Karlsruher Institut für Technologie

A heme oxygenase-like protein is involved in oxidative stress protection and Cryptochrome-related ROS signaling in *Aspergillus nidulans*

Zur Erlangung des akademischen Grades eines

DOKTORS DER NATURWISSENSCHAFTEN

(Dr. rer. nat.)

von der KIT-Fakultät für Chemie und Biowissenschaften

des Karlsruher Instituts für Technologie (KIT)

genehmigte

DISSERTATION

von

M.Sc. Ramon Frederic Seibeld

aus Hilden

Dekan: Prof. Martin Bastmeyer

Referent: Prof. Reinhard Fischer

Korreferent: Prof. Jörg Kämper

Tag der mündlichen Prüfung: 22.10.2024

Die Arbeiten im Rahmen dieser Dissertation wurden von 2019-2023 am Institut für angewandte Biowissenschaften des Karlsruher Insituts für Technologie (KIT) durchgeführt. Die Arbeiten wurden von Prof. Dr. Reinhard Fischer betreut.

Eigenständigkeitserklärung

Hiermit erkläre ich, dass ich diese Arbeit selbstständig angefertigt, keine anderen als die angegebenen Quellen oder Hilfsmittel verwendet und alle Stellen, die wörtlich oder sinngemäß aus veröffentlichten Schriften entnommen wurden, als solche kenntlich gemacht habe. Die Regelung zur Sicherung guter wissenschaftlicher Praxis im Karlsruher Institut für Technologie (KIT), in gültiger Fassung vom 27.06.2017, habe ich beachtet.

_____ _____

Datum / Ort Seibeld, Ramon Frederic

List of Publications

Yu, Z., Streng, C., Seibeld, R.F., Igbalajobi, O.A., Leister, K., Ingelfinger, J., Fischer, R., Genome-wide analyses of light-regulated genes in *Aspergillus nidulans* reveal a complex interplay between different photoreceptors and novel photoreceptor functions. *PLOS GENETICS* 17(10) (2021)

Table of Contents

Summary

Filamentous fungi are among the most diverse groups of organisms on the planet. They are very important for the decomposition of organic matter in their ecosystems, utilizing a large array of enzymes and secondary metabolites to accomplish this task. While some fungi produce valuable enzymes industrially, other pathogenic fungi pose health threats. Precise adaptation to environmental cues is essential to mount appropriate responses to various stresses they may be challenged by. Representatively, the filamentous fungus *Aspergillus nidulans* is an ideal model organism to study how fungi perceive and respond to common stress such as light, changes in temperature or oxidative stress. Its genome encodes 3 functional light receptors, such as the red-light receptor phytochrome and the blue-light receptor cryptochrome. Phytochrome functions as one of 15 histidine kinases used to evaluate biotic and abiotic stresses utilizing the phosphorelay system of the high-osmolarity glycerol (HOG) pathway to facilitate transcriptional adaptation. Light receptors heavily influence gene expression of *A. nidulans*. In previous studies, it was shown that more than 10% of the *A. nidulans* genome is differentially expressed in response to red and blue light after 15 minutes of illumination.

In this work, HoxB, a heme oxygenase-like protein, was investigated. Heme oxygenase typically catalyzes the first step of heme degradation. Furthermore, they produce biliverdin which acts as the functional chromophore for phytochrome. AlphaFold-modeling in conjunction with docking simulations showed that HoxB may not function as a heme oxygenase despite its observed impact on red-light sensing. Instead, HoxB appeared to more closely resemble a largely uncharacterized family of proteins somewhat resembling TenA-E of *A. thaliana* by potentially binding amino-pyrimidine compounds and forming homotetramers. The protein localized in the cytoplasm and in nuclei in a manner dependent on the developmental regulator VeA. Deletion of *hoxB* reduced hyphal growth when grown on meadia containing peroxides, menadione and paraquat. This mutant phenotype was rescued by re-complementation of the mutant with a wildtype *hoxB* gene. Furthermore, the *hoxB*-deletion strain showed an abnormally large increase in intracellular reactive oxygen species upon illumination with blue light and failed to express oxidative stress genes like catalase upon induction with hydrogen peroxide. Interestingly, HoxB interacted with the cryptochrome CryA in nuclei and mutants of CryA and VeA partially mimicked the growth and transcriptional

phenotypes displayed by *hoxB*-deletion and overexpression. Genome-wide expression comparison of wild type *A. nidulans* and a *hoxB*-mutant strain revealed a small set of genes relating to combating oxidative stress such as catalase, thioredoxin, peroxidases and bilirubin and glutathione transporters in response to hydrogen peroxide. While the exact mode of action by which HoxB facilitates these changes requires further investigation, it is feasible that HoxB it functions as a peroxide detector through cysteine oxidation and disulfide bond-formation in the cytoplasm and in nuclei. Additionally, in the presence of oxidative stress, HoxB may act as a negative regulator of CryA to derepress the stress-related transcription factor AtfA. In the absence of oxidative stress HoxB may disengage and CryA may downregulate AtfA to prevent the expression of genes relating to combatting oxidative stress. This work details the first characterization of HoxB-like proteins in *A. nidulans*.

Zusammenfassung

Filamentöse Pilze gehören zu den vielfältigsten Organismen der Welt. Ausgestattet mit einer Vielzahl an Enzymen und Sekundärmetaboliten spielen sie eine wichtige Rolle für die Dekomposition organischen Materials in ihren Lebensräumen. Während manche Pilze Enzyme im industriellen Maßstab produzieren sind stellen andere eine Gefahr als Pathogene dar. Eine präzise Wahrnehmung der eigenen Umgebung ist Voraussetzung um angemessen mit Stressfaktoren umzugehen mit denen sie konfrontiert werden. Der filamentöse Pilz *Aspergillus nidulans* fungiert als ein idealer Modellorganismus für Studien die sich damit befassen wie Pilze Stressfaktoren wie Licht, Temperaturveränderungen und oxidativem Stress wahrnehmen und mit ihnen umgehen. *A. nidulans* besitzt 3 funktionelle Lichtrezeptoren wie den Rotlichtrezeptor Phytochrom und den Blaulichtrezeptor Cryptochrom. Phytochrom agiert als eine von 15 Histidinkinasen die *A. nidulans* benutzt um biotische und abiotische Stressfaktoren zu bewerten indem es das Phosphorelay des „high-osmolarity glycerol (HOG)"-Signalweges benutzt um transkriptionelle Veränderungen zu bewirken. Lichtrezeptoren haben starken Einfluss auf Genexpression in *A. nidulans*. So konnte gezeigt warden dass mehr als 10% des Genoms von *A. nidulans* nach 15 Minuten Beleuchtung mit rotem und blauem Licht differentiell reguliert werden.

In dieser Arbeit wurde HoxB, ein Hämoxygenase-ähnliches Protein untersucht. Hämoxygenasen katalysieren den ersten Schritt des Hämaabaus. Außerdem generieren sie Biliverdin welches Phytochrom als Chromophor funktionalisiert. Modellierungen mit AlphaFold kombiniert mit Docking-Simulationen konnten zeigen dass HoxB nicht als Hämoxygenase fungiert obwohl ein Einfluss auf die Rotlichtwahnehmung beobachtet werden konnte. Stattdessen konnte gezeigt werden dass HoxB Aminopyrimidin-verbdingungen binden könnte und ein Homotetramer bildet wodurch es Ähnlichkeit mit der größtenteils uncharakterisierten Proteinfamilie TenA-E aus *A. thaliana* aufweist. Es wurde beobachtet dass das Protein in Abhängigkeit des globalen Regulators VeA in Zytoplasma und Nukleus lokalisiert. Die entsprechende Deletion wieß defektes Hyphenwachstum auf peroxid-, menadion- und paraquathaltigen Medien auf. Dieser Phänotyp konnte durch Rekomplementation mit einer Kopie des Wildtyp *hoxB*-Gens revertiert warden. Des Weiteren zeigte die *hoxB*-Deletion nach Beleuchtung mit Blaulicht einen höheren Anstieg reaktiver Sauerstoffspezies und war defizient in der Expression oxidativer Stressgene wie

Katalase nach Induktion durch Wasserstoffperoxid. Zusätzlich konnte eine Interaktion zwischen HoxB und dem Cryptochrom CryA im Zellkern nachgewiesen werden und Mutanten von CryA und VeA zeigten verglichen mit HoxB Deletion und Überexpression teilweise ähnliche wachstumsbezogene und transkriptionelle Phänotypen. Vergleiche genomweiter Expression zwischen Wildtyp *A. nidulans* und der *hoxB*-Mutante zeigten dass HoxB nach Induktion durch Wasserstoffperoxid die Expression von Katalase, Thioredoxin, Peroxidasen und Bilirubin- sowie Glutathiontransporter reguliert. Während die exakte Wirkungsweise in der HoxB agiert weitere Forschung benötigt besteht die Vermutung dass es durch Oxidierung von Cysteinen und Disulfidbrückenbildung als Peroxiddetektor in Zytoplasma und Nuklei aktiv ist. Weiterhin könnte HoxB nach Detektion oxidativen Stresses als negativer Regulator von CryA agieren um den Transkriptionsfaktor AtfA zu dereprimieren. In Abwesenheit von oxidativem Stress würde sich HoxB lösen und CryA erlauben AtfA zu reprimieren um die Expression oxidativer Stressgene zu unterdrücken. Diese Arbeit stellt die erste Charakterisierung eines HoxB-ähnlichen Proteins in *A. nidulans* dar.

1. Introduction

1.1 The model organism *A. nidulans*

Fungi are organisms of ubiquitous importance to their ecosystems through decomposition of a large variety of organic materials. Additionally, they provide a vast array of secondary metabolites and are commonly used for the biotechnological production of compounds. For example, *A. nidulans* produces useful enzymes such as cellulase and laccase (Jabasingh et al., 2011; Vivekanandan et al., 2014) while A. oryzae has uses in food fermentation and production of therapeutics (Gomi, 2019; Huynh et al., 2020). Simultaneously, many species of fungi are involved in food spoilage, causing economic losses across various industries and some pose a threat to human health by being pathogenic or producing mycotoxins (Stéphane et al., 2013; Kanaujia et al., 2023; Khan et al., 2024). Consequently, there is interest in researching their growth, metabolism and stress reception to understand how to utilize and manage them.

A. nidulans presents an ideal choice as a model for investigating these aspects of fungal biology due to its simple cultivation and haploid nature (Li et al., 2017). The ascomycete represents the largest division of filamentous fungi presently known and carries numerous molecular pathways found in more inconvenient or pathogenic representatives. Furthermore, its genome has been sequenced for nearly two decades (Galagan, et al., 2005) providing a large set of data to draw upon for further research. *A. nidulans* may reproduce sexually or asexually which is strongly influenced by environmental conditions, such as oxygen availability, light conditions, temperature and osmotic and oxidative stress (Rodriguez-Romero et al., 2010). In high oxygen, light and temperature conditions and the related oxidative stress, asexual reproduction is triggered, resulting in the production of conidiophores and conidiospores while in opposite conditions, sexual reproduction is triggered which results in the production of cleistothecia and ascospores (Figure 1). Proper adaptation of development relies on accurate assessment of environmental conditions and concrete stresses that may challenge survival of the fungus. One major environmental cue that *A. nidulans* relies on is light because it often determines and precedes the presence of other factors such as increases in temperature and oxidative stress. Consequently, the light reception and the corresponding signaling pathways of *A. nidulans* are highly sophisticated, tying into other stress related pathways, or being directly involved by partially doubling as

temperature sensors (Yu et al., 2019; Schuhmacher et al., 2024). In total, over 10% of *A. nidulans* genes are differentially regulated in presence of red, far-red or blue light (Yu et al., 2021). Similar, or even higher ratios have been reported in other fungi like *N. crassa* (Wu et al., 2014).

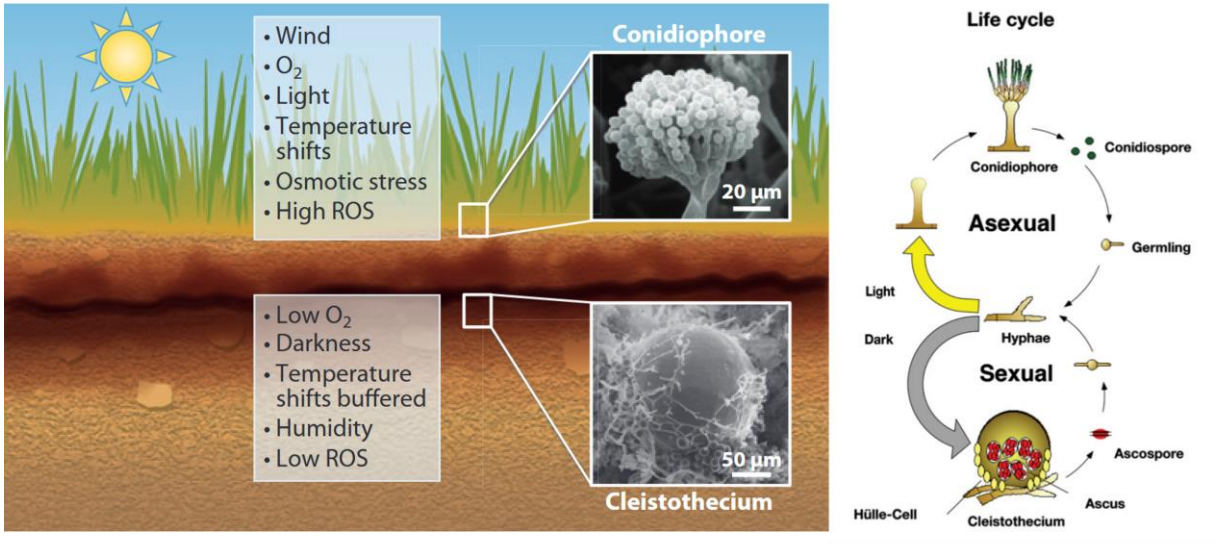

Figure 1: Sexual and Asexual Development of *A. nidulans*. Depending on environmental conditions, *A. nidulans* undergoes sexual or asexual reproduction, inducing the generation of Cleistothecia and Ascospores or Conidiophores and Conidiospores (adapted from Rodriguez-Romero et al., 2010 and Bayram et al., 2010)

1.2 Mechanisms of light reception

Perception of light generally relies on the adaptation of up to four photoreceptor systems differentiated by detected wavelength, being phytochrome for red and far-red light, opsin for green light, white collar for blue light and cryptochrome for blue/ultraviolet light (Wang et al., 2004; Saito et al., 2019; Schuhmacher et al., 2024; Vanderstraeten et al., 2020). These receptors and related chromophores as well as regulatory components are strongly conserved across different species with marginal variation due to specific environmental necessities (Pham et al., 2018; Cheng et al., 2003).

The Red-Light Receptor Phytochrome

The first discovery and research of phytochrome was performed in plants in 1959, determining the name of the receptor (Butler et al., 1959; Borthwick et al., 1960). Later,

phytochromes were identified in cyanobacteria and fungi, indicating that a common ancestor may have evolved millions of years ago, barring the option of horizontal transfer of information (Yoshihara et al., 2000; Blumenstein et al., 2005; Lane, 2011; Lamparter et al., 2017). Compositionally, phytochromes typically contain a photosensory core that consist of multiple conserved domains, a histidine kinase domain and a response-regulator domain which may be found as a separate protein (Figure 2) (Lamparter et al., 2017). The photosensory core, which binds a linear tetrapyrrole chromophore, comprises the PAS, GAF and PHY (Per-Arnt-Sim; cGMP-specific phosphodiesterases, adenylyl cyclases and FhlA; Phytochrome) domains. The location of a cysteine residue required for chromophore binding may vary case by case with *A. thaliana* phytochrome binding phytochromobilin in the GAF domain and fungal phytochromes of *A. alternata* and *A. nidulans* phytochrome assembling with biliverdin in the PAS domain (Andel et al., 1996; Blumenstein et al., 2005; Leister et al., 2019). Cyanobacteria utilize phycocyanobilin bound in the GAF-domain while other bacteria bind biliverdin in the PAS-domain (Park et al., 2000; Lamparter et al., 2017).

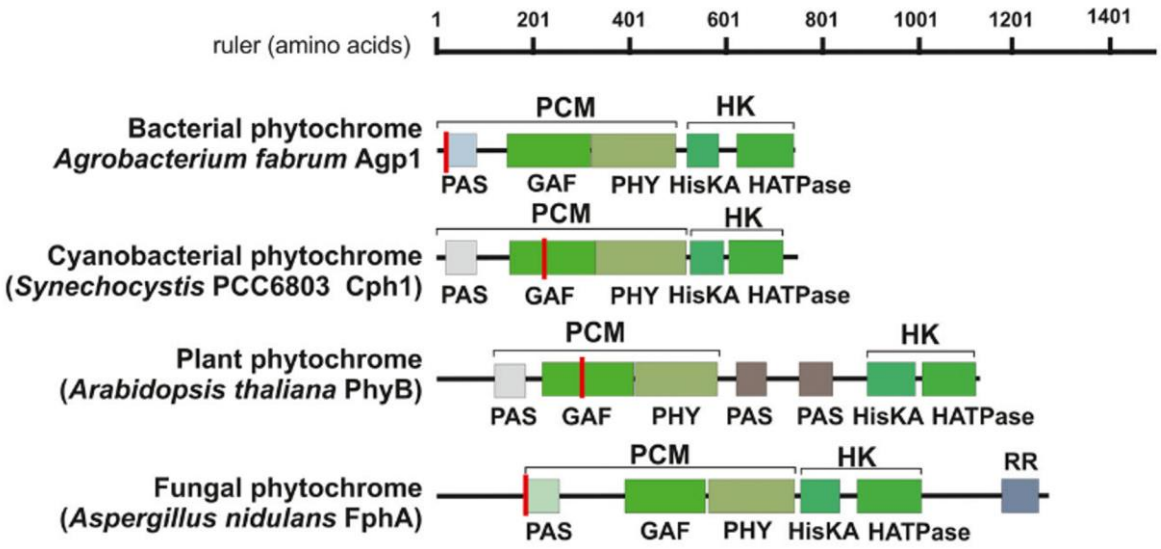

Figure 2: Composition of phytochromes in bacteria, cyanobacteria, plants and fungi. Phytochromes contain an N-terminal photosensory domain (PMC) and a C-terminal histidine kinase domain (HK). The response regulator (RR) may be coded as a separate protein. Chromophore-binding (red) situationally occurs either in the PAS or GAF-domains. (adapted from Lamparter et al., 2017)

Upon illumination with red light (~ 660 nm), the chromophore of bacteriophytochrome undergoes a cis-trans isomerization from the Pr- into the Pfr-state, involving two intermediate stages, causing structural changes along the so-called PHY tongue, translating through the helical spine of the protein into an activation of the kinase domain (Wang et al., 2004; Isaksson et al., 2021; Morozov et al., 2022). Reversion into

the Pr-state is time- and temperature-dependent or results from illumination with far-red light (~730 nm) (Figure 3) (Wang et al., 2004; Burgie et al., 2021). In *A. alternata*, heme oxygenase A is required for red-light sensing, likely by catalyzing the first step of heme degradation to form the biliverdin chromophore (Streng et al., 2021) and producing CO2, Fe3+ and biliverdin in the process (Ryter, 2022). This process is conserved in plants and bacteria and mammals (Davis et al., 2001; Wegele et al., 2004; Ryter, 2022) with some variance in the specific location of linearization of heme and the generated byproducts (Matsui et al., 2013). It has not been previously found how the biliverdin chromophore of *A. nidulans* phytochrome is produced and delivered to the protein due to the apparent lack of a functional heme oxygenase in the *A. nidulans* genome (Streng, 2020).

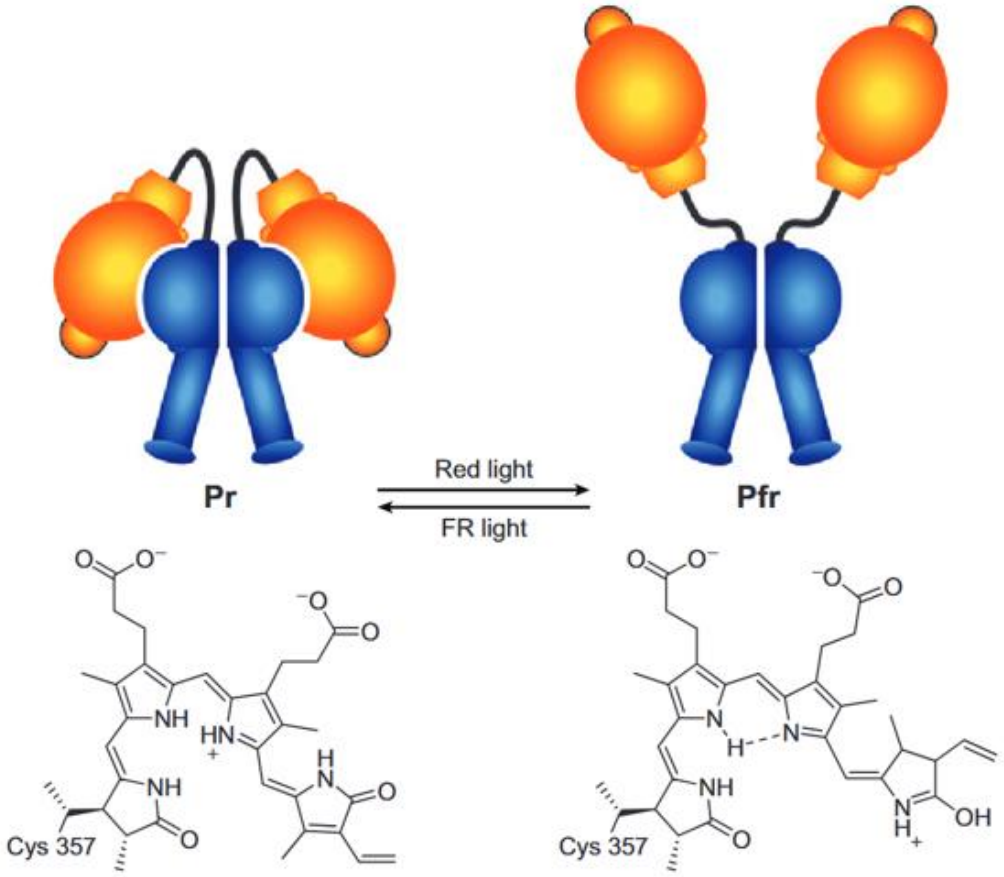

Figure 3: Photoconversion of plant phytochrome and phytochromobilin Depiction of dimeric plant phytochrome. Red light causes isomerization of phytochromobilin at the C15 position causing activation of phytochrome into the Pfr-state. Far-red light reverses this process to the Pf-state. (Bae et al., 2008)

The signal output of phytochrome of *A. nidulans* occurs via a phosphorelay system initiated by the histidine kinase domain and the response regulator using the SakA (HOG – high osmolarity glycerol) pathway (Brandt et al., 2008; Yu et al., 2016).

Mechanically, phosphorylation of the phosphorelay-components YpdA and SskA may occur in the dark, preventing the activation of SskB (Figure 4). Activation of phytochrome may reduce phosphorylation of these components, allowing SskB to activate the downstream MAPK cascade, finalizing in activation of the transcription factor AtfA (Yu et al., 2016). The precise dynamics of phosphorylation dynamics in this process have not been shown although a reverse phosphorylation of FphA by YpdA has been demonstrated *in vivo* (Azuma et al., 2007).

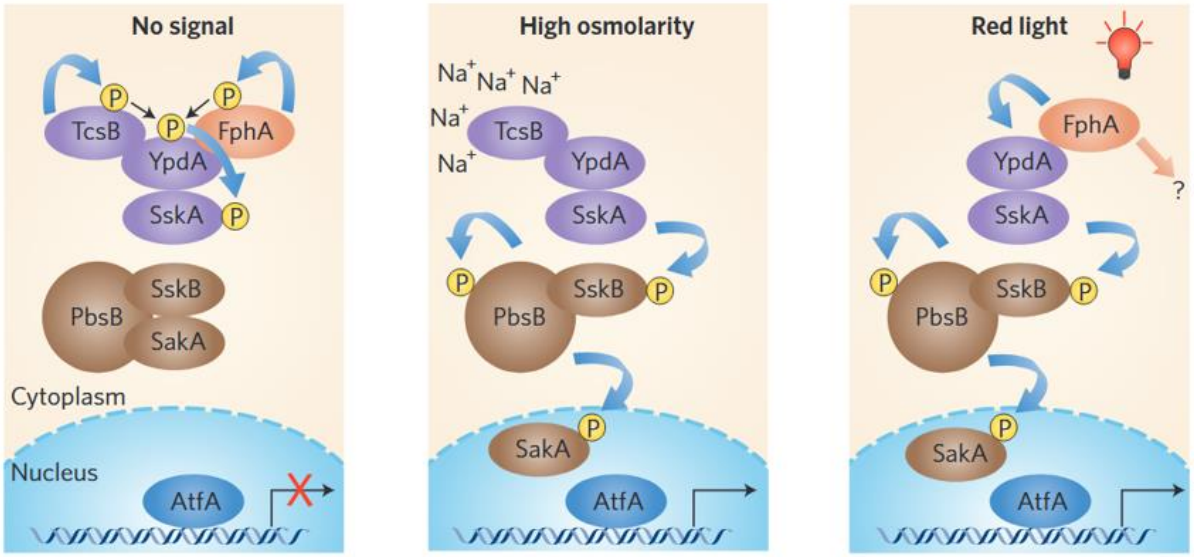

Figure 4: Fungi utilize the SakA (HOG) pathway for red-light perception. Activation of phytochrome releases phosphorylation of YpdA and SskA, activating the downstream MAPK signaling cascade including SskB, PbsB and SakA. The transcription factor AtfA regulates the response to osmotic and red-light related stress. Further effects of phytochrome may include more immediate transcriptional modulation including chromatin remodeling. (Idnurm et al., 2016)

The Blue-Light Receptor White Collar

The blue light sensors of the white-collar system, WC-1 and WC-2 have been thoroughly investigated for over 20 years in the fungus *N. crassa* (Ballario et al., 1997; Cheng et al., 2003; Gil-Sánchez et al., 2022). WC-1 consists of an N-terminal Light-Oxygen-Voltage (LOV) domain, 2 PAS domains and a C-terminal zinc-finger DNA-binding (ZF) domain. Illumination with blue light (~430-450 nm) causes the LOV domain to covalently bind an FAD chromophore (Horwitz et al., 1987; Froehlich et al., 2002). The PAS domains facilitate interactions with other proteins, such as WC-2 which contains only one PAS and ZF domains each (Ballario et al., 1998; Cheng et al., 2002). Upon illumination, the dimer conformationally changes and binds to light responsive

elements of the DNA (Froehlich et al., 2003; Schafmeier et al., 2006). A. nidulans harbors the White-Collar orthologues LreA and LreB with similar domain structures and one nuclear localization sequence each (Figure 5) (Purschwitz et al., 2008). A notable difference between white-collar of *N. crassa* and *LreA/B* in A. nidulans is their effect on the balance of sexual development in the fungi. In *A. nidulans*, corresponding deletions cause enhanced asexual development and defective cleistothecia, unlike in *N. crassa* (Purschwitz et al., 2008).

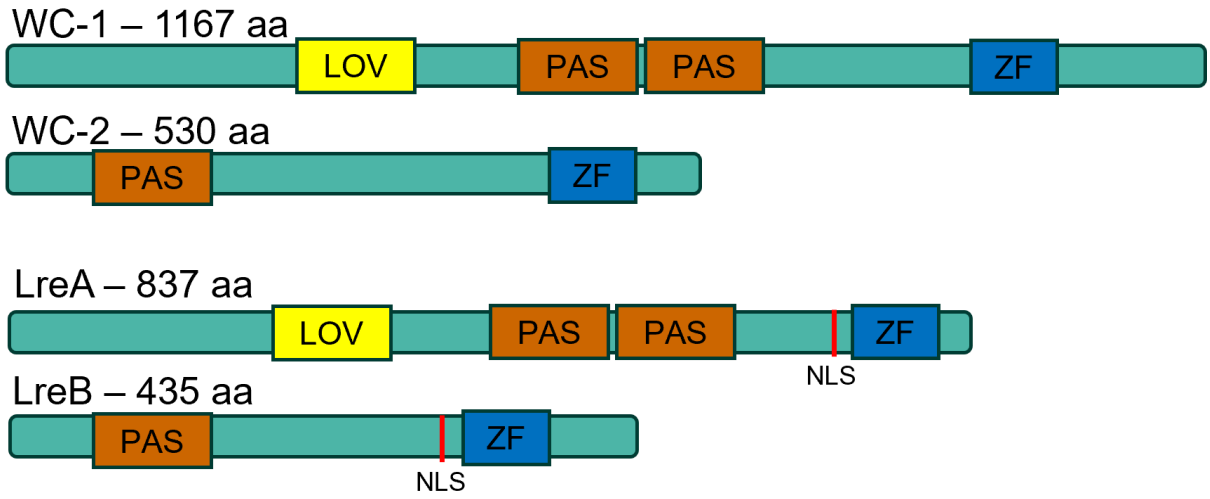

Figure 5: *N. crassa* White Collar and *A. nidulans* LreA/B proteins White Collar 1 and LreA contain a LOV domain, binding an FAD chromophore, 2 PAS domains mediating protein-protein interactions and a ZF-domain for DNA-binding. White Collar 2 and LreB contain only one PAS domain and a ZF-domain. Nuclear localization of LreA and LreB is facilitated through respective targeting sequences (red)

The Blue-Light Receptor Cryptochrome

Cryptochromes are blue-light receptors assumed to evolve from a family of DNA photolyase proteins and have adapted into multiple subsets of DNA-repair and regulatory proteins (Figure 6) (Bayram et al., 2008a; Tagua et al., 2015; Navarro et al., 2020). Photolyases bind an antenna chromophore like methyltetrahydrofolate (MTHF) which transfers the excitation energy to a non-covalently bound flavin-adenine dinucleotide (FAD) chromophore (Figure 7) (Yu et al., 2018; Aguida et al., 2024). Excitation of the FAD chromophore causes the reduction of FAD through the transfer of an electron to the bound site of DNA damage, releasing the damaged structure (Sancar, 1994). The DNA photolyases may release DNA damage in form of cyclobutene pyrimidine dimers (CPDs) or 6-4 pyrimidine-pyrimidone photoproducts (6-4s) (Maul et al., 2008; Vechtomova et al., 2021). The functionally diverse

cryptochromes may exhibit partial functionality in DNA repair like *A. nidulans* CryA (Bayram et al., 2008a; Navarro et al., 2020), but mainly perform signaling functions relevant to their host organisms. Their photocycle of the FAD chromophore remains the same, releasing reactive oxygen species like hydrogen peroxide during its recovery process although they do not necessarily require an MTHF cofactor for initial absorption of blue light (Figure 7) (Kottke et al., 2018; Romero et al., 2018; Aguida et al., 2024). Most commonly, cryptochromes are involved in regulating the circadian rhythm of their hosts through induction of transcriptional changes (Wang et al., 2008; Jiang et al., 2018; Shafi et al., 2021; Lopez et al., 2021).

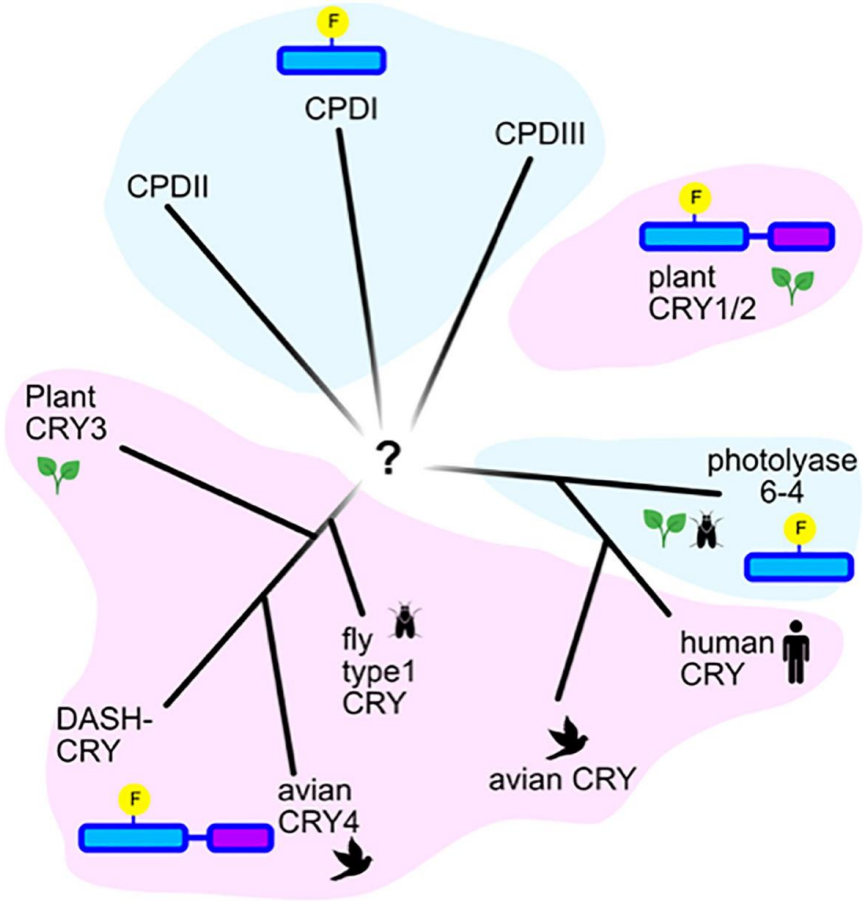

Figure 6: Evolution of Photolyase/Cryptochrome proteins Photolyases differentiate in Type I, II and III CPD- and 6-4-type photolyases. Cryptochromes have adapted as regulatory proteins in the Cry1-4- and CRY-DASH-type cryptochromes (Aguida et al., 2024)

In *A. thaliana*, Cry1 and Cry2 are phosphorylated and form oligomers upon illumination, modulating transcription factors, hormone activity and chromatin-remodeling (Ponnu et al., 2022). Cryptochrome may function in conjunction with phytochrome to affect expression of circadian clock-related genes (Tóth et al., 2001; Yanovsky et al., 2001). In *A. thaliana* and mammalian cryptochromes, the C-terminal extensions folded into

the flavin-binding pocket are modified and required for downstream activities (Chaves, et al., 2006; Ponnu et al., 2022; Aguida et al., 2024). Additionally, the reactive oxygen species produced during the cryptochrome photocycle may perform signaling functions in the nucleus. *A.thaliana* Cry2 causes accumulation of nuclear ROS and photoactivation of overexpressed *A. thaliana* Cry1 leads to cell death while the resulting accumulation of ROS in the nucleus induces transcriptional regulation of stress genes, even in morphologically deficient cryptochrome mutants (Jourdan et al. 2015; El-Esawi et al., 2017). In *N.crassa*, WC-1 and WC-2 are central components of the circadian clock while cryptochrome may be a negative regulator of WC activity (Dunlap et al., 2007; Olmedo et al., 2010). The only cryptochrome of *A. nidulans*, CryA, has not been shown to promote circadian rhythmicity in the fungus. However, it promotes sexual differentiation through transcriptional regulation of fruiting body formation (Bayram et al., 2008a). Similarly, BcCRY2 represses conidiation in B. cinerea (Cohrs et al., 2017).

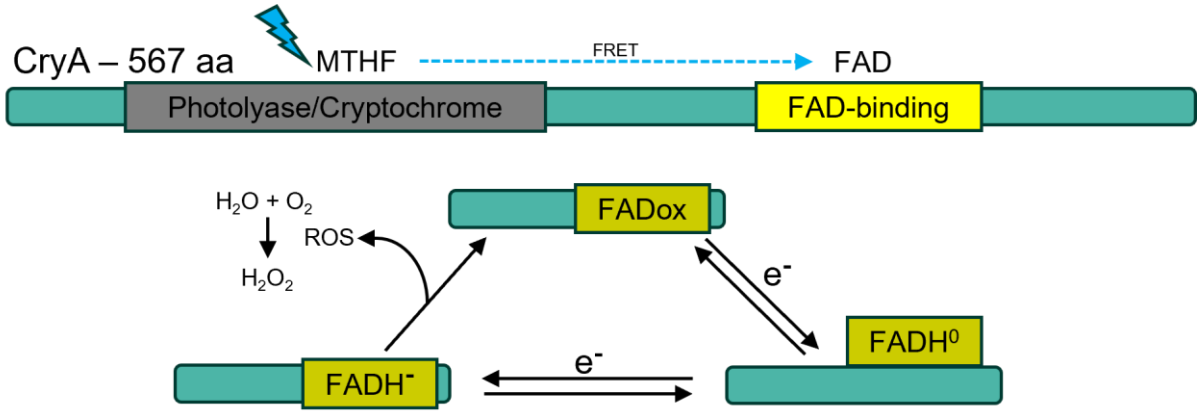

Figure 7: Cryptochrome of *A. nidulans* Cryptochrome contains one typical photolyase/cryptochrome domain (grey). It binds the chromophores MTHF which is excited by blue light and transfers this energy to FAD. During the photocycle of FAD it is reduced twice. Recovery into the oxidized state generates reactive oxygen species (mainly hydrogen peroxide).

The major regulatory protein Velvet A

Velvet A (VeA) of *A. nidulans* is a highly disordered protein involved in morphological, sensory and metabolic pathways (Spröte et al., 2007; Bayram et al., 2008b; Hou et al., 2024). Regulation of some of these processes involves interaction with the light receptor FphA (Purschwitz et al., 2008; Purschwitz et al., 2009). This dynamic may be modulated by LreA and LreB (Purschwitz et al., 2008; Hedtke et al., 2015). VeA was originally discovered in 1965 in a UV-mutagenesis screening (Käfer, 1965). The

described mutant, termed *veA1*, encodes a truncated version of the original protein and undergoes asexual development in the dark (Figure X). Mechanistically, the protein is fully unable to enter the nucleus due to a mutation of the original start codon which shifts the open reading frame by 36 positions, partially deleting a nuclear localization sequence encoded upstream of it (Kim et al., 2002). VeA heavily relies on post-translational modification through phosphorylation and interactions with other regulators, such as VelB and LaeA to perform its tasks relating to development, light sensing and secondary metabolism (Bayram et al., 2008b; Rauscher et al., 2015). In the dark, VeA localizes to the nucleus and in light, VeA translocates to the cytoplasm. This dynamic may be heavily regulated by phosphorylation of residues T167 and T170, as their mutation caused light-independent nuclear localization and affected interactions with VelB and FphA (Rauscher et al., 2015).

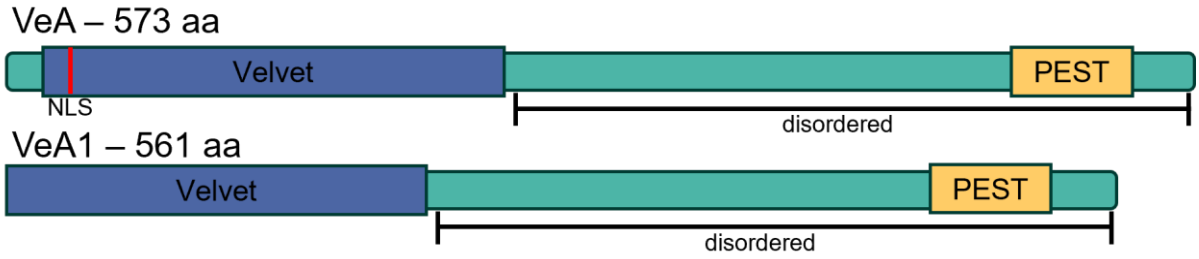

Figure 8: Velvet A of *A. nidulans* Velvet A contains a velvet domain (blue) and a PEST (rich in Proline- (**P**), Glutamic acid- (**E**), Serine- (**S**) and Threonine- (**T**)) domain (orange). The remaining protein is largely disordered. A nuclear localization sequence (NLS) is located near the N-terminus (red). The VeA1 mutation is a truncated protein. The partial deletion of the NLS causes VeA1 to remain cytoplasmic.

Evidentially, regulation of gene expression by VeA-complexes relies on epigenetic control through methyltransferases VipC, VapB and LimF (Sarikaya-Bayram et al., 20014; Palmer et al., 2013). Expression of 11 secondary metabolite clusters were shown to depend on VeA and LaeA while being heavily influenced by temperature with 4 clusters being regulated exclusively at 37°C but not at lower temperatures (Lind et al., 2016). In A. flavus, VeA was found to regulate the oxidative stress response by modulating the promoters of *cat1* and *trxB* (Baidya et al., 2014). Correspondingly, absence of VeA resulted in lower expression of these genes and increased sensitivity to reactive oxygen species. Furthermore, VeA was shown to enhance expression of the stress related transcription factor AtfB. The SvfA protein may depend on VeA to facilitate oxidative stress resistance in A. nidulans (Lim et al., 2020).

The Green-Light receptor Opsin

Opsins are green light receptors, binding a retinal chromophore. They are G-protein coupled receptors with a seven-transmembrane domain structure (Terakita, 2005). Data on opsins that operate in non-visual systems in fungi is sparce. RNA of opsin Nop1 of *N. crassa* selectively accumulates during asexual and sexual development and deletion mutants showed were defective in adapting the appropriate developmental state (Bieszke et al., 1999; Wang et al., 2018). Deletion of the opsin NopA of *A. nidulans* did not result in a notable phenotype (Ruger-Herreros et al., 2011).

1.3 Mechanisms of oxidative stress resistance

Oxidative stress is a highly diverse set of distinct stimuli posing a challenge to survival. Sources of oxidative stress may result from environmental conditions, such as high intensity blue light, interactions with other organisms utilizing it for offensive or defensive strategies like *S. oralis* or the mammalian immune system or from internal sources like metabolic processes (Erttmann et al., 2019; Sen et al., 2021; Yu et al., 2021). Filamentous fungi may encounter all of these conditions and therefore require appropriate methods to perceive, characterize and respond to oxidative stress.

Perception of oxidative stress

Mechanistically, perception of oxidative stress in fungi involves multiple histidine kinases and signal transduction through the HOG-pathway and detection by specific proteins modified by molecular sources of oxidative stress. *C. albicans* was found to leverage Hog1 via the HOG pathway for oxidative stress signaling in response to hydrogen peroxide (Figure 9A) (Smith et al., 2004; Enjalbert et al., 2005). Finetuning of Hog1 for oxidative stress sensing requires lateral control through thioredoxin peroxidases like Tsa1 through an unknown mechanism (Da Silva Santas, et al., 2010). Correspondingly, *S. pombe* uses the stress activated protein kinase Sty1 which requires lower peroxide concentrations to become activated (Chen et al., 2003; Asp et al., 2008). *E. coli* and S. typhimurium detect peroxide utilizing OxyR, a transcription factor oxidized and activated directly upon contact with hydrogen peroxide (Figure 9B) (Christman et al., 1989). Oxidation occurs at two cysteine residues that form a disulfide bond intramolecularly which promotes tetramerization of OxyR and recruitment of

RNA-Polymerase (Tao et al., 1993; Zheng et al., 1998; Choi et al., 2001). Media concentrations higher than 5 µM of hydrogen peroxide were found to be highly restrictive to growth of E. coli knockout mutants (Li et al., 2018). The Gpx3/Yap1 system of *S. cerevisiae* constitutes another cysteine-based sensory system with the transcription factor Yap1 cycling between cytoplasm and nucleus depending on cysteine oxidation (Figure 9C) (Delaunay et al., 2000). Oxidation of Yap1 may depend on elevated cytoplasmic concentrations or the glutathione peroxidase Gpx3. The respective disulfide bond was found to be released by thioredoxin and export of Yap1 from the nucleus requires the exportin Crm1 (Delauny et al., 2000; Delaunay et al., 2002; Wood et al., 2004).

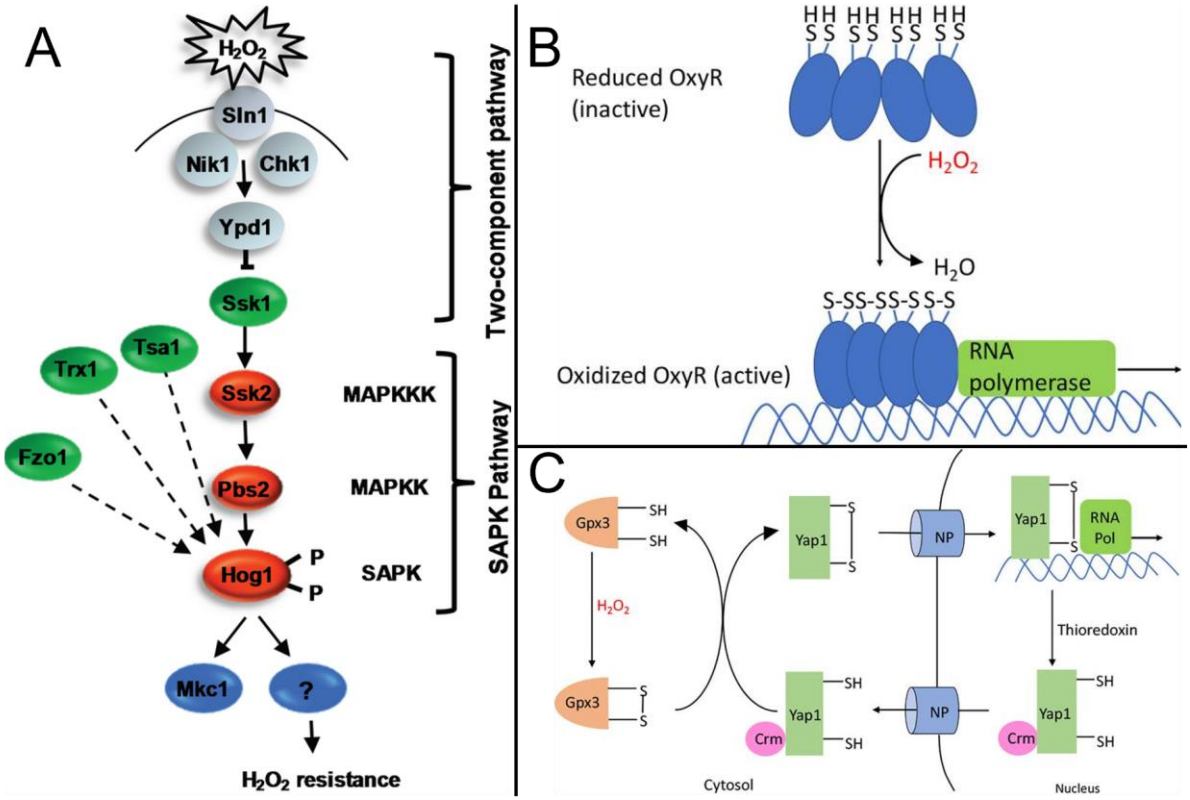

Figure 9: Mechanisms of Oxidative Stress (Peroxide) detection (A) *C. albicans* uses histidine kinases Nik1, Sln1 and Chk1 signaling into the HOG-pathway for peroxide stress perception. Modulation of MAPK Hog1 tunes Hog1 to address transcription factors responsible for relaying resistance to the perceived stress. (B) *E.coli* detects peroxide stress using the transcriptionally active OxyR. Formation of disulfide bonds within the OxyR multimer causes activation and nuclear translocation, allowing transcriptional regulation. (C) In a similar fashion, *S. cerevisiae* uses the Gpx3/Yap1 system to detect peroxide stress. Oxidized Yap1 shuttles into the nucleus and is transcriptionally active. Release of the disulfide bond by thioredoxin allows Crm1 to export Yap1 from the nucleus. The dynamics of Yap1 localization are controlled by Gpx3 which is oxidized by peroxide and in turn oxidizes Yap1. (adapted from: Da Silva Dantas et al., 2015 & Sen et al., 2021)

In *A. nidulans*, multiple histidine kinases like HysA, NikA and FphA regulate oxidative stress utilizing the HOG pathway and the HOG associated transcription factor AtfA is

required for adaptation to oxidative stress (Hayashi et al., 2014; Emri et al., 2015; Orosz et al., 2017; Kanamaru et al., 2022). Mitochondria undergo rapid changes in response to oxidative stress, indicating that they may also use a separate mechanism of detection and response to oxidative stress (Loriette et al., 2023). A signaling pathway for sensing other sources of oxidative stress like menadione or paraquat in filamentous fungi is not known in detail, although the ubiquitous nature in stress signaling of the HOG pathway may imply that it is involved. In *A. flavus*, the regulatory protein VeA increases resistance to hydrogen peroxide by promoting binding of AtfB to catalase and thioredoxin promoters (Baidya et al., 2014).

Responses to oxidative stress

The individual transcriptional responses to oxidative stress may vary in intensity depending on its source. In various filamentous fungi, paraquat primarily increases superoxide dismutase while hydrogen peroxide primarily increases catalase expression (Angelova et al., 2005; Abrashev et al., 2011). However, most genes of the core oxidative stress response, such as catalase, peroxiredoxin, thioredoxin, superoxide dismutase, glutaredoxin and glutathione peroxidase are increased in response to hydrogen peroxide in *C. albicans* (Wysong et al., 1998; Enjalbert et al., 2003; Enjalbert et al., 2006; Li et al., 2008; da Silva Dantas et al., 2010). Furthermore, bilirubin may exert cytoprotective effects, acting as an antioxidant and inhibition of NADPH oxidase-related reactive oxygen species indicating that metabolic changes are involved in oxidative stress resistance (Barañano et al., 2002; Datla et al., 2007; Weaver et al., 2018). The secondary metabolism of *A. flavus* changes regulates oxidative stress resistance by potentially consuming excess oxygen species (Fountain et al., 2016). In *A. nidulans*, expression of two catalases CatA and CatB is spore- and growth-specific respectively, with partial overlap during germination (Kawasaki et al., 1997). While expression of CatA was found to depend on AtfA, the same was not found for CatB (Orosz et al., 2017; Kocsis et al., 2023). Similarly, the glutathione peroxidase GpxA, the glutathione reductase and cytochrome c peroxidase Ccp1 depend on AtfA in response to menadione sodium bisulfate and diamide in *A. nidulans*. The thioredoxin peroxidase PrxA and thioredoxin reductase TrxR do not depend on AtfA under the same conditions (Orosz et al., 2017).

1.4 Thiamine

Thiamine, also known as vitamin B1, is a molecule with large biological relevance. Its derivatives like thiamine pyrophosphate are important cofactors for pyruvate dehydrogenase among other things (Naito et al., 2002). An important precursor in generating this cofactor is the scavenging of 4-amino-5-hydroxymethyl-2-methyl-pyrimidine (HMP) (Figure 10). In *A. thaliana*, scavenging of HMP occurs via amino- or formylamino-HMP using the TenA_C enzyme, termed after a conserved cysteine residue responsible for catalysis (Zallot et al., 2014). Similar proteins lacking this active site residue have been termed TenA_E and exhibit marginal catalytic activity with a binding-cavity fitting HMP found deep in the core of the protein in crystallographic analyses of *P. furiosus* and *B. subtilis* TenA_E (Rajan et al., 2004; Benach et al., 2005; Levin et al., 2007; Zallot et al.; 2014). Supplementation of thiamine and thiamine pyrophosphate may enhance tolerance of A. thaliana against oxidative stress induced by paraquat (Tunc-Ozdemir et al., 2009). TenA_E-like proteins have not been characterized beyond *in vitro* biochemical characterization and no phenotypes in filamentous fungi have been described previously.

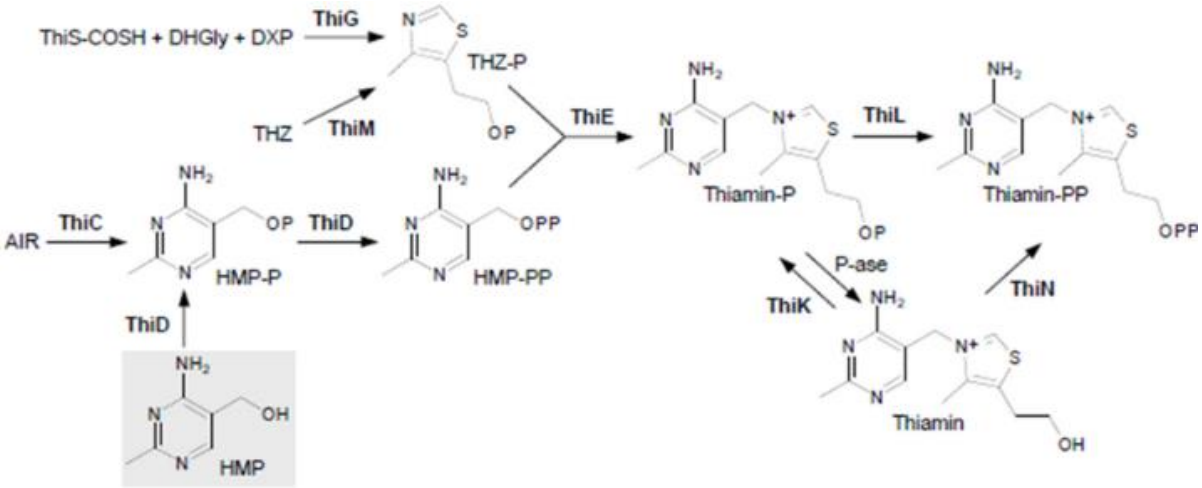

Figure 10: HMP in synthesis of the cofactor thiamine pyrophosphate 4-methyl-5-(2-hydroxyethyl)-thiazole (THZ) and HMP moieties are required for synthesis of thiamine and thiamine pyrophosphate in bacteria. Enzymatic conversion is facilitated by ThiC, ThiD, ThiE, ThiG, ThiK, ThiL, ThiM and ThiN. TenA_C (and possibly TenA_E) scavenges HMP from amino-HMP. -P: Phosphate, -PP: diphosphate, -COSH: thiocarboxylate, DXP: deoxy-D-xylulose 5-phosphate, DHGly: dehydroglycerine, AIR: 5-aminoimidazole ribotide (Zallot et al., 2014)

1.5 Objectives of this work

In previous studies, heme oxygenases have been determined to be proteins with varying functionality. The protein family is known to contribute to environmental fitness by producing biliverdin, a chromophore necessary for red light sensing in filamentous fungi and protection against ROS species in mammals, planta and fungi (Blumenstein et al., 2005; Jansen et al., 2012). Previous work (Streng et al., 2021) details two heme oxygenases termed HoxA and HoxB in *A. alternata* that were fundamentally used to search for heme oxygenases in *A. nidulans*. HoxA (*A. alternata*) was found to be a biliverdin-producing heme oxygenase, but HoxB (*A. alternata*) was determined to be an atypical heme oxygenase unlikely to be directly involved in biliverdin synthesis while still being involved in light perception. Therefore, the aim of this work was to determine whether and for what purpose *A. nidulans* expresses a HoxB protein and how it may be involved in light sensing.

2. Results

2.1 Identification of heme-oxygenase-like proteins in *A. nidulans*

This work aimed to identify and characterize HoxB-like proteins as detailed in previous work (Streng et al., 2021). A pBlast analysis within Geneious Prime was used to search for proteins resembling HoxA and HoxB of *A. alternata* in *A. nidulans* (Figure 11) (Sayers et al., 2022). A set of biliverdin-producing heme oxygenases from various organisms was compared to the genome of *A. nidulans*.

A

	KAF7586857	KOC10151	QMW36992	XP_0318947...	OOG00224	A. nidulans ...	KAB8212943	XP_0253817...	XP_0266298...	XP_0415555...	PWY69027	KAF5857597	A. alternata ...	A. alternata ...
KAF7586857		80.12%	83.33%	94.97%	69.06%	0%	71.97%	68.72%	69.27%	68.72%	66.67%	93.18%	50.23%	0%
KOC10151	80.12%		94.61%	84.81%	63.71%	0%	69.92%	65.06%	65.86%	66.53%	65.22%	80.16%	52.25%	0%
QMW36992	83.33%	94.61%		86.08%	66.80%	0%	69.49%	68.87%	67.70%	67.18%	65.90%	81.57%	52.53%	0%
XP_031894730	94.97%	84.81%	86.08%		65.00%	0%	70.28%	67.63%	68.46%	70.49%	63.60%	87.30%	49.32%	0%
OOG00224	69.06%	63.71%	66.80%	65.00%		0%	58.72%	87.21%	87.21%	75.29%	69.32%	66.67%	50.68%	0%
A. nidulans HoxB	0%	0%	0%	0%	0%		0%	0%	0%	0%	0%	0%	23.53%	0%
KAB8212943	71.97%	69.92%	69.49%	70.28%	58.72%	0%		62.71%	61.86%	63.29%	59.26%	72.24%	50.17%	0%
XP_025381759	68.72%	65.06%	68.87%	67.63%	87.21%	0%	62.71%		93.80%	77.78%	72.28%	69.38%	53.69%	0%
XP_026629813	69.27%	65.86%	67.70%	68.46%	87.21%	0%	61.86%	93.80%		77.78%	71.16%	68.99%	53.02%	0%
XP_041555547	68.72%	66.53%	67.18%	70.49%	75.29%	0%	63.29%	77.78%	77.78%		75.56%	68.85%	56.48%	0%
PWY69027	66.67%	65.22%	65.90%	63.60%	69.32%	0%	59.26%	72.28%	71.16%	75.56%		64.43%	53.57%	0%
KAF5857597	93.18%	80.16%	81.57%	87.30%	66.67%	0%	72.24%	69.38%	68.99%	68.85%	64.43%		49.85%	0%
A. alternata HoxA	50.23%	52.25%	52.53%	49.32%	50.68%	23.53%	50.17%	53.69%	53.02%	56.48%	53.57%	49.85%		0%
A. alternata HoxB	0%	0%	0%	0%	0%	0%	0%	0%	0%	0%	0%	0%	0%	

B

	BAE65044	KAE8410614	RLL92876	PYH92625	EHA23093	PKX92215	RAH60376	RDH33801	XP_0255686...	XP_0223847...	XP_0266060...	A. nidulans ...	A. alternata ...	A. alternata ...	XP_0255507...
BAE65044		0%	0%	0%	0%	0%	0%	0%	0%	0%	0%	0%	0%	0%	0.39%
KAE8410614	0%		0%	0%	0%	0%	0%	0%	0%	0%	0%	0%	0%	0%	0%
RLL92876	0%	0%		60.25%	67.51%	96.50%	68.02%	67.51%	68.02%	69.00%	70.50%	71.14%	0%	62.81%	0%
PYH92625	0%	0%	60.25%		79.36%	62.68%	81.19%	79.36%	79.82%	73.06%	76.26%	72.60%	0%	66.04%	0%
EHA23093	0%	0%	67.51%	79.36%		67.89%	97.57%	100%	98.38%	78.95%	75.89%	76.17%	0%	68.42%	0%
PKX92215	0%	0%	96.50%	62.68%	67.89%		68.70%	68.29%	68.29%	69.35%	69.76%	71.89%	0%	62.10%	0%
RAH60376	0%	0%	68.02%	81.19%	97.57%	68.70%		97.57%	98.79%	79.76%	77.08%	75.78%	0%	68.42%	0%
RDH33801	0%	0%	67.51%	79.36%	100%	68.29%	97.57%		97.98%	79.76%	76.28%	76.56%	0%	68.83%	0%
XP_025568693	0%	0%	68.02%	79.82%	98.38%	68.29%	98.79%	97.98%		79.35%	75.89%	75.78%	0%	68.83%	0%
XP_022384745	0%	0%	69.00%	73.06%	78.95%	69.35%	79.76%	79.76%	79.35%		77.95%	77.43%	0%	67.59%	0%
XP_026606042	0%	0%	70.50%	76.26%	75.89%	69.76%	77.08%	76.28%	75.89%	77.95%		86.38%	0%	65.49%	0%
A. nidulans HoxB	0%	0%	71.14%	72.60%	76.17%	71.89%	75.78%	76.56%	75.78%	77.43%	86.38%		0%	67.44%	0%
A. alternata HoxA	0%	0%	0%	0%	0%	0%	0%	0%	0%	0%	0%	0%		0%	0%
A. alternata HoxB	0%	0%	62.81%	66.04%	68.42%	62.10%	68.42%	68.83%	68.83%	67.59%	65.49%	67.44%	0%		0%
XP_025550756	0.39%	0%	0%	0%	0%	0%	0%	0%	0%	0%	0%	0%	0%	0%	

Figure 11: HemeO-like proteins in multiple organisms. (A) Comparison of HoxA and HoxB of *A. nidulans* and *A. alternata* with biliverdin-producing heme oxygenases. HoxA of *A. alternata* shows higher than 50% homology with all candidates except HoxB of *A. alternata* and *A. nidulans*. HoxB of A. nidulans shows 23.53% homology with HoxA of *A. alternata* while HoxB of *A. alternata* shows 0% homology with it. *A. nidulans* does not carry a protein resembling HoxA of *A. alternata*. (B) Comparison of HoxA and HoxB of *A. nidulans* and *A. alternata* with hemeO-like transcriptional regulators. HoxA of *A. alternata* shows no homology with any candidates while HoxB of *A. nidulans* and *A. alternata* show higher than 60% sequence homology with some, although not all, candidates.

No proteins resembling biliverdin-producing heme oxygenases were found (Figure 11A). Furthermore, a set of atypical heme oxygenases from various organisms was compared to the genome of *A. nidulans*. One protein resembling HoxB from *A. alternata* was found in the genome of *A. nidulans*. This protein resembled proteins classified as heme oxygenase-like transcriptional regulators (Figure 11B) and will subsequently be referred to as HoxB (Figure 12).

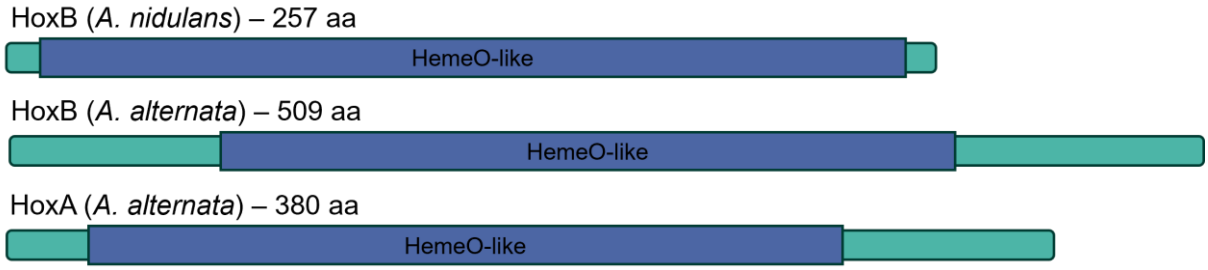

Figure 12: HoxB of *A. nidulans* and *A. alternata* and HoxA of *A. alternata*. The three Hox-proteins contain a central HemeO-like domain. HoxA and HoxB of A. alternata have long N- and C-terminal extensions beyond the central domain that are not found in HoxB of A. nidulans.

2.2 HoxB may be a TenA_E-like protein

In an effort to determine the potential function of HoxB, the protein was analyzed *in silico* and compared to similar proteins in other filamentous fungi. A conserved domain search (Marchler-Bauer et al., 2007) revealed that the classification as a heme oxygenase-like transcriptional regulator is based on the similarity to proteins in the TenA_E (transcriptional enhancer A_E) subfamily of *Arabidopsis thaliana* which has been hypothesized to be a transcriptional regulator in *Bacillus subtilis* (Pang et al., 1991). In each case, the observed effects on gene transcription were discussed to potentially be indirect since the proteins lack typical characteristics of transcription factors such as motifs and positive surface charges. Similarly, heme oxygenases, such as human heme oxygenase 1 (hHO-1) have been known to enter the nucleus under certain conditions to affect gene transcription (Lin et al., 2007). However, both proteins are mainly known for their enzymatic roles in heme oxidation or thiamin metabolism respectively (Duvigneau et al., 2019; Streng et al., 2021; Zallot et al., 2014). Accordingly, an *in silico* assessment was performed to determine whether HoxB may be active enzymatically and whether it may be active as a transcriptional regulator. Members of the heme oxygenase and TenA_E families are characterized by specific residue patterns each within their active sites.

Relevant residues for heme binding and the enzymes active site in human heme oxygenase (hHO-1) were identified to be "^{49}LVMASLYHIYVALEEEIER^{67}" and "^{205}TAFLLNIQLFEELQELLTHDTK^{226}", including an additional conserved histidine residue - being responsible for coordination of the iron center – found in heme-binding proteins (Wilks et al., 1998; Lynn et al., 1999; Sun & Loehr, 1994). Alignment of these sequences against HoxB showed that this heme binding pocket is not found within the

protein (Figure 13). Furthermore, no highly conserved histidine residues were found in HoxB (Figure 14).

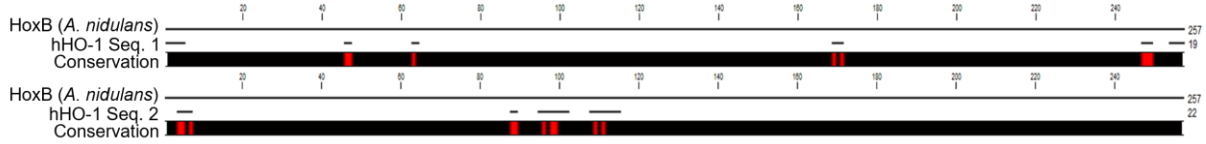

Figure 13: HoxB does not show sequence conservation with the active site of human heme oxygenase 1 Neither of the 2 active site sequences "^{49}LVMASLYHIYVALEEEIER^{67}" nor "^{205}TAFLLNIQLFEELQELLTHDTK^{226}" of human heme oxygenase 1 are found in HoxB of *A. nidulans*. Instead, short elements of these sequences are found widely spaced across the protein at positions marked conserved (red)

Similarly, TenA_E of A. thaliana binds 4-amino-5-hydroxymethyl-2-methylpyrimidine (HMP) as a ligand (Levin et al., 2007). Binding of this ligand is facilitated by Aspartate 47, Glutamate 210 and Valin 39 providing stability through hydrogen bonding as well as Phenylalanine 50 and Tyrosine 143 which stack the aromatic component of HMP (Blommel et al., 2004). While not all these residues are conserved in orthologues of TenA_E, some of them are generally present (Zallot et al., 2014). Alignment of TenA-like proteins found in filamentous fungi showed 5 series of highly conserved residues within the sequence of HoxB (Figure 14A). Notably, many conserved residues found within HoxB were predicted to be found in the core of the protein while surface residues are not highly conserved (Figure 14B). Considering that transcription factors commonly rely on specific basic surface residues to bind DNA (Chen et al., 2022; Bartas et al., 2021), this is indicative of HoxB not directly functioning as a transcription factor while not excluding the possibility of HoxB interacting with other proteins.

Among the conserved residues, multiple residues relevant for TenA_E functionality were found, such as Aspartate in positions 44 and 216, Glutamate in positions 94, 151, 160 and 248, Valine in positions 155, 215 and 244, Phenylalanine in positions 23, 98, 204 and 207 and Tyrosine 47, 105 and 163.

An assessment of whether any of these residues might be involved in ligand binding was performed by modeling HoxB using AlphaFold (Jumper et al., 2021) and potential ligands, as well as their predicted corresponding binding affinities, were modeled with the protein using Autodock Vina (Trott et al., 2010). The majority of per-residue model confidence scores (pLDDT-score) for the model of HoxB produced by AlphaFold fell within a range of high certainty (Figure 15), indicating a high degree of reliability of the model.

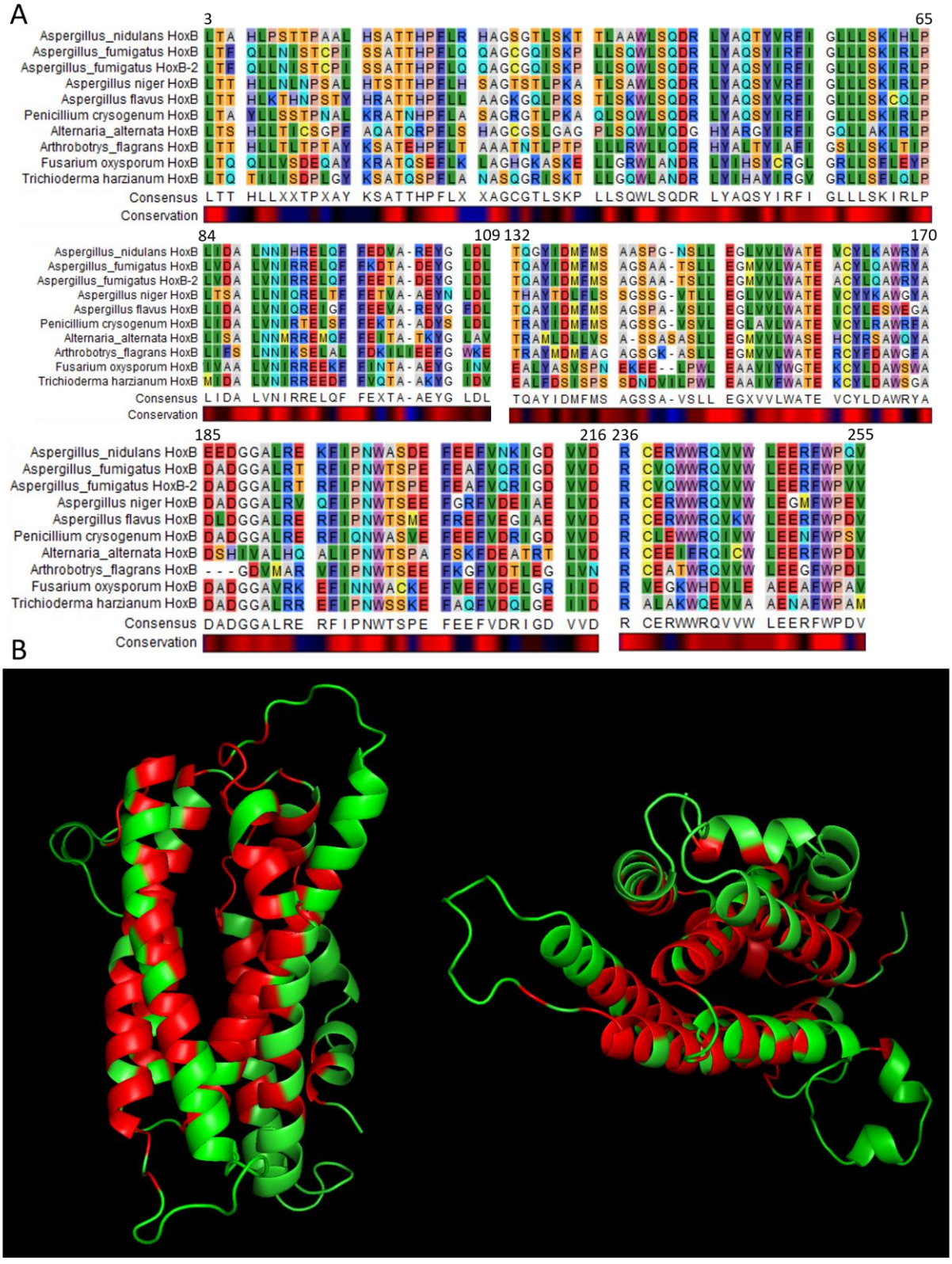

Figure 14: Conservation of HoxB in filamentous fungi (A) Alignment of HoxB-like proteins found in filamentous fungi. 5 distinct sections showing high conservation of residues between positions 3 and 65, 84 and 109, 132 and 170, 185 and 216 and 236 and 255 were found. (high conservation in red, medium conversation in blue and little conservation in black (B) Conserved regions of HoxB modelled using AlphaFold. The conserved sequences (red) point, although not exclusively, towards the core of the protein.

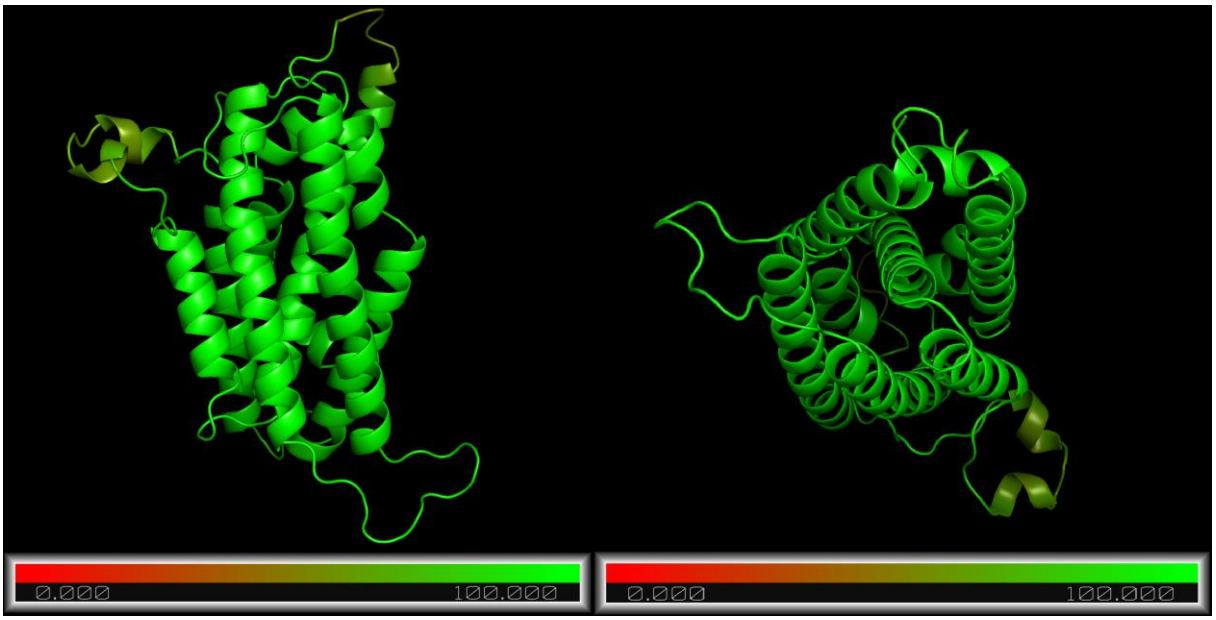

Figure 15: Per-residue model confidence scores (pLDDT-score) for HoxB modelled with AlphaFold Ranking of model confidence per residue from high (green) to low (red). The central helices of the model are ranked with high certainty. Small outer sections of the model are ranked with medium certainty, although the overall certainty in model accuracy is high.

Heme oxygenases bind protoporphyrin IX containing Fe^{3+} (heme) as substrate (Fleischhacker et al., 2020). Modeling HoxB of *A. nidulans* with heme yielded a range of binding positions on the protein surface near its N-terminus with binding affinities ranging from -5.1 to -4.0 kcal per mol. However, the orientation of the molecule was inconsistent with heme binding observed in other heme oxygenases (Okunlola et al., 2021). The models produced for HoxB show heme pressed flat against the surface of the protein (Figure 16A). Typical heme binding occurs with the molecule lodged in the heme binding pocket between two neighbouring alpha-helices as shown by modeling heme oxygenase of *C. synechocystis* (pdb-ID: 1WE1) with heme (Figure 16B). The predicted binding affinities for this model ranged from -10.5 to -9.6 kcal per mol. This indicates a strong unlikelihood that HoxB binds heme as its ligand.

TenA_E of *B. subtilis* and *A. thaliana* bind HMP as a ligand (Rajan et al., 2004; Levin et al., 2007). Modeling HoxB of *A. nidulans* with HMP, the scoring function produced possible binding positions with calculated binding affinities ranging from -4.9 to -4.6 kcal per mol. Of these, only one position was located near the predicted binding pocket found in TenA_E of *A. thaliana* (Zallot et al., 2014). In comparison, TenA_E from *A. thaliana* (pdb-ID: 2Q4X), modeled with HMP in the same fashion produced binding affinities between -6.1 and -5.7 kcal per mol, indicating stronger binding of the ligand compared to HoxB (Figure 17B).

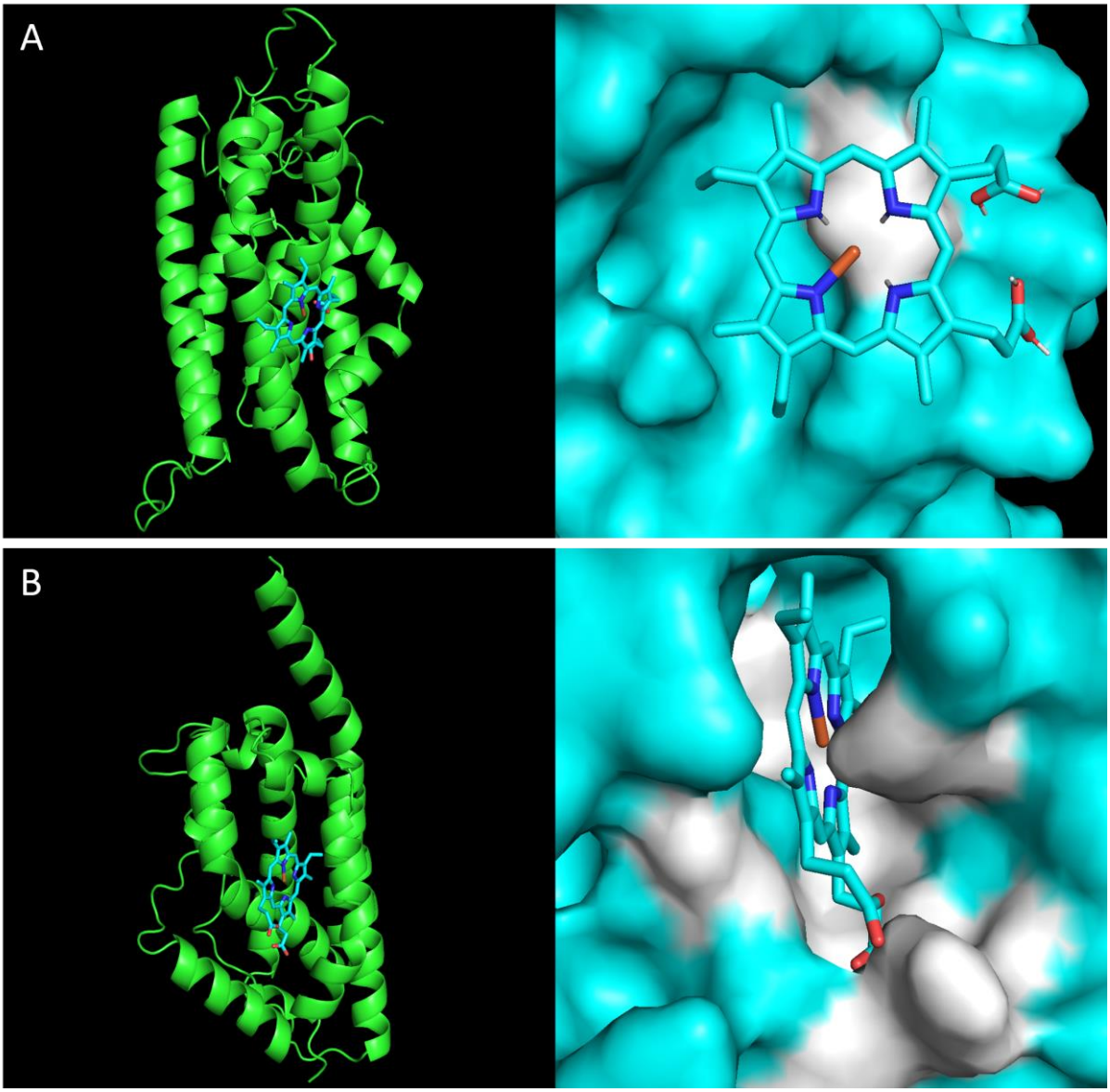

Figure 16: Modeling of HoxB and heme oxygenase (pdb-ID: 1WE1) with heme Both proteins with the modeled ligand shown in ribbon structure (left) and electrostatic surface potential (right). Residues showing a polar interaction with the ligand in the surface view are shown in white. (A) HoxB does not contain a heme-binding pocket. The ligand instead models flush against the surface of the protein, indicating that HoxB may not bind heme. (B) Heme oxygenase of *C. synechocystis* contains a heme-binding pocket including a histidine residue to stabilize the central Fe^{3+}

While the most highly ranked binding position was still calculated with a low binding affinity of -4.9 kcal per mol, the interaction with potentially relevant residues was examined (Figure 17A).

Notably, the difference in predicted affinities is likely due to the lack of alternative binding positions for the ligand within the predicted binding pocket. Multiple charged and polar residues likely involved in binding were found in both molecules, such as D44, Y47, E160 and Y163 in HoxB and D47, E140, Y143 and W168 in TenA_E of *A.*

thaliana. However, for TenA_E of *A. thaliana* the scoring function produced multiple potential binding positions near the binding site, indicating that binding in *A. thaliana* could be assisted by entropic effects. Overall, this indicates that HoxB may bind HMP as its ligand.

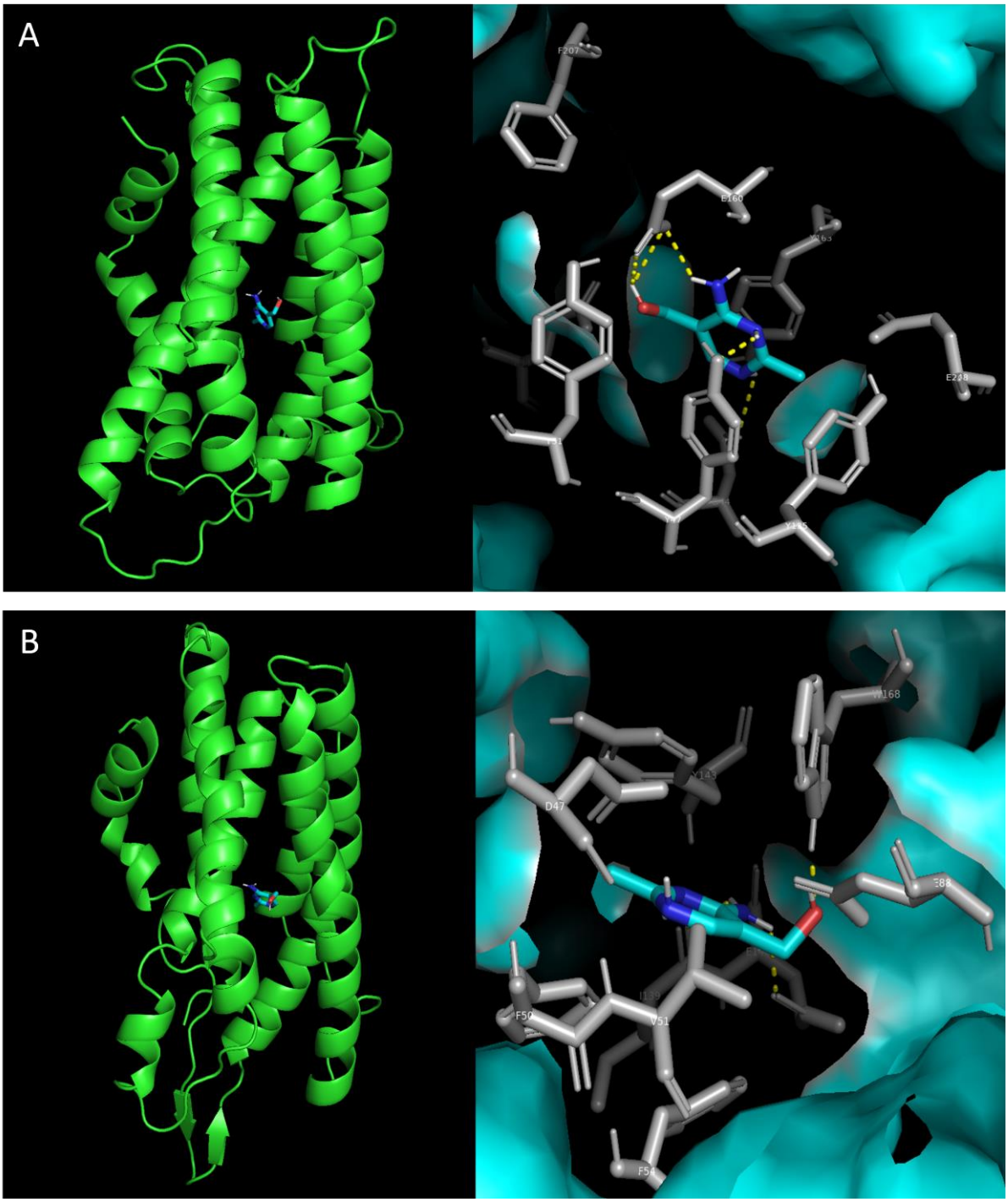

Figure 17: Modeling of HoxB and TenA_E (pdb-ID: 2Q4X) with HMP Both proteins with the modeled ligand shown in ribbon structure (left) and electrostatic surface potential (right). Residues showing a polar interaction with the ligand in the surface view are shown in white. (A) Binding of HMP occurs near the core of HoxB. The residues D44, Y47, E160 and Y163 are likely involved in ligand binding (B) Binding of HMP occurs in a similar position in TenA_E of *A. thaliana*. The residues D47, E140, Y143 and W168 associate with the ligand.

TenA_E of *P. furiosus* binds (4-amino-2-methylpyrimidin-5-yl)methyl dihydrogen phosphate (MP5) as its ligand (Benach et al., 2005). Modeling HoxB of *A. nidulans* with MP5 produced possible binding positions with calculated binding affinities ranging from -6.0 to -5.6 kcal per mol (Figure 18A).

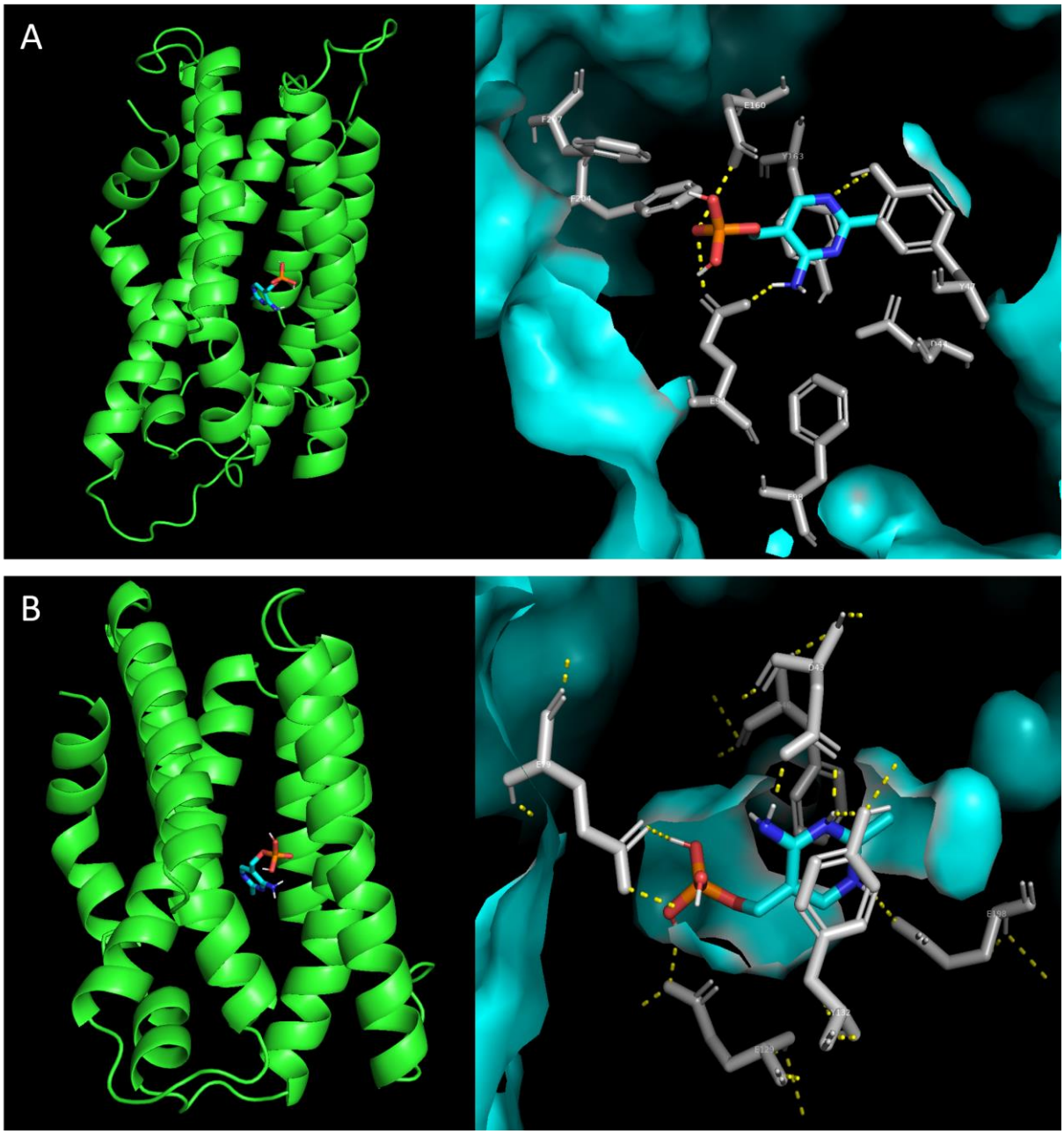

Figure 18: Modeling of HoxB and TenA_E (pdb-ID: 1RTW) with MP5 Both proteins with the modeled ligand shown in ribbon structure (left) and electrostatic surface potential (right). Residues showing a polar interaction with the ligand in the surface view are shown in white. (A) Binding of the ligand occurs near the core of HoxB. The residues D44, Y47, E94, F98, E160, F204 and F207 are likely involved in ligand binding. (B) Binding of MP5 occurs in a similar position in TenA_E of *P. furiosus*. The residues D43, F46, E79, E129, Y132 and E198 associate with the ligand.

In this model, the conserved residues E94 and E160 as well as Y47 coordinated the binding of the ligand through polar contacts while Y163 may coordinate with the aromatic component of MP5. Further conserved residues D44, F98, F204 and F207 located near the binding site may aid in moving the ligand towards the binding site. In comparison, TenA_E from *P. furiosus* (pdb-ID: 1RTW) was simulated to bind MP5 with -6.0 to -5.4 kcal per mol (Figure 18B). The predicted binding position for both models were similar although the orientation of the ligand molecule to nearby residues varies. In this model, the residues D43, F46, E79, E129, Y132 and E198 were in similar positions surrounding the ligand molecule. This indicates that HoxB may bind MP5 as a ligand.

In general, the sequences of HoxB from *A. nidulans* and *A. alternata* show very low conservation to TenA_E like proteins from *A. thaliana*, *B. subtilis* and *P. furiosus* (Figure 19). However, residues likely to be involved in ligand binding as identified above were conserved. Specifically, D44, E94, Y163 were found to be conserved. Further residues such as Y47 were conserved aromatic, being either tyrosine or phenylalanine, while F98 and E160 were found in all species except *B. subtilis*. There were several additional residues conserved that wereunlikely to be related to ligand binding, such as F23, E248, F251 and W252 which may therefore play a role in proper protein function. Furthermore, the residues T31 and S141 were conserved as either threonine or serine which are residues commonly phosphorylated to modulate protein function.

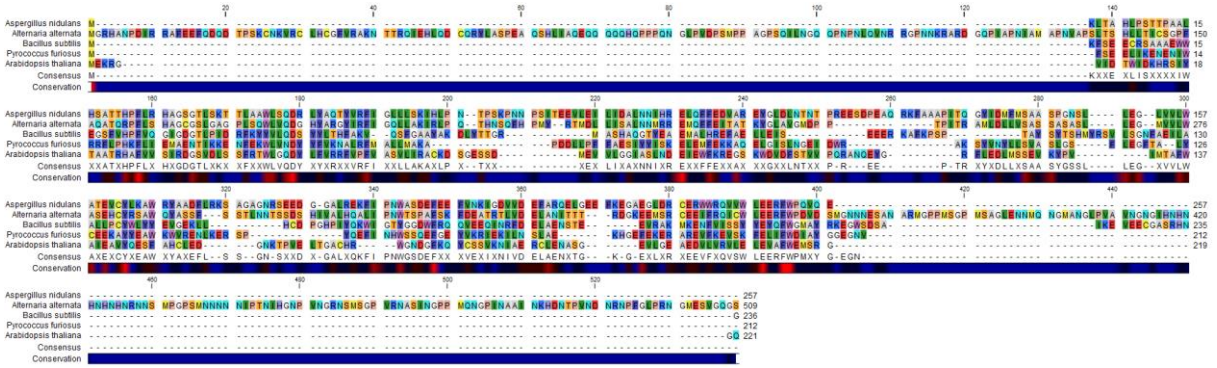

Figure 19: Ligand-associated residues are conserved between HoxB and TenA_E of distantly related organisms Alignment of HoxB of A. nidulans and TenA_E of *A. thaliana, B. subtilis* and *P. furiosus*. Core amino acids such as D44, E94, Y163 are conserved while additional residues are Y47, F98 and E160 are largely conserved. Additional conserved residues unlikely to be involved in ligand binding such as F23, E248, F251 and W252 were found and the two residues T31 and S141 are conserved as threonine or serine.

Finding these residues likely to be involved in ligand binding and protein function conserved in species as distantly related as the ones observed here further solidifies

the theory of HoxB in *A. nidulans* and *A. alternata* being proteins in the TenA_E family of proteins.

A phylogenetic analysis was performed to assess the prevalence of proteins similar to HoxB of *A. nidulans* in other, similar fungi. Protein sequences extracted from a pBlast search of the non-redundant protein sequences database against HoxB of *A. nidulans* were aligned and a circular phylogram was created (Figure 20).

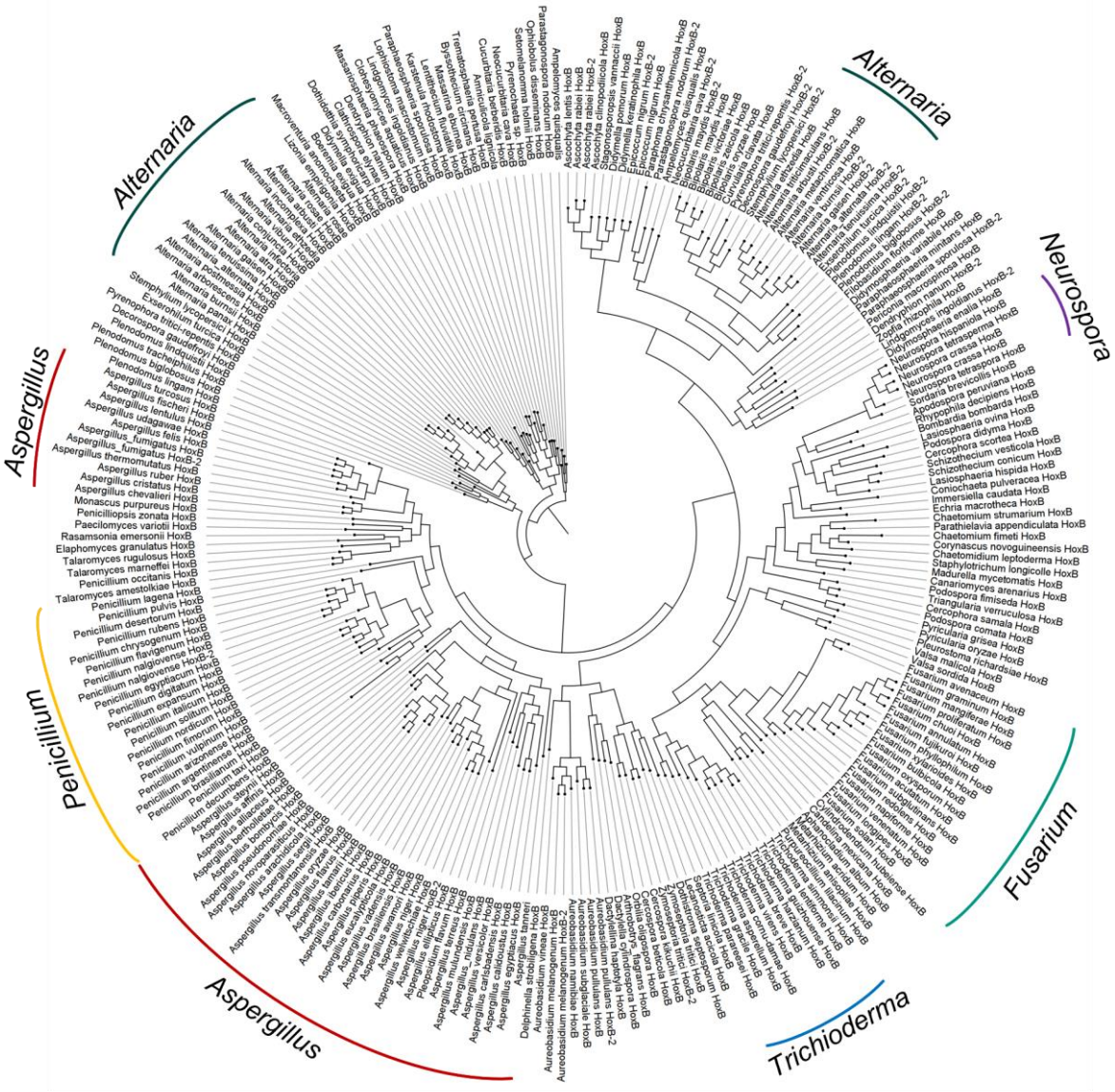

Figure 20: Distinct HoxB-like proteins are found in filamentous fungi Circular phylogram generated with CLC-workbench. HoxB-like proteins found in families of Aspergillus, Alternaria, Penicillium, Trichioderma, Fusarium, Neurospora and more were used. Some species like *A. fumigatus* and *A. alternata* host multiple HoxB-like proteins that present a further evolutionary distance to each other than to HoxB-like proteins in other organisms, indicating that HoxB-like proteins of the same organism may be functionally distinct.

The resulting tree indicates a large variety of HoxB-like proteins in different filamentous fungi. Some species, such as *A. alternata*, contain multiple HoxB-like proteins.

Furthermore, HoxB-like proteins of members of the same genus may present a larger evolutionary distance between each other than to proteins of members of different genera. Exemplary, *Aspergillus fumigatus* carries two HoxB-like proteins while *A. nidulans* only carries one. Both homologues of *A. fumigatus* presented a larger evolutionary distance to HoxB of *A. nidulans* than the HoxB of many *Penicillium* species, although the differences were small. Similarly, many *Alternaria* species contained two variations of HoxB-like proteins which present a larger evolutionary distance to each other than to HoxB-like proteins of most other genera within the phylogram.

This is an indication that the composition and potentially the function of HoxB-like proteins may vary, despite being classified as members of the same superfamilies. Consequently, experimental approaches were chosen to determine the function of HoxB of *A. nidulans*.

2.3 HoxB contributes to red light sensing in *A. nidulans*

Descriptions of proteins in the TenA_E family in literature record a set of common characteristics. HoxB of *A. alternata* is known to be necessary for red light perception. Furthermore, the GFP-fusion of the protein localizes to the mitochondria when expressed in *A. nidulans* and regulates oxidative stress resistance to hydrogen peroxide, menadione and tert-Butyl hydroperoxide (Streng et al., 2021). Furthermore, it was shown that HoxB forms homomultimers and crystal structures of TenA_E-like proteins show that the protein may form homotetrameric structures hypothesized to assist in resistance against proteases (Streng et al., 2021; Benach et al., 2005; Begum et al., 2013). An assessment of the effects of HoxB was performed using a knockout strain (SRFS16) verified via Southern blot (Figure 21A). Red light perception was evaluated by illuminating the strains with red light at 10 µmol photons per square meter and second and subsequent qPCR testing the red-light marker genes *ccgA*, *conJ* and *ccgB* (Ruger-Herreros et al., 2011; Yu et al., 2019).

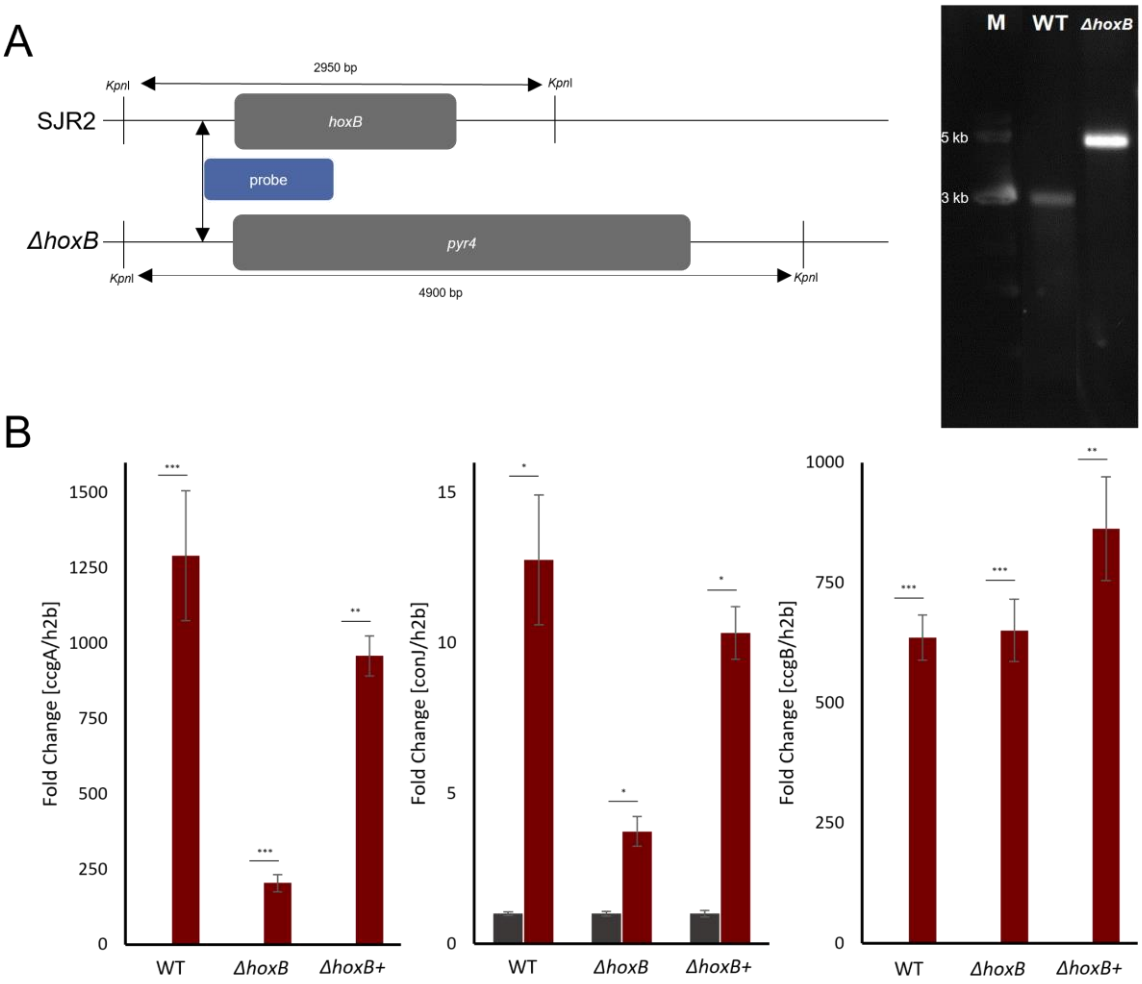

Figure 21: The *hoxB*-knockout is partially blind to red light (A) Generation of the *hoxB*-knockout was performed in the strain SJR2 by replacing the open reading frame with a *pyr4* deletion cassette. A Southern Blot using a probe binding the upstream sequence between *Kpn*I restriction sites was used to confirm the ~3000 base and ~5000 base segments in wildtype and knockout respectively. (B) Fold changes of red-light response genes *ccgA*, *conJ* and *ccgB*. Fold changes of *ccgA* and *conJ* increase above baseline (grey) when induced with red light (red), but do not reach wildtype levels. Fold change of *ccgB* is unaffected by *hoxB*. The phenotype is rescued by re-complementation. * - p<0.05; ** - p<0.01; *** - p<0.001

All three genes are, among other stimuli, regulated in a red-light/phytochrome-dependent manner through the HOG pathway in *A. nidulans* (Yu et al., 2016; Yu et al., 2019, Hedke et al., 2015). Red-light sensing remained functional in the knockout strain but was severely impaired (Figure 21B). Specifically, the expression of *ccgA* and *conJ* appears less responsive to red light in the knockout strain which is reversible through re-complementation of the *hoxB* gene. Interestingly, the expression of *ccgB* is unaffected in the knockout strain, indicating that the effect of HoxB on red light sensing is nuanced. Similarly, the localization of HoxB in *A. nidulans* differs somewhat from the localization described previously for HoxB of *A. alternata*. HoxB of *A. alternata* expressed heterologously in *A. nidulans* was found to localize to the mitochondria (Streng et al.,

2021). The localization of the GFP-fusion including the *A. nidulans* protein is found ubiquitously throughout the hyphae in an overexpression approach using the inducible *alcA*-promoter (Figure 22). The signal does not appear to spare any intracellular compartments including the nucleus as shown by the fusion of mCherry with the nuclear localization sequence of StuA. Expressing the GFP-fusion of HoxB using the native promoter shows similar results (Figure 22). However, in this fusion, a varying localization of the GFP signal was observed. In most cases, nuclei would still exhibit a signal which was non- or barely differentiable from the surrounding signal. However, in some cases, nuclei would exhibit a dim signal which was clearly distinct from their surrounding. This was true for a fraction of hyphae within an individual culture whenever it was observed. A search for specific conditions to replicate this change in localization without further genetic modification remained unsuccessful. This raises the question why an enzyme involved in thiamine scavenging would conditionally localize to the nucleus among other intracellular compartments normally not involved with metabolic processes.

Further similarities to other descriptions of HoxB and TenA_E-like proteins were found by determining it's multimerization state. A bimolecular fluorescence complementation assay using split YFP was used to determine whether HoxB shows multimerization *in vivo* (Figure 23A) while co-immunoprecipitation (Figure 23B) and size exclusion chromatography (Figure 24) were chosen as *in vitro* methods. Previous descriptions of HoxB found the protein from *A. alternata* to form homomultimers localizing at the mitochondria when expressed in *A. nidulans* (Streng et al., 2021). While the multimerization of *A. nidulans* HoxB was shown to be consistent with results obtained using HoxB of *A. alternata*, the localization of this interaction was different again. As in case of the GFP-signal, the YFP-signal is found ubiquitously throughout the cell, suggesting that the multimer formed may be the naturally occurring state of the protein. For co-immunoprecipitation, three strains expressing one copy of a GFP-fusion and HA-fusion as well as both copies were created. These fusions present with the molecular mass of approximately 56 kDa and 29 kDa respectively. The purification was performed using anti-HA antibodies. The corresponding western blots indicate a multimeric interaction of HoxB monomers *in vitro* as protein running at a height between 50 and 60 kDa was found in the GFP+HA section of the immunoprecipitation when developing with anti-GFP antibodies.

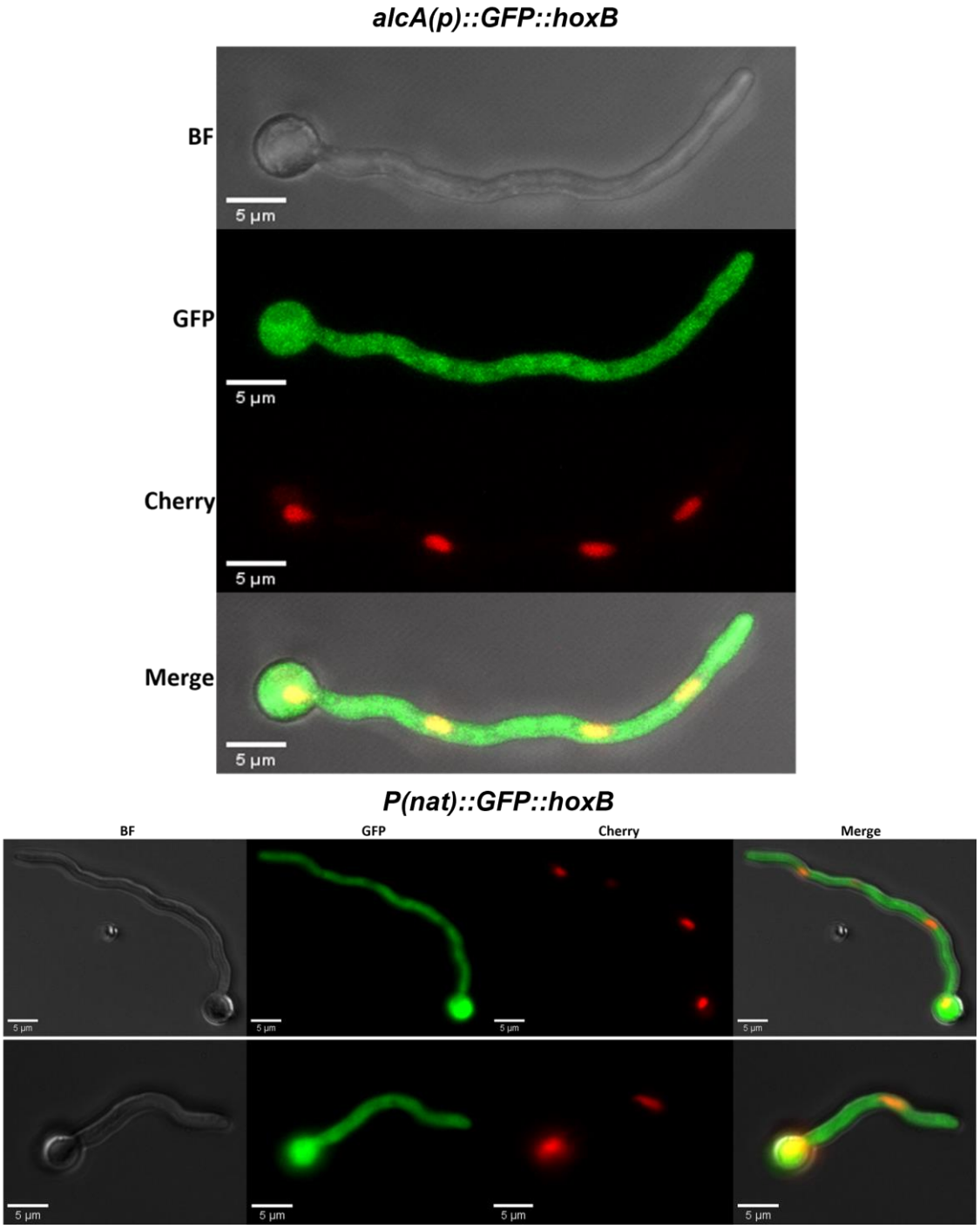

Figure 22: HoxB localizes in the cytoplasm and nuclei Overexpression of GFP-*hoxB* using the alcA-promoter showed an evenly distributed GFP-signal throughout the hyphae. Expression of GFP-*hoxB* under control of its native promoter (P(nat)) showed either an evenly distributed GFP-signal or a comparably dim nuclear GFP-signal. Nuclei were marked with mCherry fused to the nuclear localization sequence of StuA. BF: Brightfield

Within this same blot, similar bands are found at the same height in samples taken as the input control. Since HA-antibodies were used for purification, no protein was found in the immunoprecipitated sample containing only GFP-HoxB. Similarly, no bands are found in samples containing only HA-HoxB indicating specificity of the GFP-antibodies used during detection. On the blot developed with anti-GFP antibodies, some additional

bands are found at the wrong heights of approximately 30 and 15 kDa each. These are likely to be degradation products of GFP-HoxB. The blot developed using anti-HA antibodies complements the blot described above by showing bands at a height between 25 and 30 kDa which is consistent with the size of HA-HoxB. These bands are exclusively found in the 4 samples of input control and immunoprecipitation containing HA-HoxB.

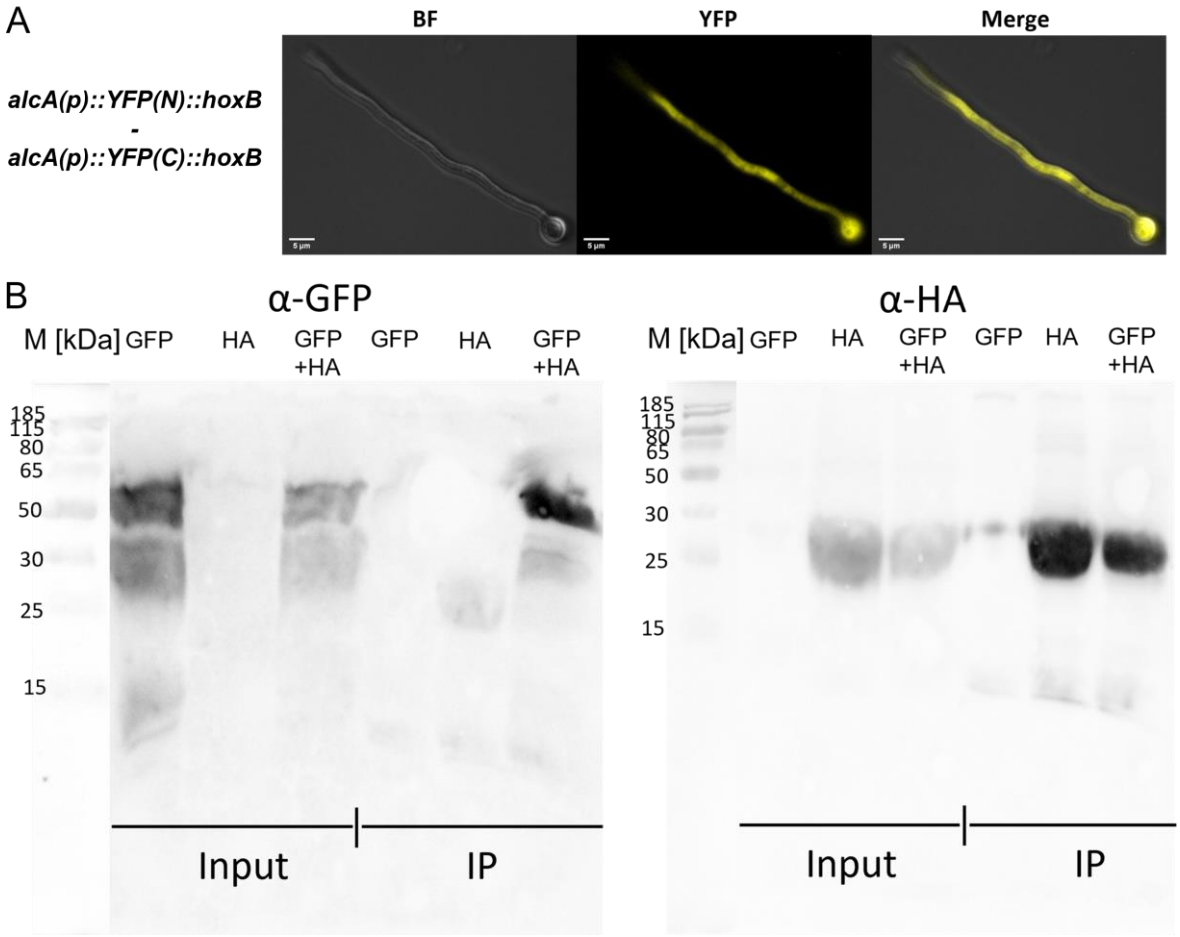

Figure 23: HoxB forms homo-multimers (A) Bimolecular fluorescence recovery assay using yellow fluorescent protein (Split-YFP) indicates multimerization of HoxB *in vivo*. BF: Brightfield (B) Western blot of co-immunoprecipitation (IP) of GFP-HoxB and HA-HoxB. Three Input samples of protein extract and IP samples after purification of GFP-HoxB, HA-HoxB and GFP-HoxB+HA-HoxB were loaded respectively. Immunoprecipitation was performed using anti-HA antibodies. The blot developed with anti-GFP antibodies shows multimerization of HoxB through the presence of a band at approximately 56 kDa corresponding to GFP-HoxB. The blot developed with anti-HA antibodies functions as a loading control of HA-HoxB (~29 kDa).

In this blot, some weak additional bands are found at a height below 15 kDa and at a height of 30 kDa in the GFP-sample of the immunoprecipitation. The band at 30 kDa likely constitutes spillage of a small amount of sample from an overloaded neighbouring well while the ones below 15 kDa are likely due to the HA-antibodies used for purification

originating from mice and the secondary antibody used for detection being anti-mouse. Consequently, some antibody remnants could be detected at a low molecular mass.

Further clarification of the multimerization state of HoxB was obtained via analytical size exclusion chromatography (SEC). The his-tagged protein used was expressed in and purified from *E. coli*. Including the tag, the HoxB protein is calculated to be just under 30 kDa in mass (29.96 kDa). The graph showing absorption in dependence of elution volume shows one clear peak centered at 12.83 mL if just HoxB is loaded (Figure 24). This volume corresponds to a molecular mass of 122.14 kDa which is slightly larger than the calculated molecular mass of the HoxB-tetramer of 119.84 kDa. The difference between these masses is approximately 1.9%. Proteins commonly appear slightly larger than their calculated molecular masses in size exclusion chromatography (Hong et al., 2012), indicating that the protein occurs in tetrameric form naturally.

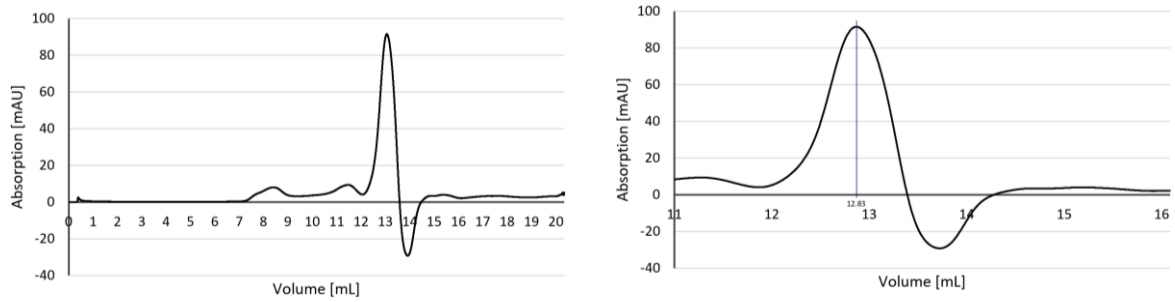

Figure 24: HoxB forms Homo-tetramers His-tagged HoxB protein was extracted from E. coli and used for size exclusion chromatography. The major peak observed at 12.83 mL corresponds to 122.14 kDa. This molecular mass is 1.9% larger than the predicted mass of the HoxB-tetramer.

One oddity of the analytical SEC is the presence of a dip of the absorption signal to approximately -30 mAU which tails the peak of the HoxB-tetramer. This downwards peak was present in repeated runs with different batches of protein. Considering the uniqueness and location of the peak at approximately 13.7 mL it is likely that this occurrence is due to an analyte presenting a lower absorption than the mobile phase such as a buffer component or aggregated protein. In any case, it should not influence the peak of the tetramer since it elutes after it.

Finding only one peak in size exclusion chromatography without introduction of any notable stimuli indicates that the tetrameric state of HoxB may be its base state under native conditions as well. A model for the HoxB-tetramer was created using AlphaFold (Figure 25) to determine where the relevant conserved residues described in chapter 2.2 are located within the tetramer. The HoxB-tetramer is expected to be nearly

symmetrical in composition with each monomer being mirrored vertically or horizontally compared to its neighbour. The predicted ligand binding site as well as both termini of the protein – particularly the C-termini – are exposed in this model.

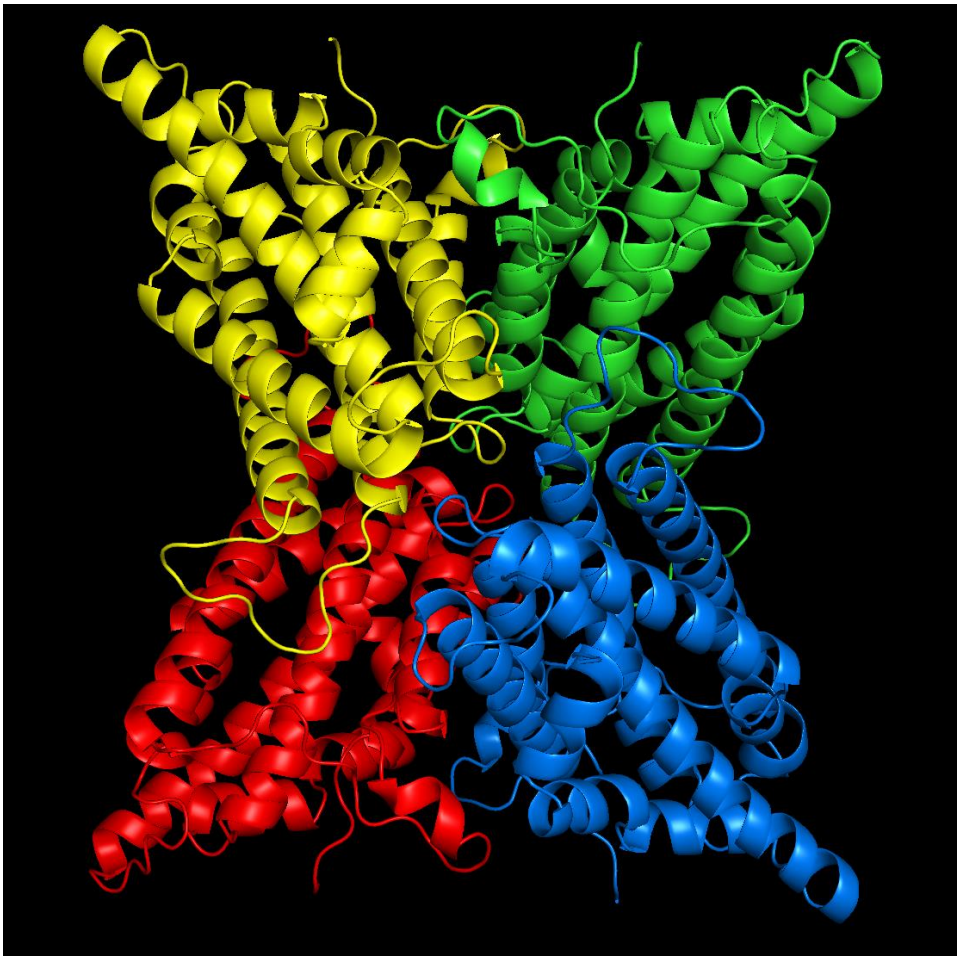

Figure 25: Model of tetrameric HoxB produced via AlphaFold Individual monomers are coloured in different colours each. The monomers in opposite corners are mirrored to each other and expose their C-termini. The ligand binding site appears accessible in the model.

The conserved residues observed in chapter 2.2 were color-coded based on their relevance for their function within the tetramer (Figure 26). Residues likely involved in stabilization of the tetramer were colored in red, those found in the ligand-binding site were colored blue and other residues with other not immediately discernible function were colored in yellow. Distances of 5 Ångstrom between residues of neighbouring proteins is generally considered as a good cutoff for protein-protein interactions (Viloria et al., 2017) and was therefore chosen as a cutoff for determining residues likely to be involved in stabilizing the tetramer. Therefore, residues of HoxB found highly conserved in other filamentous fungi found within 5 Ångstrom of another monomer were considered candidates for stabilizing the HoxB tetramer. Among them are R45,

L59, L88, D137 and R242. Residues likely to be responsible for ligand binding were D44, Y47, E94, F98 Y163 and E160.

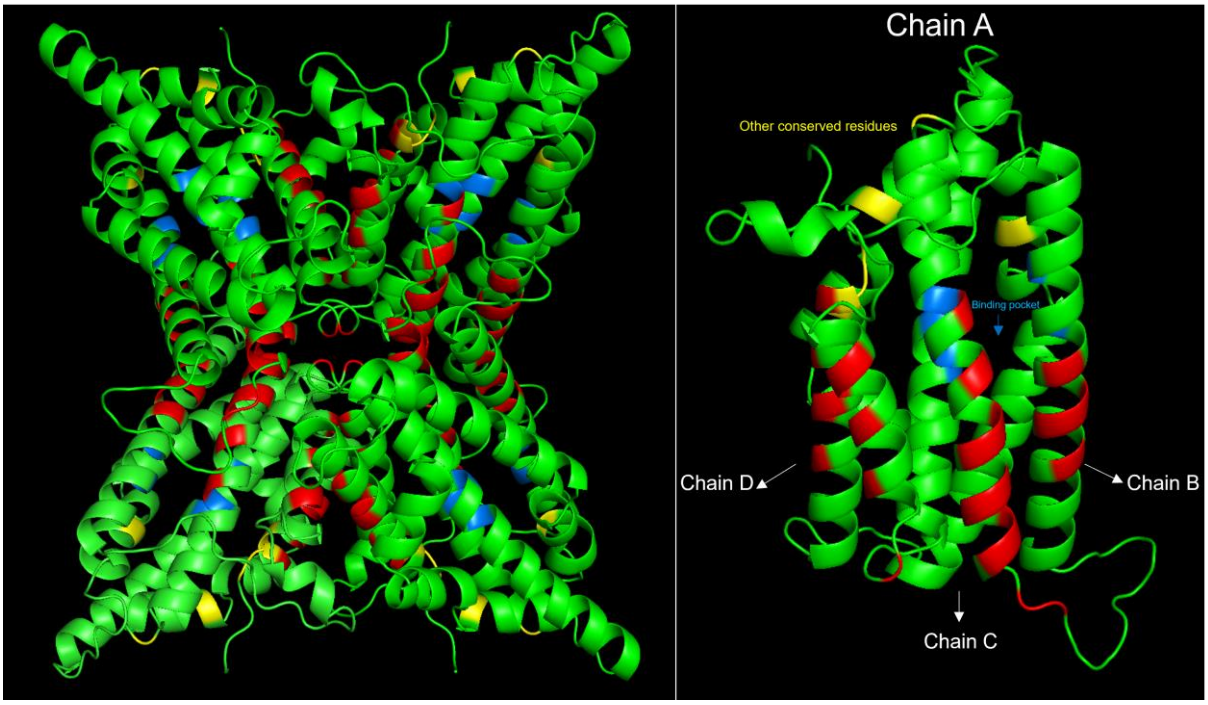

Figure 26: Colour coding of relevant residues within the HoxB-tetramer Residues considered relevant for tetramer stabilization (R45, L59, L88, D137, R242) were coloured in red. Residues likely responsible for ligand binding (D44, Y47, E94, F98, Y163, E160) were coloured in blue. Additional conserved residues with undiscernible function (F23, T31, S141, F194, E248, F251, W252) were coloured in yellow. Relative position of other HoxB monomers are displayed in white.

Additional residues found in other TenA_E proteins which were exposed but did not have a potential discernible function were F23, T31, S141, F194, E248, F251 and W252. These might facilitate further protein-protein interactions or, in case of T31 and S141, be the target of posttranscriptional modifications to modulate protein activity. Residues found to be highly conserved in filamentous fungi (Figure 14) that were not sufficiently close to neighbouring monomers, likely functional in ligand binding or conserved in other, more distantly related TenA_E proteins (Figure 19) were considered relevant for folding of the monomer and not colored.

Considering the intricate effects that HoxB appears to have on light stress perception in *A. nidulans*, further experimental approaches were chosen to elucidate the potential function and mode of action.

2.4 HoxB interacts with *Aspergillus nidulans*' light receptors

As shown in chapter 2.3, HoxB has a considerable effect on red light sensing in *A. nidulans*. Consequently, it was determined whether the protein interacts with *A. nidulans* light receptors using *in vivo* and *in vitro* methods. Considering that phytochrome functions as the red-light receptor in *A. nidulans*, a direct or indirect interaction with phytochrome was likely and a bimolecular fluorescence complementation assay in form of Split-YFP was performed. An interaction of HoxB with HoxB of *A. alternata* was shown previously (Streng et al., 2021). A total of three fragments of phytochrome were tested for an interaction with HoxB. Only the combination of the phytochrome photosensory domain showed a positive result (Figure 27) while no fluorescence signal was observed with the full-length protein and the histidine kinase domain.

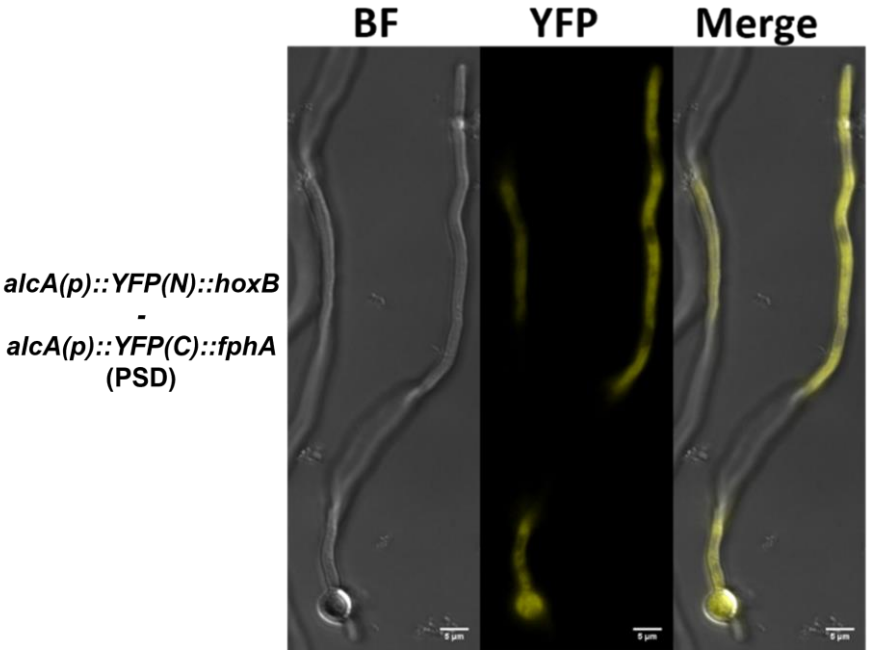

Figure 27: Interaction between HoxB and the photosensory domain (PSD) of FphA Bimolecular fluorescence recovery assay using yellow fluorescence protein (Split-YFP) of HoxB with the photosensory domain of phytochrome expressed under control of the alcA-promoter. Fluorescence indicates an interaction in some parts of the hyphae. An interaction between full length FphA and HoxB could not be observed in the same fashion. BF: Brightfield

The signal observed displayed differences in intensity within the hyphae observed at regular intervals. The dips in intensity may be where nuclei are located within the hyphae, indicating an interaction limited to the cytoplasm, though this was not investigated further due to an inconsistency of results. This may indicate that while phytochrome does not interact with phytochrome in *A. nidulans* but it may also indicate

an interaction between HoxB and FphA under specific circumstances such as phytochrome being in its Pr- or Pfr-state or HoxB being modified posttranscriptionally.

Other light receptors that was investigated for a potential interaction with HoxB were *A. nidulans* blue light receptors. These are the white-collar system LreA/LreB and the cryptochrome photolyase CryA (Bayram et al., 2010). These blue light sensors display a close relationship with phytochrome-dependent red-light sensing through either directly interacting with phytochrome or requiring phytochrome to regulate their blue-light response (Purschwitz et al., 2008; Yu et al., 2021). No corresponding fluorescence signal could be detected in strains expressing a combination of Split-YFP fusions including LreA and HoxB. However, fusions testing the interaction between HoxB and CryA showed signals localizing to the nuclei (Figure 28). Notably, this interaction is indicated in the nucleus underlining the potential transcriptional effect of HoxB mentioned previously.

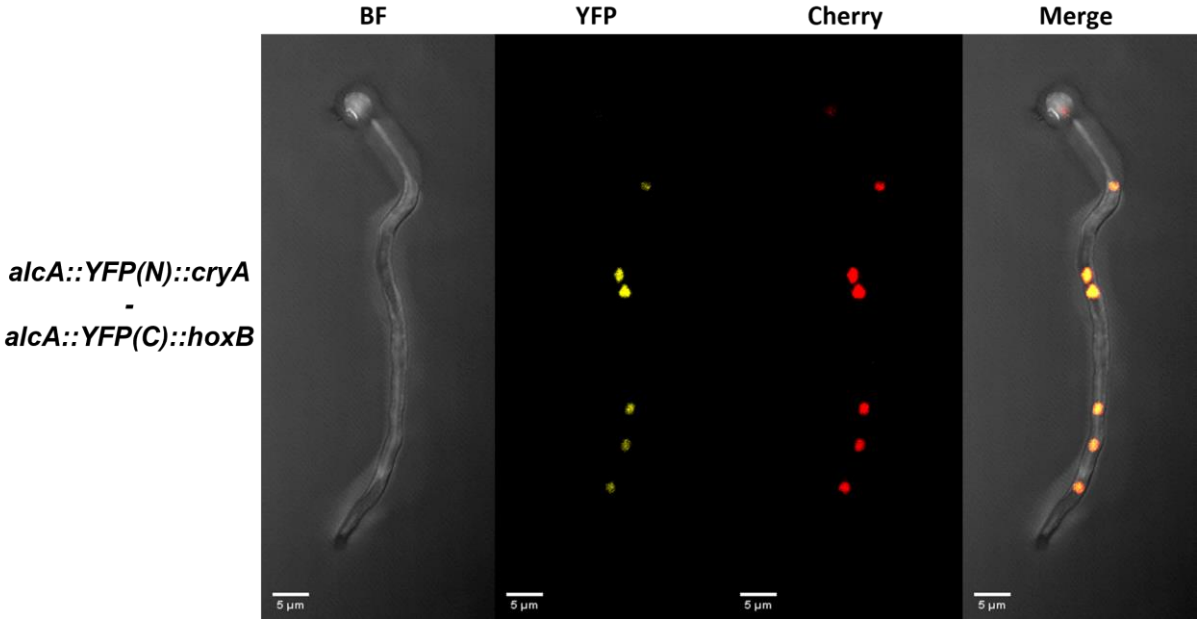

Figure 28: HoxB interacts with cryptochrome in nuclei Bimolecular fluorescence recovery assay using yellow fluorescence protein (Split-YFP) of HoxB with CryA expressed under control of the alcA-promoter. Nuclei were marked using mCherry fused to the nuclear localization sequence of StuA. YFP-signals colocalize with nuclear markings, indicating the interaction to be exclusive to nuclei. BF: Brightfield

Multiple *in vitro* approaches were chosen to validate this interaction. Firstly, a co-immunoprecipitation approach using GFP-HoxB and HA-CryA was performed (Figure 29). These fusions present with molecular masses of approximately 56 kDa and 66 kDa respectively. Three strains were generated expressing the individual fusions and both fusions at once. The purification was performed with HA-antibodies. The

corresponding western blots do not confirm an interaction as the bands running at the corresponding heights are not found in the GFP-blot.

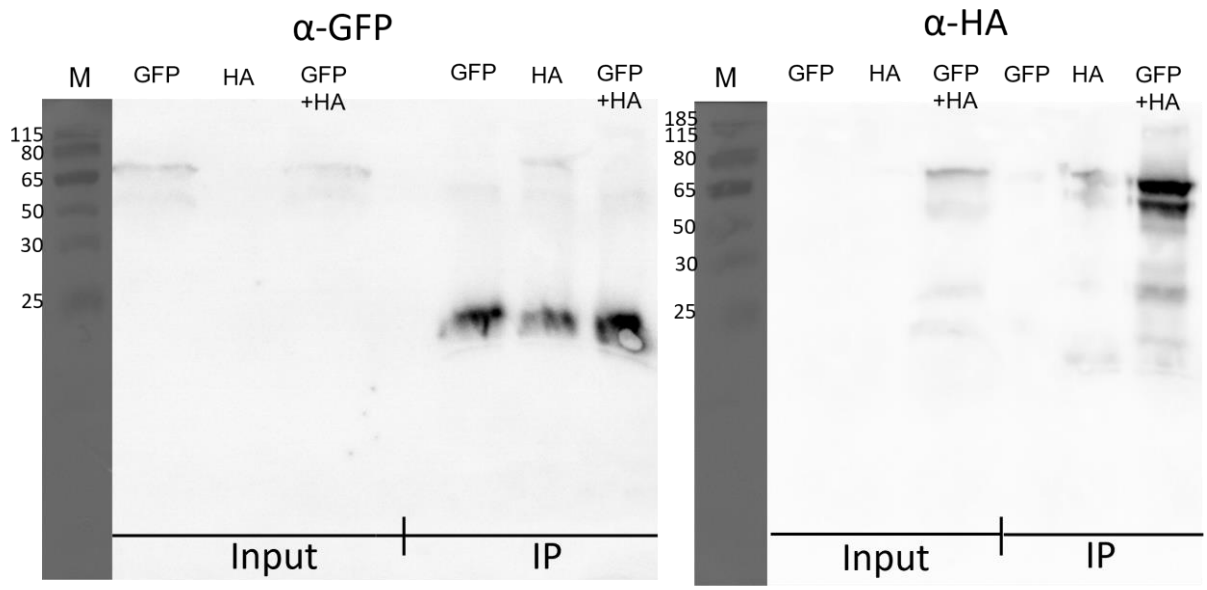

Figure 29: Co-Immunoprecipitation (IP) of HoxB and CryA Western blot of co-immunoprecipitation (IP) of GFP-HoxB and HA-CryA. Three Input samples of protein extract and IP samples after purification of GFP-HoxB, HA-CryA and GFP-HoxB+HA-CryA were loaded respectively. Immunoprecipitation was performed using anti-HA antibodies. The blot developed with anti-GFP antibodies did not show the presence of HoxB at approximately 56 kDa corresponding to GFP-HoxB. The blot developed with anti-HA antibodies functions as a loading control of HA-CryA (~66 kDa).

The HA-blot shows 2 major bands at heights corresponding to approximately 65 kDa in size for samples of strains expressing HA-CryA and both fusions simultaneously, indicating that the HA-CryA is expressed in purified properly. However, detection of the GFP-HoxB fusion at 56 kDa largely failed. Some miniscule signals appear at heights corresponding to between 50 kDa and 65 kDa in input and immunoprecipitation samples but they are overshadowed by stronger signals at incorrect heights. Three strong signals appear at a height corresponding to approximately 25 kDa. However, these are unlikely to be free GFP from degraded samples as the signal also appears in the sample containing only HA-CryA. They are more likely to be a part of the antibody used for purification as this antibody originates from mouse and the secondary antibody used for developing the blot was designed to detect the primary antibody which also originates from mouse. Considering the possibility that the interaction between HoxB and CryA may be transient or otherwise not strong enough to be detected using immunoprecipitation, an approach using biolayer interferometry (BLItz) was chosen (Figure 30).

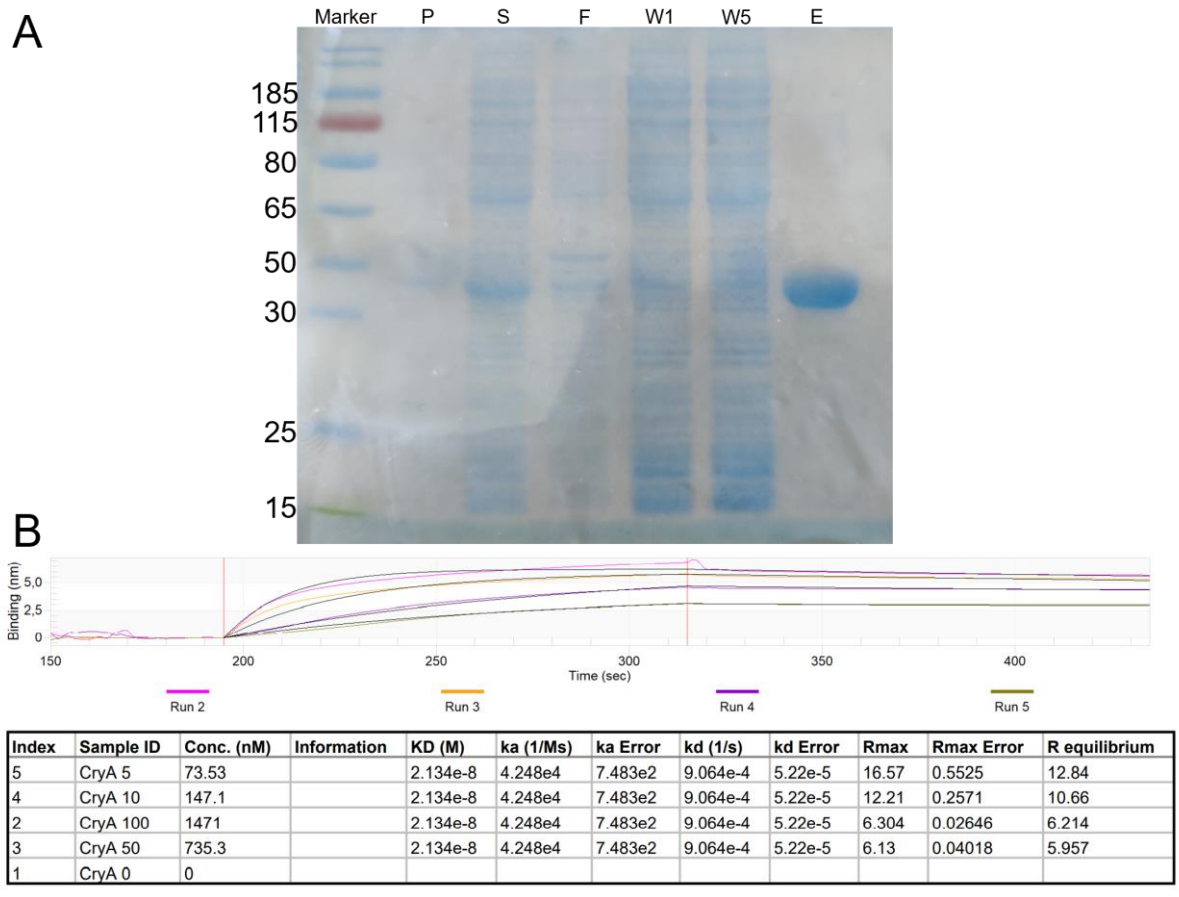

Index	Sample ID	Conc. (nM)	Information	KD (M)	ka (1/Ms)	ka Error	kd (1/s)	kd Error	Rmax	Rmax Error	R equilibrium
5	CryA 5	73.53		2.134e-8	4.248e4	7.483e2	9.064e-4	5.22e-5	16.57	0.5525	12.84
4	CryA 10	147.1		2.134e-8	4.248e4	7.483e2	9.064e-4	5.22e-5	12.21	0.2571	10.66
2	CryA 100	1471		2.134e-8	4.248e4	7.483e2	9.064e-4	5.22e-5	6.304	0.02646	6.214
3	CryA 50	735.3		2.134e-8	4.248e4	7.483e2	9.064e-4	5.22e-5	6.13	0.04018	5.957
1	CryA 0	0									

Figure 30: Interaction of HoxB and CryA in biolayer interferometry (A) Blot of purification of his-tagged HoxB from *E. coli*. P: Pellet; S: Supernatant; F: Flowthrough; W1: Washing Step 1; W5: Washing Step 5; E: Eluate. The eluate band at approximately 30 kDa shows successful purification. (B) Biolayer Interferometry of HoxB and CryA. Purified HoxB was fixed to the solid phase and presented with varying concentrations (0 to 100 µM) of CryA in the liquid phase. Increase of the curve indicates and interaction between HoxB and CryA. CryA protein was provided by Alexander Landmark.

A 6xhis-tagged construct of HoxB (approximately 30 kDa in size) was expressed from *E.coli* (Figure 30A) while the CryA protein used for analysis was purified and provided by Alexander Landmark. BLItz analyses were performed using solid-phase bound HoxB protein at saturation which was presented with CryA in concentrations between 0 to 100 µM (Figure 30B). The three sections shown are measuring against the blank in section 1, binding of CryA in section 2 and the detachment phase in section 3. The data shows an increase in signal upon addition of various concentrations of CryA, indicating an interaction between the proteins. Signal strength increases up to the concentration of 100 µM where artifacts may manifest as irregularities in the signal. Interestingly, the detachment phase does not show a fast decrease in signal, indicating that the interaction may be somewhat strong which is contrary to previous results. However, the actual affinity of the interaction were not calculated considering the effect

that tetramerization of HoxB in vitro may have on its affinity to CryA. These potential dynamics were sought out via size exclusion chromatography using the same purified proteins. Attempting to determinately show the interaction of HoxB and CryA and to determine whether the HoxB tetramer or another mono- or multimeric form partakes in the interaction using size exclusion chromatography (Figure 31) was unsuccessful. The respective curve largely resembles the size exclusion chromatography of just HoxB (Figure 24, chapter 2.3) described previously. The tetramer peak at approximately 12.7 mL elution volume is found while no peak corresponding to CryA was observed. While there is a small peak present at approximately 14.8 mL elution volume, this corresponds to 49 kDa and therefore does not match either of the proteins. It is likely that the negative absorption presenting between 13 mL and 14 mL elution volume is covering the peak corresponding to CryA.

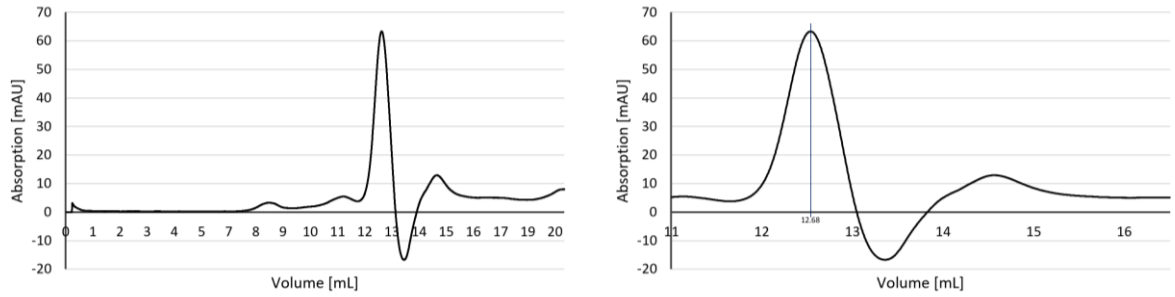

Figure 31: Size exclusion chromatography of HoxB and CryA Purified HoxB and CryA protein were loaded for size exclusion chromatography. The major peak at 12.68 mL elution is equivalent to the peak observed for the HoxB tetramer (Figure 24). A peak corresponding to CryA was not observed. CryA protein was provided by Alexander Landmark.

A modeling of a potential heterodimer of HoxB and CryA using AlphaFold confirms that the interaction between the two proteins may require a dissolution of the HoxB tetrameric structure (Figure 32). In particular, the residues 215 to 235 of HoxB are in proximity to CryA in this model. While this region is largely unconserved in other filamentous fungi or other TenA_E proteins, some conserved residues such as D215 and K228 may be relevant for this interaction. In the tetrameric model of HoxB, these residues are covered by HoxB monomers mirroring each other, negating any potential interaction with CryA. Lastly, it was tested whether the *in vivo* interaction between HoxB and CryA was dependent on red light sensing via phytochrome.

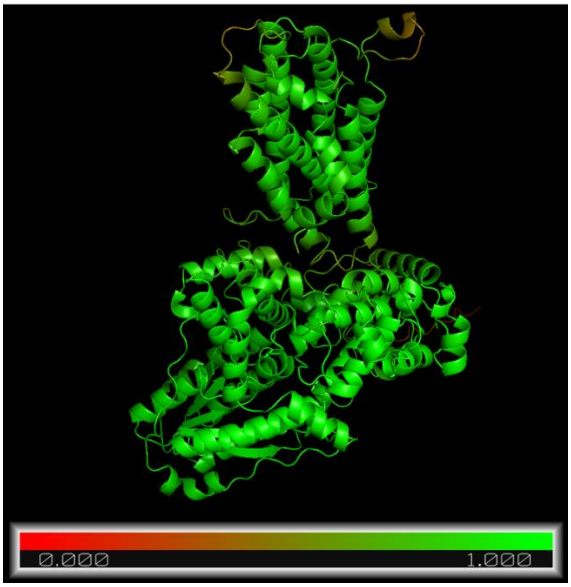

Figure 32: Model of the HoxB-CryA dimer AlphaFold model of a potential HoxB-CryA dimer. Interaction between HoxB and CryA may require resolution of the HoxB tetramer. The residues 215 to 235 of HoxB which may be used for tetramerization are near CryA. Particularly, D215 and K228 may be involved as they are conserved in other filamentous fungi. Per residue certainties within the model are high (green). Only some residues not involved in protein interaction show a low certainty (red).

In *A. nidulans*, cryptochrome expression is partially dependent on phytochrome and subsequently contributes to further phytochrome signaling (Yu et al., 2021). Therefore, the interaction was tested in an *fphA*-deletion background (Figure 33).

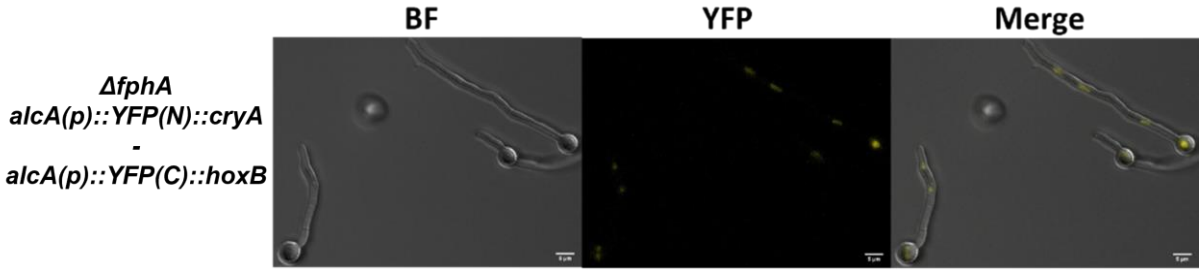

Figure 33: HoxB interacts with CryA in nuclei in absence of FphA Bimolecular fluorescence recovery assay using yellow fluorescence protein (Split-YFP) of HoxB with CryA expressed under control of the alcA-promoter. Expression was performed in an FphA-deletion background. Signal is observed in regular spaced intervals likely to be nuclei as previously observed (Figure 28) BF: Brightfield

Indeed, the interaction was also present in the absence of phytochrome. The signal strength of this interaction appeared to be weaker than observed in the wildtype background but always present. Further interest was directed towards a potential involvement of the developmental regulator VeA.

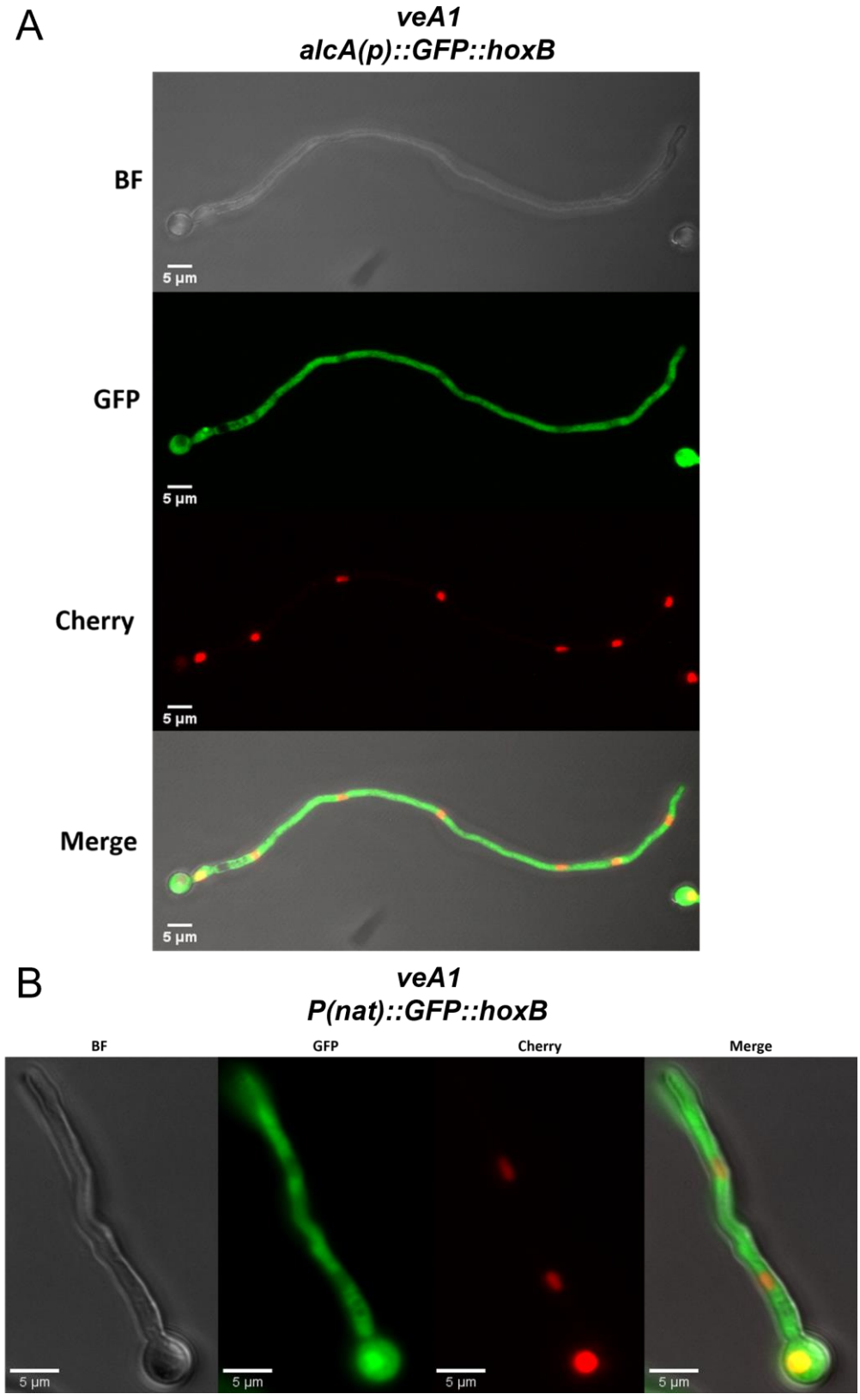

Figure 34: Localization of HoxB depends on VeA (A) Overexpression of GFP-*hoxB* using the alcA-promoter in a *veA1* background. Unlike in the wildtype background (Figure 22), a reduced GFP-signal is observed in nuclei in the overexpression of HoxB. (B) Expression of GFP-*hoxB* under control of its native promoter (P(nat)) in the same background always showed a comparably dim nuclear GFP-signal in a *veA1* background. Nuclei were marked with mCherry fused to the nuclear localization sequence of StuA. BF: Brightfield

It was shown previously that the regulation of the *ccgA* gene in response to light is dependent on VeA in tandem with phytochrome and the white-collar complex (Hedtke et al., 2015). Consequently, it is feasible that the reduced capacity for red light sensing in Δ*hoxB* is not facilitated due to an interaction with phytochrome or white-collar, but through direct influence on VeA. Henceforth, the localization of HoxB was observed in a *veA1* background. This point mutation in the start codon of *veA* leads to a partial deletion of the protein N-terminally and prevents VeA from entering the nucleus (Kim et al., 2002). The GFP-signal observed for both the overexpression model and expression under the native promoter showed a distinct lack of signal in areas of marked nuclei (Figure 34). Nuclei were marked using the nuclear localization sequence of stuA tagged to mCherry. This contrasts the native promoter in wildtype where the nuclear omission of the signal was only observed sometimes in a fraction of hyphae if HoxB was expressed under its native promoter (Figure 22). Considering that the *veA1* mutation prevents VeA from entering the nucleus, this may indicate that the localization of HoxB to the nucleus depends on the presence of VeA in the nucleus. This may be facilitated through a direct interaction, which could shuttle HoxB into the nucleus despite its lack of a nuclear localization sequence or VeA may affect transcription of a regulatory system which may lead to HoxB's localization to the nucleus. Consequently, a potential direct interaction between HoxB and VeA was investigated using a Split-YFP approach as previously described. However, no direct interaction between HoxB and VeA could be shown in this way. Modeling a potential interaction between HoxB and VeA using AlphaFold was similarly unsuccessful (Figure 35A). Although the pDockQ-value determined for this interaction is 0.233 and therefore barely passes the threshold value of 0.23 for a likely interaction, the corresponding models show a low certainty for large sections of the VeA protein. This illustrates the high disordered nature of the VeA protein, preventing unambiguous determination of (Figure 35B). Similar to the modeled interaction with CryA, the potential interaction between HoxB and VeA occurs within a similar surface region of HoxB including the residues 210 to 225, indicating that a dissolution of the HoxB tetramer would be necessary to facilitate the interaction with VeA.

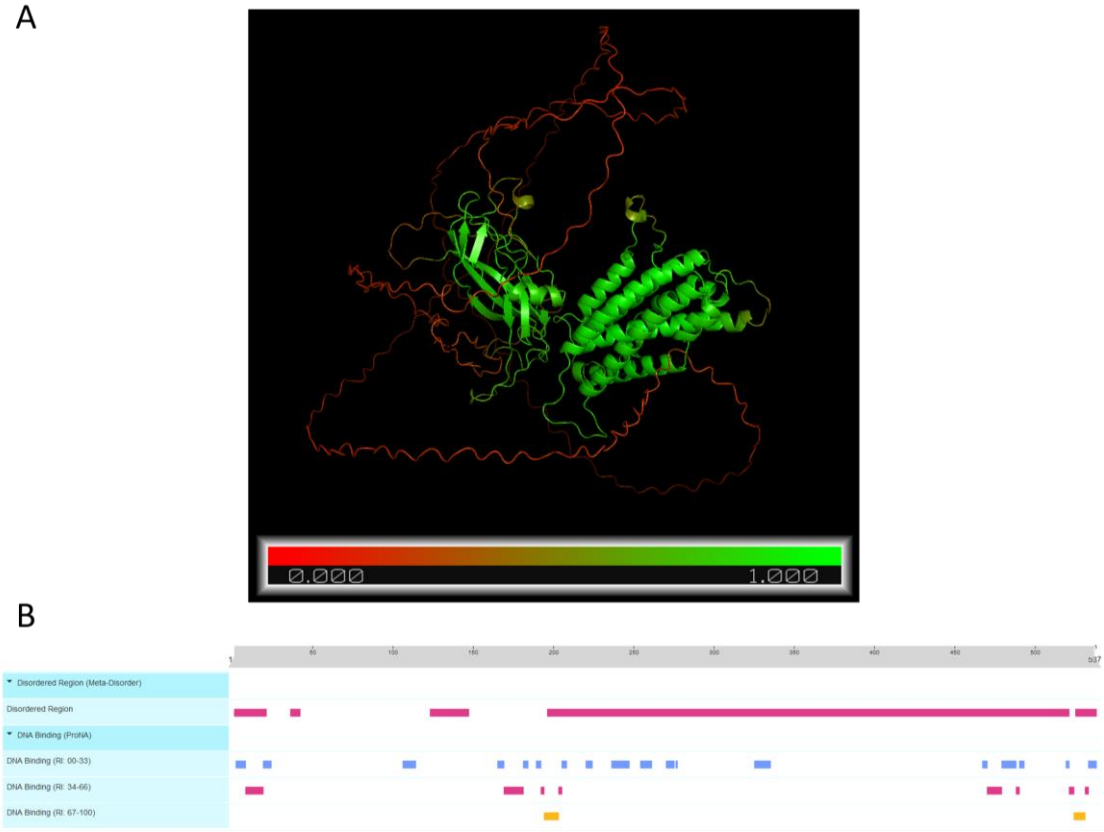

Figure 35: A direct interaction between HoxB and VeA is unlikely (A) AlphaFold modeling of a potential dimer between HoxB and VeA. High per residue certainty coloured in green; Low per residue certainty coloured in red (B) Predict Protein analysis of VeA. VeA is a highly disordered protein which disables AlphaFold from constructing a proper dimer. *In vivo* assessment of the interaction between HoxB and VeA yielded negative results.

2.5 HoxB is involved oxidative stress responses

Considering the potential implication of HoxB's involvement in the *A. nidulans* red- and blue-light sensory pathways, a phenotypical analysis in terms of growth assays under the influence of related stimuli was performed. The *ΔhoxB* strain created previously (chapter 2.3) was plated alongside the recomplemented strain and strains with *ΔfphA* (SJP1) and *ΔcryA* (SCK44) backgrounds. Phytochrome is involved in red-light sensing, osmotic stress regulation and cell wall integrity stress signaling (Blumenstein et al., 2005; Gavassi et al., 2017; Balke et al., 2023; Csillag et al., 2023). Consequently, the conditions tested involved illumination with red light, media supplementation with sodium chloride and sorbitol to induce osmotic stress, as well as congo red to induce cell wall integrity stress. Cryptochrome functions as a blue light sensor and is involved in oxidative stress signaling (Bayram et al., 2008a). Consequently, illumination with blue light as well as oxidative stress through media supplementation with hydrogen peroxide were tested (Figure 36). There did not appear to be a large influence on

strains grown on sodium chloride, sorbitol or congo red in darkness or in red light. Similarly, blue light only appeared to have the effect of introducing additional stress, which reduced growth of all strains. However, the three knockout strains of *ΔhoxB*, *ΔfphA* and *ΔcryA* showed a lack of growth on medium supplemented with hydrogen peroxide in darkness and red light. The wildtype and re-complemented knockout of *ΔhoxB* display unimpeded growth in darkness and red light. In blue light, these strains also display no growth. Colony size was not measured to determine individual differences for these growth assays as the different conditions required different growth times to obtain interpretable growth in either case.

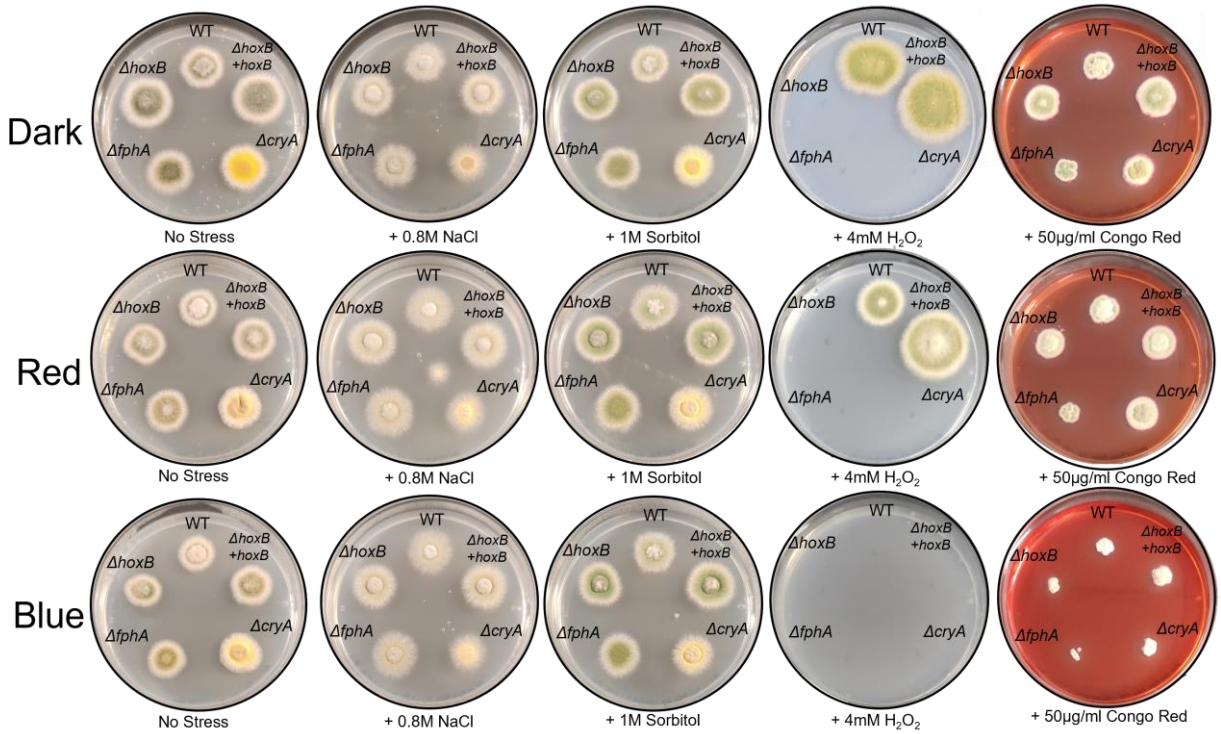

Figure 36: HoxB is required for growth on hydrogen peroxide Wildtype (WT), *ΔhoxB*, re-complemented *ΔhoxB+hoxB*, *ΔfphA* and *ΔcryA* were grown on minimal media containing no supplements, sodium chloride, sorbitol, peroxide and congo red in the dark, red and blue light. Hyphal growth does not occur in the *ΔhoxB*, *ΔfphA* and *ΔcryA* strains on hydrogen peroxide in either dark or red light and no strain grew in blue light.

Following these results, the *ΔhoxB* strain was crossed with the strain RSMO11 to reduce or remove potential strain background factors which may affect growth on specific media. The growth assay was repeated with additional stimuli for oxidative stress including tert-butylhydroperoxide, paraquat and menadione. Considering that osmotic stress did not lead to notable results, they were omitted. Furthermore, the ΔfphA strain was replaced in favor of an overexpression of *hoxB* and a strain carrying the *veA1* mutation to observe potential effects of velvet instead of phytochrome.

Considering that the overexpression functioned inducibly, the media contained threonine. As previously observed, the *ΔhoxB* strain displayed increased sensitivity to oxidative stress induced by hydrogen peroxide (Figure 37) while displaying no difference in growth on minimal medium and medium supplemented with congo red.

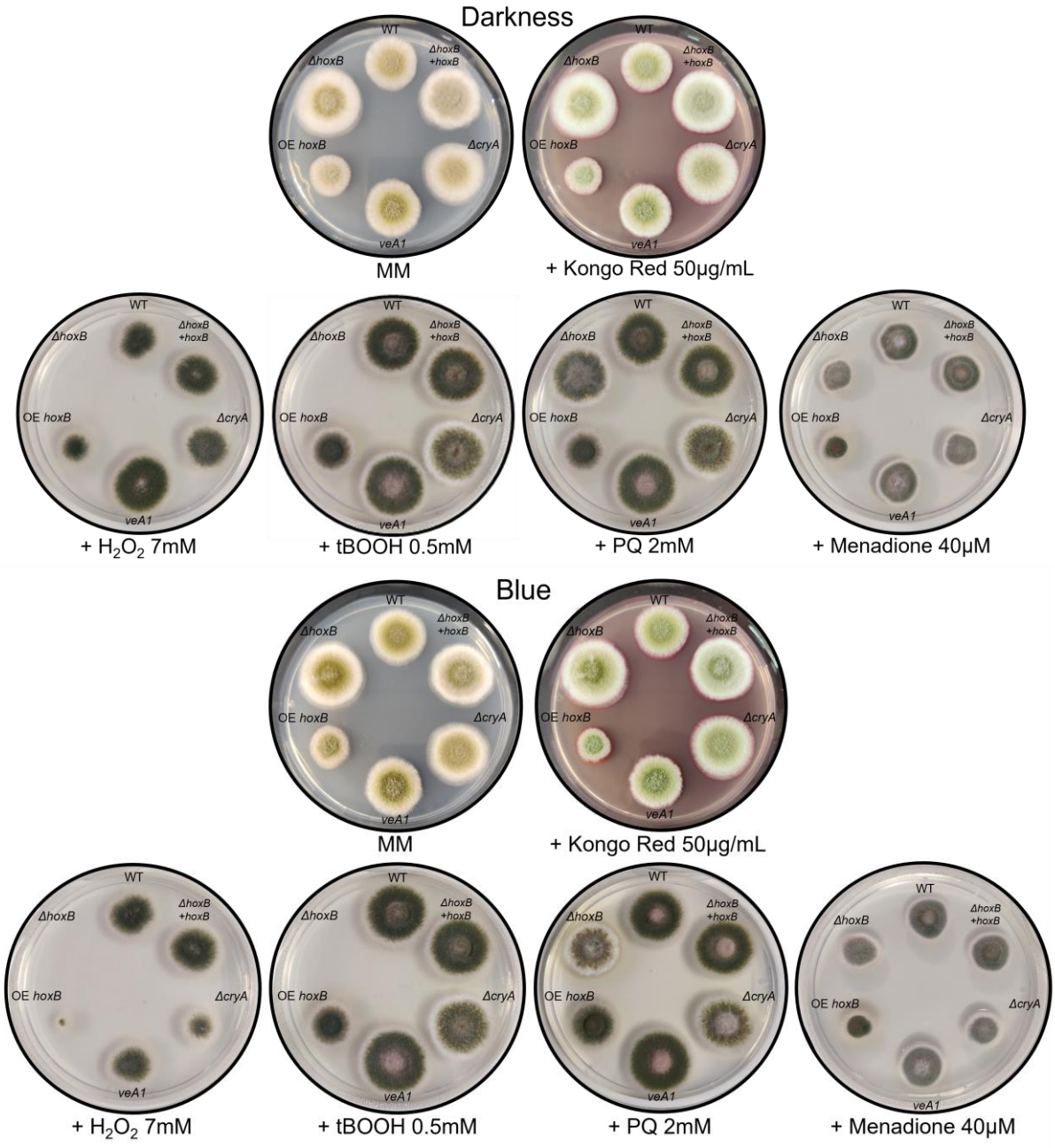

Figure 37: HoxB is required for growth on peroxide Wildtype (WT), *ΔhoxB*, re-complemented *ΔhoxB+hoxB*, *hoxB* overexpression (OE), *ΔcryA* and *veA1* were grown on minimal media containing no supplements, kongo red, hydrogen peroxide, tert. butylhydroperoxide, paraquat (PQ) and menadione in the dark and blue light. *ΔhoxB* displayed no hyphal growth on media containing peroxide and discolouration on media containing paraquat and menadione.

This sensitivity to oxidative stress was mirrored for other sources of oxidative stress and was absent in the re-complemented knockout. Specifically, the knockout did not grow on media containing hydrogen peroxide and tert-butylhydroperoxide and displayed irregular growth with discoloured colonies on media containing paraquat and menadione. The irregular growth and discoloration of *ΔhoxB* was largely mirrored by *ΔcryA* but not by *veA1* regardless of the respective light conditions. Notably, the overexpression of *hoxB* also displayed reduced growth compared to other strains without induction of oxidative stress although the difference was further exaggerated through the introduction of additional stress. This may indicate some function of HoxB in a stress signalling pathway as it appeared necessary to accommodate some oxidative stresses while an overabundance of the protein similarly resulted in reduced growth, although no lethality was observed. Simultaneously, the similarities in irregular growth between the *ΔhoxB* and *ΔcryA* strains may indicate a conjunctive function of these proteins in signaling these kinds of stress.

HoxB was previously found to be a TenA-E-like protein (chapter 2.2). Considering the potential function in thiamine salvage presented in literature (Zallot et al., 2014), the growth assay was repeated on YAG media (Figure 38). These media were supplemented with thiamine to determine whether lack of growth and growth irregularities observed may present due to a lack of thiamine. However, the supplementation of thiamine did not rescue the phenotypes observed previously. The *ΔhoxB* strain did not grow on media containing hydrogen peroxide or tert-butylhydroperoxide and displayed discoloration on media containing paraquat and menadione regardless of the respective light conditions. Similarly, the *ΔcryA* strain presented with discoloration and increased growth of aerial mycelia and the overexpression of *hoxB* displayed reduced growth regardless of light conditions. This indicates that the observed phenotypes are not a direct result of a lack of thiamine and instead may be related to another regulatory function performed by HoxB.

Furthermore, it was tested how HoxB may be involved in regulation of the response to oxidative stress in *A. nidulans*. The SVK103 wildtype, the SRFS26 *ΔhoxB* knockout and the SRFS29 *hoxB* re-complementation strains of *A. nidulans* were illuminated with high intensity blue light (approximately 20 $\mu mol*m^{-2}*s^{-1}$) to induce oxidative stress as described (Yu et al., 2021) and treated with the conditionally fluorescent dye CellROX Orange. The dye switches from a non-fluorescent state to an orange-fluorescent state

when oxidized by reactive oxygen species. As the concentration of intracellular reactive oxygen species increases, the fluorescence intensity may increase accordingly. In wildtype, the observed fluorescence intensity was highest near the hyphal tip and comparably lower near the spore (Figure 39).

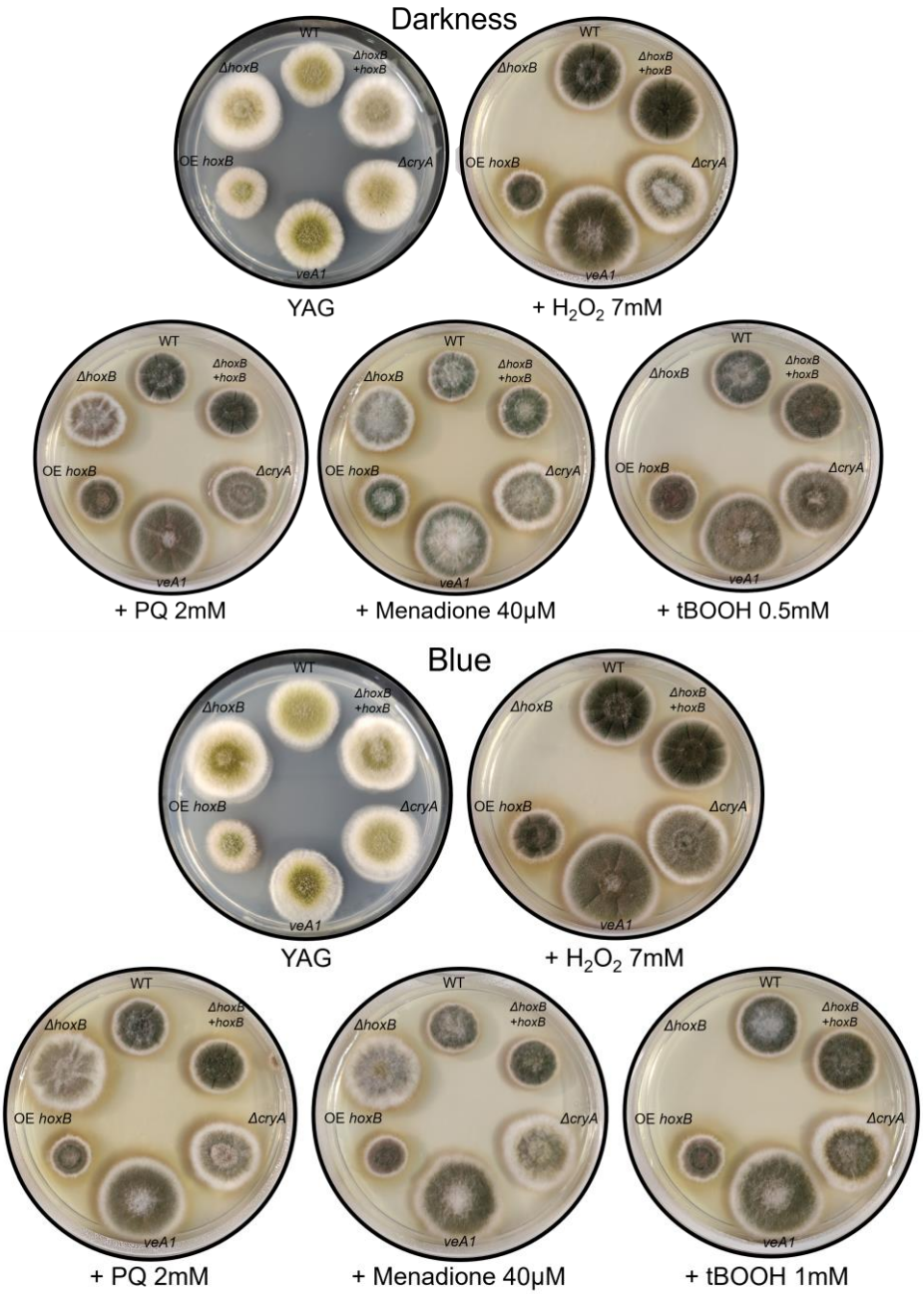

Figure 38: The *ΔhoxB* growth phenotype is not conveyed by thiamine deficiency Wildtype (WT), *ΔhoxB*, re-complemented *ΔhoxB+hoxB*, *hoxB* overexpression (OE), *ΔcryA* and *veA1* were grown on YAG media containing thiamine in combination with kongo red, hydrogen peroxide, tert. butylhydroperoxide, paraquat (PQ) and menadione in the dark and blue light. *ΔhoxB* displayed no hyphal growth on media containing peroxide and discolouration on media containing paraquat and menadione.

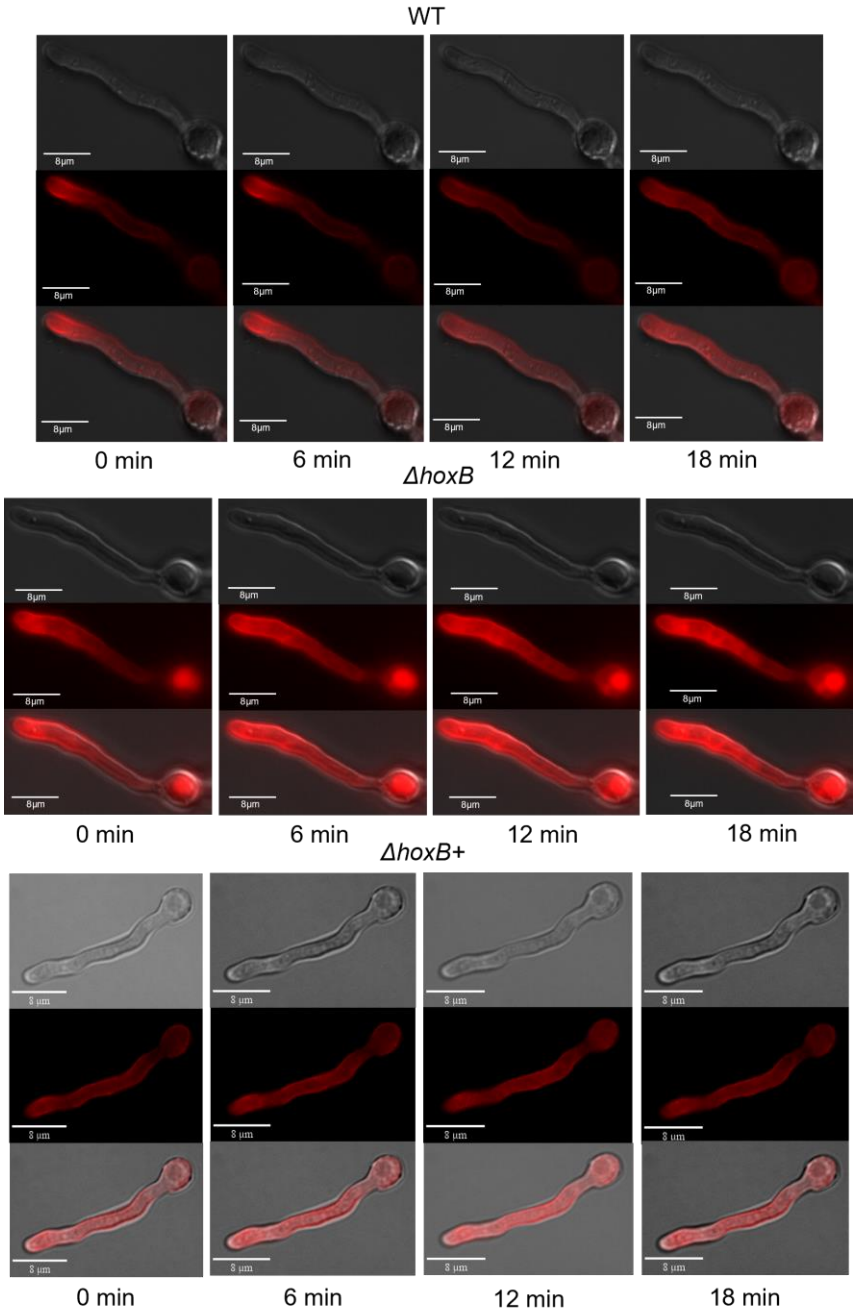

Figure 39: HoxB reduces reactive oxygen species upon blue light illumination Illumination with high-intensity blue light (approximately 20 µmol*m^{-2}*s^{-1}) increased fluorescence of CellROX Orange in *ΔhoxB*, but not in wildtype or re-complemented *ΔhoxB+hoxB*. Images were taken every six minutes.

Upon illumination, the signal increased slightly up to 6 minutes and then decreased until 18 minutes. This signal distribution and timing were mirrored by the *ΔhoxB* strain and additionally, the spore also displayed a much stronger fluorescent signal. The stronger signal may indicate a higher amount of reactive oxygen species present within the hyphae of the knockout. In the re-complementation strain, the signal was distributed more evenly but was overall much weaker than was observed in the other strains. This may indicate a reduced concentration of reactive oxygen species in this

strain. In conjunction this indicates that *hoxB* may be involved in oxidative stress management through facilitating the reduction of reactive oxygen species within the cell. Considering all previous results, specifically the ligand modelling, the change in localization in the velvet mutant background and the interaction with cryptochrome in the nucleus, it is unlikely that this facilitation of reactive oxygen species reduction is due to a catalytic function and instead the result of indirect transcriptional modulation as has been shown for TenA_E-like proteins (Pang et al., 1991).

Consequently, was tested whether stimuli which directly induce oxidative stress (high intensity blue light and hydrogen peroxide) or may function as predictors of future oxidative stress (red light) may induce the transcription of *hoxB* (Figure 40).

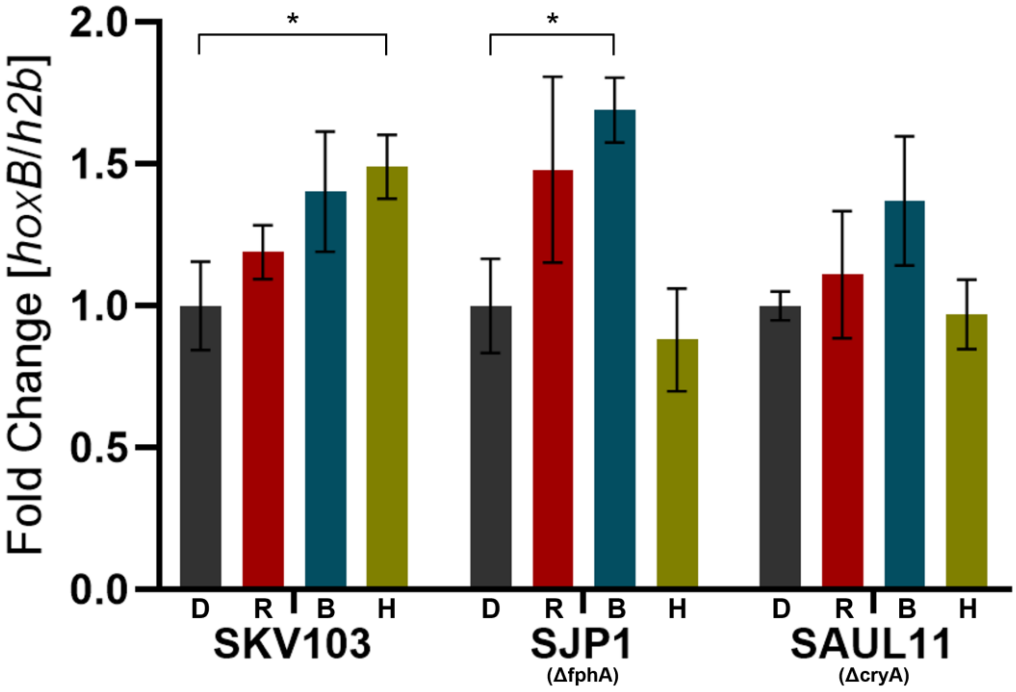

Figure 40: *hoxB* is induced by hydrogen peroxide Transcription of *hoxB* in wildtype (SKV103), *ΔfphA* and *ΔcryA* in the dark (D), red light (R), blue light (B) and hydrogen peroxide (H) after 15 min of induction. *hoxB* was induced by hydrogen peroxide in wildtype, but not *ΔfphA* and *ΔcryA*. In *ΔfphA*, *hoxB* was induced by blue light. * - p<0.05

In wildtype, only hydrogen peroxide was able to induce transcription of *hoxB* significantly by approximately 1.5 times. Illumination with blue light yielded a similar increase. However, this was not found to be significant. Notably, in backgrounds lacking photoreceptors phytochrome or cryptochrome, this upregulation in response to hydrogen peroxide was not observed. Additionally, phytochrome appeared to slightly affect *hoxB* transcription as in the phytochrome knockout the upregulation of *hoxB* in response to blue light was found to be significant. In the cryptochrome knockout none

of the chosen conditions were able to significantly affect transcription of *hoxB*. The small increase in transcription of *hoxB* in response to these stimuli may indicate a function in signal transduction of oxidative stresses as the expression of such genes typically is not altered strongly in response to the respective stimuli due to them being a pre-requisite to perceive the stimulus in the first place. An assessment of the transcriptional changes to various stress genes of A. nidulans in response to illumination with high intensity (20 µmol photons/m^{-2}*s) red or blue light or exposure to 4 mM hydrogen peroxide for 15 min each was performed to determine the effects of *hoxB* in detail. These analyses were performed in wildtype, *ΔhoxB*, the recomplemented knockout. Additionally, an overexpression of HoxB, ΔcryA and a strain carrying the *veA1* mutation. Firstly, transcription of phytochrome-dependent red-light marker genes *ccgA* (Figure 41), *ccgB* (Figure 42) and *conJ* (Figure 43) was observed as described in chapter 2.3.

In case of *ccgA*, illumination with red light led to a 175x increase in transcription which was noticeably lower in SRFS26 (97x) and noticeably higher in the SRFS29 (445x). Illumination with blue light led to a similar pattern with a 16x increase in SKV103 which was lower in SRFS26 (10x) and a strong increase in SRFS29 (285x). In contrary, treatment with hydrogen peroxide resulted in an approximately 1.85x increase in transcription and did not yield changes in transcription between those three strains. The expression pattern of SRFS40 resembled that of the SRFS29 with a 473x increase in response to red light, a 92x increase in response to blue light and a 4x increase in response to hydrogen peroxide. The expression pattern of SAUL11 mirrored that of SRFS40 with a 228x increase in response to red light, a 66x increase in response to blue light and a 3.8x increase in response to hydrogen peroxide. In SRF200, the response largely resembled the wildtype with an 83x increase in response to red light and a 21x increase in response to blue light. Merely the response to hydrogen peroxide was much larger, increasing transcription 7.6-fold. All increases measured met significance criteria with a p-value smaller than 0.05. This data indicates that transcription of the stress gene *ccgA* may be influenced by *hoxB* as indicated by the reduced transcription in response to red and blue light in the knockout. However, *hoxB* appears to only have a supportive effect as the lack of *hoxB* does not abolish the transcription fully. The increase in transcription of *ccgA* in response to hydrogen peroxide – and overall similar transcription pattern in response to all tested stimuli - in

the *hoxB* overexpression, the cryptochrome knockout and the *veA1* mutation may indicate an interaction between these proteins within the same pathway.

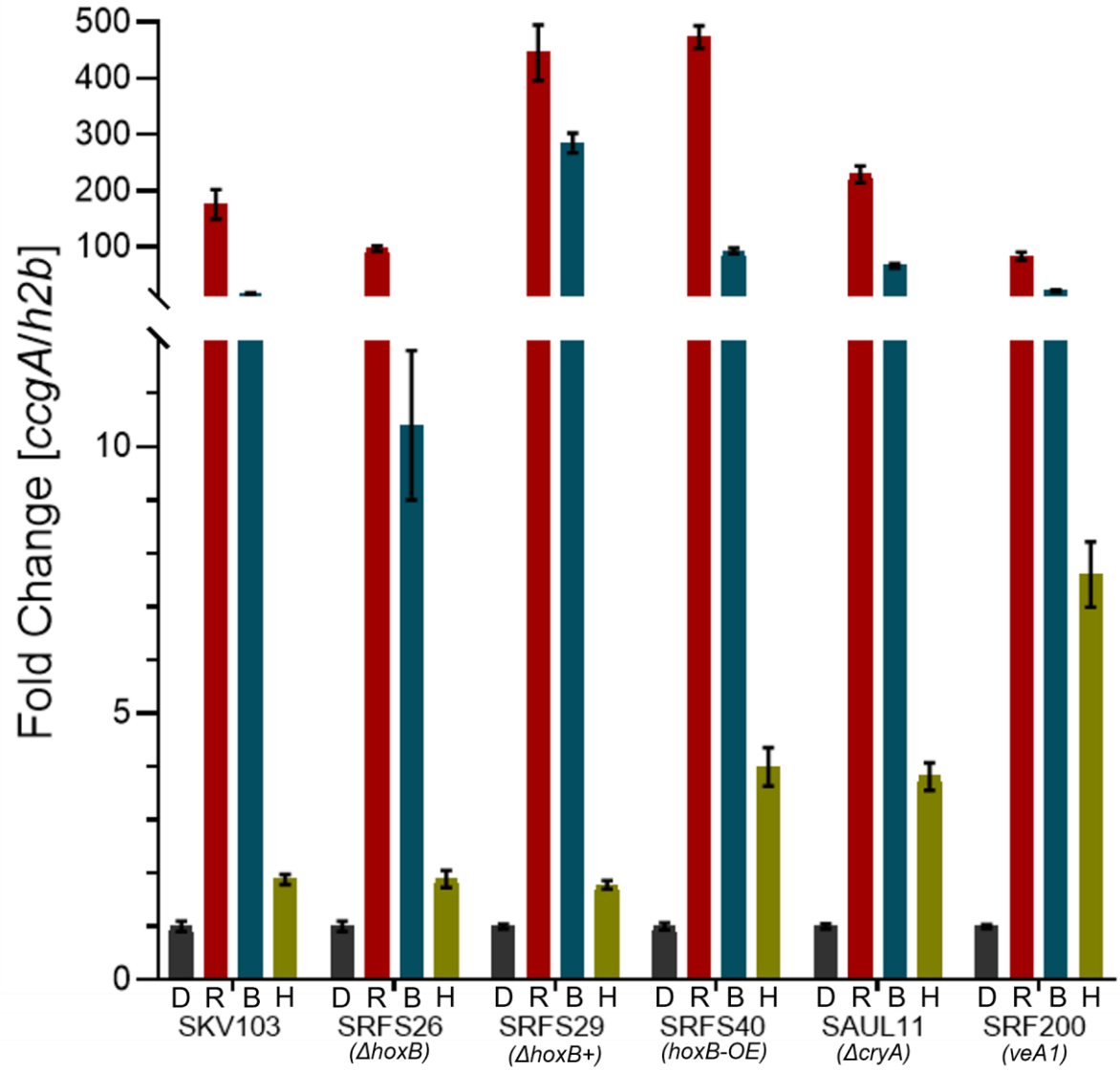

Figure 41: Transcription of *ccgA* is increased in *hoxB* overexpression, *ΔcryA* and *veA1* in response to hydrogen peroxide Transcription of *ccgA* in wildtype (SKV103), *ΔhoxB*, re-complemented *ΔhoxB*+, *hoxB* overexpression, *ΔcryA* and *veA1* in response to red light (R), blue light (B) and hydrogen peroxide (H). Induction by hydrogen peroxide in *hoxB* overexpression, *ΔcryA* and *veA1* was increased above levels observed in wildtype, *ΔhoxB* and re-complemented *ΔhoxB*+. Induction was decreased in response to red and blue light in *ΔhoxB*.

In case of *ccgB* (Figure 42), illumination with red light led to an increase in transcription in all strains observed that was approximately 400x compared to strains not illuminated. This increase was larger in SAUL11 (708x) and lower in SRF200 (188x). However, the pattern of transcription for all strains in response to blue light was similar to the one observed for *ccgA*. In SRFS26, transcription decreased from 37x in SKV103 to 10x and this decrease was recovered in SRFS29 (349x). In SRFS40, SAUL11 and SRF200, the transcription was also increased to approximately 95x, 203x and 62x

respectively. In response to hydrogen peroxide, transcription of *ccgB* increased twofold in SKV103. This increase was not present in the knockout but was observed in SRFS29 where transcription increased fourfold. In SRFS40, SAUL11 and SRF200 was much larger at 6x, 26x and 45x respectively. This may indicate that transcription of *ccgB* in response to hydrogen peroxide is suppressed by cryptochrome and velvet.

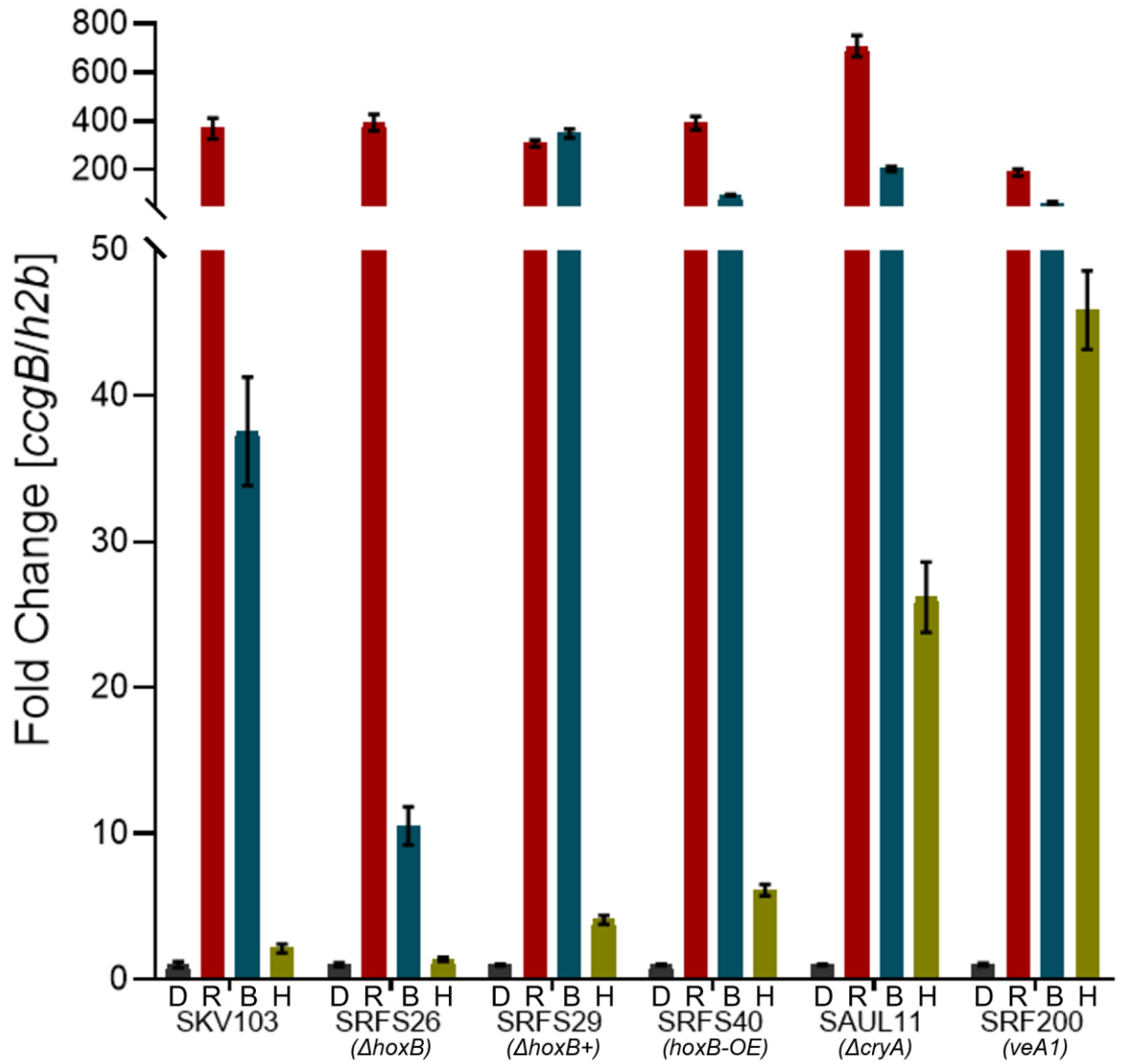

Figure 42: Transcription of *ccgB* is increased in *hoxB* overexpression, *ΔcryA* and *veA1* in response to hydrogen peroxide Transcription of *ccgB* in wildtype (SKV103), *ΔhoxB*, re-complemented *ΔhoxB+*, *hoxB* overexpression, *ΔcryA* and *veA1* in response to red light (R), blue light (B) and hydrogen peroxide (H). Induction by hydrogen peroxide in *hoxB* overexpression, *ΔcryA* and *veA1* was increased above levels observed in wildtype, *ΔhoxB* and re-complemented *ΔhoxB+*. Induction was decreased in response to blue light in *ΔhoxB*.

Considering the lack of induction in the *hoxB* knockout and the increased transcription in the *hoxB* overexpression, this may implicate HoxB as a negative regulator of this suppression by cryptochrome and velvet. The absence of a notable transcriptional change in response to illumination with red light and limited reduction in transcription

in the knockout may again indicate that *hoxB* has a supportive effect on the light signaling response leading to the transcription of these stress genes.

In case of *conJ* (Figure 43), the observed transcriptional changes do not match the patterns previously observed for *ccgA* and *ccgB*. In SKV103, red and blue light illumination led to a 21x and 9.8x increase in transcription of *conJ* respectively.

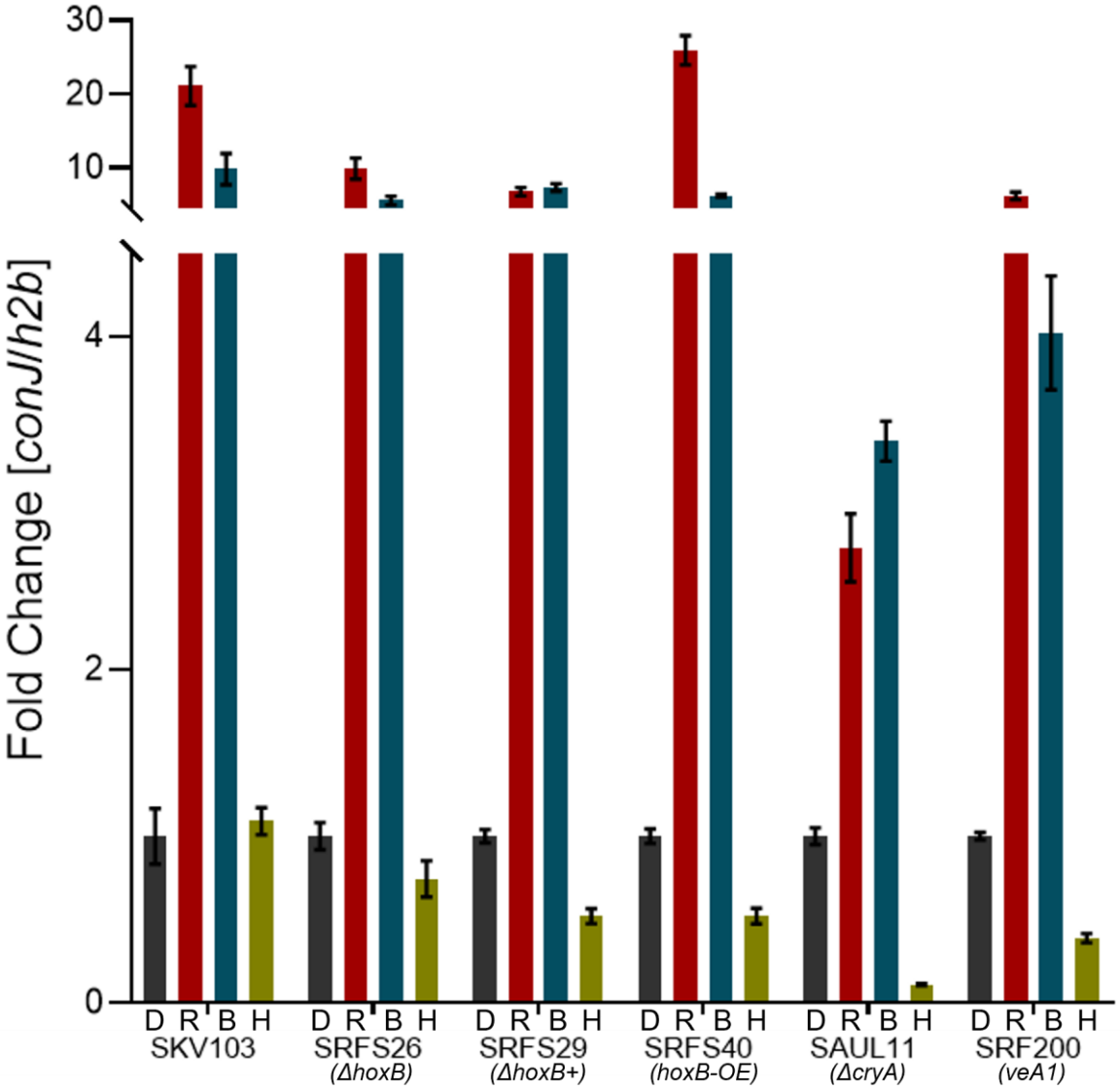

Figure 43: Transcription of *conJ* is increased in *hoxB* overexpression, *ΔcryA* and *veA1* in response to hydrogen peroxide Transcription of *conJ* in wildtype (SKV103), *ΔhoxB*, re-complemented *ΔhoxB+*, *hoxB* overexpression, *ΔcryA* and *veA1* in response to red light (R), blue light (B) and hydrogen peroxide (H). Induction by all conditions was lowest in *ΔcryA* and *veA1*.

This expression was lower in SRFS26 at 9.9x and 5.5x respectively though this was not reverted in SRFS29 where the expression was even lower at 6.7x and 7.3x respectively. In SRFS40, the expression of conJ in response to red light rose to 26x and to 6.2x in response to blue light. This may indicate that the lower expression in

SRFS26 and SRFS29 may be a feature of the strains' genetic background. In SAUL11, an increase in transcription in response to red (2.7x) and blue (3.4x) light was still present although that increase was much smaller than in other strains. In SRF200, the increases in transcription in response to red and blue light were found to be 6x and 4x respectively. In response to hydrogen peroxide, a notable difference in transcription between strains could be observed. In SKV103, there was no change in transcription of conJ in response to hydrogen peroxide. In SRFS26, the transcription was lower at approximately 0.75x. However, this decrease did not meet significance criteria. In SRFS29 and SRFS40, a significant decrease in transcription to approximately 0.5x was observed. In SRF200, a similar decrease to 0.4x was observed and in SAUL11 transcription decreased to 0.1x. This may be further evidence of a direct or indirect interaction between HoxB and cryptochrome and velvet in the same pathway as the general transcriptional pattern of the corresponding strains resembled each other although the magnitude of the transcriptional changes varied.

Considering the phenotypical effects of *hoxB* on the sensitivity to multiple oxidative stresses, the expression of the oxidative stress genes *prxA* (Figure 44A) and *trxA* (Figure 44B) in the peroxiredoxin system of *A. nidulans*, as well as the catalase genes *catA* (Figure 45A) and *catB* (Figure 45B) were tested in a similar fashion. In case of *trxA*, no notable significant transcriptional changes were observed regardless of stimulus. In case of prxA, notable significant changes were observed, specifically in response to hydrogen peroxide. In SKV103, hydrogen peroxide led to a small but significant increase in *prxA* transcription of 1.6x. This increase was not observed in SRFS26 and in SRFS29, the transcription increased to 3.4x, indicating a necessity for *hoxB* in this response to hydrogen peroxide.

In SRFS40, all tested stimuli were able to increase the transcription of *prxA* significantly. Red light exposure increased transcription 3.1-fold while blue light exposure increased transcription 2.6-fold. Upon exposure to hydrogen peroxide, transcription showed an extreme 45-fold increase. This transcriptional pattern resembled that of SRF200 which showed a 2.1-fold increase upon exposure to red light, a 2-fold increase upon exposure to blue light and a 27-fold increase upon exposure to hydrogen peroxide. In SAUL11, only hydrogen peroxide induced a significant transcriptional increase by 9.6x. This may provide further evidence that HoxB, cryptochrome and velvet are functional in the same pathway.

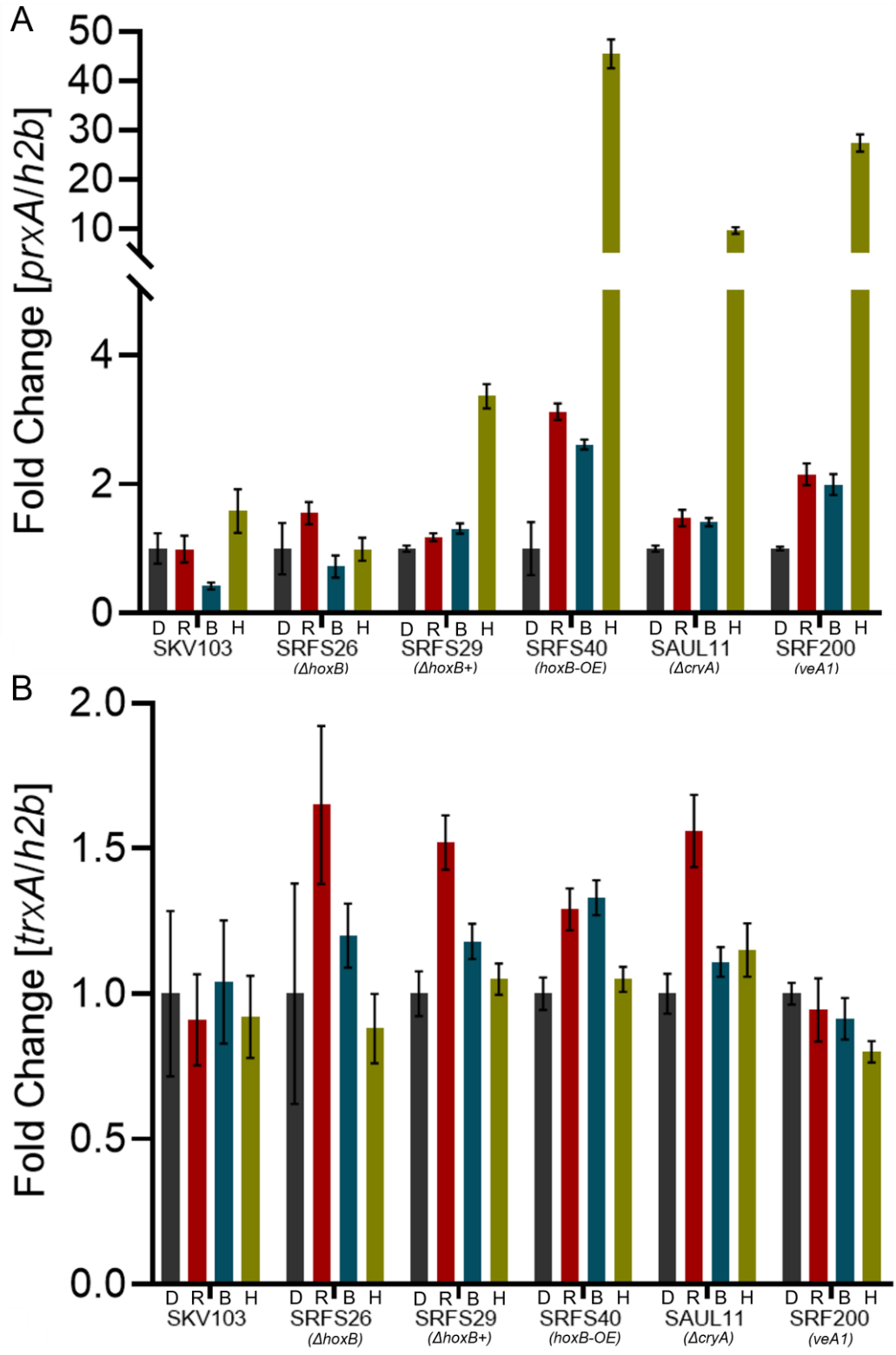

Figure 44: Transcription of the peroxiredoxin system in *hoxB* overexpression, *ΔcryA* and *veA1* in response to hydrogen peroxide (A) Transcription of *prxA* in wildtype (SKV103), *ΔhoxB*, re-complemented *ΔhoxB+*, *hoxB* overexpression, *ΔcryA* and *veA1* in response to red light (R), blue light (B) and hydrogen peroxide (H). Induction by hydrogen peroxide in *hoxB* overexpression, *ΔcryA* and *veA1* was increased above levels observed in wildtype, *ΔhoxB* and re-complemented *ΔhoxB+*. (B) Transcription of *trxA* in wildtype (SKV103), *ΔhoxB*, re-complemented *ΔhoxB+*, *hoxB* overexpression, *ΔcryA* and *veA1* in response to red light (R), blue light (B) and hydrogen peroxide (H). No noteworthy induction was observed in any strain or condition.

Considering the effect of the *hoxB* overexpression mirroring a cryptochrome knockout and *veA1*, it is feasible that HoxB may function as a negative regulator of cryptochrome and velvet as stated previously. Investigation of transcription of the *catA* and *catB* genes may allow distinguishing the effects of *hoxB* during development of *A. nidulans*. The *catA* gene of A. nidulans is primarily expressed during sporulation and shows reduced expression during mycelial growth and is required for resistance to hydrogen peroxide (Navarro et al., 1996). *CatB* is expressed during vegetative growth of A. nidulans and an increase in its expression is normally accompanied by an ablation of *catA* expression, as it takes over its protective function (Kawasaki et al., 1997). In case of *catA*, transcriptional changes were observed in response to illumination with red light in SRFS26, SRFS29 and SAUL11. Specifically, in these strains, illumination with red light caused an increase in *catA* transcription to 4.4x, 3.3x and 5.3x respectively. In SRFS40, all tested stimuli increase *catA* transcription. In response to red light, transcription increased to 17x, in response to blue light, transcription increased to 6x and in response to hydrogen peroxide transcription increased to 10x. Considering the RNA during these experiments was extracted from vegetative mycelia, the change in *catA* expression, particularly in SRFS40, is unusual and may indicate a positive effect of HoxB on *catA* transcription during sporulation. In case of *catB*, SKV103, SRFS40, SAUL11 and SRF200 showed notable transcriptional changes in response to the tested stimuli. In SKV103, transcription increased to approximately 1.5x in response to hydrogen peroxide only. In SRFS40, red light illumination increased transcription to 4.6x, blue light illumination increased transcription to 6.6x and hydrogen peroxide increased transcription to 105x. In a similar fashion, in SRF200, red light illumination increased transcription to 5.6x, blue light illumination increased transcription to 4.8x and hydrogen peroxide increased transcription to 36x. In SAUL11, only hydrogen peroxide led to a significant increase to 3.2x. Conjoinedly, this indicates a direct or indirect interaction between HoxB, CryA and VeA to affect the oxidative stress response through *catB* during vegetative growth. While the transcription of *catB* decreased to approximately 0.5x in SRFS26 in response to hydrogen peroxide and remained at base level in SKV103 and SRFS29, this decrease did not meet significance criteria. Consequently, *hoxB* may not be necessary for the expression of *catB* but it may exert an amplificatory effect.

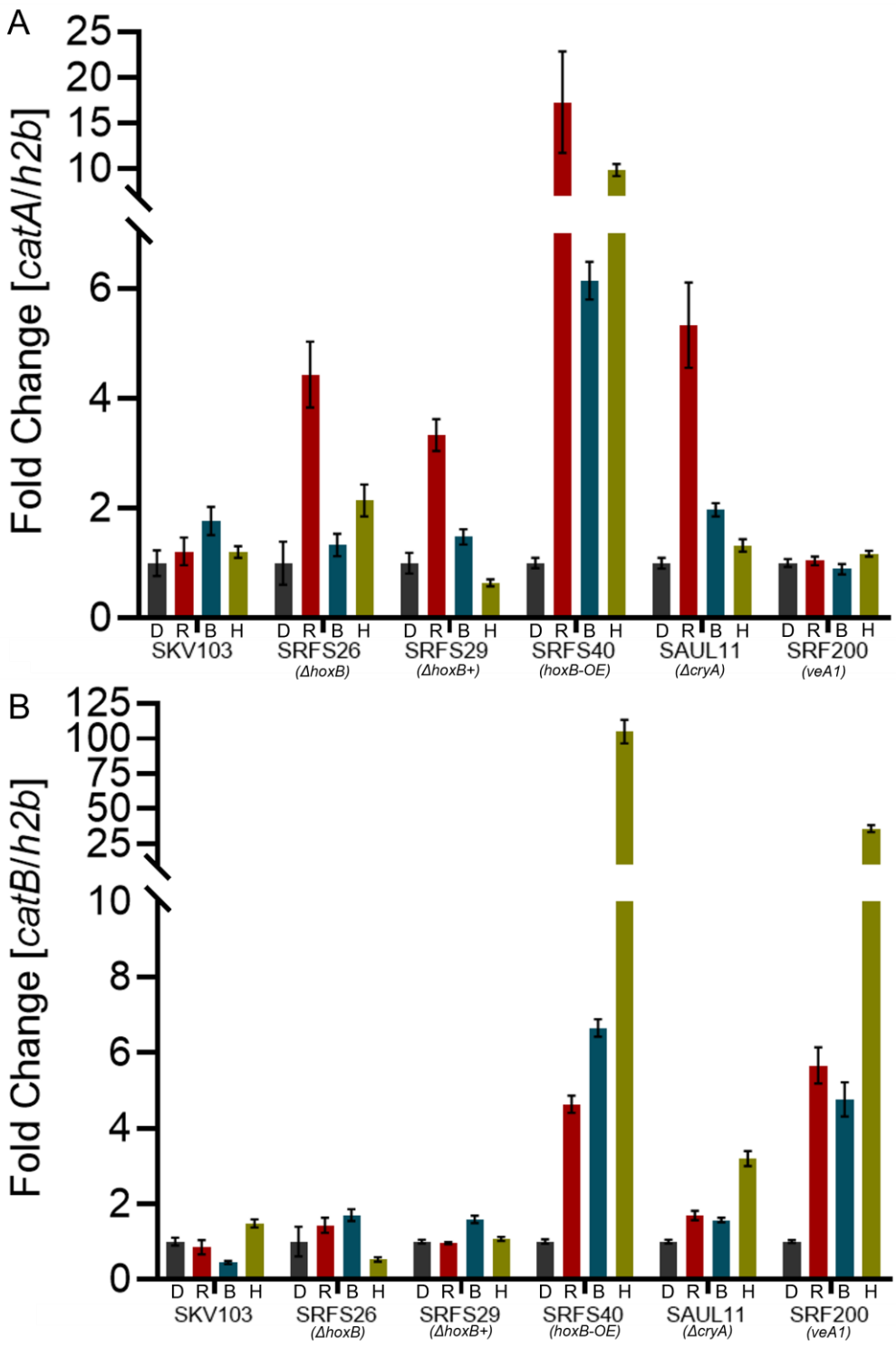

Figure 45: Transcription of catalases in *hoxB* overexpression, *ΔcryA* and *veA1* in response to hydrogen peroxide (A) Transcription of *catA* in wildtype (SKV103), *ΔhoxB*, re-complemented *ΔhoxB*+, *hoxB* overexpression, *ΔcryA* and *veA1* in response to red light (R), blue light (B) and hydrogen peroxide (H). Induction occurred in response to red light in *ΔhoxB*, re-complemented *ΔhoxB*+, *hoxB* overexpression and *ΔcryA*. Induction occurred for all tested conditions in the *hoxB* overexpression. (B) Transcription of *catB* in wildtype (SKV103), *ΔhoxB*, re-complemented *ΔhoxB*+, *hoxB* overexpression, *ΔcryA* and *veA1* in response to red light (R), blue light (B) and hydrogen peroxide (H). Induction by hydrogen peroxide in *hoxB* overexpression, *ΔcryA* and *veA1* was increased above levels observed in wildtype, *ΔhoxB* and re-complemented *ΔhoxB*+. Similarly, induction was increased by red and blue light in *hoxB* overexpression and *veA1*.

2.6 HoxB triggers gene expression changes

A broad assessment of the effects and functions of *hoxB* was performed through comparative RNA-sequencing of SKV103, SRFS26 and SRFS40 in response to hydrogen peroxide in two distinct approaches for the knockout and overexpression models. RNA-Sequencing and initial comparative analysis was performed by the company BGI. Only genes, GO- and KEGG-analyses found to be significantly differentially regulated in and between comparisons are reported in the following chapter. In the first approach, the SKV103 wild type was compared to SRFS26 (*ΔhoxB*). Both strains were either left untreated or treated with 4 mM hydrogen peroxide to compare which genes are differentially regulated within an individual strain upon treatment and how these differentially expressed genes may vary between the strains. The second approach compared the SKV103 wild type and SRFS40 (*hoxB*-OE) under the same conditions and using a similar comparative approach.

In SKV103, 1501 genes were found to be differentially regulated upon treatment with hydrogen peroxide. Similarly, in SRFS26, 1366 genes were found to be differentially regulated in response to hydrogen peroxide. There was an overlap of 818 genes which were found to be differentially regulated in both genes while 683 genes were unique to SKV103, and 548 genes were unique to SRFS26 (Figure 46). A full list of uniquely differentially regulated genes may be found in the appendix, including 8 novel genes found during this sequencing. In both strains, genes relating to specific GO-terms were found to be differentially regulated more often when compared to other genes within the *A. nidulans* genome. In SKV103, 494 unique genes relating to “Integral Component of Membrane”, “Intrinsic Component of Membrane”, “Membrane” and “Plasma Membrane” were differentially regulated. Furthermore, 249 unique genes with “Oxidoreductase Activity” and 158 unique genes relating to “Small Molecule Catabolic Process”, “Organic Acid Metabolic Process”, “Oxoacid Metabolic Process”, “Small Molecule Metabolic Process”, “Carboxylic Acid Metabolic Process”, “Monocarboxylic Acid Metabolic Process” and “Organic Acid Catabolic Process” were found to be differentially regulated. In SRFS26, 451 unique genes relating to “Integral Component of Membrane”, “Intrinsic Component of Membrane” and “Membrane” were differentially regulated. Furthermore, 378 unique genes relating to “Oxidoreductase Activity”, “Transmembrane Transporter Activity”, “Transporter” and “Solute:Sodium Symporter Activity” and 174 unique genes relating to “Small Molecule Metabolic Process“,

“Organic Hydroxy Compound Metabolic Process”, “Ethanol Metabolic Process”, “Secondary Metabolic Process”, “Ethanol Catabolic Process”, “Primary Alcohol Catabolic Process”, “Monocarboxylic Acid Biosynthetic Process”, “Organic Acid Metabolic Process”, “Monocarboxylic Acid Metabolic Process”, “Primary Alcohol Metabolic Process”, “Oxoacid Metabolic Process”, “Fatty Acid Biosynthetic Process” and “Carboxylic Acid Metabolic Process” were found differentially regulated. Considering the previously observed differences between the two strains, attention was paid to the genes uniquely regulated in each strain.

Eliminating the 818 genes which were similarly differentially regulated in both strains from those found during the GO-analysis left 330 genes in SKV103 and 270 genes in SRFS26 uniquely regulated and being attached to significantly changed genes attached to identical GO-terms (Figure 46). In SKV103, 134 of the 330 uniquely regulated genes were found to be upregulated while 196 genes were downregulated. Of the upregulated genes, 72 were involved in modifying cell membrane or cell wall composition, 31 were oxidoreductases with no strict metabolic involvement, 14 genes related to changing organelle related membrane composition, 12 genes related to metabolic changes and 5 genes related to mitochondrial changes. Furthermore, some transcription factors and transcriptional modulators were found. Of the downregulated genes, 90 were involved in modifying cell membrane or cell wall composition, 40 were oxidoreductases with no strict metabolic involvement, 25 genes related to changing organelle related membrane composition, 34 genes related to metabolic changes and 7 genes related to mitochondrial changes. Notably, some genes observed imply an upregulation of TORC2-signaling and a downregulation of TORC1-signaling in response to hydrogen peroxide that is unique to SKV103. In SRFS26, 143 of the 271 uniquely regulated genes were found to be upregulated while 128 genes were downregulated. Of the upregulated genes, 77 were involved in modifying cell membrane or cell wall composition, 19 were oxidoreductases with no strict metabolic involvement, 16 genes related to changing organelle related membrane composition, 28 genes related to metabolic changes and 3 genes related to mitochondrial changes. Multiple genes involved in regulation of secondary metabolism were found. Of the downregulated genes, 55 were involved in modifying cell membrane or cell wall composition, 25 were oxidoreductases with no strict metabolic involvement, 14 genes related to changing organelle related membrane composition, 17 genes related to metabolic changes and 5 genes related to mitochondrial changes. The majority of

transcriptional regulators found unique to SRFS26 pertain to metabolic changes. Notably, some genes whose orthologues in *S. cerevisiae* are related to promoting apoptosis were observed.

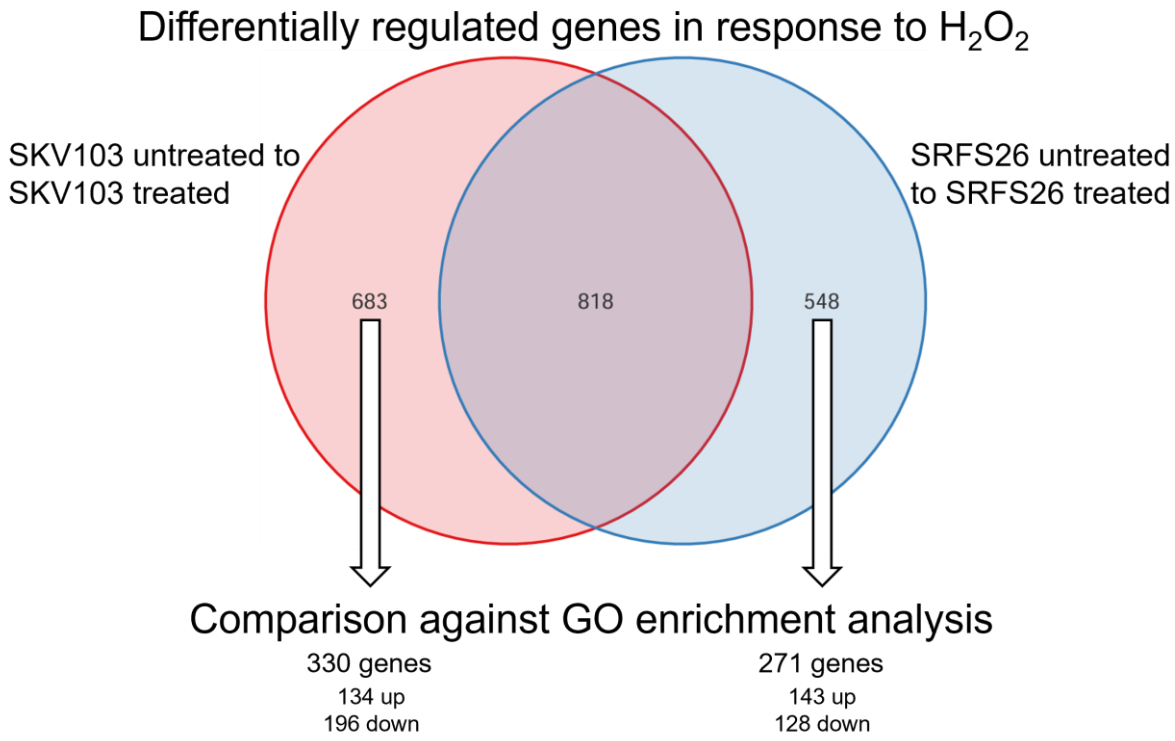

Figure 46: Comparative transcriptomic analysis between wildtype (SKV103) and *ΔhoxB* (SRFS26) Wildtype and *ΔhoxB* were treated with hydrogen peroxide. RNA-sequencing revealed that 683 genes were regulated only in wildtype, 548 genes were regulated only in *ΔhoxB* and 818 genes were regulated in both strains. Comparison against a GO enrichment analysis left 330 genes regulated in wildtype and 271 genes regulated in the knockout. Due to the likelihood of the observed phenotypes being the result of a failure to initiate an appropriate response in the knockout the focus was put on genes upregulated in either strain.

Considering the previously observed sensitivity of the knockout to hydrogen peroxide, it was seen as likely that this was the result of a failure to express genes involved in resolving the stress caused by hydrogen peroxide. While secondary regulatory genes – such as transcription factors – involved in expression of the direct effectors may be either up- or downregulated, particular attention was paid to genes upregulated in response to hydrogen peroxide in SKV103 that were not found to be upregulated in SRFS26. Despite the genes found to be uniquely differentially regulated in each strain belonging to similar GO-categories, there were strong functional differences in the types of genes in each category between SKV103 and SRFS26. In SKV103, several uniquely upregulated genes were found to be or were likely to be involved with the resolution of oxidative stress to peroxide and cell membrane or cell wall damage. A list of notable uniquely upregulated genes may be found in Table 1. In SRFS26, only 3

genes were found that may be involved in the resolution of oxidative stress induced by hydrogen peroxide. Otherwise, the response seemed to be centered on metabolic changes and restructuring of the cell wall and membrane. Furthermore, which may be associated with autolysis and apoptosis were found to be upregulated while in SKV103, genes involved in supressing apoptosis were upregulated. A list of notable uniquely upregulated genes may be found in Table 2. The respective full lists of upregulated genes are found in the appendix.

Table 1: Notable genes upregulated in wildtype (SKV103) upon exposure to hydrogen peroxide

Gene	Description	Source
AN0170	Thioredoxin trxA; control of intracellular redox homeostasis	Le Marechal et al., 1992; Thön et al., 2007
AN9339	Catalase catB; degradation of H_2O_2	Kawasaki et al., 1997; Calera et al., 2000
AN10220	Putative Cytochrome C peroxidase ccp1; Yeast orthologue CCP1 functions as hydrogen peroxide sensor in mitochondria	Martins et al., 2013; Sato et al., 2009
AN7729	Uncharacterized protein; ABC type C transporter; Yeast orthologue YCF1 transports bilirubin and glutathione from vacuole	Li et al., 1996; Petrovic et al. 2000
AN6779	Uncharacterized protein; ABC type C transporter; Yeast orthologue YCF1 transports bilirubin and glutathione from vacuole	Li et al., 1996; Petrovic et al., 2000
AN0374	Uncharacterized protein; MFS type transporter; Yeast orthologue GEX1 is a proton:glutathione antiporter	Dhaoui et al., 2011
AN1671	Uncharacterized protein; Putative Diacylglycerol pyrophosphatase with haloperoxidase-domain (Interpro domain assignment)	-
AN8104	Uncharacterized protein; Yeast orthologue PUG1 is involved in conditional protoporphyrin IX uptake	Protchenko et al., 2008
AN6304	Uncharacterized protein; Yeast orthologue AVO1 is TORC2 subunit regulating plasma membrane homeostasis	Loewith et al., 2002; Riggi et al., 2020
AN8796	Uncharacterized protein; Yeast orthologue GTR1 is TORC1 subunit that regulates sensitivity to H_2O_2	Sekiguchi et al., 2022
AN3329	Uncharacterized protein; ABC-2 type transporter; Yeast orthologue SNQ2 conveys resistance to 4NQNO-induced oxidative stress	Servos et al., 1993; Ververidis et al., 2001
AN1882	Uncharacterized protein; Yeast orthologue OYE2 suppresses apoptosis induced by H_2O_2	Odat et al., 2007

AN0754	Uncharacterized protein; S. pombe orthologue uvi15 exhibits sensitivity to tert.butylhydroperoxide	Rodríguez-López et al., 2023
AN1753	Uncharacterized protein; Yeast orthologue FMP52 induced upon UVA-induced DNA-damage	Dardalhon et al., 2007
AN2684	Uncharacterized protein; Ergosterol biosynthesis protein; Yeast orthologue ERG4 may be used to offset membrane damage	Aguilera et al., 2006
AN8395	Uncharacterized protein; likely heme haloperoxidase (Interpro domain assignment); fold change WT/KO: 5.6x/3.5x	-
AN2846	Putative glutathione peroxidase gpxA; induced by H2O2 and farnesol; fold change WT/KO: 2x/1.3x	Balász et al., 2010; Wartenberg et al., 2012

These results may indicate that the knockout is partially able to recognize a form of oxidative stress. However, there may be some misinterpretation regarding the source of this stress. This RNA-sequencing approach clearly shows that SRFS26 was unable to mount a proper response to hydrogen peroxide whereas the wildtype was able to react appropriately to the hydrogen peroxide induced stress by inducing thioredoxin, catalase B, putative peroxidases and potential components of glutathione and bilirubin transport as well as regulation of TORC-signaling.

The KEGG-analyses performed did not detect major differences between the SKV103 and SRFS26 which may indicate that transcriptional changes induced by HoxB are not occurring on a broad scale and are instead limited to the genes described above. In both strains, a differential regulation of genes affecting metabolism was found (Figure 47). Specifically, metabolic pathways relating to amino acid and sugar metabolism such as “tyrosine metabolism”, “tryptophane metabolism”, “phenylalanine metabolism” and “alanine metabolism”, as well as “glycolysis/gluconeogenesis”, “fructose and mannose metabolism” and “pentose and glucuronate interconversions” were subject to differential regulation. Furthermore, “biosynthesis of secondary metabolites”, “aflatoxin biosynthesis”, “indole alkaloid biosynthesis” and “biosynthesis of antibiotics” were differentially regulated in both strains. Some pathways uniquely differentially regulated in SKV103 included “glycerophospholipid metabolism”, “fatty acid degradation”, “N-glycan biosynthesis”, “nicotinate/nicotinamide metabolism” and “vitamin B6 metabolism” among others.

Table 2: Notable genes upregulated in *ΔhoxB* (SRFS26) upon exposure to hydrogen peroxide

Gene	Description	Source
AN1967	Putative fatty acid dioxygenase with heme peroxidase domain	Brodhun et al., 2009
AN8984	Uncharacterized protein; Bears similarity to Pth11 of M. oryzae which assists ROS homeostasis	Kou et al., 2017
AN10038	Putative glutathione S-transferase and elongation factor 1-gamma	Sato et al., 2009; Chiang et al., 2010
AN3882	Predicted Ca2+-dependent endopeptidase; Yeast orthologue MCA1 is caspase-like and regulates apoptosis in repsonse to H_2O_2	Madeo et al., 2002; Kaushal et al., 2023
AN8881	Uncharacterized protein; Yeast orthologue ORT1 is required to undergo apoptosis induced by human caspase-10	Lisa-Santamaría et al., 2012
AN0973	BrlA; Transcription factor controlling development	Adams et al., 1988; Pócsi et al., 2009
AN4871	Class V Chitinase ChiB	Yamazaki et al., 2006
AN10838	Uncharacterized protein; Chitinase-domain; A. niger orthologue CfcI is a chitinase potentially involved in autolysis	van Munster et al., 2012
AN1314	Uncharacterized protein; Carboxylesterase-domain; likely lipase function	-
AN8743	Uncharacterized protein; Fungal lipase_3-domain (Diacylglycerol lipase)	-
AN3281	Putative Cytochrome P450; Yeast orthologue DIT2 assists spore wall maturation	Kelly et al., 2009
AN2706	Putative Cytochrome P450; cell wall structure-related gene	De Groot et al., 2008
AN10049	MdpB; required for monodictyphenone synthesis	Chiang et al., 2010
AN0146	Putative versicolorin reductase MdpC; resembles sterigmatocystin- and aflatoxin-producing enzymes	Chiang et al., 2010
AN0147	MdpD; production of prenylated xanthone	Sanchez et al., 2011
AN10022	MdpH; potential endocrocin decarboxylase	Chiang et al., 2010
AN10044	MdpK; required for monodictyphenone synthesis	Chiang et al., 2010
AN0807	LaeA; necessary for sterigmatocystin-, penecillin- and lovastatin-production in Aspergillus spp.	Bok et al., 2004
AN11191	AlnA; necessary for (+)-asperlin-production	Grau et al., 2018

On the other hand, uniquely differentially regulated pathways in SRFS26 included “MAPK signaling pathways (orthologue to) yeast”, “fatty acid metabolism”, “sphingolipid metabolism”, “thiamine metabolism”, “riboflavine metabolism” and “folate biosynthesis”.

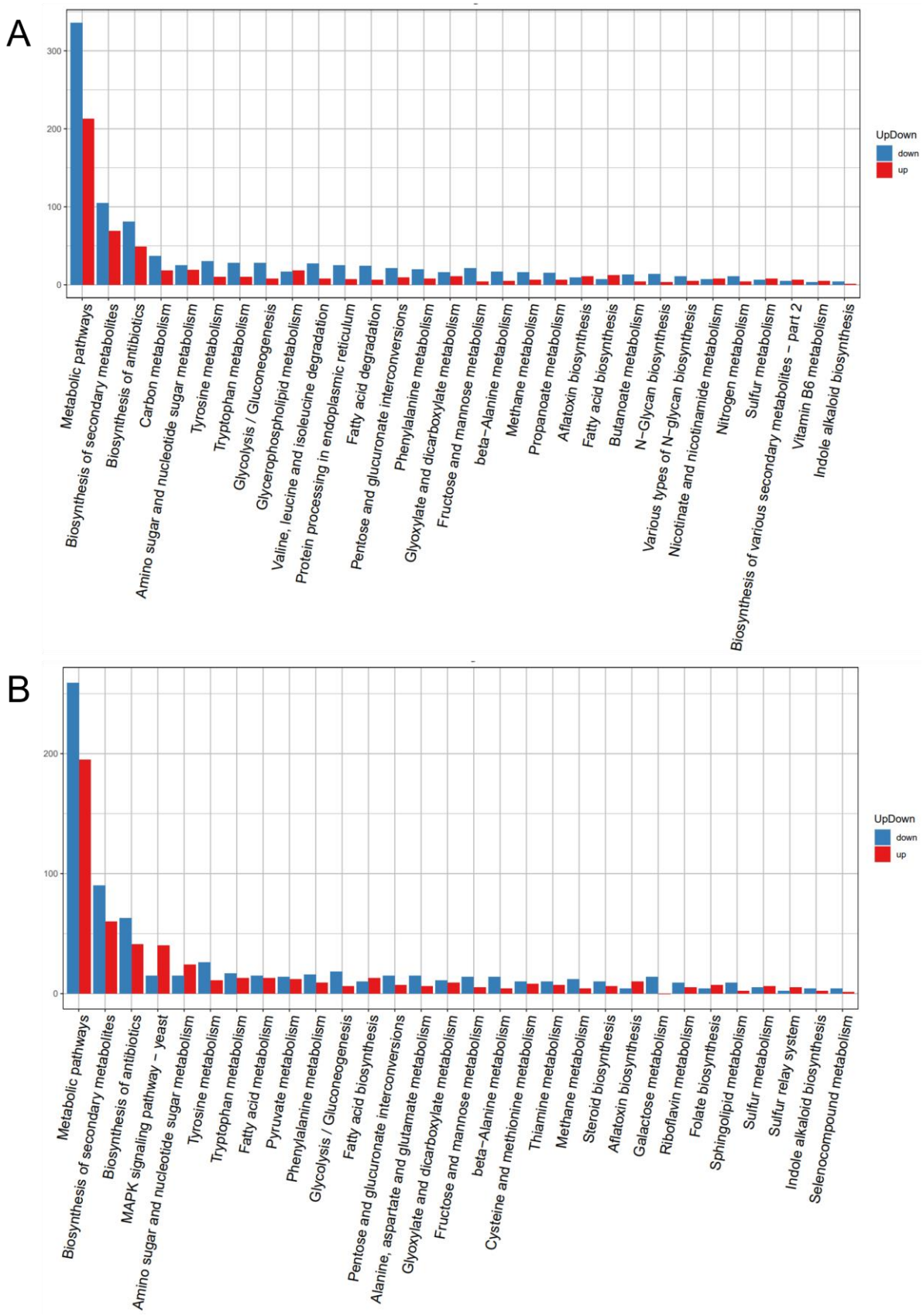

Figure 47: KEGG analyses of (A) wildtype (SKV103) and (B) *ΔhoxB* (SRFS26) in response to hydrogen peroxide Pathways induced by hydrogen peroxide in both strains are very similar, indicating that HoxB may specifically regulate genes responsible for combatting peroxide stress.

While most of the pathways affected in SKV103 met significance criteria at their respective Rich-Factor, most pathways affected in SRFS26 were not enriched significantly (Figure 48).

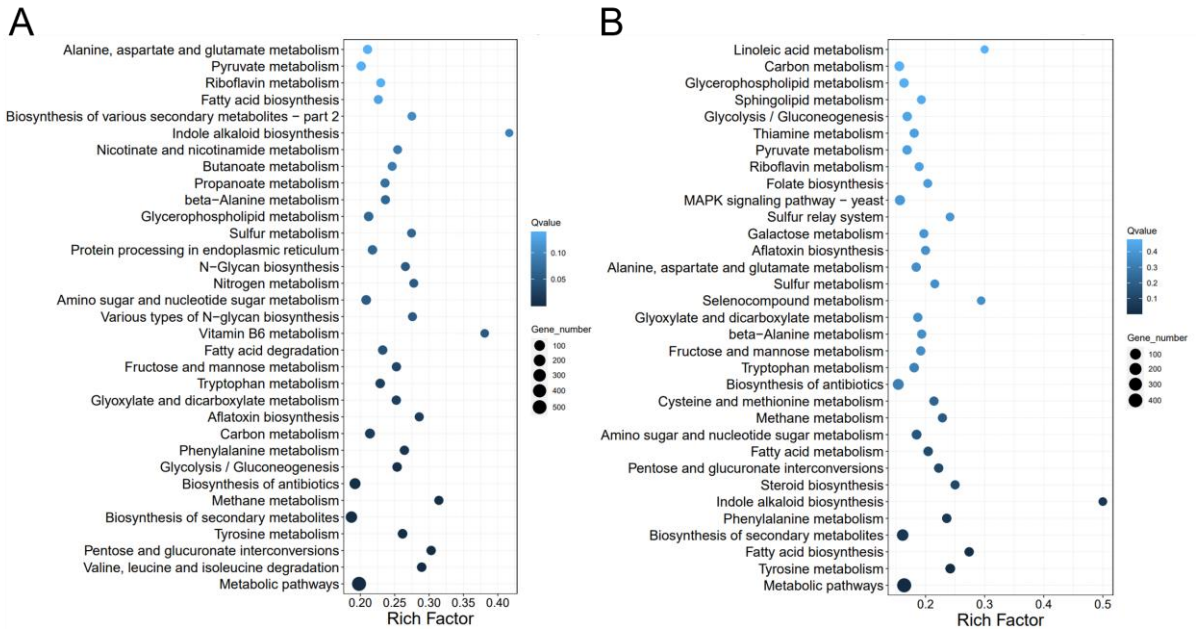

Figure 48: Significance of KEGG analyses in (A) wildtype (SKV103) and (B) *ΔhoxB* (SRFS26) in response to hydrogen peroxide Pathways induced by hydrogen peroxide in both strains sorted by Qvalue. The size of the blue circles indicates the number of genes regulated in that pathway while the darkness of the colouration indicates the significance.

The construction and comparison of SRFS40 involved some constraints in experimental design as the overexpression of *hoxB* required induction with L-threonine. For internal consistency, SKV103 was grown on the same media for this approach. As a result, the comparison between RNA-sequencing approaches regarding knockout and overexpression is limited due to the strains being grown on media with differences in composition and the overexpression-approach was deemed particularly artificial (Figure 49). Therefore, the only comparison performed involved analyzing whether genes that appeared as noteworthy in the comparison between SKV103 and SRFS26 also appeared differentially regulated in the comparisons between SKV103 and SRFS40. Of the 36 genes found in the RNA-sequencing detailed above (Table 1 and 2), 15 genes were found as well in this sequencing approach. The majority of these genes (11) were previously found to be upregulated uniquely in SKV103 while 4 genes were upregulated uniquely in SRFS26. Of the 11 genes, 8 (AN0170, AN9339, AN10220, AN7729, AN6304, AN8796, AN1882, and AN2846) were found to overlap between SKV103 and SRFS40, 2 (AN6779 and AN0754) remain

uniquely differentially regulated in SKV103 and 1 (AN0374) appeared uniquely regulated in SRFS40. Of the 4 genes previously uniquely regulated in SRFS26, 2 (AN8881 and AN0807) were found unique to SKV103, 1 (AN1314) was found unique to SRFS40 and 1 (AN0973) was found to overlap between SKV103 and SRFS40.

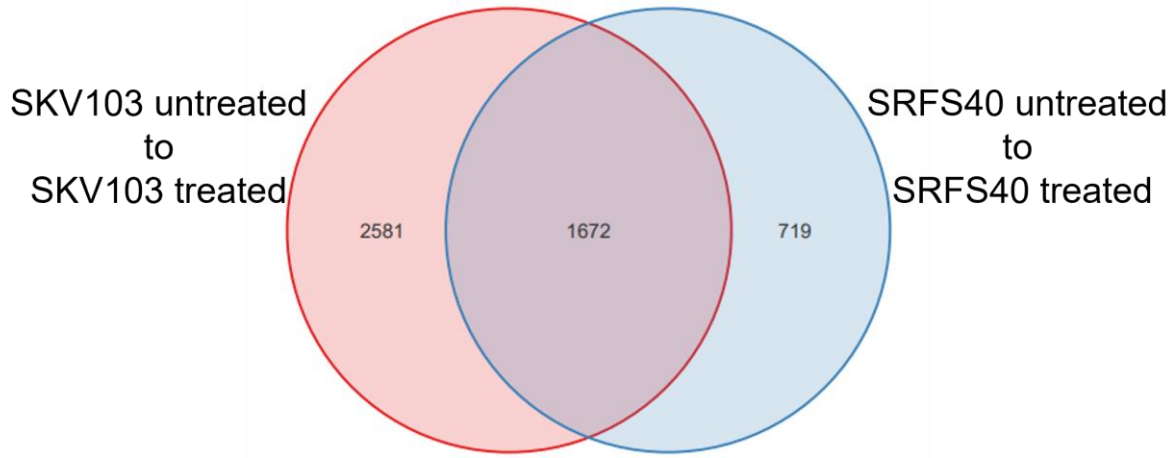

Figure 49: Comparative transcriptomic analysis between wildtype (SKV103) and *hoxB* overexpression (SRFS40) Wildtype and *hoxB* overexpression were treated with hydrogen peroxide. RNA-sequencing revealed that 2581 genes were regulated only in wildtype, 719 genes were regulated only in *ΔhoxB* and 1672 genes were regulated in both strains.

The reason for the appearance of some genes in the comparison is not immediately obvious. The similar regulation of 8 genes between SRFS40 and SKV103 relating to the resolution of hydrogen peroxide-induced oxidative stress further indicates that HoxB is involved in this resolution process by affecting the expression of the peroxiredoxin/thioredoxin-system, catalase B, putative peroxidases and potential components for the transport of glutathione and bilirubin, as well as modulation of TORC-signaling. The expression of 2 genes being unique to SKV103 may indicate that the expression of these genes may not be dependent on HoxB and may instead be a feature unique to SKV103. The remaining genes uniquely regulated in SKV103 in the knockout approach but not in the overexpression approach may be a result of the growth on different, more restrictive media. Similarly, the appearance of 4 genes found uniquely regulated in SRFS26 in the overexpression approach was unexpected. However, the genes AN0807 and AN0973 were downregulated in SKV103 and both strains respectively which is consistent with the results of the knockout approach. Only the appearance of AN8881 in SKV103 and AN1314 in SRFS40 may be a result of inconsistent experimental conditions.

3. Discussion

In this work, a heme oxygenase-like protein termed HoxB and its corresponding gene *hoxB* were investigated regarding their functionality in *A. nidulans*. This examination was performed bioinformatically and biochemically, using various methodologies of molecular biology. The protein was identified previously without being thoroughly investigated and bears similarity to the heme oxygenase-like protein HoxB in *A. alternata* (Streng et al., 2021; Streng, 2020). In this work, HoxB of *A. nidulans* was shown to resemble TenA_E-like proteins based on sequence and docking simulations with potential ligands of these proteins. Furthermore, it was shown to conditionally localize in cytoplasm and nucleus (Figure 22 & 34), partially affect phytochrome-dependent red light signaling (Figure 21), likely govern the resistance to peroxide through transcriptional modulation (Figure 41 - Figure 45; Table 1 & Table 2) and to interact with the blue light receptor cryptochrome *in vivo* (Figure 28 & 33).

3.1 HoxB-like proteins are functionally distinct in different organisms

Particularly in context of previous work, some results appear counterintuitive at surface level. HoxB of *A. alternata* was found to be required for the expression of the *ccgA* gene in response to red light, localize to the mitochondria when expressed in *A. nidulans* and interact in a homomer and with phytochrome in vivo when expressed in *A. nidulans*. Furthermore, the *hoxB* knockout showed increased resistance to menadione and hydrogen peroxide while showing decreased resistance to tert-butyl hydroperoxide (Streng et al., 2021; Streng, 2020). In this work it was found that HoxB is partially required for the expression of *ccgA* in response to red light while having no effect on the expression of *ccgB* and *conJ* under red light conditions (Figures 41-43). The localization of HoxB was found to be partially cytoplasmic and partially nuclear (Figures 22 & 34) while it was shown to form a homotetramer *in vivo* and *in vitro* (Figures 23 & 24) and interact with cryptochrome *in vivo* (Figure 28 & 33). An interaction with phytochrome remained unlikely *in vivo* (Figure 27). The partial functional overlap and partially opposite functions of HoxB in *A. nidulans* may result from the presence of two HoxB-like proteins in *A. alternata* (Figure 12 & 20). The previously investigated protein termed HoxB has a length of 509 amino acids which are sectioned into a central hemeO-like domain and N- and C-terminal extensions of unpredicted purpose. The second HoxB-like protein consisting of 331 amino acids

contains a similar hemeO-like domain but lacks extensions at both termini (Figure 50). While sequence homology of HoxB in *A. nidulans* is slightly more consistent with the previously described HoxB of *A. alternata* (approx. 42% identity) than the shorter HoxB-like protein (approx. 35% identity), the shorter HoxB-like protein resembles HoxB of A. nidulans more closely due to the nearly absent terminal extensions. It was shown in this work that HoxB of A. nidulans forms a homotetramer (Figure 24). Considering that the hemeO-like domain is sufficient for homotetramer formation, it is feasible that both HoxB-like proteins in *A. alternata* interact in a similar tetramer, either homo- or heterotetrametric. This may convey partially opposite phenotypical effects due to the shorter HoxB-like protein of *A. alternata* potentially being the proper functional homologue of HoxB of *A. nidulans*. Alternatively, the interaction between both proteins in *A. alternata* may convey changes in localization and allow additional or different protein interactions leading to different phenotypes. These speculations remain conjecture until an interaction between the proteins in *A. alternata* and the knockout phenotype of the second HoxB-like protein are investigated.

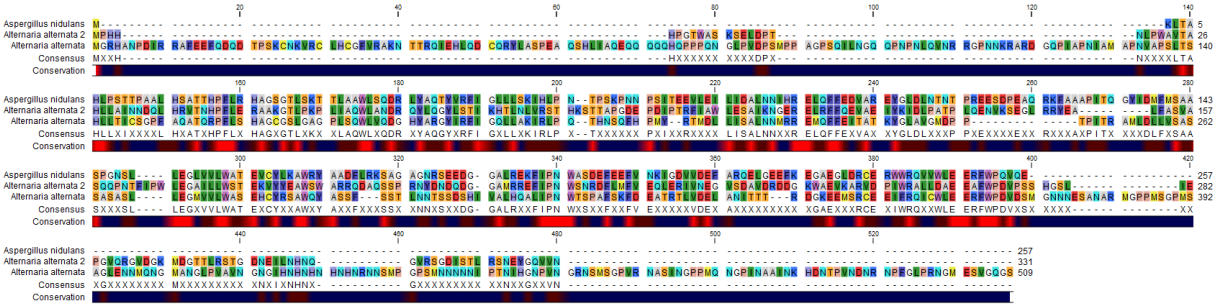

Figure 50: HoxB of *A. nidulans* may not be the functional homologue of previously described HoxB of *A. alternata* Alignment of *A. nidulans* HoxB with 2 HoxB-like proteins from *A. alternata*. The central domains of both proteins of *A. alternata* are conserved. However, the previously described HoxB (509 aa) (Streng et al., 2021) contains long N- and C-terminal extensions which may explain functional differences.

HoxB of A. nidulans was shown to resemble other TenA_E-like proteins (Figure 17 – Figure 19). While there have been speculations that these proteins are involved in thiamine metabolism or salvage, there are limited data supporting these hypotheses. Specifically, a cavity for MP5 which resembles the pyrimidine component of thiamine was found in a TenA homologue of P. furiosus and TenA_E in *A. thaliana* and maize were shown to have limited catalytic activity in a thiamine-related metabolic pathway centered on HMP despite lacking an active-site cysteine residue found in enzymes which catalyze similar reactions (Benach et al., 2005; Zallot et al, 2014). In this work, HoxB was shown to potentially bind MP5 akin to TenA_E of *P. furiosus* (Figure 18) or

HMP akin to *B. subtilis* and *A. thaliana* (Figure 17). However, the sensitivity to peroxides present in the *hoxB* knockout was not resolved through the addition of thiamine (Figure 38), indicating that the observed phenotype is not the result of dysfunctional thiamine metabolism. Furthermore, an interaction with cryptochrome was shown *in vivo* (Figure 28) which underlines the relation of HoxB with oxidative stress signaling as cryptochromes are known to act during periods of – mostly blue light-related – oxidative stress and to be a source of oxidative stress themselves through the production of nuclear ROS during their photocycle which have signaling functions in *A. thaliana* (Kleine et al., 2007; Bluhm et al., 2008; El-Esawi et al., 2017).

3.2 Potential signaling function of HoxB in *A. nidulans*

However, it remains unclear in which manner, directly or indirectly, and through which modes of action an interaction between HoxB and CryA may facilitate the observed effects. Considering that the direct interaction between both proteins was shown *in vivo* in multiple genetic backgrounds (Figure 28 & 33) it is somewhat likely that a direct instead of an indirect interaction is taking place. This direct interaction could not be confirmed with certainty *in vitro* (Figure 29 & 30); hence an indirect interaction still needs to be considered. Since a partially similar pattern of transcriptional changes between *hoxB*-overexpression and *cryA*-knockout was observed (Figure 41 - Figure 45), an interaction in the same signaling pathway is likely either way. Considering HoxB also resides outside the nucleus while CryA of *A. nidulans* localizes to the nucleus exclusively (Bayram et al., 2008a), these data may suggest a model in which HoxB has a negative downstream influence on CryA-signaling regardless of a direct or indirect nature of the interaction.

One consideration for specific HoxB activity may be a peroxide-sensor function with subsequent translocation to the nucleus. Typical peroxide sensors like bacterial OxyR and yeast YAP1 activate through oxidation of cysteine residues by reacting with peroxides to form disulfide bonds (Zheng et al., 1998 & Okazaki et al., 2007). HoxB does contain 2 highly conserved cysteine residues (Figure 14) and does form homotetramers (Figure 24) akin to a proposed model for OxyR (Jo et al., 2015). The conserved cysteine residues of HoxB are 15.4 Ångström apart from each other within the proposed model and the relevant cysteine residues of OxyR were found to be 17 Ångström apart (Choi et al., 2001) while the general distance of cysteines engaging in

disulfide bonds is between 3 and 7.5 Ångström (Gao et al., 2020), likely necessitating an unexplained conformational change prior to potentially generating a disulfide bond (Figure 14 & 51A). However, HoxB was not found to have DNA-binding domains or other characteristics of transcription factors like OxyR or YAP1 (Figure 51B & Figure 55) indicating that unlike OxyR or YAP1, HoxB may rely on other proteins to enact its transcriptional modulation. Assuming this potential functionality of HoxB, it may be feasible that HoxB captures ROS produced by CryA during its photocycle (Arthaut et al., 2017). These ROS produced by CryA specifically have been found to be involved in regulation in *A. thaliana* and *D. melanogaster* (Arthaut et al., 2017; El-Esawi et al., 2017). Notably, work performed by Alexander Blumhofer (unpublished work) has shown that CryA produces a diminished amount of ROS during its photocycle in the presence of HoxB. However, in this model, HoxB would act downstream of CryA which may be unlikely due to aforementioned factors.

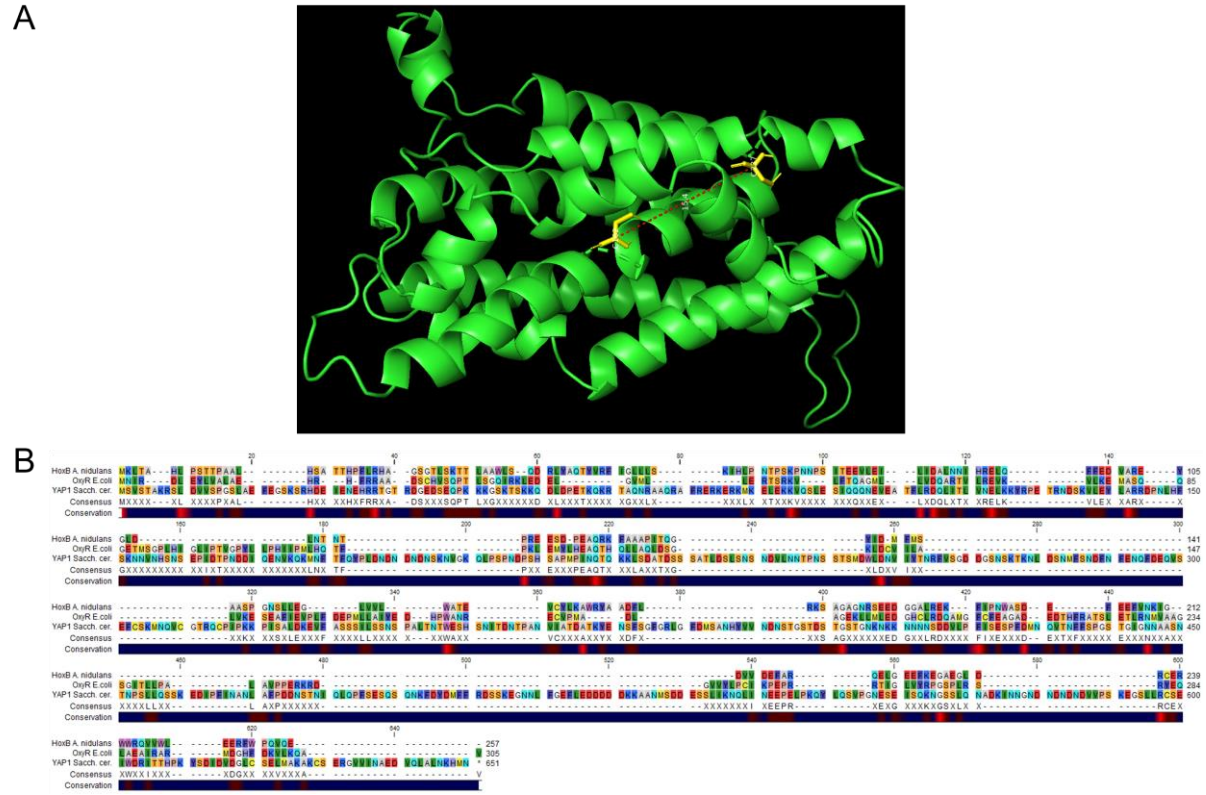

Figure 51: HoxB may detect peroxide stress through cysteine oxidation (A) Two conserved cysteines of HoxB are located within 15.4 Ångström of each other within the AlphaFold model. Comparatively, the distance between 2 conserved cysteines used for peroxide detection within bacterial OxyR are 17 Ångström apart. (B) Sequence alignment of HoxB, OxyR of *E. coli* and Yap1 of *S. cerevisiae*. HoxB does not share the DNA-binding features of OxyR and Yap1.

Alternatively, HoxB may simply function in relaying oxidative stress without a sensory function. In this context, the potential translocation from cytoplasm to nucleus is of particular interest (Figure 22 & 34). Although the translocation was not directly observed in one strain, it is implicated due to the presence of HoxB-GFP signal in cytoplasm and nucleus in what appeared to be similar ratios in wildtype while the signal appeared primarily in the cytoplasm and was rarely observed in the nucleus in a VeA-deficient background.

Regarding the facilitation of the nuclear translocation of HoxB, the modification of the protein needs to be considered. Firstly, the size of the HoxB monomer is 29.16 kDa while the tetramer was found to appear with a size of 122.14 kDa (Figure 24). The maximum size of proteins able to freely diffuse into the nucleus via the nuclear pore is generally considered to be around 50 kDa although ranges between 30 kDa and 60 kDa have been discussed (Shimozono et al., 2009). Therefore, diffusion of the monomeric form into the nucleus may be possible while the diffusion of the tetrameric form would be restricted. The indication of an interaction between HoxB and CryA *in vivo* but not *in vitro* may be indicative of the monomeric, but not the tetrameric form of HoxB interacting with CryA since the necessary conditions for release of the tetramer are not present *in vitro* may match with the concept that disruption of a tetramer enables translocation into the nucleus. The specific mechanism may involve interaction with an unknown interaction partner or posttranslational modification. In *A. nidulans*, stress signaling commonly involves MAPK pathways (Kanamaru, 2011; Hagiwara et al., 2016; Yu et al., 2019). Particulary, the histidine kinases HysA and FphA are involved in control of reactive oxygen species and the related stimuli light and temperature sensing in *A. nidulans* respectively (Hayashi et al., 2014; Yu et al., 2016). In this work, 2 potential phosphorylation sites, T31 and S141 of HoxB were identified based on sequence homology to distantly related proteins (Figure 14 & 19). Although comparison between such distantly related proteins is questionable, other residues involved in ligand binding, such as D44, E94 and Y163, were found to be conserved as well, implicating that other conserved residues may be of similar importance to HoxB functionality. Notably, previous work by Christian Streng (unpublished work) has shown the removal of a C-terminal segment of HoxB in *A. alternata* to be sufficient to induce nuclear localization. While some amino acids were found conserved at the C-terminus of HoxB in *A. nidulans*, the low conservation between residues in the residues of the C-terminal extension of HoxB in *A. alternata* and residues of the HoxB C-terminus in

A. nidulans indicate that the C-terminal residues found - E248, F251 and W252 (Figure 19) - are not involved in nuclear translocation and may fulfil another unknown purpose.

Regarding the apparent contribution of VeA to HoxB translocation, some contrary data was obtained, indicating that it's involvement may be complex and require some further research to elucidate. While VeA appears to impact the dynamics of localization of HoxB in cytoplasm and nucleus (Figure 22 & 34) where HoxB is proposed to fulfil its main functions, the expression pattern of oxidative stress genes in a *veA1* background mimics the HoxB overexpression (Figure 41 – Figure 45). One possible explanation involves a potential mechanical similarity to YAP1. This leucine zipper contains an active nuclear export sequence which causes it to predominantly localize to the cytoplasm under normal conditions (Kuge et al., 1997). However, upon formation of disulfide bonds through oxidation by peroxide, the export sequence becomes inactive, causing a dominantly nuclear localization. Using the LocNES-Tool (Xu et al., 2015) a potential export sequence of HoxB can be found (Figure 52).

Sequence	Score
QDRLYAQTYVRFIGL	0.148
RLYAQTYVRFIGLLL	0.306
AQTYVRFIGLLLSKI	0.058
TYVRFIGLLLSKIHL	0.075
PNNPSITEEVLEILI	0.242
TEEVLEILIDALNNI	0.262
ILIDALNNIHRELQF	0.500
LIDALNNIHRELQFF	0.239
ASDEFEEFVNKIGDV	0.030
FEEFVNKIGDVVDEF	0.014

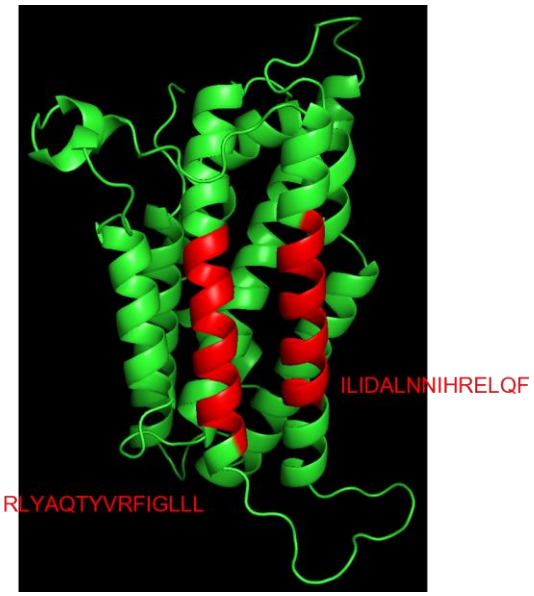

Figure 52: Nuclear localization of HoxB may be regulated by an exportin The LocNES-Tool trained on the nuclear export sequences of human Crm1 predicted a potential export sequence (score above 0.4) in a conserved region of HoxB. Another potential sequence with lower certainty is located next to the sequence with the highest score within the AlphaFold model of HoxB.

This sequence lies within a region (position 83 to 98) highly conserved in other filamentous fungi (Figure 14). Considering no direct interaction between HoxB and VeA could be shown in this work and work performed by Alexander Blumhofer (unpublished work), VeA may be involved in regulating the expression or activity of a protein which

uses the potential nuclear export sequence to regulate HoxB localization. A possible exporting protein may be KapK (Markina-Iñarrairaegui et al., 2011).

VeA, in tandem with *atfB*, was found to be important for catalase and thioxiredoxin expression to convey resistance to hydrogen peroxide in *A. flavus* (Baidya et al., 2014). Both genes were detected to be upregulated in wildtype but not in the *hoxB* knockout in RNA-sequencing in this work (Table 1 & Table 2), indicating that HoxB may be involved in oxidative stress regulation in this pathway. Notably, this pathway was found to regulate both oxidative stress response and secondary metabolism in *A. flavus* and *A. parasiticus* (Cary et al., 2015; Roze et al., 2011) which matches with the changes to secondary metabolism in the *hoxB* knockout that were observed in this work. In *A. nidulans*, both AtfA and AtfB have been implicated for their regulation of the response to oxidate stress induced by menadione with AtfA being the dominantly responsible transcription factor (Kocsis et al., 2023). Particularly, transcription of cryptochrome, the red-light stress-related gene *ccgA* and catalase A was found to depend on AtfA. Consequently, relating to this work, the observed transcriptional effects on *ccgA* and catalase may result from HoxB addressing AtfA rather than AtfB. Furthermore, cryptochromes commonly engage in regulatory loops to tune circadian clock feedback loops, but also to finetune red-light responses produced downstream of AtfA activity (Lopez et al., 2021; Yu et al., 2021). Therefore, the interaction between HoxB and CryA (Figure 23) in conjunction with HoxB overexpression and CryA deletion producing similar transcriptional changes (Figure 41 - Figure 45) indicate that HoxB may fulfil the role of a negative regulator of CryA activity in modulating both red-light sensing and oxidative stress perception along AtfA-related signaling. Previously described mechanisms of red-light dependent AtfA modulation downstream of the HOG pathway use the SakA protein which translocates to the nucleus to modulate AtfA function (Yu et al., 2016). Consequently, HoxB may likely utilize another MAPK pathway if it is involved in some phosphorelay system.

Some possible functions of HoxB, such as the involvement in a CryA- and AtfA related feedback loop, relay of information as part of a MAPK signaling pathway or sensing of oxidative stress through oxidation of cysteines are likely mutually exclusive due to the stark contrast of these concepts. Although speculative in nature, the hypotheses around functionalization of HoxB regarding protein modulation and signaling pathway

involvement presented based on data produced in this work and literature research provide multiple avenues to elucidate the specifics of HoxB action in future.

3.3 HoxB may modulate CryA function

The question of HoxB potentially being a negative regulator of CryA requires further consideration. Although CryA of *A. nidulans* itself has not previously been shown to directly impact oxidative stress signaling, it has been shown to impact fungal development by modulating gene transcription and have some function in DNA repair as a bimodal, transitory protein acting similar to more distinct CRY-DASH proteins while retaining some functionality as a photolyase (Bayram et al., 2008a). Nevertheless, cryptochromes rely on their chromophores to function as photolyases or regulatory proteins through photoactivation (Li et al., 2010; Hitomi et al., 2000; El-Esawi et al., 2017). Upon modeling HoxB with a variety of ligands it was determined that some core amino acids may aid in binding MP5 or HMP as its ligand (Figure 17 & Figure 18). Primarily, these molecules consist of an amino-methyl-pyrimidine element with a variable side group. The pyrimidine moiety within the adenine component of the FAD-chromophore bound by cryptochrome closely, although only partially, resembles this element (Figure 53).

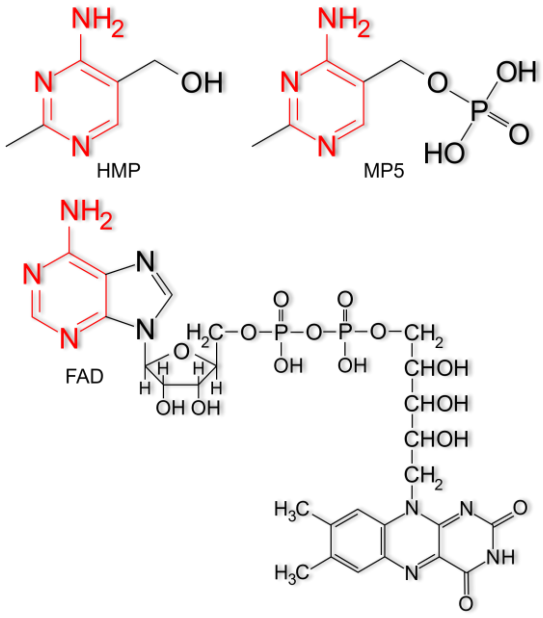

Figure 53: HoxB may bind FAD The pyrimidine moiety within FAD partially resembles MP5 and HMP, indicating a potential for association with the molecule.

The provided models appear to heavily rely on association with the ligands through pi-stacking and polar interactions of the pyrimidine moieties and amino groups of MP5 and HMP.

Feasibly, the interaction between HoxB and CryA may revolve around HoxB accessing the FAD chromophore of CryA. The FAD chromophore of cryptochrome is typically not covalently bound to the protein (Wang et al., 2015) and HoxB modulating availability of FAD may enable some dynamic shifting of chromophore-associated effects.

Considering the size difference between the complete molecules, it is not possible to successfully model FAD with the model of HoxB obtained using AlphaFold (chapter 2.2) because the binding cavity for MP5 and HMP was predicted buried within the protein. Consequently, a shift of surface residues near the binding cavity would be required to potentially enable binding of FAD. Until the possibility of HoxB binding FAD or interacting with FAD-binding proteins relating to oxidative stress to modulate their activity is experimentally explored, other standard modes of action of HoxB still need to be considered. For instance, cryptochrome C-terminal extensions have been tightly linked to proper cryptochrome activity with C-terminal mutants still undergoing a normal photocycle while being unable to produce corresponding effects (Chaves et al., 2006; El-Esawi et al., 2017). Consequently, masking of the cryptochrome C-terminus by HoxB may affect proper cryptochrome functionality and may result in the transcriptional effects observed, especially regarding HoxB overexpression.

3.4 Proposed model of HoxB function

Using the data gathered in this work, as well as the hypotheses presented above, a proposed model of HoxB function and activity may be assembled (Figure X). These models rely on speculations proposed above and further experimentation may elucidate the specific mechanics of HoxB signaling. Specifically, this work was focused on describing the HoxB-related phenotypes involving peroxide stress and how they are caused transcriptionally by regulating the expression of stress genes such as catalase, thioredoxin and *ccgA*. These genes, and cryptochrome, are expressed under the control of AtfA in *A. nidulans*. The speculative portion of the model involves the dynamics and purpose of HoxB interacting with cryptochrome as well as its localization to nucleus and cytoplasm. A CryA/HoxB-complex may be involved in regulating the

expression of the stress genes. HoxB may regulate CryA by either shifting its FAD-binding dynamics, binding to its C-terminus or capturing ROS produced during its photocycle. The dynamics of cytoplasmic and nuclear translocation of HoxB may depend on generation of disulfide bridges by ROS or phosphorylation in a MAPK pathway responding to peroxide stress and export from the nucleus through an unknown protein under control of the regulatory protein VeA.

Clarification of these hypotheses may be obtained through further experimentation. Verification of the AtfA-dependence of the observed phenotypes may be obtained through interaction studies of HoxB and CryA with AtfA via bimolecular fluorescence complementation and Co-immunoprecipitation, as well as transcriptional studies in double knockout mutants of HoxB or CryA and AtfA similar to those presented in this work. The presented proposition includes the active form of HoxB being a monomeric state. Assuming that a generation of disulfide bonds is a driving factor for transitioning to the monomeric state, purified HoxB protein may transition upon being exposed to an oxidizing agent, such as hydrogen peroxide. This may be shown using size exclusion chromatography. Similarly, oxidation of HoxB may allow an interaction between HoxB and CryA *in vitro*. If HoxB binding FAD in a spectrometric analysis may not occur naturally, it may occur upon oxidation of HoxB. If oxidation of HoxB does not result in monomerization or functionalization of HoxB, other potential avenues include the introduction of phosphomimetic mutations at the positions proposed above or the point mutations of amino acids proposed to be involved in tetramerization. Although potentially less stable, these mutations could also be studied *in vivo* for their localization and phenotypes upon introduction to the knockout strain. The translocation dynamics of HoxB may be elucidated by investigating the localization of protein with mutations introduced in the proposed export sequence or through interaction studies of with potential exportins, such as KapK.

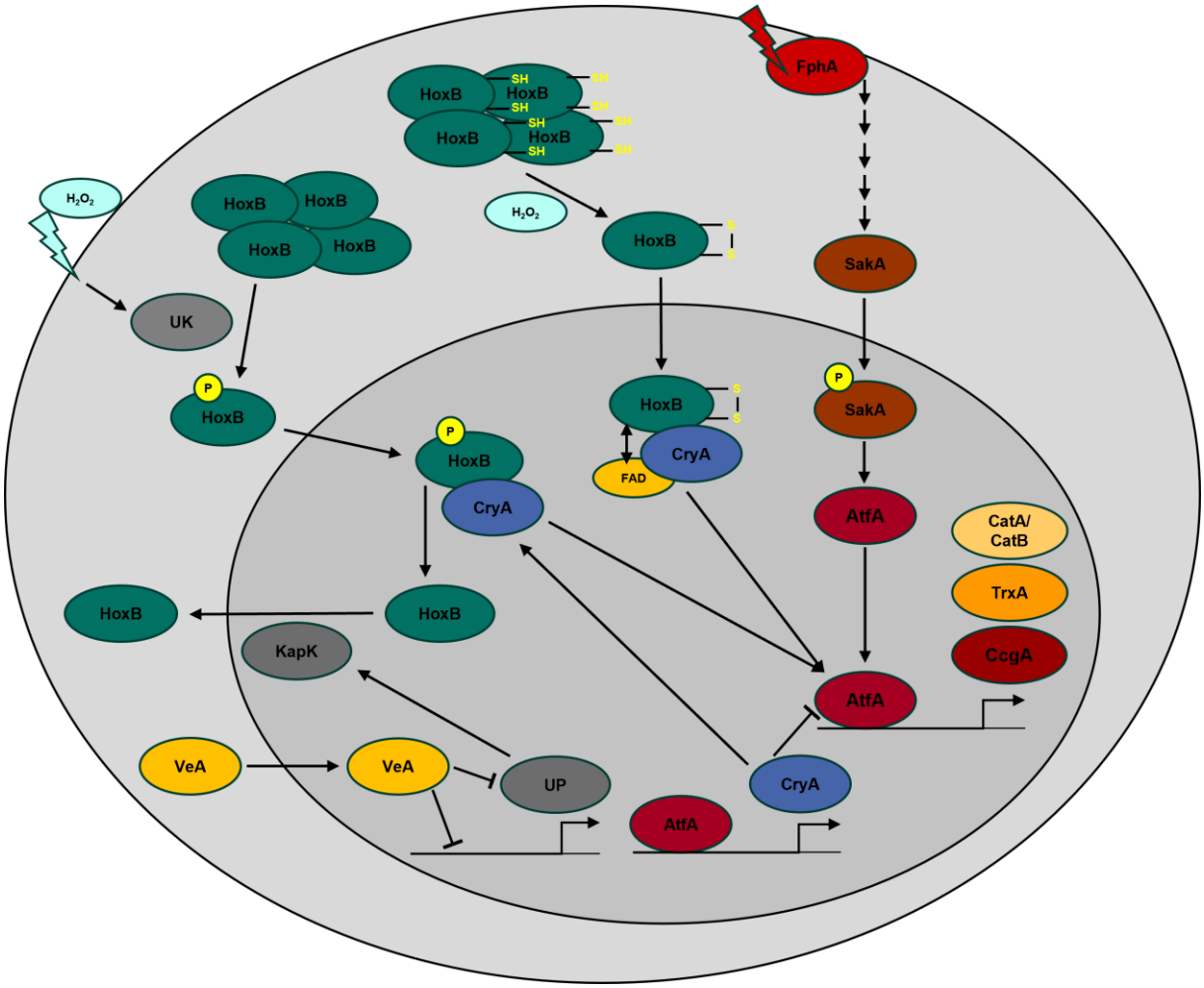

Figure 54: Proposed model of HoxB action Expression of red-light related stress genes, oxidative stress genes and CryA may depend on AtfA. In turn, CryA may repress AtfA unless it interacts with and is inhibited by HoxB. HoxB may regulate CryA through association with its chromophore or interaction with the protein itself. Activation of HoxB may depend on oxidation of conserved cysteine residues by peroxide or phosphorylation of the protein by an unknown kinase (UK) in response to peroxide induced stress. Activation of HoxB may cause a shift of the tetrameric to monomeric form, allowing for nuclear localization and interaction with CryA. Export of the HoxB monomer from the nucleus upon inactivation may involve activity of an exportin like KapK. Export may be regulated by VeA through transcriptional or direct regulation of an unknown protein (UP).

4. Materials and Methods

4.1 Chemicals

All chemicals, unless stated otherwise, were supplied by Roth (Karlsruhe, Germany), Biozym (Hessisch Oberdorf, Germany), Invitrogen (Karlsruhe, Germany), Roche (Mannheim, Germany), Sigma Aldrich (Steinheim, Germany), Biomol (Hamburg, Germany), Thermo Fisher (Waltham, USA) and Applichem (Darmstadt, Germany). Protein markers and restriction enzymes were supplied by New England Biolabs (Frankfurt, Germany) and Thermo Fisher. Oligonucleotides were supplied by Eurofins Genomics (Ebersberg, Germany).

4.2 Devices and Tools

All used devices are listed below in Table 3. Unless stated otherwise, all consumable goods and materials were supplied by Sarstedt (Nümbrecht, Germany).

Table 3: List of used devices

Device	Model	Supplier
Labcycler Basic	3x21	SensoQuest GmbH
	48	SensoQuest GmbH
Realtime-PCR Cycler	CFX Connect	BioRad Laboratories GmbH
Autoclave	3870EL V-D	Biomedis Laborservice
	3870EL VCG-D	GmbH
Thermoblock	Thermomixer 5436	Eppendorf SE
	Thermomixer comfort	Eppendorf SE
Incubator	HT Infors Minitron	Infors AG
	HT Infors Electron	Infors AG
	New Brunswick™ Innova® 44	Eppendorf SE
	BB6220	Heraeus Holding GmbH
	B40	Memmert GmbH & Co.KG
	ICP600	Memmert GmbH & Co.KG
Shaker	ROTAMAX 120	Heidolph Instruments
	VortexGenie™ 1 Touch	Scientific Industries Inc.
Spectrophotometer	ND-1000	NanoDrop

Spectrofluorometer	QuBit Fluorometer	Invitrogen
Scale	440-47N	Kern & Sohn GmbH
	PCB1000-2	Kern & Sohn GmbH
	R-200 D	Sartorius
	CS 200	OHAUS
Centrifuge	Universal 320R	Andreas Hettich GmbH & Co.K
	5415 R	Eppendorf SE
	Fisher AccuSpin Micro 17	Thermo Fisher Scientific
Microscope	AxioImager Z1	Zeiss
	AxioCamMR	
	Airyscan	
	Eclipse E200	Nikon GmbH
Gel electrophoresis system	PerfectBlue™ Gelsystem Mini L	VWR Peqlab
	Chemi-Smart 5100	VWR International GmbH
Gel documentation system	GP-FAS-V	NIPPON Genetics Europe
Homogenizer	Emulsiflex-C3	Avestin Europe GmbH
Compressor	6-15	Jun-Air
SDS-PAGE and Western Blot Equipment	Power Pac Basic	Bio-Rad Laboratories GmbH
	Mini-PROTEAN Tetra Vertical Electrophoresis Cell	
	Mini Trans-Blot® Cell	
Stirrer (magnetic)	MR 3000	Heidolph Instruments GmbH & Co.KG
	80	Kniese Apparatebau GmbH
pH-meter	HI 208	Hanna Instruments GmbH
Waterbath	GFL 1002	LAUDA-GFL GmbH
Water purification system	PURELAB® flex Reinstwasseranlage	ELGA LabWarer Veolia Water Technologies GmbH
Fast Gene Gel/PCR Extraction Kit		NIPPON Genetics

NucleoSpin Plasmid EasyPure Kit	Macherey & Nagel GmbH & Co.KG
Zymoclean Gel DNA Recovery Kit	Zymo Research
Luna® Universal One-Step RT-qPCR Kit	New England Biolabs
Vivaspin 30,000 MWCO	Sartorius

4.3 Media and Solutions

All used media and solutions are listed below in Table 4. Additives used in combination with these media are listed in Table 5.

Table 4: List of used media

Medium	Component	Composition
E. coli		
Luria Bertani (LB)	Trypton	10 g/l
	Yeast Extract	5 g/l
	NaCl	5 g/l
	(Agar-Agar)	(15 g/l)
		pH7.5
A. nidulans		
Minimal medium (MM)	Glucose	20 g/l
	20x Salt Stock	50 ml/l
	1000x Trace Element Solution	1 ml/l
	(Agar-Agar)	(15 g/l)
		pH6.5
Minimal medium regeneration (MMR)	Saccharose	342 g/l
	Glucose	20 g/l
	20x Salt Stock	50 ml/l
	1000x Trace Elements	1 ml/l
	Agar-Agar	15 g/l

		pH6.8
Minimal medium regeneration Top	Saccharose	342 g/l
	Glucose	20 g/l
	20x Salt Stock	50 ml/l
	1000x Trace Elements	1 ml/l
	Agar-Agar	7.5 g/l
		pH6.8
Yeast Agar Dextrose (YAG)	Yeast Extract	5 g/l
	Glucose	10 g/l
	1000x Trace Elements	1 ml/l
	$MgSO_4$ x 7 H_2O	2.47 g/l
	1000x Vitamin Solution	1 ml/l
		pH6.5
20x Salt Stock	$NaNO_3$	120 g/l
	KCl	10.4 g/l
	$MgCl_2$ x 7 H_2O	10.4 g/l
	KH_2PO_4	30.4 g/l
1000x Trace Elements	$ZnSO_4$ x 7 H_2O	22 g/l
	H_3BO_3	11 g/l
	$MnCl_2$ x 4 H_2O	5 g/l
	FeSO4 x 7 H2O	5 g/l
	CuSO4 x 5 H2O	1.6 g/l
	$(NH_4)_6Mo_7O_{24}$ x 4 H_2O	1.1 g/l
	$CoCl_2$ x 5 H_2O	1.6 g/l
	Na_4-EDTA	50 g/l
		pH6.8
1000x Vitamin Solution	Biotin	0.01 g/l
	Pyridoxine	0.01 g/l
	Thiamin	0.01 g/l
	Riboflavin	0.01 g/l
	para-Aminobenzoic acid (PABA)	0.01 g/l
	Nicotinic acid	0.01 g/l

Table 5: List of used media additives

Additive	Concentration
E. coli	
Ampicillin	100 µg/ml
Kanamycin	50 µg/ml
A. nidulans	
Uridine	1 g/l
Uracil	1 g/l
Pyridoxin-HCl	0.05 mg/l
PABA	0.02 mg/l
L-Arginine	0.1 g/l

4.4 Organisms

All organisms used for this work are listed below in Table 6.

Table 6: List of all used and generated strains

Strain	Genotype	Source
SKV103	*pyrG89, veA+, pyroA4*	Vienken et al., 2005
SJR2	*pyrG89, veA+, pyroA4*	Herr & Fischer, 2014
RSMO11	*ΔargB::trpCΔB, pabaA1 yA2, veA+,*	Stringer et al., 1991
SRF200	*yA1, pyrG89, argB2; pyroA4;*	Toews et al., 2004
SJP1	*ΔfphA, pyrG89, veA+, pyroA4*	Purschwitz et al., 2008
SCK44	*ΔcryA, yA1, pabaA1; argB2; pyroA4; nkuA::bar*	Röhrig et al., 2013
SAUL11	*ΔcryA, veA+, pyroA4*	Alexander Landmark
SRFS16	*ΔhoxB* in SJR2	This Work
SRFS17	*alcA:GFP-hoxB* (pRS35) in SKV103	This Work
SRFS18	*alcA:GFP-hoxB(Δctr)* (pRS38) in SKV103	This Work
SRFS19	*hoxB+* (pRS48) in SRFS16	This Work

SRFS20	*alcA:YFPN-hoxB* (pRS47) and *alcA:YFPC-hoxB* (pRS46) in SKV103	This Work
SRFS21	*alcA:YFPN-hoxB* (pRS47) and *alcA:YFPC-fphA* (pJP5) in SKV103	This Work
SRFS22	*alcA:YFPC-hoxB* (pRS46) and *alcA:YFPN-cryA* (pAUL4) in SKV103	This Work
SRFS23	*alcA:YFPN-hoxB* (pRS47) and *alcA:YFPC-cryA* (pAUL3) in SKV103	This Work
SRFS24	*alcA:YFPC-fphA(phot.)* (p1605) and *alcA:YFPN-hoxB* (pRS47) in SKV103	This Work
SRFS25	*alcA:YFPC-lreA* (p1626) and *alcA:YFPN-hoxB* (pRS47) in SKV103	This Work
SRFS26	*ΔhoxB* (SRFS16 x RSMO11)	This Work
SRFS27	*ΔhoxB*, *pyroA4* (SRFS16 x RSMO11)	This Work
SRFS28	*ΔhoxB*, *pyroA4, pabaA1* (SRFS16 x RSMO11)	This Work
SRFS29	*hoxB+* (pRS48) in SRFS27	This Work
SRFS30	*P(nat):GFP-hoxB* (pRS49) in SJR2	This Work
SRFS31	*alcA:GFP-hoxB:trpC* (pRS68) and a*lcA:mCherry:stuA(NLS):trpC* (pJW18) in SKV103	This Work
SRFS32	*alcA:GFP-hoxB:trpC* (pRS68) and *alcA:mCherry:stuA(NLS):trpC* (pJW18) in SRF200	This Work
SRFS33	*alcA:YFPN-hoxB* (pRS47) *and alcA:YFPC-cryA* (pAUL3) in SRF200	This Work

SRFS40	*alcA:hoxB:trpC* (pRS69) in SKV103	This Work
SRFS41	*P(nat):GFP-hoxB* (pRS67) in SKV103	This Work
SRFS42	*alcA:GFP-hoxB:trpC* (pRS68) in SKV103	This Work
SRFS43	*alcA:3xHA-hoxB:trpC* (pRS70) in SKV103	This Work
SRFS44	*alcA:GFP-hoxB:trpC* (pRS68) and *alcA:3xHA-hoxB:trpC* (pRS70) in SKV103	This Work
SRFS45	*alcA:3xHA-cryA:trpC* (pAUL7) in SKV103	This Work
SRFS46	*alcA:GFP-hoxB:trpC* (pRS68) and *alcA:3xHA-cryA:trpC* (pAUL7) in SKV103	This Work
SRFS47	*alcA:GFP-cryA:trpC* (pAUL6) in SKV103	This Work
SRFS48	*alcA:GFP-hoxB:trpC* (pRS68) and *alcA:mCherry:stuA(NLS):trpC* (pJW18) in SKV103	This Work
E. coli BL21 (DE3)	F– *omp*T *hsd*SB (rB– mB–) *gal* *dcm* (DE3)	Invitrogen (Karlsruhe, Germany)
E. coli Top10	F- *mcrA* Δ(*mrr-hsd*RMS-*mcr*BC), *Φ80lacZΔM15* *ΔlacX*74, *rec*A1, *araD139*Δ (*araleu*)7697, *gal*U, *gal*K, *rps*L (StrR) *end*A1, *nup*G	Invitrogen (Karlsruhe, Germany)

4.5 Plasmids

All plasmids used for this work are listed below in Table 7.

Table 7: List of all used and generated plasmids

Name	Insert	Source
pRFS35	alcA::GFP-hoxB; pyr4; Amp	This Work
pRFS37	RB(hoxB)::pyr4::LB(hoxB); pyr4; Amp	This Work
pRFS38	alcA::GFP-hoxB(ΔCTR);pyr4; Amp	This Work
pRFS46	alcA::YFP(C)-hoxB; pyr4; Amp	This Work
pRFS47	alcA::YFP(N)-hoxB; pyro; Amp	This Work
pRFS48	RB(hoxB)::hoxB::LB(hoxB)	This Work
pRFS49	p(nat)::GFP-hoxB; pyr4; Amp	This Work
pRFS66	p(Tet)::6xHis-hoxB; Kan	This Work
pRFS67	p(nat)::GFP-hoxB; pyro; Amp	This Work
pRFS68	alcA::GFP-hoxB; pyro; Amp	This Work
pRFS69	alcA::hoxB; pyr4; Amp	This Work
pRFS70	alcA::3xHA-hoxB; pyr4; Amp	This Work
pRFS71	mCherry-stuA(NLS); pyro; Amp	This Work
pAUL1	p(Tet)::6xHis-cryA; Kan	Alexander Landmark
pAUL3	alcA::YFP(C)-cryA; pyr4; Amp	Alexander Landmark
pAUL4	alcA::YFP(N)-cryA; pyro; Amp	Alexander Landmark
pAUL7	alcA::3xHA-cryA; pyr4; Amp	Alexander Landmark
p1605	alcA::YFP(C)-fphA(PPG-domain); pyr4; Amp	Janina Purschwitz
p1626	alcA::YFP(C)-lreA; pyr4; Amp	Janina Purschwitz
pJP5	alcA::YFP(C)-fphA; pyr4; Amp	Janina Purschwitz
pJP16	alcA::YFP(C)-fphA(HKRR-domain); pyr4; Amp	Janina Purschwitz
pJet	-	Thermo Fisher (Waltham, USA)

4.6 Oligonucleotides

All oligonucleotides used for this work are listed below in Table 8.

Table 8: List of all used oligonucleotides and their purpose

Name	Sequence	Purpose
AN2853_GFP_fw	CATGGATGAACTATACAAAGGCGCGCCCATGAAACTAACCGCCCACCTC	pRFS35/38/49 generation
AN2853_GFP_rev	AGGTCGACTCTAGAGGATCCTTAATTAACCGTATGCGTCAAGGACACTA	pRFS35 generation
AN2853_KO_upfw	CTCGAGTTTTTCAGCAAGATGTTCATGCCAATGAGCTCACC	pRFS37 generation
AN2853_KO_uprev	GCCCCGAAGAACGTTTTCCATTTCGAGCTTGCGGGATTGAA	pRFS37 generation
AN2853_KO_downfw	AGAAAATACCGCATCAGGCGGCCAGGAGCTTCTAATATACAAT	pRFS37 generation
AN2853_KO_downrev	AGGAGATCTTCTAGAAAGATGGCTTTTATAGCGCCCCGA	pRFS37 generation
PyrG_fw	TGGAAAACGTTCTTCGGGGC	pRFS37 generation
PyrG_rev	CGCCTGATGCGGTATTTTCTCC	pRFS37 generation
AN2853gene_dCTR_GFP_rev	CTAACATCGATCCAGCCCTTCAG	pRFS38 generation
AN2853down_dCTR_GFP_fw	AAGGGCTGGATCGATGTTAGGCCAGGAGCTTCTAATATACAATCA	pRFS38 generation
AN2853_YFPN_fw	TCATGCGCTCCATCGCCACGGGCGCGCCGATGAAACTAACCGCCCACCTC	pRFS46 generation
AN2853_YFPN_rev	AGGTCGACTCTAGAGGATCCTTAATTAACCGTATGCGTCAAGGACACTA	pRFS46/47 generation

AN2853_YFPC_fw	AACAGAAGGTCATGAACCACGGCGCGCC GATGAAACTAACCGCCCACCTC	pRFS47 generation
HoxB_recomp_fw	CTCGAGTTTTTCAGCAAGATGTTCATGCCA ATGAGCTCACC	pRFS48 generation
HoxB_recomp_rev	AGGAGATCTTCTAGAAAGATGGCTTTTATA GCGCCCCGA	pRFS48 generation
(p)HoxB_fornatGFP _fw	AAAACGACGGCCAGTGAATTGTTCATGCC AATGAGCTCACC	pRFS49 generation
(p)HoxB_fornatGFP _rev	TCGATACCGTCGACCTCGAGTTTCGAGCT TGCGGGATTGAA	pRFS49 generation
GFP-HoxB_fw	CTCGAGGTCGACGGTATC	pRFS49 generation
GFP_rev	TTTGTATAGTTCATCCATGCCATGT	pRFS49 generation
HoxB-Expr_fw	GCCTGGTGCCGCGCGGCAGCCATATGAA ACTAACCGCCCACCTC	pRFS66 generation
HoxB-Expr_rev	CAGTGGTGGTGGTGGTGGTGCTCGAGCT CCTGGACTTGCGGCC	pRFS66 generation
EfiPyro_fw	GGATCCTCTAGAGTCGACCT	pRFS67/68 generation
EfiPyro_rev	GGTACCGCTAATTAACTGAGTAGA	pRFS67/68 generation
HoxB-OE_EfiAlcA_fw	TTCTCTACTCAGTTAATTAGGGCGCGCCAA TGAAACTAACCGCCCACCTC	pRFS69 generation
HoxB-OE_EfiAlcA_rev	TGATTTCAGTAACGTTAAGTTTAATTAACTA CTCCTGGACTTGCGGC	pRFS69 generation
Cherry_stuAnls_fw	CTCAGTTAATTAGCGGTACCATGAGCAAG GGCGAGGAG	pRFS71 generation
Cherry_stuAnls_rev	AGGTCGACTCTAGAGGATCCTTAATTAATC ATGCAGCCCAAGAGGAAC	pRFS71 generation
RT_AN_h2b_fw	GAAGAAGCGCGGAAAGACC	qPCR H2B
RT_AN_h2b_rev	TAGACATAGCACGGGTGGAG	qPCR H2B
RT_AN_ccgA_fw	CGCTTCCCTCACTTCTCGT	qPCR ccgA

RT_AN_ccgA_rev	TTCTTAGCGGCCTCCTTGTG	qPCR ccgA
RT_AN_ccgB_fw	ATAACGCCGACCTGACTACG	qPCR ccgB
RT_AN_ccgB_rev	TTGGCGGCTTCCTTGTAAAC	qPCR ccgB
RT_AN_conJ_fw	ACCAGAACCCCGGTAACTTC	qPCR conJ
RT_AN_conJ_rev	CAGAGTCCATACTGGCAAAGC	qPCR conJ
qAN_hoxB-fw	TTCATACCCAACTGGGCGAG	qPCR hoxB
qAN_hoxB-rev	TGAATTCCTCCCCAAGCTCC	qPCR hoxB
qAN_prxA-fw	GGGTAAGGCCAACGGTGTTA	qPCR prxA
qAN_prxA-rev	CGGAAAGGAAGAGCTAGGGAA	qPCR prxA
qAN_trxA-fw	CCTGGGATTGACAAATCAGGC	qPCR trxA
qAN_trxA-rev	TCTAGGTGCTTTGAATGGGGG	qPCR trxA
qAN_catA-fw	CAAATGACCGCGACTGAGTG	qPCR catA
qAN_catA-rev	TTGTTATGGGCCGTCTGGG	qPCR catA
qAN_catB-fw	CTGGGCAAGATGACCCTCAA	qPCR catB
qAN_catB-rev	ACGGCAAAGAGAGGGATACAG	qPCR catB
AlcA_MCSSeq_fw	CCCAAGGTTCTCAGTCTCAC	Sequencing
AN2853_Koscreen_fw	GCCTCCAAGCACTGCTCAG	Screening hoxB KO
AN2853_Koscreen_rev	CGTTCATCGGGCGTTCATTG	Screening hoxB KO
PyrG_screen_fw	AGACCACAAGGCCAAGGATG	Screening hoxB KO
PyrG_screen_rev	AGTAGCCAGTTCCCGAAAGC	Screening hoxB KO

4.7 Bioinformatic Methods

The operating system for most applications used in this Work were Windows-based. The work was produced and written on Windows 10 Home Version 22H2, the AxioVision v4.8.1 Zen 2012 Blue Edition v1.20 software was operated on Windows 7 Professional (Service Pack 1) and the SpectraSuite software was operated on Windows 7 Professional 32bit (Service Pack 1). The Microsoft Office 365 software package was used to generate this work.

4.7.1 Procurement and analysis of DNA and protein sequences

DNA and protein sequences were procured from the database of the national center for biotechnology information (pBlast, NCBI) (Sayers et al., 2022) and fungidb.org (Basenko et al., 2018). For the identification of homologous sequences, the NCBI Blast search (Altschul et al., 1990) and subsequent updates (Altschul et al., 1994) and upgrades like NCBI conserved domain search (Marchler-Bauer et al., 2007) were used. Further analyses were performed using PredictProtein2013 (Yachdav et al., 2014) and PFAM (Mistry et al., 2021)/InterPro (Paysan-Lafosse et al., 2022) and HMMER (Potter et al., 2018).

4.7.2 Processing of Sequences

For the *in silico* cloning of plasmids, the plasmid editor application ApE version 3.0.8 (Wayne Davis) was used. This application also supplied information about the location of restriction sites, the size of restriction fragments and the size of PCR fragments. Protein sequences, alignments and phylogenetic trees were generated using CLC Sequence Viewer v.23.0.4 (Qiagen, Venlo, Netherlands) and Geneious Prime 2022.2.2.

4.7.3 Picture Processing

Pictures taken were processed either directly within the Zen 2012 Blue Edition v.1.20 software (Zeiss, Oberkochen, Germany) or using the application Fiji/ImageJ (Schindelin et al., 2012).

4.7.4 Calculation and Visualization of 3D protein models

Protein models were calculated using AlphaFold (Jumper et al., 2021) run in the laboratory of Tilman Lamparter and the protein data bank (PDB) (Berman et al., 2000). The calculated models were visualized using the application PyMOL v.2.5.4 (Schrödinger et al., 2020). Modelling of protein-ligand interactions was performed using the web application AlphaFill (Hekkelman et al., 2023) and Autodock Vina (Trott et al., 2010). Autodock Vina was used in accordance with the instructions for molecular

docking using MGL Tools v1.5.7 provided by the Scripps Research Institute (Dr. Oleg Trott, 2014). Ligands and other protein files were obtained using the Ligand Reader & Modeler of CHARMM-GUI (Kim et al., 2017).

4.7.5 Processing of transcriptomics

Initial analyses of RNA-Sequencing raw data were performed by the company (BGI group, Shenzhen, China). Further analysis of relevant genes was performed through processing of the obtained Microsoft Excel spreadsheets.

4.8 Methods of Molecular Biology

4.8.1 T4 Plasmid Cloning

For T4-DNA ligation, T4 ligase (New England Biolabs, Frankfurt, Germany) was used according to the manufacturer's instructions. Vector fragments were generated using appropriate restriction digests and isolated from a gel upon gel electrophoresis. Insert fragments were generated via PCR followed by an appropriate restriction digest. After inactivation of the restriction enzymes, the ligation reaction was composed as described in Table 9. The reaction was performed for 45 min at room temperature.

Table 9: Contents of a 20 µL T4 plasmid cloning reaction

Component	Volume
T4 DNA Ligase Buffer (10x)	2 µl
Vector DNA (50 ng/µl)	1 µl
Insert DNA (variable; 3:1 surplus to vector)	variable
T4 DNA Ligase	1 µl
Nuclease-free water	to 20 µl

4.8.2 Plasmid Cloning via Gibson Assembly

Some plasmids were cloned using the *NEBuilder® Hifi DNA Assembly* method (New England Biolabs, Frankfurt, Germany). The vector backbone was linearized via PCR or restriction digest. The insert fragment was generated via PCR. The length of the matching overlaps between vector and insert was 20 base pairs. The reaction was composed using 50 ng vector and a 3:1 molar surplus of insert in a total reaction volume of 20 µL. The details of the reaction composition are noted in Table 10 and 11. A thermocycler (SensoQuest GmbH, Göttingen, Germany) was used to keep the reaction temperature at 50°C for 30 minutes.

Table 10: Composition of a Gibson Assembly reaction

Component	Volume
Reaction Mix	15 µl
Linearized Vector (50 ng/µL)	1 µl
Insert	variable
ddH_2O	to 20 µl

Table 11: Composition of the reaction mix used for Gibson Assembly

Component	Volume
ISO-Buffer (5x)	320 µl
Tris-HCl (pH 7.5)	3 ml
$MgCl_2$ 1M	300 µl
dATP 100 mM	60 µl
dTTP 100 mM	60 µl
dGTP 100 mM	60 µl
dCTP 100 mM	60 µl
PEG-8000	1.5 g
DTT 1M	300 µl
NAD 100 mM	300 µl
ddH_2O	to 6 ml
T5 Exonuclease (10 U/µL)	0.64 µl
Q5® High-Fidelity DNA Polymerase (2 U/µL)	20 µl

Taq DNA Ligase (40 U/µL)	160 µl
ddH_2O	699.36 µl

4.8.3 Gel Electrophoresis

DNA restriction digests and PCR products were analysed using agarose gel electrophoresis. The gel electrophoresis system PerfectBlue™ Gelsystem Mini L (VWR Peqlab, Darmstadt, Germany) was used. A 1% agarose gel in 0.5x TAE buffer was used (Table 12). Prior to pouring the agarose gel in the electrophoresis system, 1 µl of *MIDORI*^{GREEN} *Advance* (NIPPON Genetics Europe, Düren, Germany) was added for each 80 µl of liquid agarose solution. For determination of fragment sizes, the *1 kb DNA ladder* (New England Biolabs, Frankfurt, Germany) was used. Prior to loading, all samples were mixed with 6x staining buffer (Table 13). Gels were run for 30 min at 135 V and were observed using the gel observation system *GP-FAS-V* (Nippon Genetics Europe, Düren, Germany). DNA bands were cut from the gel in the observation system if required.

Table 12: Concentration of additives used in a 1% agarose gel

Component	Concentration
Tris-Acetate	40 mM
EDTA	1 mM pH8

Table 13: Composition of the 6x staining buffer used for DNA visualization after gel electrophoresis

Component	Concentration
Bromophenol blue	0.25 % (w/v)
Xylenecyanol FF	0.25 % (w/v)
Glycerin	30 % (v/v)

4.8.4 DNA-Fragment Purification

DNA fragments were purified using the *FastGene Gel/PCR Extraction Kit* (NIPPON Genetics Europe, Düren, Germany). For PCR products, 10% of the reaction were loaded for gel electrophoresis. If the reaction yielded a pure product, the PCR extraction protocol of the kit was performed according to the manufacturer's instructions. Digested plasmids or impure PCR products were fully loaded for gel electrophoresis and the required band was cut from the gel using a scalpel. The gel extraction protocol of the kit was performed according to the manufacturer's instructions.

4.8.5 Determination of DNA and RNA concentrations

The concentrations of DNA and RNA were determined using a ND-1000 Spectrophotometer (NanoDrop, USA). The extinction of nucleic acid solutions at 260, 280 and 230 nm were observed. An A_{260}/A_{280} ratio of approximately 1.8 and 2.0 was considered acceptable for DNA and RNA respectively. An A_{260}/A_{230} ratio of higher than 2.0 was considered acceptable for both types of nucleic acids.

4.8.6 Transformation of *E. coli*

The *E.coli* strains Top10 and BL21 DE3 were used in transformation. The Top10 strain was used for plasmid replication while BL21 DE3 was used for protein expression. Both strains were transformed identically. Approximately 100 ng of plasmid was added to 50 µL of bacteria solution. The mixture was incubated on ice for 10 min, followed by a heat shock for 1 min at 42°C and another incubation on ice for 5 min. The heat shock was performed on a heating block (Eppendorf SE, Hamburg, Germany). The bacterial solution was then supplemented with 200 µl *super optimal broth with catabolite repression* (SOC-) medium (Table 14). This mixture was incubated on a heating block at 37°C for 30 minutes while shaking at 180 rpm. The bacterial solution was plated on LB-Agar media containing the necessary selection markers and the plates were incubated for approximately 16 hours at 37°C.

Table 14: Composition of SOC-medium used for *E. coli* transformation

Component	Concentration
Trypton	20 g/l
Yeast Extract	5 g/l
NaCl	0.58 g/l
KCl	0.185 g/l
$MgCl_2$ x 7 H_2O	2.03 g/l
$MgSO_4$ x 7 H_2O	2.46 g/l
D(+)-Glucose Monohydrate	3.6 g/l
	pH7

4.8.7 Plasmid Isolation from *E. coli*

Plasmids were isolated from *E. coli* for the purpose of screening and transformation using separate methods. In each case, *E. coli* were cultured for approximately 16 hours at 37°C while shaking at 180 rpm in approximately 15 ml of LB media containing the proper selection markers.

For screening, plasmids were isolated using cell suspension buffer, lysis buffer and neutralization buffer (Table 15, 16 and 17) which were made in house, followed by precipitation in 100% isopropanol and 70% ethanol. Part of the overnight culture was pelleted in an reaction tube, resuspended in 200 µl of cell suspension buffer and lysed by adding 200 µl of lysis buffer. After 3 minutes of incubation, 200 µl of neutralization buffer was added and the mixture was centrifuged at 13,000 rpm for 5 min at 4°C. Afterwards, 500 µl of supernatant were mixed with 500 µl 100% isopropanol, incubated at -20°C for 10 min and centrifuged at 13,000 rpm. The supernatant was discarded, and the pellet was washed with 500 µl 70% ethanol at 13,000 rpm. The pellet was then dried on a heating block at 68°C for 10 min and resuspended in 50 µl ddH_2O.

Table 15: Composition of cell suspension buffer for plasmid isolation

Component	Volume
Tris-HCl 1 M pH7.5	5 ml
EDTA 0.5 M pH8	2 ml
ddH_2O	to 100 ml

Table 16: Composition of lysis buffer for plasmid isolation

Component	Volume
NaOH 10 M	2 ml
SDS 10 %	5 ml
ddH_2O	to 100 ml

Table 17: Composition of neutralization buffer for plasmid isolation

Component	Amount
KAc pH4.8	19.6 g
ddH_2O	to 200 ml

For transformation, plasmids were isolated using the *NucleoSpin® Plasmid Easy Pure Kit* (Macherey-Nagel, Düren, Germany). The isolation was performed according to the manufacturer's protocol.

4.8.8 Restriction Digests

Restriction digests of DNA were performed using restriction enzymes (New England Biolabs, Frankfurt, Germany) according to the manufacturer's instructions. The reaction was performed using 1 to 5 µg DNA and 0.3 to 1 µl enzyme in 20 µl total volume.

4.8.9 DNA Sequencing

Sequencing of DNA was performed externally (Eurofins Genomics, Ebersberg, Germany). Samples were prepared according to the instructions of the service provider.

4.8.10 Protoplastation of *A. nidulans*

For protoplastation of *A. nidulans*, spores were inoculated in approximately 100 ml of appropriate media at 30°C for 16 hours while shaking at 180 rpm. Any solutions used during protoplastation and transformation are noted in Table 18. The overnight culture was filtered through sterile Miracloth (Merck, Darmstadt, Germany) and washed with solution 1. Some of the mycelial pellet was added to a 50 ml reaction tube containing 10 ml solution 1, 200 mg Glucanex (VinoTaste® Pro, Novozymes, Bagsveard, Denmark) and 10 mg of BSA. The additives were completely dissolved prior to adding the mycelia. The cell wall digest was performed at 30°C while shaking at 100 rpm for 1.5 hours. The digested mycelia were filtered through sterile miracloth again and filled to 20 ml with solution 1. 10 ml solution 2 was added carefully so the solutions would not mix. Centrifugation at 5000 rpm for 12 min and 4°C separated settled protoplasts in the interphase between the two solutions. Appropriate break settings were used to prevent mixing of the phases. The protoplasts were collected in another 50 ml reaction tube and supplemented with 2x volumes of solution 3. Protoplasts were pelleted by centrifugation at 5000 rpm and 4°C for 12 minutes. The supernatant was discarded, and the pellet was washed in 1 ml of solution 3. Afterwards, the pellet was resuspended in solution 4. Aliquots of 200 µl protoplast suspension were generated and used for transformation. Until transformation, protoplasts were kept on ice or at 4°C.

Table 18: Composition of solutions for protoplastation of *A. nidulans*

Solution	Composition
Solution 1 (50 ml)	14.9 g $MgSO_4$ 1.8 ml Na_2HPO_4 0.2 M 0.7 ml NaH_2PO_4 0.2 M pH5.5

	sterile filtrated and stored at 4°C
Solution 2 (100 ml)	10.9g Sorbitol 10 ml Tris-HCl 1 M pH7.5 Stored at 4°C
Solution 3	18.2 g Sorbitol 1 ml Tris-HCl 1 M pH7.5 Stored at 4°C
Solution 4	18.2 g Sorbitol 1 ml Tris-HCl 1 M pH7.5 1 ml $CaCl_2$ 1 M Stored at 4°C
Solution 5	30 g PEG4000 0.5 ml Tris-HCl 1 M pH7.5 0.5 ml $CaCl_2$ 1 M

4.8.11 Transformation of *A. nidulans*

For transformation, a 200 µl aliquot of protoplasts (4.8.10) was supplemented with approximately 10 µg of DNA in a 50 ml reaction tube. 50 µl of solution 5 was added and mixed through careful inverting. The transformation mix was incubated on ice for 20 min. Afterwards, 1 ml of solution 5 was added and mixed until homogenous. Following incubation for 5 min at room temperature, 5 ml of solution 4 were added. The reaction tube was filled to 50 ml with MMR-Top medium and mixed thoroughly. The transformation mix was poured onto 3 petri dishes containing appropriate MMR media. Control mixtures containing no DNA were prepared separately and poured onto petri dishes containing appropriate MMR media. Plates were incubated at 37°C for approximately 4 days. Colonies were picked onto appropriate MM media and validated by extracting gDNA and PCR.

4.8.12 Isolation of gDNA from *A. nidulans*

For isolation of genomic DNA from *A. nidulans* a standing culture was incubated for 16 hours at 37°C in a petri dish (150 million spores per dish). Grown mycelia were dried using Miracloth (Merck, Darmstadt, Germany) and transferred into a mortar. Liquid

nitrogen was added, and the mycelia were ground into fine powder. The mycelial powder was transferred to a reaction tube and incubated in 1 ml extraction buffer (Table 19) for 1.5 hours. The cell debris was pelleted by centrifugation and 100 µl of KAc solution (Table 20) was added. Following incubation on ice for 5 min, the mixture was centrifuged at 13,000 rpm for 5 min and the supernatant was mixed with 100% Isopropanol in a 1:1 ratio. After incubation at -20°C for 10 min the pellet was washed with 70% ethanol by centrifugation at 13,000 rpm for 5 min. The genomic DNA was then dried on a heating block for 10 min at 68°C before resuspending it in 200 µL ddH_2O.

Table 19: Composition of gDNA-extraction buffer

Component	Amount
SDS 10%	2 ml
EDTA 0.5 M pH8	10 ml
ddH_2O	to 100 ml

Table 20: Composition of KAc solution for DNA extraction

Component	Amount
KAc	14.7g
Acetic Acid	5.7 ml
	pH 4.2

Alternatively, a small portion of agar containing hyphae was excised from a petri dish and crushed in a 2 ml reaction tube containing 1 ml extraction buffer. This mixture was incubated at 68°C for approximately 1 hour and neutralized with 100 µl KAc solution. After centrifugation at 13,000 rpm for 5 min, the isolation was continued as described above.

4.8.13 Southern Blot

Southern Blotting was performed to confirm gene knockouts. Genomic DNA of wildtype (control) and candidate knockout strains of *A. nidulans* were obtained (4.8.14) and digested with an appropriate restriction digest (4.8.8) such that DNA fragments of

differing lengths around the site of the gene locus and deletion cassette were obtained. All buffers and solutions are detailed in Table 21. In a total volume of 30 µL, the restriction digest was performed according to the manufacturer's instructions. The next day, the DNA was run on a 0.8% TAE gel for 2.5 hours at 90 Volt. The gel was washed in 0.25 M HCl for 30 min, shortly rinsed with ddH_2O, washed in DENAT solution for 30 min, rinsed with water and washed in RENAT solution for 30 min. A sandwich of three pieces of whatman paper surrounding the gel and nitrocellulose membrane on both sides was constructed to blot the DNA to the membrane over night. The whatman paper pieces were soaked in 20x SCC buffer and the blot was performed in 20x SCC buffer. Any air bubbles were removed by rolling a glass pipette over the blot sandwich. After blotting, the membrane was dried using whatman paper and the DNA was crosslinked to the membrane using UV-light.

A probe was generated by DIG-labeling PCR and gel extraction using the PCR DIG Probe Synthesis Kit (Roche, Basel, Switzerland). The PCR was performed like a standard PCR using the Kit components according to the manufacturer's instructions. Probes matching one kilobase of the left border of the deletion cassette were synthesized. The shift of the PCR product on the gel was controlled for using a standard PCR reaction.

For hybridization, the membrane was prehybridized with 40 ml Southern-Hybridization buffer at 65°C for 15-30 min. The probe was resuspended in 1 ml of Southern-Hybridization buffer and denatured at 95°C for 10 min. The prehybridization buffer was discarded and the probe was hybridized using 15 ml fresh hybridization buffer at 65°C over night.

For detection, the membrane was washed with in 2x SSPE+0.1% SDS buffer, 1x SSPE+0.1% SDS buffer and 0.1x SSPE+0.1% SDS buffer at 65°C for15 min each. The membrane was then washed with 20 ml DIG-Wash buffer at 25°C for 5 min and incubated with 25 ml DIG2 buffer for 30 min. Afterwards, the membrane was incubated with 10 ml Anti-DIG antibody solution (1:10000 in DIG2 buffer). The membrane was washed with 50 ml DIG buffer twice for 15 min, incubated in 40 ml DIG3 buffer for 5 min, incubated in CDP-Star solution for 5 min. Finally, the membrane was tested for chemiluminescence using the Chemismart-5000 (Peqlab, Darmstadt, Germany).

Table 21: Composition of solutions used for Southern blotting

Buffer/Solution	Composition
0.25 M HCl Solution	20.7 ml 37% HCl 979.3 ml ddH_2O
DENAT Buffer	1.5 M NaCl 0.4 M NaOH
RENAT Buffer	1.5 M NaCl 282 mM Tris-HCl 218 mM Tris-Base
20x SSC Buffer	3 M NaCl 0.3 M Na-citrate pH7 (HCl)
Southern Hybridization Buffer	0.5 M Na_2HPO_4 0.5M NaH_2PO_4 7 % SDS autoclave
20x SSPE Buffer	3 mM NaCl 227 mM Na_2HPO_4 20 mM Na_2-EDTA pH7.4 (NaOH)
DIG1 Buffer	0.1 M Maleic Acid 0.15 M NaCl pH7.5 (NaOH)
DIG-Wash Buffer	0.3 % (v/v) Tween20 Prepared in DIG1
DIG2 Buffer	5% fat-free milk powder Prepared in DIG1
DIG3 Buffer	0.1 M NaCl 0.05 M $MgCl_2$ pH9.5 (Tris-HCl)
CDP-Star Solution	20 µl CDP-Star in 10 ml DIG3

4.8.14 Polymerase Chain Reaction

For PCR reactions the *Q5® High-Fidelity DNA Polymerase* (New England Biolabs, Frankfurt, Germany) was used. Reactions were performed in a thermocycler (SensoQuest GmbH, Göttingen, Germany). Oligonucleotides were ordered externally (Eurofins Genomics, Ebersberg, Germany). In order to reach higher specificity for the desired amplicon a touch-down PCR with varying annealing temperatures was used. The reaction volume of 25 µl was composed as described in Table 22 and performed as described in Table 23.

Table 22: Composition of a 25 µL PCR reaction

Component	Volume
DNA (300 ng/µl gDNA, 10 ng/µL Plasmid)	1 µL
Q5® High-Fidelity Polymerase	0.25 µl
Q5 Reaction Buffer (5x)	5 µl
Q5 GC-Enhancer (5x)	5 µl
dNTPs 10 mM	0.5 µl
Oligonucleotide 1 (10 pmol/µl)	1.25 µl
Oligonucleotide 2 (10 pmol/µl)	1.25 µl
ddH_2O	10.75 µl

Table 23: Thermocycler protocol for a standard PCR reaction

Step	Temperature	Time
Initial Denaturing	98°C	3 min
Denaturing	98°C	15 sec
Primer Annealing	Ideal annealing temperature +2°C	30 sec
Elongation	72°C	30 sec per kilobase
Repeat from step 2 (5x)		
Denaturing	98°C	15 sec
Primer Annealing	Ideal annealing temperature +1°C	30 sec
Elongation	72°C	30 sec per kilobase

Repeat from step 5 (5x)		
Denaturing	98°C	15 sec
Primer Annealing	Ideal annealing temperature (varies by Oligonucleotide)	30 sec
Elongation	72°C	30 sec per kilobase
Repeat from step 8 (30x)		
Final Elongation	72°C	5 min

4.8.15 RNA Isolation from A. nidulans

For isolation of total RNA from *A. nidulans* a standing culture was incubated for 16 hours at 37°C in a petri dish (150 million spores per dish). For each strain and condition tested, a biological triplicate was inoculated. After each sample was treated as desired, the extraction was performed in green light to prevent unwanted light receptor activation. Grown mycelia were dried using Miracloth (Merck, Darmstadt, Germany), frozen in liquid nitrogen and transferred to a reaction tube. The tube was submerged in liquid nitrogen prior to further processing. The weight of the frozen mycelia was determined using a precision scale. The isolation was performed by filling a mortar with liquid nitrogen and grinding the mycelia into a fine powder. This powder was transferred to a 15 ml reaction tube and suspended in Trizol (1 ml per 100 mg of mycelia). From this suspension, an amount corresponding to 15 mg of mycelia were transferred to a 2 ml reaction tube and filled to 1 ml with Trizol. Afterwards, 200 µl of chloroform were added. The sample was vortexed and incubated at room temperature for 5 min. The sample was then centrifuged at 4°C for 15 min at 13,000 rpm. From the phase-separated solution, 400 µl of the upper, watery phase containing the RNA was recovered. Afterwards, the RNA was precipitated by adding 500 µl of isopropanol and incubating for 30 min at 4°C. The samples were centrifuged at 4°C at 13,000 rpm for 10 min. The supernatant was largely removed and a second centrifugation step with the same parameters was performed. The remaining isopropanol was removed, and Thermothe pellet was washed with 1 ml of 70% ethanol. The samples were allowed to dry for 20 min at room temperature under a fume hood. The RNA was resuspended in 50 µl of RNAse-free water.

4.8.16 Quantitative Real-Time PCR

The *Luna® Universal One-Step RT-qPCR Kit* (New England Biolabs, Frankfurt, Germany) was used for qRT-PCR. Isolated RNA was diluted to 50 ng/µl and 100 ng of RNA were used. For every sample, a technical duplication was applied. The thermocycler CFX Connect (BioRad Laboratories GmbH, Hercules, California, USA) was used. The composition of the reaction mixture and the protocol used for qRT-PCR are noted in Table 24 and Table 25 respectively.

Table 24: Composition of a qRT-PCR reaction mixture

Component	Volume
Luna Universal One-Step Reaction Mix (2x)	10 µl
Luna WarmStart® RT Enzyme Mix (20x)	1 µl
Oligonucleotide 1 (10 pmol/µl)	0.8 µl
Oligonucleotide 2 (10 pmol/µl)	0.8 µl
RNA (50 ng/µl)	2 µl
Nuclease-free H_2O	to 20 µl

Table 25: Thermocycler protocol of a qRT-PCR reaction

Step	Temperature	Time
Reverse Transcription	55°C	10 min
Initial Denaturing	95°C	1 min
Denaturing	95°C	10 sec
Elongation	58°C	30 sec
Repeat from step 3 (40x)		
Melting Curve	55°C to 95°C	5 sec
Repeat step 5 (40x)		

4.8.17 RNA-Sequencing

RNA sequencing was performed as an external service (BGI group, Shenzen, China). Samples were isolated as biological triplicates. The individual triplicates were pooled such that identical amounts of RNA (approximately 2 µg) were used from each sample.

Samples were prepared and shipped according to the instructions of the service provider.

4.8.18 Microscopy of *A. nidulans*

Fluorescence Microscopy of *A. nidulans* was performed using the Zeiss AxioImager Z.1, an AxioCamMR (Zeiss, Jena, Germany), using a 63x/1.4 oil DIC objective and an Osram HXP120 mercury vapor lamp. The microscope was operated using the AxioVision v4.8.1 Zen 2012 Blue Edition v1.20 software (Zeiss, Jena, Germany). Images were processed using the same software or the open-source Fiji software.

For fluorescence microscopy, constructs under the control of the AlcA-promoter were used. As such, any glucose in the media was replaced with equivalent amounts of glycerin as the carbon source. Samples were inoculated on 170 ± 5 µm precision coverslips (Roth, Karlsruhe, Germany). Approximately 4 x 10^4 spores were inoculated in 450 µl of microscopy media for 16 hours at 28°C.

4.8.19 Qualitative intracellular ROS measurement

Qualitative intracellular ROS measurement was performed using CellROX™ Orange reagent (ThermoFisher Scientific, Karlsruhe, Germany). Prior to microscopy, the reagent was diluted 1:1000 in respective media and cells were incubated for 30 min in the dark. Afterwards cells were illuminated at variable light intensities and wavelengths for 20 min. The fluorescence was detected in the Alexa Fluor 555 channel in correspondence with the absorption and emission maxima of CellROX™ Orange reagent of 545 nm and 565 nm respectively.

4.8.20 Growth Assay

Growth Assays were performed in a qualitative or quantitative manner on media containing all necessary selection markers for the strain with the most required media supplementations. Further supplementation was performed to induce a variety of stresses. For qualitative evaluation, a toothpick was used to transfer an unspecified number of spores from to the growth plate. For quantitative evaluation, a

hemocytometer was used to prepare spore suspensions containing 1000 spores per microliter. From this suspension, 5 µl were plated for a total of 5000 spores.

4.8.21 Spore Counting

Quantification of spores was performed by suspending 25,000 spores in 5 ml of MMR-Top medium and plating on plates containing minimal media with appropriate selection markers. The plates were further overlaid with corresponding liquid media. After incubating for 20 hours at 37 °C the liquid medium was removed, and plates were incubated for another 24 hours for conidiospores or 120 hours for cleistothecia. Spores were counted from a block of agar with a diameter of 1 cm. The block of agar was incubated in 500 µl of water containing 1% Tween 20. Illumination was performed using lightboxes at various intensities.

4.9 Methods of Protein Biochemistry

4.9.1 Recombinant Expression of HoxB in *E. coli*

Heterologous expression of the HoxB protein was performed in the *E. coli* strain BL21 DE3. The inducible *tet*-promotor was used to control the expression of the gene. The concentration of Anhydrotetracyclin (AHT) used for induction was 50 mg per ml, leading to a strong overproduction of the protein. Kanamycin was used as a selection marker. A 6x-his-tag was fused N-terminally to the protein in order to facilitate purification. Prior to purification, the required plasmid was procured from a Top10 *E. coli* culture and transformed into *E. coli* BL21 DE3. The next day, a preculture of a transformed colony was inoculated in 50 ml LB media with selection marker while shaking at 180 rpm for 20 hours at 37 °C. The next day, a 2 l culture in LB media with selection marker was inoculated using 1% (V/V) of the preculture, growing at 37 °C while shaking at 180 rpm until an OD_{600} of 0.8 was reached. Afterwards, the promotor system was induced using 50 mM AHTC. Expression of the protein was performed for 20 hours at 20 °C while shaking at 180 rpm.

4.9.2 Isolation of HoxB expressed in *E. coli*

Isolation of the protein was facilitated by first centrifuging the entire culture for 10 min at 4°C and 9000 rpm. The supernatant was discarded, and the cell pellet was collected in 40 ml lysis buffer (Table 26). Afterwards, the same centrifugation was repeated using the smaller volume. The supernatant was discarded again, and the pellet was resuspended in 40 ml of lysis buffer containing 1 mM PMSF and 5 mM DTT. PMSF was repeatedly added at a concentration of 1 mM every 1.5 hours over the course of the purification process. Cell lysis was performed twice using an Emulsiflex-C3 high pressure homogeniser (Avestin Europe GmbH, Mannheim, Germany) at 1000 to 1500 bar. The sample was cooled during the lysation process using a cooling spiral. Cell debris was removed from the sample by centrifuging for 1 hour at 18;000 rpm and 4 °C. The supernatant and pellet were separated, and the pellet was resuspended in lysis buffer corresponding to the volume of removed supernatant. Samples for an SDS-PAGE and a Western Blot consisting of samples of supernatant, resuspended pellet, sample after washing and sample after elution were taken and mixed with 5x SDS sample buffer (Table 29). The pellet was then discarded, and the protein was purified from the supernatant using gravity flow. Gravity flow purification was performed using His-Select® Nickel Affinity Gel (Sigma-Aldrich, Taufkirchen, Germany) and a gravity flow plastic XL column (Roth, Karlsruhe, Germany) according to the manufacturer's instructions. The sepharose beads were equilibrated using one column volume of lysis buffer five times. The sample was incubated with the beads at 4 °C for 1 hour while rotating. The column was washed with one column volume of lysis buffer 10 times. Elution of the protein was performed using half a column volume of elution buffer (Table 27) 6 times. After elution, Imidazole was removed from the sample using a PD-10 Desalting Column (GE Healthcare, USA) according to the manufacturer's instructions. Afterwards, the protein sample was concentrated using a 30,000 MWCO Vivaspin Ultrafiltration Column (Sartorius, Göttingen, Germany) according to the manufacturer's instructions. The sample was concentrated to a total volume of 600 µl. The protein concentration was determined using the QuBit Spectrofluorometer (Invitrogen, Karlsruhe, Germany) according to the manufacturer's instructions.

Table 26: Composition of lysis buffer for protein extraction

Component	Concentration
Tris-HCl	50 mM
NaCl	300 mM
Glycerol	10%
Tween 20	0.05%
Imidazole	90 mM
	pH 7.4

Table 27: Composition of elution buffer for protein extraction

Component	Concentration
Tris-HCl	50 mM
NaCl	300 mM
Glycerol	10%
Tween 20	0.05%
Imidazol	340 mM
DTT	5 mM (added freshly)
PMSF	1 mM (added freshly)
	pH 7.4

4.9.3 Co-Immunoprecipitation

For co-immunoprecipitation, relevant strains were inoculated in 100 mL liquid minimal media in which the glucose component was exchanged for L-threonine and containing suitable auxotrophy markers. The cultures were inoculated for 24 hours at 180 rpm at 30°C. Mycelia were harvested by filtering the culture through sterile Miracloth (Merck, Darmstadt, Germany). They were dried, frozen in liquid nitrogen and ground into fine powder before 800 µl of extraction buffer (Table 28) were added. Samples were resuspended by vortexing and incubated on ice for 30 min. Afterwards samples were centrifuged twice at 13,000 rpm and the pellet was discarded each time. The total protein concentration was determined using Qubit™ (Thermo Fisher Scientific, Karlsruhe, Germany) according to the manufacturer's instructions. All samples were diluted to the same concentration and input samples were mixed with 5x SDS sample

buffer (Table 29) and boiled at 95 °C for 5 min. Afterwards, at least 7 mg of remaining total protein were used for immunoprecipitation. A total of 80 µl of HA epitope antibody solution (Thermo Fisher Scientific, Karlsruhe, Germany) per sample were equilibrated in extraction buffer three times and added to the samples. The samples were inoculated for 3 hours at 4°C while spinning slowly. After centrifugation, the supernatant was discarded, and the beads were resuspended in 50 µl 2x SDS sample buffer and boiled at 95°C for 5 min. The total of 6 samples were then separated using SDS Polyacrylamide Gel Electrophoresis (4.9.3) and a Western Blot (4.9.4) was performed.

Table 28: Composition of extraction buffer used for co-immunoprecipitation

Component	Concentration
Tris-HCl	20 mM
NaCl	150 mM
Tween20	0.05%
PMSF	1 mM (added every 1.5h during extraction)
Protease Inhibitor Cocktail	1 tablet per 10 ml
	pH 8

Table 29: Composition of 5x SDS sample buffer

Component	Concentration (5x)	Concentration (2x)
Tris-HCl	200 mM	80 mM
SDS	10 %	4 %
Bromophenol blue	0.05 %	0.02 %
Glycerol	40 %	16 %
DTT	10 mM (added freshly)	4 mM (added freshly)
	pH 6.8	

4.9.4 SDS Polyacrylamide Gel Electrophoresis

To analyze purified proteins, SDS-PAGE according to Laemmli (Laemmli, 1970) was performed. The Mini-PROTEAN Tetra Vertical Electrophoresis Cell and Power Pac Basic electrophoresis system (BioRad, Feldkirchen, Deutschland) were used. SDS-Gels were used in tandem with SDS-Electrophoresis buffer (Table 30 & 31). The stacking gel was concentrated at 5 % while the separation gel was concentrated at 10%. All samples were mixed with 5x SDS sample buffer (Table 29) and boiled for 5 min prior to electrophoresis. Varying amounts of samples between 3 µl and 20 µl were loaded based on protein concentration. The protein marker *PageRuler* 180 kDa *prestained protein ladder* (Thermo Fisher Scientific, Karlsruhe, Germany) was used. The stacking of samples in the stacking gel was performed at 80 V for 15 min and the separation of samples was performed at 120 V for 1 hour. Upon completion of the SDS-PAGE, a Western Blot (4.9.5) was performed, or the gel was stained using 25 ml Coomassie-Brilliantblau staining solution (Table 32) while shaking (ROTAMAX 120, Heidolph Instruments, Schwabach, Germany) at 60 rpm. The gel was destained by shaking at 60 rpm, alternating Coomassie-Brilliantblau Destaining Solution (Table 33) and ddH_2O. The gel was imaged using the GP-FAS-V imaging station (NIPPON Genetics Europe, Düren, Germany).

Table 30: Composition of SDS gels used for SDS-PAGE

Component	Stacking Gel (5 %)	Separation Gel (10 %)
30 % Acrylamide-Bisacrylamide Solution	0.83 ml	6.6 ml
10 % SDS	0.05 ml	0.2 ml
ddH_2O	3.4 ml	8 ml
10% APS	0.05 ml	0.2 ml
Tris-HCl	0.63 ml (0.5 M, pH 6.8)	0.2 ml (1.5 M, pH 8.8)
TEMED	0.007 ml	0.02 ml

Table 31: Composition of SDS-PAGE buffer

Component	Concentration
Tris	25 mM
SDS	0.1 %
Glycin	192 mM

Table 32: Composition of Coomassie staining solution for SDS-PAGE

Component	Concentration
Methanol	45 %
100 % Acetic Acid	10 %
ddH_2O	45 %
Coomassie-Brilliantblau R-250	0.1 %

Table 33: Composition of Coomassie destaining solution for SDS-PAGE

Component	Concentration
Methanol	40 %
100 % Acetic Acid	10 %
ddH_2O	50 %

4.9.5 Western Blot

After SDS-PAGE (4.9.4), samples were transferred to a nitrocellulose membrane at 80 V and 4°C for 2 hours. The membrane was blocked in PBST-Blocking Buffer containing 1 % (w/V) milk powder (Table 35) for 1 hour at room temperature. Upon blocking, the membrane was washed three times in PBST (Table 34). Primary Antibody Solution was obtained by diluting a suitable primary antibody in PBST. The membrane was incubated in primary antibody solution overnight at 4°C while shaking gently. Afterwards, the membrane was washed three times in PBST again and incubated with a suitable secondary antibody diluted in PBST for 1 hour at room temperature. The membrane was washed 3 more times in PBST and analyzed for chemoluminescence using the Chemismart-5000 system (Peqlab, Darmstadt, Germany). 1 ml solution A was mixed with 100 µl solution B and 0.5 µl H_2O_2 and the image was developed for up to 10 min.

Table 34: Composition of PBST for Western blotting

Component	Concentration
KH_2PO_4	4 mM
Na_2HPO_4	16 mM
NaCl	115 mM
Tween20	0.1% (V/V)

Table 35: Composition of PBST-Blocking Buffer for Western blotting

Component	Concentration
Milk powder	1 % (w/V)
Dissolved in PBST (Table 34)	

4.9.6 Size Exclusion Chromatography (SEC)

Size exclusion chromatography was performed using a Superdex 200 Increase 10/300 column (Sigma-Aldrich, Taufkirchen, Germany). The column was equilibrated, and protein was loaded in SEC-running buffer (Table 36).

Table 36: Composition of running buffer for size exclusion chromatography

Component	Concentration
NaCl	137 mM
KCl	2.7 mM
Na_2PO_4	10 mM
KH_2PO_4	1 mM
BSA	0.5%
Tween-20	0.02%
	pH 7.4

4.9.7 Biolayer Interferometry

The BLItz platform Octet® N1 (Sartorius, Göttingen, Germany) was used to perform biolayer interferometry experiments. The protocol used was in accordance with Sultana, A. & Lee, J.E. (2015). In this work, the Basic Protocol I for measuring protein-protein interactions was performed.

4.10 Other Methods

4.10.1 Calibration of Illumination in Lightboxes and during Microscopy

Absolute intensity measurements were performed using a portable JAZ-COMBO S/N:JAZA0503 with QP400-1-VIS-NIR and CC-3-UV-S spectrometer unit (Ocean Optics). Individual measurements were evaluated by extracting the raw data from the complementary SpectraSuite software. Data values obtained as Watt per square meter [W/m^2] were recalculated as micromol photons per square meter and second [µmol photons m^{-2} s^{-1}] using Formula 1.

Formula 1: $E_{QF} = I\ \left[\frac{W}{m^2}\right] *\ \lambda\ [nm] * 0.003179$

Light boxes (Yu, Streng et al, 2021) were calibrated for a range between 2 and 20 micromol photons per square meter and second (µmol photons m^{-2} s^{-1}). The voltages for each LED type were adjusted according to Formulas 2 to 6.

Formula 2: $E_{QF(White)} = 8.6383 * Output\ [V] - 38.85$

Formula 3: $E_{QF(Blue)} = 50.763 * Output\ [V] - 8.0706$

Formula 4: $E_{QF(Green)} = 101.22 * Output\ [V] - 29.073$

Formula 5: $E_{QF(Red)} = 114.74 * Output\ [V] - 116.13$

Formula 6: $E_{QF(Far\ Red)} = 37.832 * Output\ [V] - 23.268$

5. References

Abrashev, R., Krumova, E., Dishliska, V., Eneva, R., Engibarov, S., Abrashev, I,. Angelova, M., Differential Effect of Paraquat and Hydrogen Peroxide on the Oxidative Stress Response in *Vibrio Cholerae* Non O1. *Biotechnology & Biotechnological Equip.* 25, no. sup1 (2011): 72-76.

Adams, T.H., Boylan, M.T., Timberlake, W.E., brlA is necessary and sufficient to direct conidiophore development in *aspergillus nidulans*. *Cell* 54, no. 3 (1988): 353-362

Aguida, B., Babo, J., Baouz, S., Jourdan, N., Procopio, M., El-Esawi, M.A., Ahmad, M., et al., 'Seeing' the electromagnetic spectrum: spotlight on the cryptochrome photocycle. *Front. in Plant Science* 15 (2024): 1340304

Aguilera, F., Peinado, R.A., Millán, C., Ortega, J.M., Mauricio, J.C., Relationship between ethanol tolerance, H+ -ATPase activity and the lipid composition of the plasma membrane in different wine yeast strains. *Int. J. Food Microb.* 110, no. 1 (2006): 34-42

Altschul, S.F., Lipman, D.J., et al., Basic local alignment search tool. *J. Mol. Biol.* 215 (1990) :403-410

Altschul, S.F., Wootton, J.C. et al., Issues in searching molecular sequence databases. *Nature Genet.* 6 (1994) :119-129

Andel , F., Lagarias, J.C., Mathies, R.A., Resonance raman analysis of chromophore structure in the lumi-R photoproduct of phytochrome. *Biochemistry* 35, no. 50 (1996): 15997-16008

Angelova, M.B., Pashova, S.B., Spasova, B.K., Vassilev, S.V., Slokoska, L.S., Oxidative stress response of filamentous fungi induced by hydrogen peroxide and paraquat. *Mycol. Research* 109, no. 2 (2005): 150-158

Arthaut, L.-D., Jourdan, N., Mteyrek, A., Procopio, M., El-Esawi, M., d'Harlingue, A., Bouchet, P.-E., Witczak, J., Ritz, T., Klarsfeld, A., Birman, S., Usselman, R.J., Hoecker, U., Martino, C.F., Ahmad, M., Blue-light induced accumulation of reactive oxygen species is a consequence of the *Drosophila* cryptochrome photocycle. *PLoS One* 12, no. 3 (2017): e0171836.

Asp, E., Nilsson, D., Sunnerhagen, P., Fission yeast mitogen-activated protein kinase Sty1 interacts with translation factors. *Euk. Cell* 7, no. 2 (2008): 328-338

Azuma, N., Kanamaru, K., Matsushika, A., Yamashino, T., Mizuno, T., Kato, M., Kobayashi, T., *In Vitro* Analysis of His-Asp Phosphorelays in *Aspergillus nidulans*: The First Direct Biochemical Evidence for the Existence of His-Asp Phosphotransfer Systems in Filamentous Fungi. *Bioscience Biotechnology Biochemistry* 71, no. 10 (2007): 2493-2502

Bae, G., Choi, G., Decoding of Light Signals by Plant Phytochromes and Their Interacting Proteins. *Annu. Rev. Plant Biol.* 59, no. 1 (2008): 281-311

Baidya, S., Duran, R.M., Lohmar, J.M., Harris-Coward, P.Y., Cary, J.W., Hong, S.-Y., Roze L.V., Calvo, A.M., VeA Is Associated with the Response to Oxidative Stress in the Aflatoxin Producer Aspergillus flavus. *Euk. Cell* 13, no. 8 (2014): 1095-1103

Balázs, A., Pócsi, I., Hamari, Z., Leiter, É., Emri, T., Miskei, M., Oláh, J., Tóth, V., Hegedüs, N., Prade, R.A., Molnár, M., Pócsi, I., AtfA bZIP-type transcription factor regulates oxidative and osmotic stress responses in *Aspergillus nidulans*. *Mol. Genet. and Genom.* 283 (2010): 289-303

Balke, J., Gutiérrez, P.D., Rafaluk-Mohr, T., Proksch, J., Koksch, B., Alexiev, U., Osmolytes Modulate Photoactivation of Phytochrome: Probing Protein Hydration. *MDPI molecules* 28, no. 16 (2023): 6121

Ballario, P., Macino, G., White collar proteins: PASsing the light signal in *Neurospora crassa*. *Trends Microbiology* 5, no. 11 (1997): 458-462

Ballario, P., Talora, C., Galli, D., Linden, H., Macino, G., Roles in dimerization and blue light photoresponse of the PAS and LOV domains of *Neurospora crassa* white collar proteins. *Molecular Biology* 29, no. 3 (1998): 719-729

Barañano, D.E., Rao, M., Ferris, C.D., Snyder, S.H., Biliverdin reductase: A major physiologic cytoprotectant. *PNAS* 99 (2002):16093-16098

Bartas, M., Červeň, J., Guziurová, S., Slychko, K., Pečinka, P., Amino Acid Composition in Various Types of Nucleic Acid-Binding Proteins. *Int J Mol Sci.* 22, no. 2 (2021): 922

Basenko, E.Y., Pulman, J.A. & Hertz-Fowler, C. et al., FungiDB: An Integrated Bioinformatic Resource for Fungi and Oomycetes. *J. Fungi (Basel).* 4, no. 1 (2018): 39

Bayram, O., Biesemann, C., Krappmann, S, Galland, P., Braus, G.H., More than a repair enzyme: Aspergillus nidulans photolyase-like CryA is a regulator of sexual development. *Mol. Biol. Cell* 19, no. 8 (2008a): 3254-3262

Bayram, O., Krappmann, S., Ni, M., Bok, J.W., Helmstaedt, K., Valerius, O., Braus-Stromeyer, S., Kwon, N.-J., Keller, N.P., Yu, J.-H., Braus, G.H., VelB/VeA/LaeA complex coordinates light signal with fungal development and secondary metabolism. *Science* 320, no. 5882 (2008b): 1504-1506

Bayram, O., Braus, G.H., Fischer, R., Rodriguez-Romero, J., Spotlight on *Aspergillus nidulans* photosensory systems. *Fung. Genet. Biol.* 47, no. 11 (2010): 900-908

Begum, A., Drebes, J., Kikhney, A., Müller, I.B., Perbrandt, M., Svergun, D., Wrenger, C., Betzel, C., Staphylococcus aureus thiaminase II: oligomerization warrants proteolytic protection against serine proteases. *Acta. Cryst. Struct. Biol.* 69, no. 12 (2013): 2320-2329

Benach, J., Edstrom, W.C., Lee, I., Das, K., Cooper, B., Xiao, R., Liu, J., Rost, B., Acton, T.B., Montelione, G.T., Hunt, J.F., The 2.35 A structure of the TenA homolog from *Pyrococcus furiosus* supports an enzymatic function in thiamine metabolism. *Acta. Cryst. Struct. Biol.* 61, no. 5 (2005): 589-598

Berman, H.M., Westbrook, J. & Bourne P.E. et al., The Protein Data Bank. *Nucl. Acids Research* (2000)

Bieszke, J.A., Braun, E.L., Bean, L.E., Kang, S., Natvig, D.O., Borkovich, K.A., The nop-1 gene of *Neurospora crassa* encodes a seven transmembrane helix retinal-binding protein homologous to archaeal rhodopsins. *Proc Natl Acad Sci U S A.* 96, no. 14 (1999): 8034-8039

Bluhm, B.H., Dunkle, L.D., PHL1 of Cercospora zeae-maydis encodes a member of the photolyase/cryptochrome family involved in UV protection and fungal development. *Fung. Genet. Biol.* 45, no. 10 (2008): 1364-1372

Blumenstein, A., Vienken, K. Tasler, R., Purschwitz, J., Veith, D., Frankenberg-Dinkel, N., Fischer, R., The *Aspergillus nidulans* Phytochrome FphA Represses Sexual Development in Red Light. *Curr. Biol.* 15, no. 20 (2005): 1833-1838

Bok, J.W., Keller, N.P., LaeA, a Regulator of Secondary Metabolism in *Aspergillus spp*. *ASM Euk. Cell* 3, no. 2 (2004): 527-535

Borthwick, H.A., Hendricks, S.B., Photoperiodism in Plants. *Science* 132, no. 3435 (1960): 1223-1228

Brandt, S., von Stetten, D., Günter, M., Hildebrandt, P., Frankenberg-Dinkel, N., The Fungal Phytochrome FphA from *Aspergillus nidulans*. *J. Biol. Chem.* 283(50) (2008): 34605–34614

Brodhun, F., Göbel, C., Hornung, E., Feussner, I., Identification of PpoA from *Aspergillus nidulans* as a Fusion Protein of a Fatty Acid Heme Dioxygenase/Peroxidase and a Cytochrome P450. *J. Biol. Chem.* 284, no. 18 (2009): 11792-11805

Bryant, P., Pozzati, G., Elofsson, A., Improved prediction of protein-protein interactions using AlphaFold2. *Nature Comm.* 13, no. 1 (2022): 1265

Burgie, E.S., Gannam, Z.T.K., McLoughlin, K.E., Sherman, C.D., Holehouse, A.S., Stankey, R.J., Vierstra, R.D., Differing biophysical properties underpin the unique signaling potentials within the plant phytochrome photoreceptor families. *PNAS* 118, no. 22 (2021): e2105649118

Butler, W.L., Norris, K.H., Siegelman, H.W., Hendricks, S.B., DETECTION, ASSAY, AND PRELIMINARY PURIFICATION OF THE PIGMENT CONTROLLING PHOTORESPONSIVE DEVELOPMENT OF PLANTS. Proc Natl Acad Sci U S A. 45, no. 12 (1959): 1703-1708

Calera, J.A., Sánchez-Weatherby, J., López-Medrano, R., Leal, F., Distinctive properties of the catalase B of *Aspergillus nidulans. FEBS Letters* 475, no. 2 (2000): 117-120

Cary, J.W., Han, Z., Yin, Y., Lohmar, J.M., Shantappa, P.Y., Harris-Coward, P.Y., Mack, B., Ehrlich, K.C., Wei, Q., Arroyo-Manzanares, N., Uka, V., Vanhaecke, L., Bhatnagar, D., Yu, J., Nierman, W.C., Johns, M.A., Sorensen, D., Shen, H., Saeger, S.D., Mavungu, J.D.D., Calvo, A.M., Transcriptome Analysis of Aspergillus flavus Reveals veA-Dependent Regulation of Secondary Metabolite Gene Clusters, Including the Novel Aflavarin Cluster. *Euk. Cell* 14, no. 10 (2015): 983-997

Chaves, I., Yagita, K., Barnhoorn, S., Okamura, H., van der Horst, G.T.J., Tamanini, F., Functional Evolution of the Photolyase/Cryptochrome Protein Family: Importance of the C Terminus of Mammalian CRY1 for Circadian Core Oscillator Performance. *Molec. Cell. Biol.* 26(5) (2006): 1743–1753

Chen, D., Toone, W.M., Mata, J., Lyne, R., Burns, G., Kivinen, K., Brazma, A., Jones, N., Bähler, J., Global transcriptional responses of fission yeast to environmental stress. *Molec. Biol. Cell* 14, no. 1 (2003): 214-229

Chen, X., Tsai, M.Y., Wolynes, P.G., The Role of Charge Density Coupled DNA Bending in Transcription Factor Sequence Binding Specificity: A Generic Mechanism for Indirect Readout. *J. Am. Chem. Soc.* 144, no. 4 (2022): 1835-1845

Cheng, P., Yang, Y., Gardner, K.H., Liu, Y., PAS domain-mediated WC-1/WC-2 interaction is essential for maintaining the steady-state level of WC-1 and the function of both proteins in circadian clock and light responses of *Neurospora. Molec. Cell. Biol.* 22, no. 2 (2002): 517-524

Cheng, P., He, Q., Yang, Y., Wang, L., Liu, Y., Functional conservation of light, oxygen, or voltage domains in light sensing. *PNAS* 100, no. 10 (2003): 5938-5943

Cheng, P., Yang, Y., Wang, L., He, Q., Liu, Y., WHITE COLLAR-1, a Multifunctional *Neurospora*Protein Involved in the Circadian Feedback Loops, Light Sensing, and Transcription Repression of wc-2. *J. Biol. Chem.* 278, no. 6 (2003): 3801-3808

Chiang, Y.-M, Szewczyk, E., Davidson, A.D., Entwistle, R., Keller, N.P., Wang, C.C.C., Characterization of the Aspergillus nidulans Monodictyphenone Gene Cluster. *Appl. Env. Microbiol.* 76, no. 7 (2010): 2067-2074

Choi, H.-J., Kim, S.-J., Mukhopadhyay, P., Cho, S., Woo, J.-R., Storz, G., Ryu, S.-E., Structural Basis of the Redox Switch in the OxyR Transcription Factor. *Cell* 105, no. 1 (2001): 103-113

Christman, M.F., Storz, G., Ames, B.N., OxyR, a positive regulator of hydrogen peroxide-inducible genes in *Escherichia coli* and *Salmonella typhimurium*, is homologous to a family of bacterial regulatory proteins. Proc Natl Acad Sci U S A 86, no. 10 (1989): 3484-3488

Cohrs, K.C., Schumacher, J., The Two Cryptochrome/Photolyase Family Proteins Fulfill Distinct Roles in DNA Photorepair and Regulation of Conidiation in the Gray Mold Fungus *Botrytis cinerea*. *Appl Environ Microbiol.* 83, no. 17 (2017): e00812-17

Csillag, K., Emri, T., Rangel, D.E.N., Pócsi, I., pH-dependent effect of Congo Red on the growth of *Aspergillus nidulans* and *Aspergillus niger*. *Fung. Biol.* 127, no. 7-8 (2023): 1180-1186

Da Silva Dantas, A., Patterson, M.J., Smith, D.A., Maccallum, D.M., Erwig, L.P., Morgan, B.A., Quinn, J., Thioredoxin regulates multiple hydrogen peroxide-induced signaling pathways in *Candida albicans*. *Molec. Biol. Cell* 30, no. 19 (2010): 4550-4563

Da Silva Dantas, Day, A., Ikeh, M., Kos, I., Achan, B., Quinn, J., Oxidative Stress Responses in the Human Fungal Pathogen, *Candida albicans*. *Biomolecules* 5, no. 1 (2015): 142-165

Dardalhon, M., Lin, W., Nicolas, A., Averbeck, D., Specific transcriptional responses induced by 8-methoxypsoralen and UVA in yeast. *FEMS Yeast Res.* 7, no. 6 (2007): 866-878

Davis, S.J., Bhoo, S.H., Durski, A.M., Walker, J.M., Vierstra, R.D., The Heme-Oxygenase Family Required for Phytochrome Chromophore Biosynthesis Is Necessary for Proper Photomorphogenesis in Higher Plants. *Plant Phys.* 126, no. 2 (2001): 656-669

Datla, S.R., Dusting, G.J., Mori, T.A., Taylor, C.J., Croft, K.D., Jiang, F., Induction of heme oxygenase-1 in vivo suppresses NADPH oxidase derived oxidative stress. *Hypertension* 50, no. 4 (2007): 636-642

De Groot, P.W.J., Brandt, B.W., Horiuchi, H., Ram, A.F.J., de Koster, C.G., Klis, F.M., Comprehensive genomic analysis of cell wall genes in *Aspergillus nidulans*. *Fung. Genet. Biol.* 46, no. 1 (2009): S72-S81

Delaunay, A., Isnard, A.-D., Toledano, M.B., H_2O_2 sensing through oxidation of the Yap1 transcription factor. *EMBO J.* 19, no. 19 (2000): 5157-5166

Delaunay, A., Pflieger, D., Barrault, M.B., Vinh, J., Toledano, M.B., A thiol peroxidase is an H_2O_2 receptor and redox-transducer in gene activation. *Cell* 111, no. 4 (2002): 471-481

Dhaoui, M., Auchère, F., Blaiseau, P.-L., Lesuisse, E., Landoulsi, A., Camadro, J.-M., Haguenauer-Tsapis, R., Belgareh-Touzé, N., Gex1 is a yeast glutathione exchanger that interferes with pH and redox homeostasis. *Molec. Biol. Cell* 22, no. 12 (2011): 2054-2067

Dunlap, J.C., Loros, J.J., Colot, H.V., Mehra, A., Belden, W.J., Shi, M., Hong, C.I., Larrondo, L.F., Lambreghts, R., et al., A Circadian Clock in *Neurospora*: How Genes and Proteins Cooperate to Produce a Sustained, Entrainable, and Compensated Biological Oscillator with a Period of about a Day. *Cold Spring Harb Symp Quant Biol.* vol. 72, (2007) pp. 57-68

Duvigneau, J.C., Esterbauer, H., Kozlov, A.V., Role of Heme Oxygenase as a Modulator of Heme-Mediated Pathways. *MDPI* 8, no. 10 (2019): 475

El-Esawi, M., Arthaut, L.-D., Jourdan, N., d'Harlingue, A., Link, J., Martino, C.F., Ahmad, M., Blue-light induced biosynthesis of ROS contributes to the signaling mechanism of *Arabidopsis* cryptochrome. *Nature Scient. Rep.* 7, no. 1 (2017): 13875

Emri, T., Szarvas, V., Orosz, E., Antal, K., Park, H., Han, K.-H., Yu, J.-H., Pócsi, I., Core oxidative stress response in *Aspergillus nidulans*. *BMC Genom.* 16 (2015): 1-19

Enjalbert, B., Nantel, A., Whiteway, M., Stress-induced gene expression in *Candida albicans*: absence of a general stress response. *Molec. Biol. Cell* 14, no. 4 (2003): 1460-1467

Enjalbert, B, Smith, D.A., Cornell, M.J., Alam, I., Nicholls, S., Brown, A.J.P., Quinn, J., Role of the Hog1 Stress-activated Protein Kinase in the Global Transcriptional Response to Stress in the Fungal Pathogen *Candida albicans*. *Molec. Biol. Cell* 17, no. 2 (2006): 1018-1032

Erttmann, S.F., Gekara, N.O., Hydrogen peroxide release by bacteria suppresses inflammasome-dependent innate immunity. *Nature Comm.* 10, no. 1 (2019): 3493

Fleischhacker, A.S., Gunawan, A.L., Kochert, B.A., Liu, L., Wales, T.E., Borowy, M.C., Engen, J.R., Ragsdale, S.W., The heme-regulatory motifs of heme oxygenase-2 contribute to the transfer of heme to the catalytic site for degradation. *J. Biol. Chem.* 295, no. 16 (2020): 5177-5191

Fountain, J.C., Bajaj, P., Pandey, M., Nayak, S.N., Yang, L., Kumar, V., Jayale, A.S., Guo, B., et al., Oxidative stress and carbon metabolism influence *Aspergillus flavus*

transcriptome composition and secondary metabolite production. *Nature Scient. Rep.* 6, no. 1 (2016): 38747

Froehlich, A.C., Liu, Y.L., Loros, J.J., Dunlap, J.C., White Collar-1, a circadian blue light photoreceptor, binding to the frequency promoter. *Science* 297, no. 5582 (2002): 815-819

Froehlich, A.C., Loros, J.J., Dunlap, J.C., Rhythmic binding of a WHITE COLLAR-containing complex to the frequency promoter is inhibited by FREQUENCY. *Proc Natl Acad Scie U S A* 100, no. 10 (2003): 5914-5919

Galagan, J.E., Calvo, S.E., Cuomo, C., Ma, L.-J., Wortman, J.R., Batzoglou, S., Birren, B.W., et al., Sequencing of *Aspergillus nidulans* and comparative analysis with *A. fumigatus* and *A. oryzae*. *Nature* 438, no. 7071 (2005): 1105-1115

Gao, X., Dong, X., Li, X., Liu, Z., Liu, H., Prediction of disulfide bond engineering sites using a machine learning method. *Nature Scient. Rep.* 10, no. 1 (2020): 10330

Gavassi, M.A., Monteiro, C.C., Campos, M.L., Melo, H.C., Cavalho, R.F., Phytochromes are key regulators of abiotic stress responses in tomato. *Scient. Hortic.* 222 (2017): 126-135

Gil-Sánchez, M.d.M., Cea-Sánchez, S., Lugue, E.M., Cánovas, D., Corrochano, L.M., Light regulates the degradation of the regulatory protein VE-1 in the fungus *Neurospora crassa*. *BMC Biology* 20, no. 1 (2022): 149

Gomi, K., Regulatory mechanisms for amylolytic gene expression in the koji mold *Aspergillus oryzae. Biosc., Biotech. & Biochem.* 83, no. 8 (2019): 1385-1401

Grau, M.F., Entwistle, R., Chiang, Y.-M., Ahuja, M., Oakley, C.E., Akashi, T., Wang, C.C.C., Todd, R.B., Oakley, B.R., Hybrid Transcription Factor Engineering Activates the Silent Secondary Metabolite Gene Cluster for (+)-Asperlin in *Aspergillus nidulans*. *ACS Chem. Biol.* 13, no. 11 (2018): 3193-3205

Hagiwara, D., Sakamoto, K., Abe, K., Gomi, K,. Signaling pathways for stress responses and adaptation in Aspergillus species: stress biology in the post-genomic era. *Biosc., Biotech. & Biochem.* 80, no. 9 (2016): 1667-1680

Hayashi, S., Yoshioka, M., Matsui, T., Kojima, K., Kato, M., Kanamaru, K., Kobayashi, T,. Control of reactive oxygen species (ROS) production through histidine

kinases in Aspergillus nidulans under different growth conditions. *FEBS Open Bio* 4 (2014): 90-95

Hedke, M., Rauscher, S., Röhrig, J., Rodríguez-Romero, J., Yu, Z., Fischer, R., Light-dependent gene activation in *Aspergillus nidulans* is strictly dependent on phytochrome and involves the interplay of phytochrome and white collar-regulated histone H3 acetylation. *Molec. Microbiol.* 97, no. 4 (2015): 733-745

Hekkelman, M.L., de Vries, I., Joosten, R.P., Perrakis, A., AlphaFill: enriching AlphaFold models with ligands and cofactors. *Nature Meth.* 20, no. 2 (2023): 205-213

Herr, A., Fischer, R., Improvement of *Aspergillus nidulans* penicillin production by targeting AcvA to peroxisomes. *Metab. Engin.* 25 (2014): 131-139

Hitomi, K., Okamoto, K., Daiyasu, H., Miyashita, H., Iwai, S., Toh, H., Ishiura, M., Todo, T., Bacterial cryptochrome and photolyase: characterization of two photolyase-like genes of *Synechocystis sp.* PCC6803. *Nucl. Acid Res.* 28, no. 12 (2000): 2353-2362

Hong, P., Koza, S., Bouvier, E.S.P., A Review Size-Exclusion Chromatography For The Analysis Of Protein Biotherapeutics And Their Aggregates. *J. Liquid Chrom. & Rel. Tech.* 35, no. 20 (2012): 2923-2950

Horwitz, B.A., Lipson, E.D., Schechtman, M.G., *In vivo* absorption spectra of*Neurospora crassa* white collar photomutants. *Experim. Mycol.* 11, no. 1 (1987): 74-76

Hou, X., Liu, L., Xu, D., Lai, D., Zhou, L., Involvement of LaeA and Velvet Proteins in Regulating the Production of Mycotoxins and Other Fungal Secondary Metabolites. *J Fungi (Basel)* 10, no. 8 (2024): 561

Huynh, H.H., Morita, N., Sakamoto, T., Katayama, T., Miyakawa, T., Tanokura, M., Chiba, Y., Shinkura, R., Maruyama, J.I., Functional production of human antibody by the filamentous fungus Aspergillus oryzae. *Fung. Biol. Biotech.* 7 (2020): 1-15

Idnurm, A., Bahn, Y.-S., Red light plugs into MAPK pathway. *Nature Microbiol. – Fung. Phys.* 1, no. 5 (2016): 1-2

Isaksson, L., Gustavsson, E., Persson, C., Brath, U., Vrhovak, L., Karlsson, G., Orekhov, V., Westenhoff, S., Signaling Mechanism of Phytochromes in Solution. *Structure* 29, no. 2 (2021): 151-160

Jabasingh, S.A., Nachiyar, C.V., Optimization of cellulase production by *Aspergillus nidulans*: application in the biosoftening of cotton fibers. *W. J. Microbiol. and Biotech.* 27 (2011): 85-97

Jansen, T., Daiber, A., Direct Antioxidant Properties of Bilirubin and Biliverdin. Is there a Role for Biliverdin Reductase?. *Front. in Pharmacol.* 3 (2012): 30

Jiang, Y.-D., Yuan, X., Zhou, W.-W. Bai, Y.-L., Wang, G.-Y., Zhu, Z.-R., Cryptochrome Regulates Circadian Locomotor Rhythms in the Small Brown Planthopper *Laodelphax striatellus* (Fallén). *Front. in Physiol.* 9 (2018): 149

Jo, I., Chung, I.-Y., Bae, H.-W., Kim, J.-S., Song, S., Cho, Y.-H., Ha, N.-C., Structural details of the OxyR peroxide-sensing mechanism. *PNAS* 112, no. 20 (2015): 6443-6448

Jourdan, N., Martino, C.F., El-Esawi, M., Witczak, J., Bouchet, P.-E., d'Harlingue, A., Ahmad, M., Blue-light dependent ROS formation by *Arabidopsis* cryptochrome-2 may contribute toward its signaling role. *Plant Sign. & Behav.* 10, no. 8 (2015): e1042647

Jumper, J., Evans, R., Pritzel, A., Green, T., Figurnov, M., Ronneberger, O., Tunyasuvunakool, K., Hassabis, D., et al., Highly accurate protein structure prediction with AlphaFold. *Nature* 596, no. 7873 (2021): 583-589

Käfer, E., Origins of Translocations in *ASPERGILLUS NIDULANS*. *Genetics* 52, no. 1 (1965): 217

Kanamaru, K., Roles of the His-Asp Phosphorelay Signal Transduction System in Controlling Cell Growth and Development in *Aspergillus nidulans*. *Biosc., Biotech. & Biochem.* 75, no. 1 (2011): 1-6

Kanamaru, K., Izuhara, K., Kimura, M., Kobayashi, T., Generation of mitochondrial reactive oxygen species through a histidine kinase, HysA in *Aspergillus nidulans*. *J. Gen. and Appl. Microbiol.* 68, no. 1 (2022): 17-23

Kanaujia, R., Singh, S., Rudramurthy, S.M., Aspergillosis: an Update on Clinical Spectrum, Diagnostic Schemes, and Management. *Curr Fungal Infect Rep.* 17, no. 2 (2023): 144-155

Kaushal, V., Klim, J., Skoneczna, A., Kurlandzka, A., Enkhbaatar, T., Kaczanowski, S., Zielenkiewicz, U., Apoptotic Factors Are Evolutionarily Conserved Since Mitochondrial Domestication. *Genome Biol. Evol.* 15, no. 10 (2023): evad154

Kawasaki, L., Wysong, D., Diamond, R., Aguirre, J., Two divergent catalase genes are differentially regulated during Aspergillus nidulans development and oxidative stress. *J Bacteriol.* 179, no. 10 (1997): 3284-3292

Kelly, D.E., Kraševec, N., Mullins, J., Nelson, D.R., The CYPome (Cytochrome P450 complement) of *Aspergillus nidulans*. *Fung. Genet. Biol.* 46, no. 1 (2009): S53-S61

Khan, R., Anwar, F., Ghazali, F.M., A comprehensive review of mycotoxins: Toxicology, detection, and effective mitigation approaches. *Heliyon* 8 (2024) e28361

Kim, H., Han, K., Kim, K., Han, D., Jahng, K., Chae, K., The *veA* gene activates sexual development in *Aspergillus nidulans*. *Fung. Genet. Biol.* 37, no. 1 (2002): 72-80

Kim, S., Lee, J., Jo, S., Brooks III, C.L., Lee, H.S., Im, W., CHARMM-GUI Ligand Reader and Modeler for CHARMM Force Field Generation of Small Molecules. *J. Comput. Chem.* (2017): 1879-1886

Kleine, T., Kindgren, P., Benedict, C., Hendrickson, L., Strand, Å., Genome-Wide Gene Expression Analysis Reveals a Critical Role for CRYPTOCHROME1 in the Response of Arabidopsis to High Irradiance. *Plant Physiol.*144, no. 3 (2007): 1391-1406

Kocsis, B., Lee, M.-L., Antal, K., Yu, J.-H., Pócsi, I., Leiter, É., Emri, T., Genome-Wide Gene Expression Analyses of the AtfA/AtfB-Mediated Menadione Stress Response in Aspergillus nidulans. *Cells* 12, no. 3 (2023): 463

Kottke, T., Xie, A., Larsen, D.S., Hoff, W.D., Photoreceptors Take Charge: Emerging Principles for Light Sensing. *Ann. Rev. Biophys.* 47, no. 1 (2018): 291-313

Kou, Y., Han Tan, Y., Ramanujam, R., Naqvi, N.I., Structure-function analyses of the Pth11 receptor reveal an important role for CFEM motif and redox regulation in rice blast. *New Phytol.* 214, no. 1 (2017): 330-342

Kuge, S., Jones, N., Nomoto, A., Regulation of yAP-1 nuclear localization in response to oxidative stress. *EMBO J* 16 (1997): 1710 - 1720

Lane, N., Energetics and genetics across the prokaryote-eukaryote divide. *BMC* 6 (2011): 1-31

Lamparter, T., Krauß, N., Scheerer, P., Phytochromes from *Agrobacterium fabrum*. *Photochem. Photobiol.* 93, no. 3 (2017): 642-655

Leister K., Photobiochemical properties of the fungal phytochrome FphA from *Alternaria alternata*. [Master's Thesis; Karlsruher Institute of Technology] (2019)

Le Marechal, P., Hoang, B.M.C., Schmitter, J.-M., Van Dorsselaer, A., Decottignies, P., Purification, properties and primary structure of thioredoxin from *Aspergillus nidulans*. *Europ. J. Biochem.* 210, no. 2 (1992): 421-429

Levin, E.J., Kondrashov, D.A., Wesenberg, G.E.,Phillips Jr., G.N., Ensemble Refinement of Protein Crystal Structures: Validation and Application. *Structure* 15, no. 9 (2007): 1040-1052

Li, J., Liu, Z., Tan, C., Guo, X., Wang, L., Sancar, A., Zhong, D., Dynamics and mechanism of repair of ultraviolet-induced (6–4) photoproduct by photolyase. *Nature* 466, no. 7308 (2010): 887-890

Li, Q., McNeil, B., Harvey, L.M., Adaptive response to oxidative stress in the filamentous fungus *Aspergillus niger* B1-D. *Free Radic. Biol. Med.* 44, no. 3 (2008): 394-402

Li, X., Imlay, J.A., Improved measurements of scant hydrogen peroxide enable experiments that define its threshold of toxicity for *Escherichia coli*. *Free Radic. Biol. Med.* 120 (2018): 217-227

Li, Y., Shuai, L., A versatile genetic tool: haploid cells. *Stem Cell Res. & Ther.* 8 (2017): 1-6

Li, Z.-S., Szczypka, M., Lu, Y.-P., Thiele, D.J., Rea, P.A., The Yeast Cadmium Factor Protein (YCF1) Is a Vacuolar Glutathione S-Conjugate Pump. *J. Biol. Chem.* 271, no. 11 (1996): 6509-6517

Lim, J.Y., Kang, E.-H., Park, Y.-H., Kook, J.-H., Park, H.-M., Survival factor SvfA plays multiple roles in differentiation and is essential for completion of sexual development in *Aspergillus nidulans*. *Scient. Rep.* 10, no. 1 (2020): 5586

Lin, Q., Weis, S., Yang, G., Weng, Y.H., Helston, R., Rish, K., Smith, A., Bordner, J., Polte, T., Gaunitz, F., Dennery, P.A., Heme Oxygenase-1 Protein Localizes to the Nucleus and Activates Transcription Factors Important in Oxidative Stress. *J. Biol. Chem.* 282, no. 28 (2007): 20621-20633

Lind, A.L., Smith, T.D., Saterlee, T., Calvo, A.M., Rokas, A., Regulation of Secondary Metabolism by the Velvet Complex Is Temperature-Responsive in *Aspergillus*. *Genes Genomes Genet.* 6, no. 12 (2016): 4023-4033

Lisa-Santamaría, P., Jiménez, A., Revuelta, J.L., The Protein Factor-arrest 11 (Far11) Is Essential for the Toxicity of Human Caspase-10 in Yeast and Participates in the Regulation of Autophagy and the DNA Damage Signaling. *J. Biol. Chem.* 287, no. 35 (2012): 29636-29647

Loewith, R., Jacinto, E., Wullschleger, S., Lorberg, A., Crespo, J.L., Bonenfant, D., Oppliger, W., Jenoe, P., Hall, M.N., Two TOR Complexes, Only One of which Is Rapamycin Sensitive, Have Distinct Roles in Cell Growth Control. *Molec. Cell* 10, no. 3 (2002): 457-468

Lopez, L., Fasano, C., Perrella, G., Facella, P., Cryptochromes and the Circadian Clock: The Story of a Very Complex Relationship in a Spinning World. *genes* 12, no. 5 (2021): 672

Loriette, V., Fragola, A., Kruglik, S.G., Sridhar, S., Hubert, A., Orieux, F., Sepulveda, E., Sureau, F., Bonneau, S., Dynamics of mitochondrial membranes under photo-oxidative stress with high spatiotemporal resolution. *Front. Cell Devel. Biol.* 11 (2023): 1307502

Lynn, A., Chandra, S., Malhotra, P., Chauhan, V.S., Heme binding and polymerization by *Plasmodium falciparum* histidine rich protein II: influence of pH on activity and conformation. *FEBS Letters* 459, no. 2 (1999): 267-271

Madeo, F., Herker, E., Maldener, C., Wissing, S., Lächelt, S., Herlan, M., Fehr, M., Lauber, K., Sigrist, S.J., Wesselborg, S., Fröhlich, K.U., A Caspase-Related Protease Regulates Apoptosis in Yeast. *Molec. Cell* 9, no. 4 (2002): 911-917

Marchler-Bauer, A., Anderson, J.B. & Bryant, S.H. et al., CDD: a conserved domain database for interactive domain family analysis. *Nucleic Acids Res.* 35, no. suppl_1 (2007): D237-D240

Markina-Iñarrairaegui, A., Etxebeste, O., Herrero-García, E., Araújo-Bazán, L., Fernández-Martínez, J., Flores, J.A., Osmani, S.A., Espeso, E.A., Nuclear transporters in a multinucleated organism: functional and localization analyses in Aspergillus nidulans. *Molec. Biol. Cell* 22, no. 20 (2011): 3874-3886

Martins, D., Kathiresan., M., English, A.M., Cytochrome c peroxidase is a mitochondrial heme-based H2O2 sensor that modulates antioxidant defense. *Free Rad. Biol. Med.* 65 (2013): 541-551

Matsui, T., Nambu, S., Ono, Y., Goulding, C.W., Tsumoto, K., Ikeda-Saito, M., Heme degradation by *Staphylococcus aureus* IsdG and IsdI liberates formaldehyde rather than carbon monoxide. *Biochemistry* 52, no. 18 (2013): 3025-3027

Maul, M.J., Barends, T.R.M., Glas, A.F., Cryle, M.J., Domratcheva, T., Schneider, S., Schlichting, I., Carell, T., Crystal Structure and Mechanism of a DNA (6-4) Photolyase. *Angew. Chem.* 47, no. 52 (2008): 10076-10080

Mistry, J., Chuguransky, S., & Bateman, A. et al., Pfam: The protein families database in 2021. *Nucl. Acids Res.* 49, no. D1 (2021): D412-D419

Morozov, D., Modi, V., Mironov, V., Groenhof, G., The Photocycle of Bacteriophytochrome Is Initiated by Counterclockwise Chromophore Isomerization. *J Physic. Chem. Lett.* 13, no. 20 (2022): 4538-4542

Naito, E., Ito, M., Yokota, I., Saijo, T., Matsuda, J., Ogawa, Y., Kitamura, S., Takada, E., Horii, Y., Kuroda, Y., Thiamine-responsive pyruvate dehydrogenase deficiency in two patients caused by a point mutation (F205L and L216F) within the thiamine pyrophosphate binding region. *Biochimica et Biophysica Acta (BBA) – Molec. Basis Dis.* 1588, no. 1 (2002): 79-84

Navarro, R. E., Stringer, M. A., Hansberg, W., Timberlake, W. E., Aguirre, J., catA, a new Aspergillus nidulans gene encoding a developmentally regulated catalase. *Curr Genet.* 29 (1996): 352-359

Navarro, E., Nieman, N., Kock, D., Dadaeva, T., Gutiérrez, G., Engelsdorf, T., Kiontke, S., Corrochano, L.M., Batschauer, A., Garre, V., The DASH-type Cryptochrome from the Fungus *Mucor circinelloides* Is a Canonical CPD-Photolyase. *Curr. Biol.* 30, no. 22 (2020): 4483-4490

Odat, O., Matta, S., Khalil, H., Kampranis, S.C., Pfau, R., Tsichlis, P.N., Makris, A.M., Old Yellow Enzymes, Highly Homologous FMN Oxidoreductases with Modulating Roles in Oxidative Stress and Programmed Cell Death in Yeast. *Molec. Basis Cell Dev. Biol.* 282, no. 49 (2007): 36010-36023

Okazaki, S., Tachibana, T., Naganuma, A., Mano, N., Kuge, S., Multistep Disulfide Bond Formation in Yap1 Is Required for Sensing and Transduction of H2O2 Stress Signal. *Molec. Cell* 27, no. 4 (2007): 675-688

Okunlola, F.O., Soremekun, O.S., Olotu, F.A., Soliman, M.E.S., East to West not North-West: Structure-Based Mechanistic Resolution of 8-Hydroxyl Replacement and Resulting Effects on the Activities of Imidazole-Based Heme Oxygenase-1 Inhibitors. *Protein J* 40 (2021): 166-174

Olmedo, M., Ruger-Herreros, C., Luque, E.M., Corrochano, L.M., A complex photoreceptor system mediates the regulation by light of the conidiation genes con-10 and con-6 in *Neurospora crassa*. *Fung. Genet. Biol.* 47, no. 4 (2010): 352-363

Orosz, E., Antal, K., Gazdag, Z., Szabó, Z., Han, K.-H., Yu, J.-H., Pócsi, I., Emri, T., Transcriptome-Based Modeling Reveals that Oxidative Stress Induces Modulation of the AtfA-Dependent Signaling Networks in *Aspergillus nidulans*. *Int. J. Genom.* no. 1 (2017): 6923849

Pang, A.S.H, Nathoo, S., Wong, S.L., Cloning and Characterization of a Pair of Novel Genes that Regulate Production of Extracellular Enzymes in *Bacillus subtilis*. *J. Bacteriol.* 173, no. 1 (1991): 46-54

Park, C.M., Bhoo, S.H., Song, P.S., Inter-domain crosstalk in the phytochrome molecules. *Semin Cell Dev Biol.* vol. 11, no. 6 (2000) pp. 449-456

Paysan-Lafosse, T., Blum, M. & Bateman, A., InterPro in 2022. *Nucleic Acids Research* 51, no. D1 (2022): D418-D427

Petrovic, S., Pascolo, L., Gallo, R., Cupelli, F., Ostrow, J.D., Goffeau, A., Tiribelli, C., Bruschi, C.V., The products of YCF1 and YLL015w (BPT1) cooperate for the ATP-dependent vacuolar transport of unconjugated bilirubin in *Saccharomyces cerevisiae. Yeast* 16, no. 6 (2000): 561-571

Pham, V.N., Kathare, P.K., Huq, E., Phytochromes and Phytochrome Interacting Factors. *Plant Physiol.* 176, no. 2 (2018): 1025-1038

Pócsi, I., Leiter, É., Kwon, N.-J., Shin, K.-S., Kwon, G.-S., Pusztahelyi, T., Emri, T., Abuknesha, R.A., Price, R.G., Yu, J.-H., Asexual sporulation signalling regulates autolysis of *Aspergillus nidulans* via modulating the chitinase ChiB production. *J. Appl. Microbiol.* 107, no. 2 (2009): 514-523

Ponnu, J., Hoecker, U., Signaling Mechanisms by *Arabidopsis* Cryptochromes. *Front. Plant Sci.* 13 (2022): 844714

Potter, S.C., Luciani, A. & Finn, R.D. et al., HMMER web server: 2018 update. *Nucl. Acids Res.* 46, no. W1 (2018): W200-W204

Protchenko, O., Shakoury-Elizeh, M., Keane, P., Storey, J., Androphy, R., Philpott, C.C., Role of PUG1 in Inducible Porphyrin and Heme Transport in *Saccharomyces cerevisiae*. *Euk. Cell* 7, no. 5 (2008): 859-871

Purschwitz, J., Müller, S., Fischer, R. et al., Functional and Physical Interaction of Blue- and Red-Light Sensors in *Aspergillus nidulans*. Curr. Biol. 18, no. 4 (2008): 255-259

Purschwitz, J., Müller, S., Fischer, R., Mapping the interaction sites of *Aspergillus nidulans* phytochrome FphA with the global regulator VeA and the White Collar protein LreB. *Mol. Genet. Genomics* 281 (2009): 35-42

Rajan, S.S., Shuvalova, L., Yang, X., Anderson, W.F., Crystal Structure of THI-4 protein from *Bacillus subtilis*. PDB DOI: https://doi.org/10.2210/pdb1to9/pdb (2004)

Rauscher, S., Pacher, S., Hedtke, M., Kniemeyer, O., Fischer, R., A phosphorylation code of the *Aspergillus nidulans* global regulator VelvetA (VeA) determines specific functions. *Molec. Microbiol.* 99, no. 5 (2015): 909-924

Riggi, M., Kusmider, B., Loewith, R., The flipside of the TOR coin – TORC2 and plasma membrane homeostasis at a glance. *J. Cell Sci.* 133, no. 9 (2020): jcs242040

Rodríguez-López, M., Bordin, N., Lees, J., Scholes, H., Hassan, S., Saintain, Q., Kamrad, S., Orengo, C., Bähler, J., Broad functional profiling of fission yeast proteins using phenomics and machine learning. *eLife* 12 (2023): RP88229

Rodriguez-Romero, J., Hedtke, M., Kastner, C., Müller, S., Fischer, R., Fungi, Hidden in Soil or Up in the Air: Light Makes a Difference. *Ann. Rev. Microbiol.* 64, no. 1 (2010): 585-610

Röhrig, J., Kastner, C., Fischer, R., Light inhibits spore germination through phytochrome in *Aspergillus nidulans*. *Curr. Genet.* 59 (2013): 55-62

Romero, E., Castellanos, J.R.G., Gadda, G., Fraaije, M.W., Mattevi, A., Same Substrate, Many Reactions: Oxygen Activation in Flavoenzymes. *Chem. Rev.* 118, no. 4 (2018): 1742-1769

Roze, L.V., Chanda, A., Wee, J., Awad, D., Linz, J.E., Stress-related Transcription Factor AtfB Integrates Secondary Metabolism with Oxidative Stress Response in Aspergilli. *J. Biol. Chem.* 286, no. 40 (2011): 35137-35148

Ruger-Herreros, C., Rodríguez-Romero, J., Fernández-Barranco, R., Olmedo, M., Fischer, R., Corrochano, L.M., Canovas, D., Regulation of Conidiation by Light in *Aspergillus nidulans*. *Genetics* 188, no. 4 (2011): 809-822

Ryter, S.W., Heme Oxygenase-1: An Anti-Inflammatory Effector in Cardiovascular, Lung, and Related Metabolic Disorders. *Antioxidants (Basel)* 11, no. 3 (2022): 555

Saito, T., Koyanagi, M., Sugihara, T., Nagata, T., Arikawa, K., Terakita, A., Spectral tuning mediated by helix III in butterfly long wavelength-sensitive visual opsins revealed by heterologous action spectroscopy. *Zool. Lett.* 5 (2019): 1-11

Sancar, A., Structure and function of DNA photolyase. *Biochem.* 33, no. 1 (1994): 2-9

Sanchez, J.F., Entwistle, R., Hung, J.H., Yaegashi, J., Jain, S., Chiang, Y.-M., Wang, C.C.C., Oakley, B.R., Genome-Based Deletion Analysis Reveals the Prenyl Xanthone Biosynthesis Pathway in *Aspergillus nidulans*. *J. Amer. Chem. Soc.* 133, no. 11 (2011): 4010-4017

Sato, I., Shimizu, M., Hoshino, T., Takaya, N., The Glutathione System of Aspergillus nidulans Involves a Fungus-specific Glutathione S-Transferase. *J. Biol. Chem.* 284, no. 12 (2009): 8042-8053

Sayers, E.W., Bolton, E.E. & Sherry, S.T. et al., Database resources of the national center for biotechnology information. *Nucl. Acids Res.* 50, no. D1 (2022): D20-D26

Schafmeier, T., Káldi, K., Diernfellner, A., Mohr, C., Brunner, M., Phosphorylation-dependent maturation of *Neurospora* circadian clock protein from a nuclear repressor toward a cytoplasmic activator. *Genes & Develop.* 20, no. 3 (2006): 297-306

Schindelin, J., Arganda-Carreras, I., Frise, E. et al. Fiji: an open-source platform for biological-image analysis. *Nat Methods* (2012)

Schuhmacher, L., Heck, S., Pitz, M., Mathey, E., Lamparter, T., Blumhofer, A., Leister, K., Fischer, R., The LOV-domain blue-light receptor LreA of the fungus *Alternaria alternata* binds predominantly FAD as chromophore and acts as a light and temperature sensor. *J. Biol. Chem.* 300, no. 5 (2024) 107238

Schrödinger, L., DeLano, W., PyMOL, 2020

Sekiguchi, T., Ishii, T., Kamada, Y., Funakoshi, M., Kobayashi, H., Furuno, N., Involvement of Gtr1p in the oxidative stress response in yeast *Saccharomyces cerevisiae*. *Biochem. Biophys. Res. Comm.* 598 (2022): 107-112

Sen, A., Imlay, J.A., How Microbes Defend Themselves From Incoming Hydrogen Peroxide. *Front. Immun.* 12 (2021): 667343

Servos, J., Haase, E., Brendel, M., Gene *SNQ2* of *Saccharomyces cerevislae*, which confers resistance to 4-nitroquinoline-N-oxide and other chemicals, encodes a 169 kDa protein homologous to ATP-dependent permeases. *Molec. Genet. and Genomics* 236 (1993): 214-218

Shafi, A.A., McNair, C.M., McCann, J.J., Alshalalfa, M., Shostak, A., Severson, T.M., Knudsen, K.E., et al., The circadian cryptochrome, CRY1, is a pro-tumorigenic factor that rhythmically modulates DNA repair. *Nature Comm.* 12, no. 1 (2021): 401

Shimozono, S., Tsutsui, H., Miaywaki, A., Diffusion of Large Molecules into Assembling Nuclei Revealed Using an Optical Highlighting Technique. *Biophys. J.* 97, no. 5 (2009): 1288-1294

Smith, D.A., Nicholls, S., Morgan, B.A., Brown, A.J.P., Quinn, J., A conserved stress-activated protein kinase regulates a core stress response in the human pathogen *Candida albicans*. *Molec. Biol. Cell* 15, no. 9 (2004): 4179-4190

Spröte, P., Brakhage, A.A., The light-dependent regulator velvet A of *Aspergillus nidulans* acts as a repressor of the penicillin biosynthesis. *Arch Microbiol* 188 (2007): 69-79

Sultana, A. & Lee, J.E., Measuring Protein-Protein and Protein-Nucleic Acid Interaction by Biolayer Interferometry. *Curr. Protoc. Protein Sci* 79, no. 1 (2015): 19-25

Sun, J. & Loehr, T.M., Identification of Histidine 25 as the Heme Ligand in Human Liver Heme Oxygenase. *Biochemistry* 33, no. 46 (1994): 13734-13740

Stéphane, D., Jeanne-Marie, M., Predicting and Preventing Mold Spoilage of Food Products. *J. Food Prot.* 76, no. 3 (2013): 538-551

Streng, C., Identifizierung neuer Komponenten der Lichtwahrnehmung in *Aspergillus nidulans* und Untersuchung der Rolle zweier Hämoxygenasen in der Chromophorbildung von Phytochrom in *Alternaria alternata* [Doctoral PhD thesis, Karlsruher Institute of Technology] (2020)

Streng, C., Hartmann, J., Fischer, R., et al., Fungal phytochrome chromophore biosynthesis at mitochondria. *The EMBO Journal* 40, no. 17 (2021): e108083

Stringer, M.A., Dean, R.A., Sewall, T.C., Timberlake W.E., Rodletless, a new Aspergillus developmental mutant induced by directed gene inactivation. Genes & Devel. 5, no. 7 (1991): 1161-1171

Tagua, V.G., Pausch, M., Eckel, M., Gutiérrez, G., Miralles-Durán, A., Sanz, C., Eslava, A.P., Pokorny, R., Corrochano, L.M., Batschauer, A., Fungal cryptochrome with DNA repair activity reveals an early stage in cryptochrome evolution. *PNAS* 112, no. 49 (2015): 15130-15135

Tao, K., Fujita, N., Ishihama, A., Involvement of the RNA polymerase alpha subunit C-terminal region in co-operative interaction and transcriptional activation with OxyR protein. *Molec. Microbiol.* 7, no. 6 (1993): 859-864

Terakita, A., The opsins. *Genome Biology* 6 (2005): 1-9

Thön, M., Al-Abdallah, Q., Hortschansky, P., Brakhage, A.A., The Thioredoxin System of the Filamentous Fungus Aspergillus nidulans. *J. Biol. Chem.* 282, no. 37 (2007): 27259-27269

Trott, O., Olson, O., J., AutoDock Vina: improving the speed and accuracy of docking with a new scoring function, efficient optimization and multithreading. *J. Comput. Chem.* 31, no. 2 (2010): 455-461

Trott, O., AutoDock Vina Video Tutorial. https://vina.scripps.edu/tutorial/ (2014)

Toews, M.W., Warmbold, J., Fischer, R. et al., Establishment of mRFP1 as a fluorescent marker in *Aspergillus nidulans* and construction of expression vectors for high-throughput protein tagging using recombination in vitro (GATEWAY). *Curr. Genet.* 45 (2004): 383-389

Tóth, R., Kevei, É., Hall, A., Millar, A.J., Nagy, F., Kozma-Bognár, L., Circadian Clock-Regulated Expression of Phytochrome and Cryptochrome Genes in *Arabidopsis*. *Plant Physiol.* 127, no. 4 (2001): 1607-1616

Tunc-Ozdemir, M., Miller, G., Song, L., Kim, J., Sodek, A., Koussevitzky, S., Misra, A.N., Mittler, R., Shintani, D., Thiamin Confers Enhanced Tolerance to Oxidative Stress in *Arabidopsis*. *Plant Physiol.* 151, no. 1 (2009): 421-432

Vanderstraeten, J., Gailly, P., Malkemper, E.P., Light entrainment of retinal biorhythms: cryptochrome 2 as candidate photoreceptor in mammals. *Cellular and Molec. Life Sci.* 77, no. 5 (2020): 875-884

Van Munster, J.M., van der Kaaij, R.M., Dijkhuizen, L., van der Maarel, M.J.E.C., Biochemical characterization of *Aspergillus niger* CfcI, a glycoside hydrolase family 18 chitinase that releases monomers during substrate hydrolysis. *Microbiology* 158, no. 8 (2012): 2168-2179

Vechtomova, Y.L. Telegina, T.A., Buglak, A.A., Kritsky, M.S., UV Radiation in DNA Damage and Repair Involving DNA-Photolyases and Cryptochromes. *Biomedicines* 9, no. 11 (2021): 1564

Ververidis, P., Davrazou, F., Diallinas, G., Georgakopoulos, D., Kanellis, A.K., Panopoulos, N., A novel putative reductase (Cpd1p) and the multidrug exporter Snq2p are involved in resistance to cercosporin and other singlet oxygen-generating photosensitizers in *Saccharomyces cerevisiae*. *Curr. Genet.* 39, no. 3 (2001) 127

Vilora, J.S., Allega, M.F., Lambrughi, M., Papaleo, E., An optimal distance cutoff for contact-based Protein Structure Networks using side-chain centers of mass. *Nature Scientific Reports* 7, no. 1 (2017): 2838

Vivekanandan, K.E., Sivaraj, S., Kumaresan, S., Characterization and purification of laccase enzyme from *Aspergillus nidulans* CASVK3 from vellar estuary south east coast of India. *IJCMAS* 3, no. 10 (2014): 213-227

Wang, H., Deng, X.W., Phytochrome Signaling Mechanism. The Arabidopsis Book (2004)

Wang, X., Wang, Q., Nguyen, P., Lin, C., Cryptochrome-mediated light responses in plants. *Enzymes* vol. 35 (2018) pp. 167-189

Wang, J., Du, X., Pan, W., Wang, X., Wu, W., Photoactivation of the cryptochrome/photolyase superfamily. *J. Phot. Photobiol. C: Photochem. Rev.* 22 (2015): 84-102

Wang, Z., Wang, J., Li, N., Li, J., Trail, F., Dunlap, J.C., Townsend, J.P., Light sensing by opsins and fungal ecology: NOP-1 modulates entry into sexual reproduction in response to environmental cues. *Mol Ecol.* 27, no. 1 (2018): 216-232

Wartenberg, D., Vödisch, M., Kniemeyer, O., Albrecht-Eckhardt, D., Scherlach, K., Winkler, R., Weide, M., Brakhage, A.A., Proteome analysis of the farnesol-induced stress response in *Aspergillus nidulans*—The role of a putative dehydrin. *J. Proteom.* 75, no. 13 (2012): 4038-4049

Weaver, L., Hamoud, A.-R., Stec, D.E., Hinds Jr., T.D., Biliverdin reductase and bilirubin in hepatic disease. *Am J Physiol Gastrointest Liver Physiol.* 314, no. 6 (2018): G668-G676

Wegele, R., Tasler, R., Zeng, Y., Rivera, M., Frankenberg-Dinkel., N., The heme oxygenase(s)-phytochrome system of *Pseudomonas aeruginosa*. *J. Biol. Chem.* 279, no. 44 (2004): 45791-45802

Wilks, A., Medzihradszky, K., F., de Montellano, P., R., O., Heme Oxygenase Active-Site Residues Identified by Heme−Protein Cross-Linking during Reduction of CBrCl3. *Biochemistry* 37, no. 9 (1998): 2889-2896

Wood, M.J., Storz, G., Tjandra, N., Structural basis for redox regulation of Yap1 transcription factor localization. *Nature* 430, no. 7002 (2004): 917-921

Wu, C., Yang, F., Smith, K.M., Peterson, M., Dekhang, R., Zhang, Y., Zucker, J., Sachs, M.S., Genome-Wide Characterization of Light-Regulated Genes in *Neurospora crassa*. *Genes Genom. Genet.* 4, no. 9 (2014): 1731-1745

Wysong, D.R., Christin, L., Sugar, A.M., Robbins, P.W., Diamond, R.D., Cloning and sequencing of a *Candida albicans* catalase gene and effects of disruption of this gene. *Inf. and Imm.* 66, no. 5 (1998): 1953-1961

Xu, D., Marquis, K., Pei, J., Fu, S.-C., Cağatay, T., Grishin, N.V., Chook, Y.M., LocNES: a computational tool for locating classical NESs in CRM1 cargo proteins. *Bioinformatics* 31, no. 9 (2015): 1357-1365

Yachdav, G., Kloppmann, E. & Rost, B. et al., PredictProtein--an open resource for online prediction of protein structural and functional features. *Nucleic Acids Res.* 42, no. W1 (2014): W337-W343

Yamazaki, H., Yamazaki, D., Takaya, N., Takagi, M., Ohta, A., Horiuchi, H., A chitinase gene, chiB, involved in the autolytic process of *Aspergillus nidulans*. *Curr. Genet.* 51 (2007): 89-98

Yanovsky, M.J., Mazzella, M.A., Whitelam, G.C., Casal, J.J., Resetting of the Circadian Clock by Phytochromes and Cryptochromes in *Arabidopsis*. *J. Biol. Rhythms* 16, no. 6 (2001): 523-530

Yoshihara, S., Suzuki, F., Fujita, H., Geng, X.X., Ikeuchi, M., Novel putative photoreceptor and regulatory genes Required for the positive phototactic movement of the unicellular motile cyanobacterium *Synechocystis sp*. *PCC 6803*. *Plant Cell Phys.* 41, no. 12 (2000): 1299-1304

Yu, Z., Armant, O., Fischer, R., Fungi use the SakA (HogA) pathway for phytochrome-dependent light signalling. *Nature Microbiol.* 1, no. 5 (2016): 1-7

Yu, Z., Fischer, R., Light sensing and responses in fungi. *Nature Rev. – Microbiol.* 17, no. 1 (2018): 25-36

Yu, Z., Ali, A., Igbalajobi, O.A., Streng, C., Leister, K., Krauß, N., Lamparter, T., Fischer, R., Two hybrid histidine kinases, TcsB and the phytochrome FphA, are

involved in temperature sensing in *Aspergillus nidulans*. *Molec. Microbiol.* 112, no. 6 (2019): 1814-1830

Yu, Z., Streng, C., Seibeld, R.F., Igbalajobi, O.A., Leister, K., Ingelfinger, J., Fischer, R., Genome-wide analyses of light-regulated genes in *Aspergillus nidulans* reveal a complex interplay between different photoreceptors and novel photoreceptor functions. *PLoS Genet.* 17, no. 10 (2021): e1009845

Zallot, R., Yazdani, M., Goyer, A., Ziemak, M.J., Guan, J.-C., McCarty, D.R., Crécy-Lagard, V.d., Gerdes, S., Garrett, T.J., Benach, J., Hunt, J.F., Shintani, D.K., Hanson, A.D., Salvage of the thiamin pyrimidine moiety by plant TenA proteins lacking an active-site cysteine. *Biochem. J.* 463, no. 1 (2014): 145-155

Zheng, M., Åslund, F., Storz, G., Activation of the OxyR Transcription Factor by Reversible Disulfide Bond Formation. *Science* 279, no. 5357 (1998): 1718-1722

6. Appendix

Figure 55: Predict Protein analysis of HoxB of *A. nidulans* It is unlikely that HoxB binds to DNA

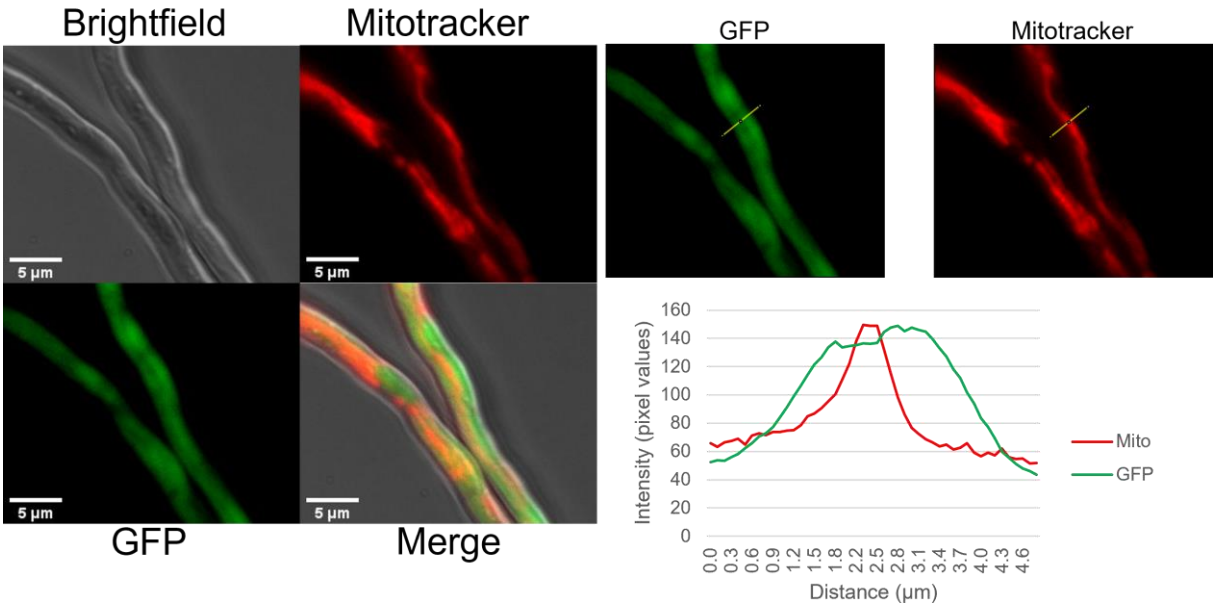

Figure 56: HoxB does not localize to mitochondria under normal conditions Visualization of mitochondria and GFP-HoxB. In some cases, increases in mitotracker-signal coincide with small dips in GFP-signal, indicating HoxB may not localize to mitochondria under standard growth conditions or may be able to localize to mitochondria conditionally.

Table 37: All genes uniquely regulated in response to hydrogen peroxide in SKV103

Symbol	Up or Down
AN 0094	Up
AN 0097	Up
AN 0170	Up
AN 0171	Up
AN 0245	Up
AN 0298	Up
AN 0304	Up
AN 0368	Up
AN 0374	Up
AN 0422	Up
AN 0435	Up
AN 0460	Up
AN 0468	Up
AN 0482	Up
AN 0498	Up
AN 0539	Up
AN 0563	Up
AN 0600	Up
AN 0723	Up
AN 0732	Up
AN 0754	Up
AN 0778	Up
AN 0884	Up
AN 0981	Up
AN 1144	Up
AN 1231	Up
AN 1240	Up
AN 1242	Up
AN 1331	Up
AN 1342	Up
AN 1429	Up
AN 1430	Up
AN 1450	Up
AN 1451	Up
AN 1490	Up
AN 1520	Up
AN 1547	Up
AN 1566	Up
AN 1620	Up
AN 1622	Up
AN 1650	Up
AN 1656	Up
AN 1671	Up
AN 1714	Up
AN 1753	Up
AN 1781	Up
AN 1800	Up
AN 1801	Up
AN 1808	Up
AN 1819	Up
AN 1868	Up
AN 1871	Up
AN 1872	Up
AN 1882	Up
AN 2029	Up
AN 2072	Up
AN 2168	Up
AN 2232	Up
AN 2255	Up
AN 2374	Up
AN 2383	Up
AN 2397	Up
AN 2407	Up
AN 2435	Up
AN 2436	Up
AN 2498	Up
AN 2503	Up
AN 2526	Up
AN 2661	Up
AN 2684	Up
AN 2695	Up
AN 2711	Up
AN 2796	Up
AN 2826	Up
AN 2837	Up
AN 2879	Up
AN 2919	Up
AN 2926	Up
AN 2931	Up
AN 2942	Up
AN 2943	Up
AN 2952	Up
AN 2953	Up
AN 2955	Up
AN 2995	Up
AN 3017	Up
AN 3031	Up
AN 3087	Up
AN 3129	Up
AN 3175	Up
AN 3191	Up
AN 3225	Up
AN 3230	Up
AN 3311	Up
AN 3329	Up
AN 3373	Up
AN 3433	Up
AN 3497	Up
AN 3506	Up
AN 3507	Up
AN 3524	Up
AN 3525	Up
AN 3632	Up
AN 3671	Up
AN 3689	Up
AN 3769	Up
AN 3848	Up
AN 3873	Up
AN 3877	Up
AN 3900	Up
AN 3979	Up
AN 3983	Up
AN 3997	Up
AN 4046	Up
AN 4089	Up
AN 4105	Up
AN 4117	Up
AN 4134	Up
AN 4139	Up
AN 4147	Up
AN 4199	Up
AN 4224	Up
AN 4248	Up
AN 4263	Up
AN 4322	Up
AN 4345	Up
AN 4372	Up
AN 4393	Up
AN 4474	Up
AN 4552	Up
AN 4608	Up
AN 4654	Up
AN 4708	Up
AN 4854	Up
AN 4933	Up
AN 4935	Up
AN 4989	Up
AN 5082	Up
AN 5110	Up
AN 5118	Up
AN 5140	Up
AN 5159	Up
AN 5172	Up
AN 5231	Up
AN 5258	Up
AN 5396	Up
AN 5409	Up
AN 5477	Up
AN 5478	Up
AN 5504	Up
AN 5509	Up
AN 5535	Up
AN 5550	Up
AN 5600	Up
AN 5623	Up
AN 5657	Up
AN 5689	Up
AN 5824	Up
AN 5831	Up
AN 5936	Up
AN 5940	Up
AN 5983	Up
AN 6023	Up
AN 6069	Up
AN 6132	Up
AN 6139	Up
AN 6215	Up
AN 6304	Up
AN 6403	Up
AN 6423	Up
AN 6430	Up
AN 6434	Up
AN 6481	Up
AN 6532	Up
AN 6581	Up
AN 6618	Up
AN 6645	Up
AN 6670	Up
AN 6693	Up
AN 6731	Up
AN 6775	Up
AN 6778	Up
AN 6779	Up
AN 6780	Up
AN 6789	Up
AN 6821	Up
AN 6861	Up
AN 6883	Up
AN 6899	Up
AN 6917	Up
AN 6931	Up
AN 6940	Up
AN 6941	Up
AN 6983	Up
AN 7050	Up
AN 7095	Up
AN 7151	Up
AN 7165	Up
AN 7166	Up
AN 7191	Up
AN 7199	Up
AN 7221	Up
AN 7222	Up
AN 7229	Up
AN 7245	Up
AN 7267	Up
AN 7268	Up

AN 7374	Up	**AN 9054**	Up	**AN 0423**	Down	**AN 1738**	Down
AN 7378	Up	**AN 9089**	Up	**AN 0484**	Down	**AN 1849**	Down
AN 7385	Up	**AN 9162**	Up	**AN 0486**	Down	**AN 1850**	Down
AN 7431	Up	**AN 9167**	Up	**AN 0507**	Down	**AN 1857**	Down
AN 7470	Up	**AN 9168**	Up	**AN 0540**	Down	**AN 1869**	Down
AN 7577	Up	**AN 9184**	Up	**AN 0541**	Down	**AN 1897**	Down
AN 7601	Up	**AN 9204**	Up	**AN 0542**	Down	**AN 1912**	Down
AN 7618	Up	**AN 9252**	Up	**AN 0543**	Down	**AN 1943**	Down
AN 7621	Up	**AN 9293**	Up	**AN 0568**	Down	**AN 1977**	Down
AN 7662	Up	**AN 9315**	Up	**AN 0595**	Down	**AN 2004**	Down
AN 7684	Up	**AN 9339**	Up	**AN 0610**	Down	**AN 2062**	Down
AN 7725	Up	**AN 9354**	Up	**AN 0638**	Down	**AN 2063**	Down
AN 7729	Up	**AN 9373**	Up	**AN 0660**	Down	**AN 2129**	Down
AN 7753	Up	**AN 9513**	Up	**AN 0712**	Down	**AN 2166**	Down
AN 7792	Up	**AN 10028**	Up	**AN 0726**	Down	**AN 2177**	Down
AN 7895	Up	**AN 10041**	Up	**AN 0739**	Down	**AN 2250**	Down
AN 7909	Up	**AN 10062**	Up	**AN 0744**	Down	**AN 2289**	Down
AN 7911	Up	**AN 10096**	Up	**AN 0746**	Down	**AN 2305**	Down
AN 7912	Up	**AN 10134**	Up	**AN 0830**	Down	**AN 2344**	Down
AN 7950	Up	**AN 10198**	Up	**AN 0834**	Down	**AN 2353**	Down
AN 7992	Up	**AN 10199**	Up	**AN 0836**	Down	**AN 2358**	Down
AN 8006	Up	**AN 10220**	Up	**AN 0847**	Down	**AN 2360**	Down
AN 8008	Up	**AN 10242**	Up	**AN 0928**	Down	**AN 2466**	Down
AN 8067	Up	**AN 10295**	Up	**AN 0967**	Down	**AN 2479**	Down
AN 8089	Up	**AN 10321**	Up	**AN 0995**	Down	**AN 2493**	Down
AN 8095	Up	**AN 10350**	Up	**AN 1006**	Down	**AN 2509**	Down
AN 8099	Up	**AN 10448**	Up	**AN 1007**	Down	**AN 2529**	Down
AN 8103	Up	**AN 10485**	Up	**AN 1041**	Down	**AN 2553**	Down
AN 8104	Up	**AN 10488**	Up	**AN 1054**	Down	**AN 2567**	Down
AN 8150	Up	**AN 10490**	Up	**AN 1056**	Down	**AN 2659**	Down
AN 8251	Up	**AN 10536**	Up	**AN 1077**	Down	**AN 2662**	Down
AN 8255	Up	**AN 10693**	Up	**AN 1080**	Down	**AN 2666**	Down
AN 8278	Up	**AN 10703**	Up	**AN 1117**	Down	**AN 2731**	Down
AN 8300	Up	**AN 10789**	Up	**AN 1170**	Down	**AN 2760**	Down
AN 8361	Up	**AN 10929**	Up	**AN 1204**	Down	**AN 2829**	Down
AN 8365	Up	**AN 10975**	Up	**AN 1271**	Down	**AN 2844**	Down
AN 8373	Up	**AN 11016**	Up	**AN 1291**	Down	**AN 2859**	Down
AN 8377	Up	**AN 11100**	Up	**AN 1303**	Down	**AN 2976**	Down
AN 8417	Up	**AN 11165**	Up	**AN 1310**	Down	**AN 3029**	Down
AN 8428	Up	**BGI_novel_G000082**	Up	**AN 1378**	Down	**AN 3080**	Down
AN 8441	Up	**BGI_novel_G000047**	Up	**AN 1461**	Down	**AN 3116**	Down
AN 8460	Up	**BGI_novel_G000056**	Up	**AN 1488**	Down	**AN 3139**	Down
AN 8478	Up	**AN 0052**	Down	**AN 1503**	Down	**AN 3178**	Down
AN 8512	Up	**AN 0055**	Down	**AN 1579**	Down	**AN 3196**	Down
AN 8562	Up	**AN 0080**	Down	**AN 1597**	Down	**AN 3209**	Down
AN 8587	Up	**AN 0104**	Down	**AN 1608**	Down	**AN 3333**	Down
AN 8608	Up	**AN 0119**	Down	**AN 1609**	Down	**AN 3349**	Down
AN 8733	Up	**AN 0120**	Down	**AN 1678**	Down	**AN 3366**	Down
AN 8796	Up	**AN 0150**	Down	**AN 1679**	Down	**AN 3402**	Down
AN 8933	Up	**AN 0174**	Down	**AN 1703**	Down	**AN 3431**	Down
AN 8939	Up	**AN 0181**	Down	**AN 1706**	Down	**AN 3517**	Down
AN 8949	Up	**AN 0200**	Down	**AN 1712**	Down	**AN 3519**	Down
AN 8969	Up	**AN 0232**	Down	**AN 1726**	Down	**AN 3520**	Down
AN 9000	Up	**AN 0338**	Down	**AN 1733**	Down	**AN 3565**	Down
AN 9004	Up	**AN 0405**	Down	**AN 1737**	Down	**AN 3573**	Down

AN 3590	Down	**AN 5076**	Down	**AN 6727**	Down	**AN 8050**	Down
AN 3599	Down	**AN 5141**	Down	**AN 6823**	Down	**AN 8069**	Down
AN 3643	Down	**AN 5155**	Down	**AN 6831**	Down	**AN 8084**	Down
AN 3654	Down	**AN 5174**	Down	**AN 6847**	Down	**AN 8111**	Down
AN 3741	Down	**AN 5181**	Down	**AN 6874**	Down	**AN 8124**	Down
AN 3778	Down	**AN 5193**	Down	**AN 6885**	Down	**AN 8193**	Down
AN 3791	Down	**AN 5205**	Down	**AN 6921**	Down	**AN 8265**	Down
AN 3799	Down	**AN 5305**	Down	**AN 6933**	Down	**AN 8307**	Down
AN 3888	Down	**AN 5306**	Down	**AN 6934**	Down	**AN 8309**	Down
AN 3974	Down	**AN 5346**	Down	**AN 7033**	Down	**AN 8399**	Down
AN 4006	Down	**AN 5378**	Down	**AN 7076**	Down	**AN 8445**	Down
AN 4008	Down	**AN 5400**	Down	**AN 7081**	Down	**AN 8481**	Down
AN 4019	Down	**AN 5415**	Down	**AN 7121**	Down	**AN 8498**	Down
AN 4020	Down	**AN 5487**	Down	**AN 7141**	Down	**AN 8532**	Down
AN 4031	Down	**AN 5557**	Down	**AN 7181**	Down	**AN 8537**	Down
AN 4048	Down	**AN 5586**	Down	**AN 7269**	Down	**AN 8546**	Down
AN 4050	Down	**AN 5602**	Down	**AN 7298**	Down	**AN 8547**	Down
AN 4058	Down	**AN 5611**	Down	**AN 7302**	Down	**AN 8559**	Down
AN 4069	Down	**AN 5650**	Down	**AN 7320**	Down	**AN 8606**	Down
AN 4070	Down	**AN 5658**	Down	**AN 7323**	Down	**AN 8609**	Down
AN 4174	Down	**AN 5672**	Down	**AN 7338**	Down	**AN 8615**	Down
AN 4186	Down	**AN 5708**	Down	**AN 7339**	Down	**AN 8657**	Down
AN 4201	Down	**AN 5725**	Down	**AN 7357**	Down	**AN 8661**	Down
AN 4209	Down	**AN 5780**	Down	**AN 7367**	Down	**AN 8737**	Down
AN 4223	Down	**AN 5823**	Down	**AN 7391**	Down	**AN 8777**	Down
AN 4255	Down	**AN 5844**	Down	**AN 7426**	Down	**AN 8781**	Down
AN 4340	Down	**AN 5846**	Down	**AN 7428**	Down	**AN 8861**	Down
AN 4353	Down	**AN 5888**	Down	**AN 7447**	Down	**AN 8899**	Down
AN 4367	Down	**AN 5907**	Down	**AN 7472**	Down	**AN 8928**	Down
AN 4392	Down	**AN 5908**	Down	**AN 7484**	Down	**AN 8938**	Down
AN 4504	Down	**AN 5929**	Down	**AN 7488**	Down	**AN 8942**	Down
AN 4583	Down	**AN 5944**	Down	**AN 7491**	Down	**AN 8977**	Down
AN 4590	Down	**AN 5947**	Down	**AN 7500**	Down	**AN 8983**	Down
AN 4623	Down	**AN 5948**	Down	**AN 7523**	Down	**AN 9047**	Down
AN 4634	Down	**AN 5977**	Down	**AN 7539**	Down	**AN 9116**	Down
AN 4685	Down	**AN 6019**	Down	**AN 7541**	Down	**AN 9124**	Down
AN 4687	Down	**AN 6061**	Down	**AN 7557**	Down	**AN 9214**	Down
AN 4688	Down	**AN 6075**	Down	**AN 7568**	Down	**AN 9289**	Down
AN 4690	Down	**AN 6084**	Down	**AN 7622**	Down	**AN 9304**	Down
AN 4739	Down	**AN 6176**	Down	**AN 7631**	Down	**AN 9313**	Down
AN 4758	Down	**AN 6189**	Down	**AN 7633**	Down	**AN 9363**	Down
AN 4774	Down	**AN 6197**	Down	**AN 7679**	Down	**AN 9369**	Down
AN 4806	Down	**AN 6224**	Down	**AN 7704**	Down	**AN 9384**	Down
AN 4817	Down	**AN 6225**	Down	**AN 7708**	Down	**AN 9444**	Down
AN 4831	Down	**AN 6281**	Down	**AN 7715**	Down	**AN 9448**	Down
AN 4929	Down	**AN 6307**	Down	**AN 7780**	Down	**AN 9460**	Down
AN 4939	Down	**AN 6345**	Down	**AN 7805**	Down	**AN 9495**	Down
AN 4957	Down	**AN 6386**	Down	**AN 7838**	Down	**AN 9522**	Down
AN 5015	Down	**AN 6418**	Down	**AN 7865**	Down	**AN 10034**	Down
AN 5020	Down	**AN 6419**	Down	**AN 7884**	Down	**AN 10081**	Down
AN 5021	Down	**AN 6438**	Down	**AN 7904**	Down	**AN 10108**	Down
AN 5027	Down	**AN 6565**	Down	**AN 7917**	Down	**AN 10171**	Down
AN 5035	Down	**AN 6613**	Down	**AN 7967**	Down	**AN 10205**	Down
AN 5050	Down	**AN 6642**	Down	**AN 7986**	Down	**AN 10217**	Down
AN 5069	Down	**AN 6654**	Down	**AN 8005**	Down	**AN 10222**	Down

AN 10255	Down
AN 10284	Down
AN 10306	Down
AN 10335	Down
AN 10354	Down
AN 10359	Down
AN 10379	Down
AN 10441	Down
AN 10455	Down
AN 10491	Down
AN 10495	Down
AN 10512	Down
AN 10518	Down
AN 10550	Down
AN 10652	Down
AN 10684	Down
AN 10706	Down
AN 10795	Down
AN 10829	Down
AN 10834	Down
AN 10898	Down
AN 10947	Down
AN 10967	Down
AN 11040	Down
AN 11117	Down
AN 11146	Down
AN 11226	Down
AN 11312	Down
AN 11359	Down
AN 11541	Down
AN 11608	Down
BGI_novel_G000073	Down
BGI_novel_G000072	Down
BGI_novel_G000057	Down
BGI_novel_G000012	Down
BGI_novel_G000078	Down

Table 38: All genes differentially regulated in SRFS26 in response to hydrogen peroxide

Symbol	Up or Down	AN 1731	Up	AN 3403	Up	AN 5414	Up
		AN 1847	Up	AN 3415	Up	AN 5427	Up
AN 0061	Up	AN 1861	Up	AN 3421	Up	AN 5430	Up
AN 0062	Up	AN 1955	Up	AN 3490	Up	AN 5437	Up
AN 0146	Up	AN 1967	Up	AN 3551	Up	AN 5510	Up
AN 0147	Up	AN 2013	Up	AN 3600	Up	AN 5659	Up
AN 0159	Up	AN 2020	Up	AN 3627	Up	AN 5667	Up
AN 0226	Up	AN 2036	Up	AN 3818	Up	AN 5687	Up
AN 0282	Up	AN 2118	Up	AN 3866	Up	AN 5709	Up
AN 0294	Up	AN 2155	Up	AN 3882	Up	AN 5775	Up
AN 0395	Up	AN 2171	Up	AN 3934	Up	AN 5813	Up
AN 0528	Up	AN 2219	Up	AN 3938	Up	AN 5900	Up
AN 0531	Up	AN 2228	Up	AN 4088	Up	AN 5943	Up
AN 0566	Up	AN 2328	Up	AN 4114	Up	AN 5945	Up
AN 0588	Up	AN 2336	Up	AN 4138	Up	AN 6081	Up
AN 0644	Up	AN 2337	Up	AN 4167	Up	AN 6275	Up
AN 0651	Up	AN 2366	Up	AN 4189	Up	AN 6299	Up
AN 0655	Up	AN 2370	Up	AN 4324	Up	AN 6321	Up
AN 0656	Up	AN 2371	Up	AN 4357	Up	AN 6347	Up
AN 0693	Up	AN 2385	Up	AN 4364	Up	AN 6377	Up
AN 0731	Up	AN 2387	Up	AN 4469	Up	AN 6411	Up
AN 0780	Up	AN 2447	Up	AN 4544	Up	AN 6429	Up
AN 0793	Up	AN 2560	Up	AN 4625	Up	AN 6433	Up
AN 0807	Up	AN 2571	Up	AN 4642	Up	AN 6444	Up
AN 0841	Up	AN 2582	Up	AN 4655	Up	AN 6447	Up
AN 0856	Up	AN 2583	Up	AN 4673	Up	AN 6450	Up
AN 0857	Up	AN 2588	Up	AN 4701	Up	AN 6456	Up
AN 0903	Up	AN 2593	Up	AN 4795	Up	AN 6460	Up
AN 0904	Up	AN 2636	Up	AN 4845	Up	AN 6527	Up
AN 0930	Up	AN 2647	Up	AN 4846	Up	AN 6550	Up
AN 0931	Up	AN 2649	Up	AN 4871	Up	AN 6633	Up
AN 0973	Up	AN 2706	Up	AN 4909	Up	AN 6700	Up
AN 0975	Up	AN 2813	Up	AN 4920	Up	AN 6757	Up
AN 0983	Up	AN 2815	Up	AN 4961	Up	AN 6784	Up
AN 1020	Up	AN 2832	Up	AN 5003	Up	AN 6787	Up
AN 1100	Up	AN 2854	Up	AN 5018	Up	AN 6797	Up
AN 1134	Up	AN 2894	Up	AN 5039	Up	AN 6803	Up
AN 1147	Up	AN 2899	Up	AN 5117	Up	AN 6812	Up
AN 1202	Up	AN 2901	Up	AN 5169	Up	AN 6836	Up
AN 1236	Up	AN 3004	Up	AN 5203	Up	AN 6943	Up
AN 1261	Up	AN 3020	Up	AN 5204	Up	AN 6985	Up
AN 1314	Up	AN 3023	Up	AN 5207	Up	AN 7001	Up
AN 1321	Up	AN 3051	Up	AN 5303	Up	AN 7035	Up
AN 1428	Up	AN 3077	Up	AN 5312	Up	AN 7071	Up
AN 1431	Up	AN 3130	Up	AN 5314	Up	AN 7073	Up
AN 1497	Up	AN 3150	Up	AN 5315	Up	AN 7074	Up
AN 1514	Up	AN 3152	Up	AN 5339	Up	AN 7075	Up
AN 1573	Up	AN 3273	Up	AN 5350	Up	AN 7110	Up
AN 1577	Up	AN 3277	Up	AN 5353	Up	AN 7200	Up
AN 1586	Up	AN 3280	Up	AN 5398	Up	AN 7253	Up
AN 1612	Up	AN 3281	Up	AN 5402	Up	AN 7532	Up
AN 1623	Up	AN 3395	Up	AN 5408	Up	AN 7580	Up

AN 7644	Up	**AN 10289**	Up	**AN 0917**	Down	**AN 3489**	Down
AN 7851	Up	**AN 10297**	Up	**AN 0918**	Down	**AN 3515**	Down
AN 7881	Up	**AN 10318**	Up	**AN 1061**	Down	**AN 3555**	Down
AN 7883	Up	**AN 10336**	Up	**AN 1073**	Down	**AN 3710**	Down
AN 7900	Up	**AN 10343**	Up	**AN 1119**	Down	**AN 3759**	Down
AN 7999	Up	**AN 10355**	Up	**AN 1169**	Down	**AN 3865**	Down
AN 8075	Up	**AN 10417**	Up	**AN 1311**	Down	**AN 3958**	Down
AN 8129	Up	**AN 10442**	Up	**AN 1318**	Down	**AN 3961**	Down
AN 8146	Up	**AN 10557**	Up	**AN 1477**	Down	**AN 4002**	Down
AN 8154	Up	**AN 10580**	Up	**AN 1563**	Down	**AN 4094**	Down
AN 8175	Up	**AN 10604**	Up	**AN 1564**	Down	**AN 4102**	Down
AN 8308	Up	**AN 10678**	Up	**AN 1587**	Down	**AN 4120**	Down
AN 8324	Up	**AN 10691**	Up	**AN 1593**	Down	**AN 4135**	Down
AN 8325	Up	**AN 10731**	Up	**AN 1607**	Down	**AN 4136**	Down
AN 8326	Up	**AN 10805**	Up	**AN 1611**	Down	**AN 4176**	Down
AN 8327	Up	**AN 10838**	Up	**AN 1614**	Down	**AN 4243**	Down
AN 8339	Up	**AN 10869**	Up	**AN 1658**	Down	**AN 4276**	Down
AN 8340	Up	**AN 10960**	Up	**AN 1682**	Down	**AN 4405**	Down
AN 8341	Up	**AN 10985**	Up	**AN 1799**	Down	**AN 4539**	Down
AN 8342	Up	**AN 11011**	Up	**AN 1832**	Down	**AN 4603**	Down
AN 8366	Up	**AN 11039**	Up	**AN 1866**	Down	**AN 4747**	Down
AN 8413	Up	**AN 11046**	Up	**AN 1911**	Down	**AN 4749**	Down
AN 8429	Up	**AN 11051**	Up	**AN 1937**	Down	**AN 4778**	Down
AN 8458	Up	**AN 11158**	Up	**AN 1981**	Down	**AN 4784**	Down
AN 8507	Up	**AN 11161**	Up	**AN 2018**	Down	**AN 4786**	Down
AN 8526	Up	**AN 11191**	Up	**AN 2021**	Down	**AN 4822**	Down
AN 8536	Up	**AN 11217**	Up	**AN 2041**	Down	**AN 4866**	Down
AN 8542	Up	**AN 11222**	Up	**AN 2107**	Down	**AN 4883**	Down
AN 8564	Up	**AN 11314**	Up	**AN 2132**	Down	**AN 4948**	Down
AN 8623	Up	**AN 11607**	Up	**AN 2197**	Down	**AN 4983**	Down
AN 8643	Up	**AN 11612**	Up	**AN 2204**	Down	**AN 5000**	Down
AN 8706	Up	**BGI_novel_G 000014**	Up	**AN 2346**	Down	**AN 5019**	Down
AN 8743	Up			**AN 2376**	Down	**AN 5037**	Down
AN 8881	Up	**AN 0016**	Down	**AN 2463**	Down	**AN 5087**	Down
AN 8930	Up	**AN 0056**	Down	**AN 2475**	Down	**AN 5134**	Down
AN 8962	Up	**AN 0122**	Down	**AN 2515**	Down	**AN 5145**	Down
AN 8984	Up	**AN 0132**	Down	**AN 2530**	Down	**AN 5191**	Down
AN 9003	Up	**AN 0209**	Down	**AN 2675**	Down	**AN 5226**	Down
AN 9206	Up	**AN 0231**	Down	**AN 2680**	Down	**AN 5276**	Down
AN 9210	Up	**AN 0246**	Down	**AN 2690**	Down	**AN 5345**	Down
AN 9220	Up	**AN 0250**	Down	**AN 2713**	Down	**AN 5463**	Down
AN 9309	Up	**AN 0256**	Down	**AN 2745**	Down	**AN 5470**	Down
AN 9361	Up	**AN 0302**	Down	**AN 2780**	Down	**AN 5496**	Down
AN 9372	Up	**AN 0331**	Down	**AN 2818**	Down	**AN 5503**	Down
AN 9483	Up	**AN 0335**	Down	**AN 2828**	Down	**AN 5524**	Down
AN 10022	Up	**AN 0339**	Down	**AN 2937**	Down	**AN 5531**	Down
AN 10038	Up	**AN 0377**	Down	**AN 2944**	Down	**AN 5749**	Down
AN 10044	Up	**AN 0399**	Down	**AN 3057**	Down	**AN 5847**	Down
AN 10049	Up	**AN 0403**	Down	**AN 3117**	Down	**AN 6001**	Down
AN 10068	Up	**AN 0466**	Down	**AN 3136**	Down	**AN 6048**	Down
AN 10104	Up	**AN 0481**	Down	**AN 3204**	Down	**AN 6093**	Down
AN 10113	Up	**AN 0585**	Down	**AN 3206**	Down	**AN 6180**	Down
AN 10119	Up	**AN 0639**	Down	**AN 3336**	Down	**AN 6242**	Down
AN 10158	Up	**AN 0640**	Down	**AN 3352**	Down	**AN 6253**	Down
AN 10288	Up	**AN 0756**	Down	**AN 3369**	Down	**AN 6262**	Down

AN 6276	Down	**AN 7641**	Down	**AN 8522**	Down	**AN 10435**	Down
AN 6283	Down	**AN 7648**	Down	**AN 8592**	Down	**AN 10478**	Down
AN 6297	Down	**AN 7652**	Down	**AN 8754**	Down	**AN 10501**	Down
AN 6319	Down	**AN 7668**	Down	**AN 8814**	Down	**AN 10554**	Down
AN 6332	Down	**AN 7683**	Down	**AN 8901**	Down	**AN 10578**	Down
AN 6333	Down	**AN 7814**	Down	**AN 8923**	Down	**AN 10600**	Down
AN 6395	Down	**AN 7867**	Down	**AN 8931**	Down	**AN 10607**	Down
AN 6477	Down	**AN 7870**	Down	**AN 8953**	Down	**AN 10639**	Down
AN 6518	Down	**AN 7918**	Down	**AN 8970**	Down	**AN 10683**	Down
AN 6604	Down	**AN 7921**	Down	**AN 8978**	Down	**AN 10720**	Down
AN 6703	Down	**AN 7934**	Down	**AN 8980**	Down	**AN 10846**	Down
AN 6743	Down	**AN 7936**	Down	**AN 9133**	Down	**AN 10979**	Down
AN 6782	Down	**AN 7953**	Down	**AN 9140**	Down	**AN 10983**	Down
AN 6837	Down	**AN 7985**	Down	**AN 9226**	Down	**AN 10994**	Down
AN 6845	Down	**AN 7989**	Down	**AN 9286**	Down	**AN 10995**	Down
AN 6888	Down	**AN 8037**	Down	**AN 9348**	Down	**AN 11003**	Down
AN 6923	Down	**AN 8122**	Down	**AN 9380**	Down	**AN 11018**	Down
AN 6946	Down	**AN 8149**	Down	**AN 9389**	Down	**AN 11044**	Down
AN 6964	Down	**AN 8206**	Down	**AN 9521**	Down	**AN 11049**	Down
AN 6973	Down	**AN 8211**	Down	**AN 10021**	Down	**AN 11092**	Down
AN 7006	Down	**AN 8223**	Down	**AN 10024**	Down	**AN 11127**	Down
AN 7112	Down	**AN 8351**	Down	**AN 10042**	Down	**AN 11274**	Down
AN 7140	Down	**AN 8374**	Down	**AN 10086**	Down	**AN 11440**	Down
AN 7148	Down	**AN 8390**	Down	**AN 10110**	Down	**AN 11584**	Down
AN 7227	Down	**AN 8416**	Down	**AN 10120**	Down	**BGI_novel_G 000010**	Down
AN 7242	Down	**AN 8431**	Down	**AN 10169**	Down		
AN 7295	Down	**AN 8434**	Down	**AN 10178**	Down	**BGI_novel_G 000070**	Down
AN 7319	Down	**AN 8435**	Down	**AN 10274**	Down		
AN 7332	Down	**AN 8437**	Down	**AN 10285**	Down	**BGI_novel_G 000074**	Down
AN 7402	Down	**AN 8454**	Down	**AN 10308**	Down		
AN 7460	Down	**AN 8469**	Down	**AN 10344**	Down		
AN 7466	Down	**AN 8505**	Down	**AN 10404**	Down		

Table 39: Genes of SKV103 upregulated in GO enrichment

Gene	AN 3031	AN 6481	AN 8104
AN 0170	AN 3087	AN 6581	AN 8150
AN 0171	AN 3225	AN 6645	AN 8278
AN 0374	AN 3311	AN 6670	AN 8361
AN 0498	AN 3329	AN 6731	AN 8365
AN 0600	AN 3497	AN 6775	AN 8428
AN 0723	AN 3507	AN 6778	AN 8512
AN 0732	AN 3524	AN 6779	AN 8587
AN 0754	AN 3769	AN 6821	AN 8733
AN 0884	AN 3873	AN 6861	AN 8796
AN 0981	AN 3979	AN 6883	AN 8933
AN 1240	AN 3997	AN 6940	AN 9000
AN 1331	AN 4046	AN 6941	AN 9004
AN 1429	AN 4117	AN 7050	AN 9162
AN 1430	AN 4199	AN 7165	AN 9168
AN 1450	AN 4224	AN 7166	AN 9184
AN 1547	AN 4248	AN 7191	AN 9252
AN 1620	AN 4854	AN 7222	AN 9315
AN 1622	AN 4989	AN 7229	AN 9339
AN 1671	AN 5140	AN 7267	AN 10028
AN 1753	AN 5258	AN 7268	AN 10041
AN 1800	AN 5409	AN 7601	AN 10062
AN 1808	AN 5477	AN 7618	AN 10134
AN 1868	AN 5478	AN 7621	AN 10220
AN 1872	AN 5550	AN 7662	AN 10321
AN 1882	AN 5600	AN 7684	AN 10448
AN 2232	AN 5689	AN 7725	AN 10488
AN 2374	AN 5824	AN 7729	AN 10693
AN 2435	AN 5983	AN 7895	AN 10703
AN 2526	AN 6023	AN 7909	AN 10789
AN 2684	AN 6139	AN 7912	AN 10929
AN 2952	AN 6215	AN 8089	AN 10975
AN 2953	AN 6304	AN 8095	AN 11016
AN 2955	AN 6434	AN 8099	

Table 40: Genes of SRFS26 upregulated in GO enrichment

Gene	AN 0395	AN 0793	AN 0973
AN 0061	AN 0528	AN 0807	AN 0983
AN 0146	AN 0566	AN 0856	AN 1134
AN 0147	AN 0651	AN 0857	AN 1202
AN 0294	AN 0731	AN 0930	AN 1236

AN 1314	AN 3882	AN 6550	AN 8881
AN 1577	AN 3934	AN 6633	AN 8962
AN 1586	AN 4114	AN 6757	AN 8984
AN 1612	AN 4167	AN 6784	AN 9003
AN 1731	AN 4642	AN 6787	AN 9210
AN 1967	AN 4673	AN 6803	AN 9220
AN 2013	AN 4845	AN 6943	AN 9309
AN 2118	AN 4846	AN 6985	AN 9483
AN 2219	AN 4871	AN 7035	AN 10022
AN 2328	AN 4920	AN 7075	AN 10038
AN 2370	AN 5018	AN 7110	AN 10044
AN 2371	AN 5039	AN 7200	AN 10049
AN 2385	AN 5303	AN 7532	AN 10158
AN 2387	AN 5312	AN 7644	AN 10288
AN 2560	AN 5315	AN 7881	AN 10318
AN 2583	AN 5339	AN 7900	AN 10343
AN 2593	AN 5350	AN 8146	AN 10355
AN 2649	AN 5398	AN 8154	AN 10557
AN 2706	AN 5414	AN 8340	AN 10580
AN 2815	AN 5427	AN 8341	AN 10604
AN 2899	AN 5430	AN 8342	AN 10678
AN 2901	AN 5900	AN 8366	AN 10691
AN 3020	AN 5943	AN 8413	AN 10805
AN 3077	AN 6299	AN 8429	AN 10838
AN 3130	AN 6321	AN 8507	AN 10960
AN 3273	AN 6377	AN 8536	AN 11011
AN 3277	AN 6411	AN 8542	AN 11161
AN 3281	AN 6429	AN 8564	AN 11191
AN 3395	AN 6444	AN 8623	AN 11217
AN 3551	AN 6450	AN 8706	AN 11222
AN 3866	AN 6460	AN 8743	AN 11607

Acknowledgement

This has been quite the extended endeavour and there are so many people without whom I would have certainly never been able to finish up.

My thanks go Prof. Dr. Reinhard Fischer for providing the opportunity to perform the PhD work in his lab, his help with ideas and his patience with me. Many thanks to the Deutsche Forschungsgemeinschaft for financing the work.

Furthermore, I'd like to thank the members of his laboratory for being so welcoming and providing an environment that made even the bad days bearable. Firstly, my thanks go to Dr. Christian Streng for introducing me to the project and helping with any questions. My gratitude also goes to Dr. Kai Leister, Lars Schuhmacher, Alexander Landmark and Alexander Blumhofer for their interest in scientific discourse. Without our discussions and your assistance, many ideas may have never come to fruition. Of course I cannot forget about my other colleagues, Birgit, Elke, Maria (both of you), Helena, Jenny, Satur and Michael.

Huge thanks go to my family who have supported me all the way. You always encouraged and enabled me to follow my passion. Unfortunately, my grandfathers Werner and Walter did not live to see the conclusion of this work. May you rest in peace!

Special thanks also go to my friends David, Christine and Lukas for all the memories and amazing times we've had over the years! May there be many more days spent together in future.